



International Workshop on
Advanced Materials and Innovative
Systems in Structural Engineering:
Seismic Practices



Süleyman Demirel Cultural Center, Istanbul Technical University
16 November 2018

Proceedings

Editors: Alper Ilki, Derya Çavunt

İTÜ



fib
CEB-FIP
Turkey

*The International Workshop on Advanced Materials and
Innovative Systems in Structural Engineering: Seismic Practices
IWAMISSE 2018, Istanbul, Turkey
16 November 2018*

**Proceedings of IWAMISSE 2018
the International Workshop
on Advanced Materials and Innovative Systems in
Structural Engineering: Seismic Practices**

Editors

Alper Ilki

Derya Cavunt

November 2018

*The International Workshop on Advanced Materials and
Innovative Systems in Structural Engineering: Seismic Practices
IWAMISSE 2018, Istanbul, Turkey
16 November 2018*



Advanced Materials and Innovative Systems in Structural Engineering: Seismic Practices
Proceedings of IWAMISSE 2018, The International Workshop on Advanced Materials and
Innovative Systems in Structural Engineering: Seismic Practices

ISBN: No. 978-975-561-500-4

Email: info@fib-tr.org

Website: www.iwamisse2018.org

All rights reserved.

Please contact info@fib-tr.org for more information.

The Workshop Organizing Committee is not responsible for the statements of opinions expressed in this publication. Any statements of views expressed in the papers contained these proceedings are those of the author(s). Mention of trade names or commercial products does not constitute endorsement or recommendation for use.

Preface

The International Workshop on Advanced Materials and Innovative Systems in Structural Engineering: Seismic Practices, IWAMISSE 2018, is co-organised by The International Federation for Structural Concrete Turkey Branch, *fib*-Turkey, and Istanbul Technical University, ITU, on November 16, 2018 at ITU.

The International Federation for Structural Concrete, *fib*, is a not-for-profit association formed by 45 national member groups and approximately 1000 corporate and individual members. The *fib*'s mission is to develop at an international level the study of scientific and practical matters capable of advancing the technical, economic, aesthetic and environmental performance of concrete construction.

Istanbul Technical University (ITU) was established in 1773 and is a state university which defined and continues to update methods of engineering and architecture in Turkey. It provides its students with innovative educational facilities while retaining traditional values, as well as using its strong international contacts to mould young, talented individuals who can compete not only within their country borders but also in the global arena. With its educational facilities, social life and strong institutional contacts, ITU has always been preferred by Turkey's most distinguished students since its foundation and has achieved justified respect.

The workshop covers the topics of advanced materials and innovative systems in structural engineering with a focus on seismic practices as well as other issues related with steel fiber reinforced concrete, anchors/fasteners, precast structures, and recent advances on different types of structural systems such as reinforced concrete, steel, and reinforced masonry structures.

This proceeding book contains sixteen papers from ten countries worldwide. We have no doubt that the up-to-date subjects covered during the workshop will be extremely beneficial for the workshop participants both from academia and industry. We would like to thank all authors for their contributions to the workshop as well as the members of the International Scientific Committee for their rigorous work for reviewing the papers. We also gratefully acknowledge the support of the sponsoring companies and we express our sincere thanks to organization committee for their tireless efforts in the overall organization of the workshop. Many thanks go as well to undergraduate and graduate students from ITU for their assistance during all stages of the workshop.

Alper Ilki, Derya Cavunt

16 November 2018

Organization

Chair

Alper Ilki

Istanbul Technical University
Istanbul / Turkey

Workshop Secretary

Derya Cavunt

Istanbul Technical University
Necmettin Erbakan University
Istanbul / Turkey

Sponsors



International Scientific Committee

Akio Kasuga	Haluk Sucuoglu	Oguz Cem Celik
Andrea Penna	Hugo Corres Peiretti	Polat Gülkan
Cem Demir	Ismail Ozgür Yaman	Riadh Al Mahaidi
Cem Topkaya	Jian Fei Chen	Scott Smith
Cüneyt Vatansever	Khalid Mosalam	Serdar Göktepe
David Fernández-Ordóñez	Koichi Kusunoki	Stefano Pampanin
Elizabeth Vintzileou	Kutay Orakcal	Thanasis Triantafillou
Eray Baran	Larbi Sennour	Ulrich Bourgund
Erdem Canbay	Metin Aydogan	Walter Berger
Erkan Özer	Michael Fardis	Yasar Kaltakcı
Faruk Karadogan	Nilüfer Ozyurt	Yuji Ishikawa
György L. Balazs		

Table of Contents

Invited Papers

<i>New fib Model Code 2020 for existing and new concrete structures</i> H. C. Peiretti, F. A. Fernandez, J. S. Delgado	1
<i>New improvements in the 2018 Turkish Seismic Code</i> H. Sucuoglu	13
<i>Collapse assessment of building columns through multi-axis hybrid simulation</i> R. Al-Mahaidi, M. J. Hashemi, H. A. Yazdi, Y. Al-Ogaidi	22
<i>Advanced pre-cast concrete system and innovative steel fibre reinforced concrete structural system in Japan</i> Y. Ishikawa	31
<i>Evolution of bridge construction in Japan</i> A. Kasuga	41
<i>Raising the bar in earthquake risk reduction: integrated low-damage building systems to enhance community resilience</i> S. Pampanin	58
<i>Fastening in seismic environment</i> U. Bourgund, R. Piccinin	79
<i>Shear behaviour of interfaces within repaired/strengthened RC elements subjected to cyclic actions</i> E. Vintzileou, V. Palieraki, G. Genesio, R. Piccinin	89
<i>Performance based mix design of steel fiber reinforced concretes - Recent advances in applications</i> M. A. Tasdemir	100
<i>Fiber reinforced cementitious composites for retrofit of reinforced concrete members-A review</i> I. Bedirhanoglu, A. Ilki	122

Regular Papers

<i>Influence of adjacent channel bolts on the lip capacity of anchor channels – a connection to withstand typhoons and earthquakes</i> C. Mahrenholtz	149
<i>Study on the behavior of RC beams strengthened with CFRP laminates under pure torsion using finite element analysis and fib Bulletin 14 method</i> M. M. Majed, M. T. Zadeh	159
<i>Experimental and numerical investigation of cyclic response of precast hybrid beam-column connections</i> S. C. Girgin, I. S. Misir, S. Kahraman	170
<i>A simplified performance based rapid seismic assessment method for mid-rise reinforced concrete structures</i> H. Gorgun, D. Kaya, M. E. Oncu, S. Y. Cetin	181
<i>Flexural behaviour of cement based composite plates for seismic retrofit of masonry walls</i> M. E. Günes, Z. C. Girgin, B. Y. Pekmezci	191
<i>A Study on effect of steel fiber content on minimum reinforcement ratio of high strength reinforced concrete beams</i> M. Gumus, A. Arslan	200
Author Index	210

International Workshop on Advanced Materials and
Innovative Systems in Structural Engineering:
Seismic Practices

Invited Papers

New fib Model Code 2020 for existing and new concrete structures

Hugo Corres Peiretti¹, Freddy Ariñez Fernández², Julio Sánchez Delgado³

¹ Prof. PhD Msc Civil Engineer, *fib* President

² PhD Msc Civil Engineer, FHECOR Structural Engineer

³ Msc Civil Engineer, FHECOR Technical Director

1 INTRODUCTION

Model Code is one of the most important documents produced by fib. The first edition was published in 1970. Since then, fib has published new and updated editions in 1978, 1990 and, the most recent one, in 2010. All of these documents have been reference documents that have influenced the production of National and Regional Codes. Model Code 1978 had a strong influence on the previous version of Eurocode 2; Model Code 1990 had the same strong influence on the current version of Eurocode 2 and Model Code 2010 similarly guides the preparatory work CEN has started for the new editions of the Eurocodes. Model Codes have always been an important reference for researchers, designers and constructors.

Some years ago, the fib started the process to produce a new updated edition to be published in 2020. This new Model Code intends to approach, at the same level, new and existing structures. It will present more general and more rational models, removing any trace of previous empirical design rules (MC2010 was an important step forward, but further steps are possible and needed). It will be an operational model code and oriented towards practical needs. It will recognize the needs of engineering communities around the world. MC 2020 has to be a real International Code.

This paper shows the content of the new Model Code 2020 and the ongoing work for its preparation.

2 MAIN IDEAS/GOALS OF THE NEW MC 2020

MC 2020 will be a single, merged structural code for new and existing structures

There were many different approaches for codes to be able to cover existing structures. A good summary of the evolutions of codes for existing structures was presented by Dr Steve Danton [1], at the first workshop to discuss the content of the new MC 2020 held in The Hague in June 2015.

The first approach/generation was to use the codes developed for new structures and apply them to existing structures. The result was not good because it failed to recognise the differences between design and assessment. Typically, the results obtained with this approach were conservative for assessment works, because it did not adequately take into account actual material properties, structural detailing and tolerances.

The second approach/generation was to write codes for existing structures. The result was also not good enough because there were cases of duplication of content, omission of content and it presented problems in the case of interventions (modification of existing structures).

The new approach, and what is often called the new generation of codes, is to develop a single, merged code structural code for both new and existing structures. And this is exactly what we decided to do for the new MC 2020.

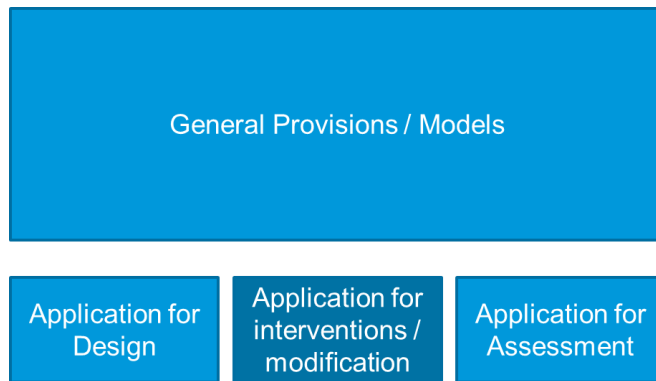


Figure 1. New generation of structural codes for new and existing structures. Figure presented by Dr. Steve Denton at the first workshop on Model Code 2020, held at The Hague on June 2015 [1]

The principles for the development of a unified Model Code will be: General provisions / models common for design, assessment and interventions. Provisions / models have to be general to be applied for the different problems we have to solve. General provisions / models capable of taking into account actual material properties, structural detailing and tolerances that may be found on existing structures.

MC2020 has to present general and more rational models, removing any trace from previous empirical design rules.

MC2010 was an important step forward in removing empirical design rules leaving space for general and rational models. This criterion has to be expanded in the new MC 2020.

Figure 2 shows the differences in using a general rational with an empirical rule for bending of a reinforced concrete section.

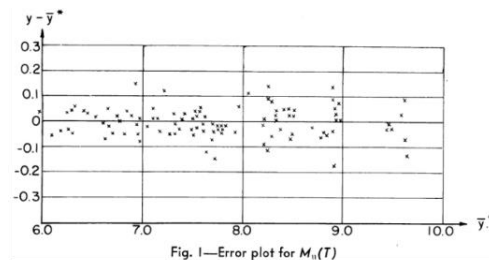
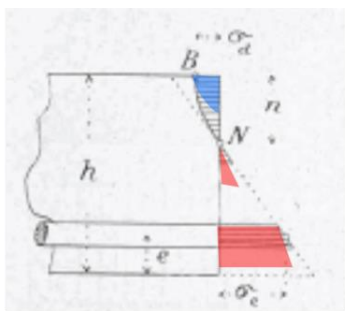


Fig. 1—Error plot for $M_u(T)$

$$M_R = 0.431 \cdot b \cdot d^2 \cdot \rho^{0.75} \cdot f_y^{0.9} \cdot f_c^{0.1} \text{ (psi, in)}$$

Ritter, W., 1899, *Die Bauweise Hennebique*, Schweizerische Bauzeitung, Zurich
 Courtesy of Aurelio Muttoni

Zsutty T.C., *Ultimate Strength Behaviour Study by Regression Analysis of Beam Test Data*, ACI Structural Journal, May 1963

Figure 2. Mechanical models vs. empirical equations, the case of bending. Figure presented by Prof Aurelio Muttoni at the first workshop on Model Code 2020, held at The Hague on June 2015 [2]

7.3.2 Bending with and without axial force

7.3.2.1 Beams, columns and slabs

This sub-clause applies to undisturbed areas of beams, slabs and similar types of members for which sections remain approximately plane before and after loading. The discontinuity regions of beams and other members, where plane sections do not remain plane, may be designed and detailed according to sub-clause 7.3.6.

When determining the ultimate bending resistance of reinforced or prestressed concrete cross-sections, the following assumptions are made:

- plane sections remain plane;
- the strain in bonded reinforcement or bonded prestressing tendons, whether in tension or in compression, is the same as that in the surrounding concrete;
- the tensile strength of the concrete is ignored;
- the stresses in the concrete are derived from stress-strain relations for the design of cross-sections as given in sub-clause 7.2.3.1.5;
- the stresses in the reinforcing and prestressing steel are derived from the design curves in sub-clause 7.2.3.2 and 7.2.3.3; and
- the initial strain in the prestressing tendons is taken into account when

Figure 7.3-1 shows the possible range of strain distributions for concrete, reinforcing steel and prestressing steel. In the figure, the following limits are shown:

- A = reinforcing strain limit;
- B = concrete compression limit; and
- C = concrete pure compression strain limit.

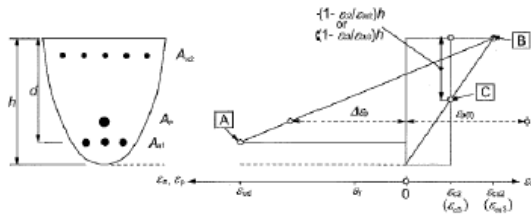
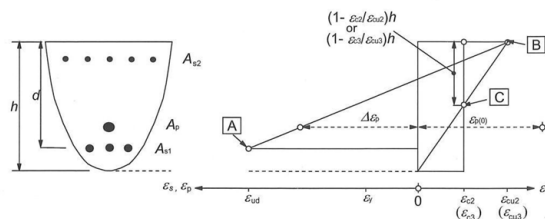


Figure 7.3-1: Possible strain distributions in the ultimate limit state.

Figure 3. *fib* MC 2010 model for bending [3].

Ritter proposed in 1899 the model which is still used in *fib*, see Figure 3 taken from MC 2010. This general approach allows considering: axial force, different cross-section shapes, several reinforcement layers, prestressing, different concrete types, different types of loads (fire, seismic loads, etc.). In addition, the model can be easily adapted to a wide variety of cases (different types of concrete, non-metallic reinforcement, sections subjected to different types of deterioration, etc.). This model may be used to consider the different situations we have in the design of new structures and in the assessment and interventions in existing structures.

In comparison, the empirical formula proposed by Zsutty in 1963 is only valid for the conditions for which was developed.



EXISTING CONCRETE						
fck	17	20	90	120	150	250
DESIGN CONCRETE						
fck	17	20	90	120	150	250
FIBRE REINFORCED CONCRETE (FRC)						
fck	17	20	90	120	150	250
UHPFRC						
fck	17	20	90	120	150	250

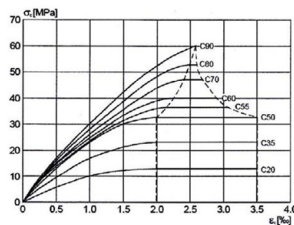


Figure 7.2-7: Design stress strain relations for various concrete strength classes (parabola-rectangle) for $\gamma_c = 1.5$

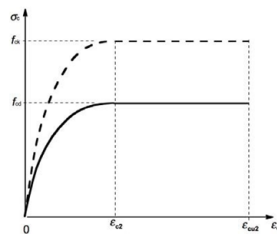


Figure 7.2-9: Parabola-rectangle diagram for concrete in compression

Figure 4. *fib* Model Code 2010 model for bending extended for assessment of existing structures or for design of new structures or interventions on existing structures. Constitutive equations for concretes with different compressive strengths.

Figure 4 shows how the same *fib* model may be used for assessment of existing structures or for design of new structures or interventions.

The top part of the figure shows different types of concretes that can be found in existing and in new structures, including new types of concrete: FRC, UHPFRC, Green Concretes, Tailor-made concretes, etc. In order to use the model for all of the different concretes it is only necessary to have the correct constitutive equations for the different cases. The bottom part of the figure shows the constitutive equations currently available in MC 2010 for concretes with different compressive strengths.

MC 2010 was drafted to take into account different types of actions, in addition to static actions, such as for example, seismic actions, fire and many others. This same philosophy was preserved in MC 2020, adopting models, like the one shown in figure 4, where different types of actions can be represented only by considering the pertinent constitutive equations. Figure 5 shows the constitutive equations proposed by MC 2010 to represent the behavior of confined concrete for seismic actions, or concrete subjected to different temperatures, to consider the influence of fire.

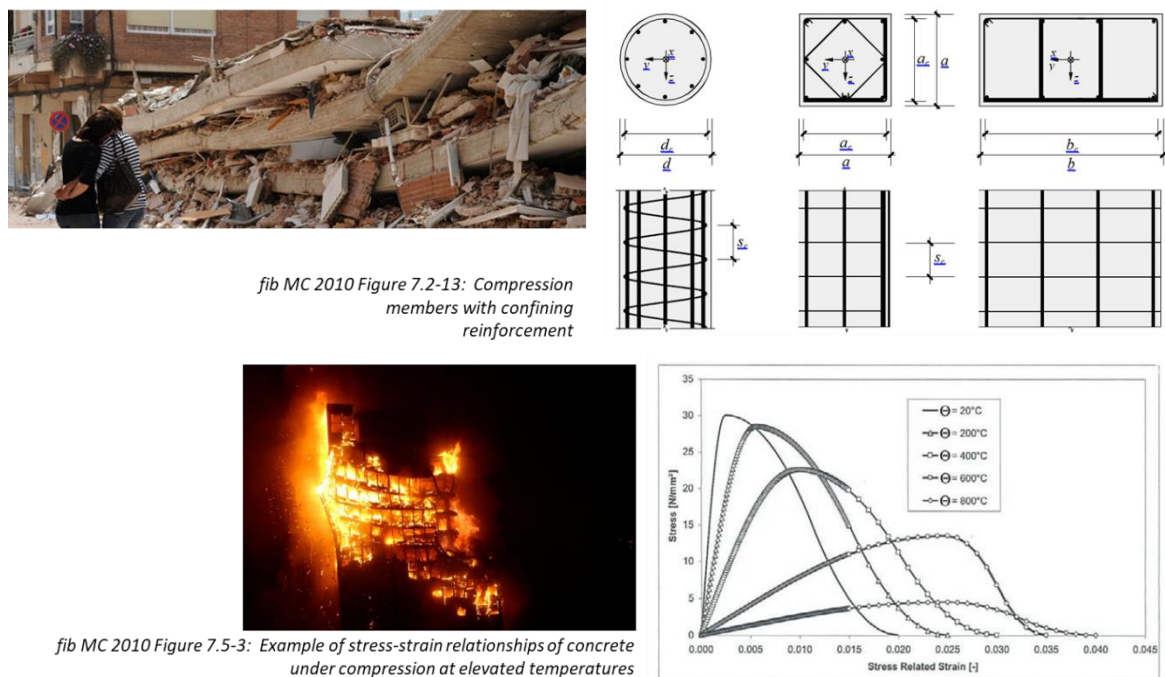
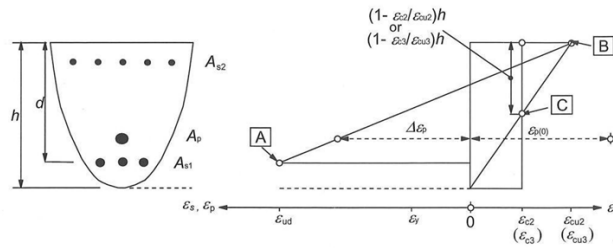


Figure 5. *fib* Model Code 2010 model for bending extended for the assessment of existing structures or for the design of new structures or interventions on existing structures. Constitutive equations for confined concrete and concrete subjected to different temperatures.

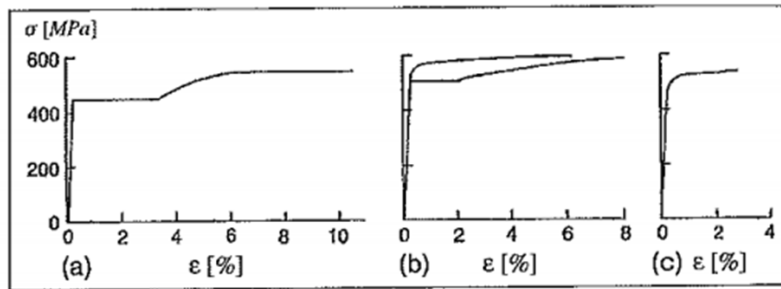
The assessment of existing structure requires setting forth criteria to estimate representative characteristics of concrete. Thus, we must define the right experimental test campaign in order to obtain results that are actually representative of the structure.

Likewise, we also need more and better models, than the ones currently available in MC 2010, in order to represent the effect of different types of deteriorations in the bearing capacity of concrete.

In the case of reinforcing and prestressing steel it is possible setting forth constitutive equations that represent the situations found in the assessment, design and intervention of structure, both for static actions and other actions that may be found in the structures. In fact, MC 2010 has already established many of these equations, see figures 6 and 7.

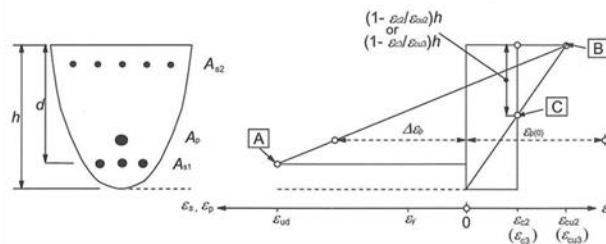


EXISTING REINFORCING STEEL		
f _{yd}	200	600
REINFORCING STEEL		
f _{yd}	400	600

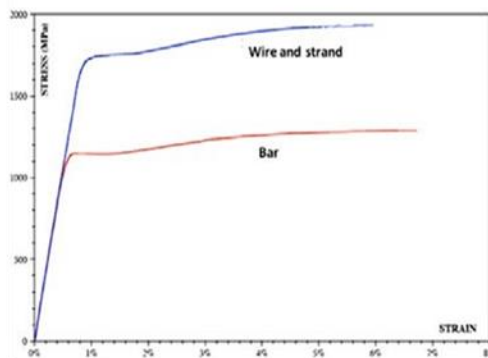


fib MC 2010 Figure 5.2-1: Stress-strain relationships of reinforcing steel: (a) hot-rolled bars; heat-treated bars; micro-alloyed bars, (b) low carbon, heat-treated bars (lower curve): cold-worked bars (upper curve); (c) cold-worked wires.

Figure 6. fib MC 2010 model for bending extended for assessment of existing structures or for design of new structures or interventions on existing structures. Constitutive equations for reinforcing steel.



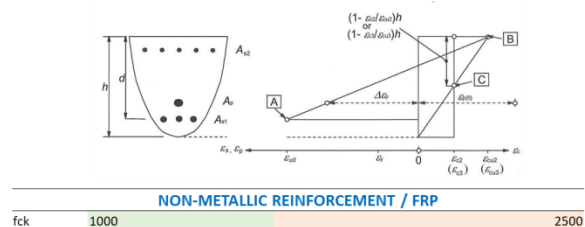
EXISTING PRESTRESSING STEEL		
f _{yp}	1700	2000
		2500
PRESTRESSING STEEL		
f _{yp}	1700	2000
		2500



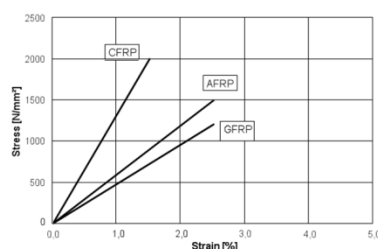
fib MC 2010 Figure 5.3-1: Typical stress-strain diagrams for prestressing steel

Figure 7. fib MC 2010 model for bending extended for assessment of existing structures or for design of new structures or interventions on existing structures. Constitutive equations for prestressing steel.

The same model can be used to represent non-metallic reinforcement, used lately in new structures and in retrofitting existing structures. For this type of material it will be necessary to revise the safety formats in order to define material safety factors that take into account the brittleness of these materials as well as other specific uncertainties.



	CFRP	GFRP	AFRP
Tensile strength f_f [MPa]	600-3000	400-1600	600-2500
Modulus of elasticity E_f [GPa]	80-500	30-60	30-125
Ultimate strain ϵ_{fu} [%]	0.5-1.8	1.2-3.7	1.8-4.0



fib MC 2010 Table 5.5-1: Tensile properties of FRP reinforcement

fib MC 2010 Figure 5.5-1: Stress-strain diagram of non-metallic reinforcement in the principal fibre direction

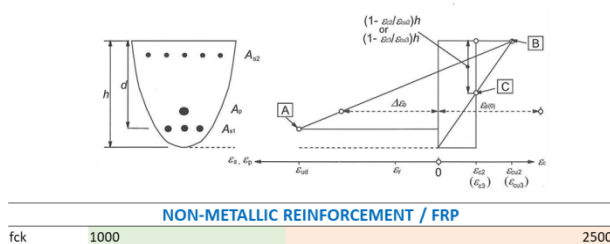


Figure 8. *fib* MC 2010 model for bending extended for assessment of existing structures or for design of new structures or interventions on existing structures. Use of non-metallic reinforcement.

The same *fib* model for normal stresses is capable of estimating the resistance of a reinforced section. In this case, it is necessary to elaborate a system to represent the tensional state in section under the loads, generally permanent loads, applied prior to the design forces. This can be materialized with a preliminary strain in all of the materials of the cross-section. Afterwards, taking into account the initial stress state, additional factored loads can be applied to the structure for a given combination.

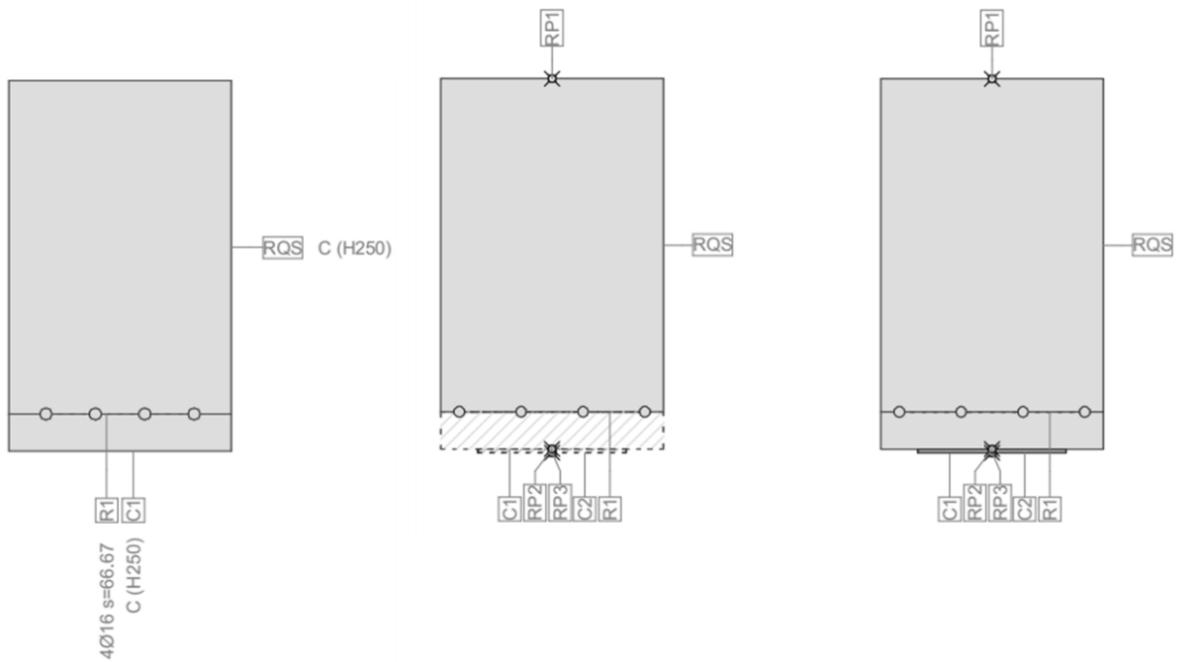
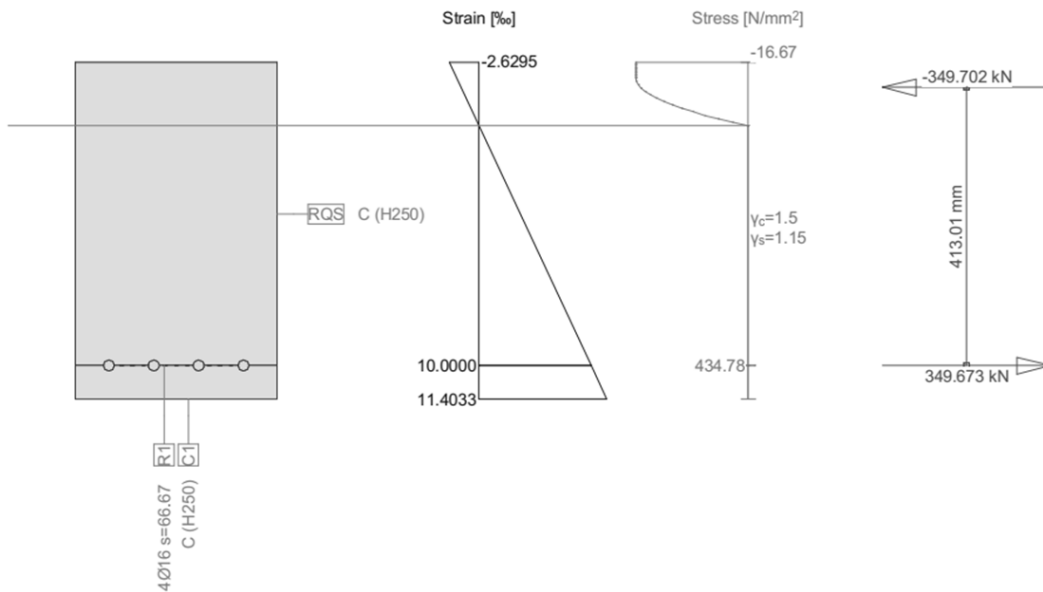


Figure 9. a) Original cross-section design b) Deteriorated cross-section, for a reinforcing steel corrosion process. C) Reinforced cross-section, where the part of the missing cover was replaced and a steel plate was added to the bottom face.

Cross-section INICIAL (H250;AEH500): Efficiency $M_y=142.000$; $\text{eff}(M,N) = 0.98$ OK Scale 1 : 10.0

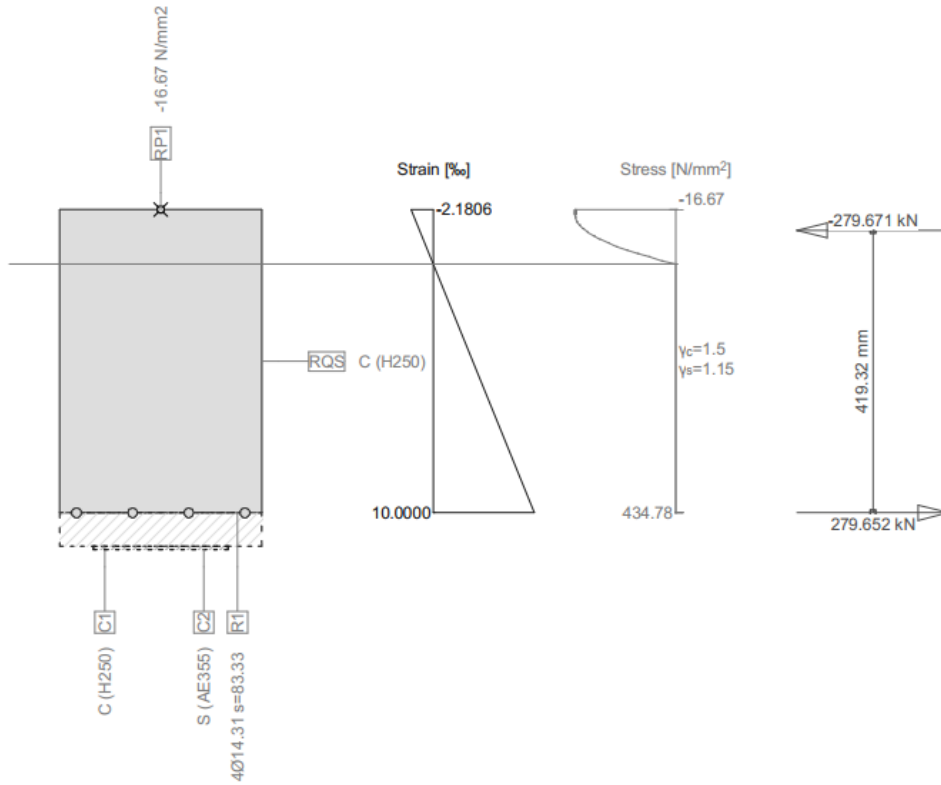


Action forces / Efficiency: $\text{eff}(M,N) = 0.98$ OK

No.	AP	P	Bending and axial force				Shear forces and torsion			Complete CS eff(M,N,V,T)
			N [kN]	M _y [kNm]	M _z [kNm]	eff(M,N) [-]	V _y [kN]	V _z [kN]	T [kNm]	
1	AP4		0	142.000	-	0.98				

- : Calculation with uniaxial bending (neutral axis is horizontal)!!

Figure 10. ULS strength of the original design of the cross-section.



Action forces / Efficiency: $eff(M,N) = 1.00$ OK

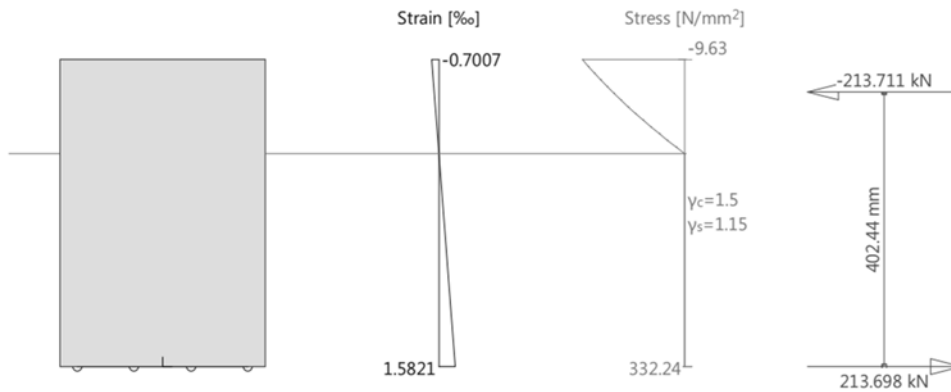
No.	AP	P	Bending and axial force				eff(M,N)	Shear forces and torsion			Complete CS eff(M,N,V,T)
			N [kN]	M_y [kNm]	M_z [kNm]	eff(V,T)		V_y [kN]	V_z [kN]	T [kNm]	
1	AP4		0	117.000	-	1.00					

- : Calculation with uniaxial bending (neutral axis is horizontal)!!

Figure 11. ULS strength of the cross-section after it was damaged by corrosion.

Stress analysis Cross section (Girder): SEGUNDA, Variante: OXIDADA

Scale 1:8.2



Action forces / Loading history - calculation with loading steps, (in-)active parts,

No.	AP	P	Bending and axial force			Shear forces and torsion			Remarks
			N [kN]	M_y [kNm]	M_z [kNm]	V_y [kN]	V_z [kN]	T [kNm]	
1			0	86.000	0				
2	AP4								Set inactiv

1 : Set inactiv: C2,C1

Figure 12. Tensional state of the cross-section subjected to the bending moment that corresponds to the permanent load.

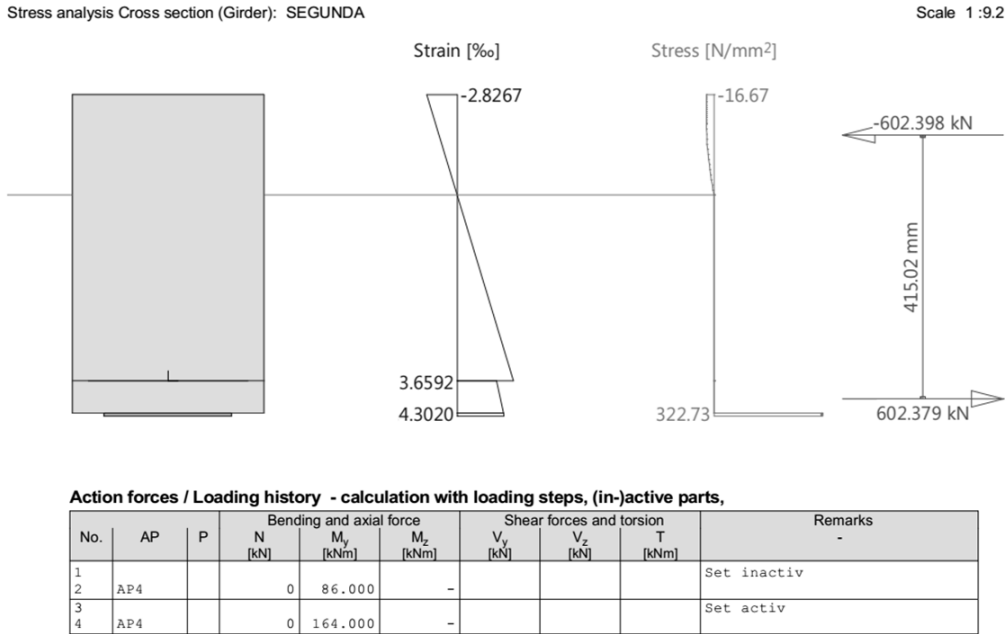


Figure 13. ULS strength of the reinforced section, considering the tensional state of the cross-section for permanent loads, prior the reinforcement installation.

Figure 9 shows a cross-section a) with dimensions of 0.30x0.50 and C25 concrete and 4 rebars with a diameter of 16 mm of B500B steel and a cover of 0.05 m. It also shows b) the section affected by a corrosion process of the reinforcing steel, showing how the concrete cover was lost as well as 80% of the original rebar area. Finally, it shows c) a section where the concrete cover was replaced and a steel plate with dimensions of 200x20 mm² was added.

The original section had ULS strength of 142 kNm, as shown in figure 10. The damaged section has ULS strength of 117 kNm, as shown in figure 11. It is clear that the resisting capacity of the structure was reduced. Figure 12 shows the tensional state of the damaged section for permanent load forces. Finally, figure 13 shows the ULS strength of the reinforced section, considering a preliminary deformation that corresponds to the permanent load forces on section b). The efficiency of the reinforcement can be strongly conditioned by the tensional state of the section prior the application of the reinforcement as well as its corresponding design loads.

The fib model for normal stresses is capable of taking into account all of the different situations that occur in a section for the design of a new structure, for the assessment of an existing structure and for the evaluation of the bearing strength of possible interventions.

Nevertheless, it will be necessary in the new MC 2020 to adequately describe the process to take into account the tensional state of the section before considering the designed reinforcement.

It will also be necessary to clarify how to deal with the ULS safety of the loads on the structure, generally, permanent loads, before the application of the reinforcement. For new structures, load factors are applied at once because, in this case, the initial deformations are not taken into account. For reinforcements and retrofitting of existing structures, we first take into account the tensional state under the loads that act prior the execution of the reinforcement, possibly with characteristics values and, afterwards, at the ULS, these loads will be considered with their corresponding safety factor, which was not considered at the initial state.

The analysis proposed in this paper corresponds to normal stress models. It is still necessary to carry out a detailed work to adapt the available models for other forces such as shear, punching shear and torsion, in order for these models to consider all of the situations described above.

Model Code 2020 will be an operational model code and oriented towards practical needs

The evolution of codes has grown in content and pages see figure 14. In addition, modern codes generate the false impression that all problems in structural engineering are solved, when it is manifestly evident that each time that we face a structural engineering problem we show how little we really know and how much we need to research, see figure 15. Research is an ever-increasing field in structural concrete but it is often not focused on practical problems.

Figure 14. Evolution of codes in time. Comparison between the Dutch code in 19xx and the current version of Eurocode.

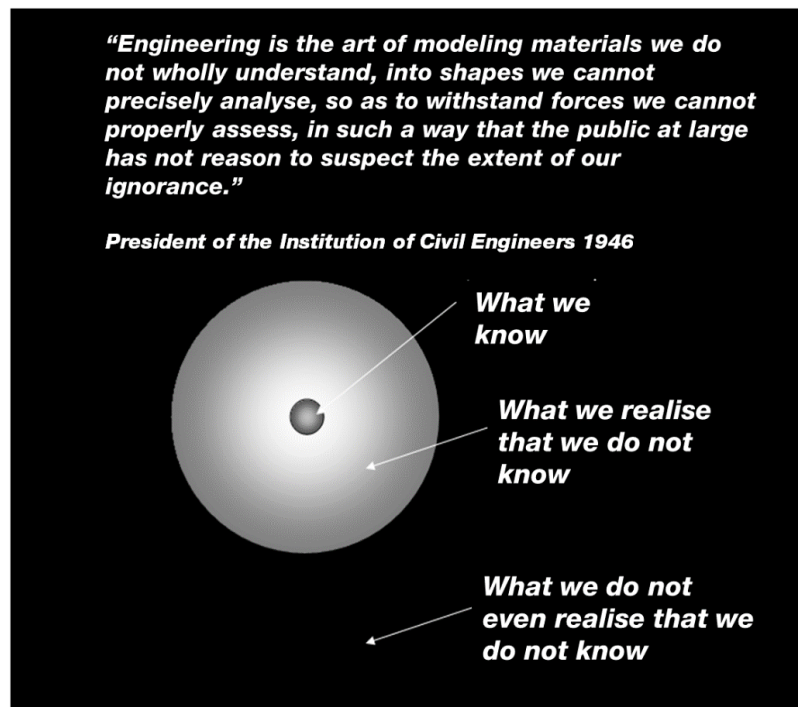


Figure 15. Words of the president of the Institution of Civil Engineers in England in 1949.

The new MC 2020 must be an example of trend change. How to solve this enormous challenge?

Traditionally, MC's have been drafted using the right part for principles and application rules and the left part for comments. The rules must be clear, general and coherent with the content in other parts of the document. The comments should be very specific and above all, referenced to other documents that support the proposed rules and even that show more specific application aspects of these rules. It has always been desired for the models and rules in Model Codes to be explained in background documents. The current goal is to publish the background documents in the bulletings, as in the recent Bulletin 80 [4] on safety formats for existing structures, or in the Structural Concrete Journal of the fib. All effort on this matter will save explanations in the code text and it will help for a better comprehension of the considered principles and rules.

The new MC 2020 has the ambition to have indications on what is currently unknown and therefore is susceptible to be studied. It is possible that this document can also help to coordinate research efforts towards necessary subjects.

MC 2010 introduced the concept of different approximation levels. This a very intelligent way to use complex models with different approximation levels to allow the use of the same conceptual base and, depending on the required precision level, the use of simplifications in determined initial design levels or the total capacity of the models when the problem requires it, see figure 16.

Levels of approximation approach (MC 2010)

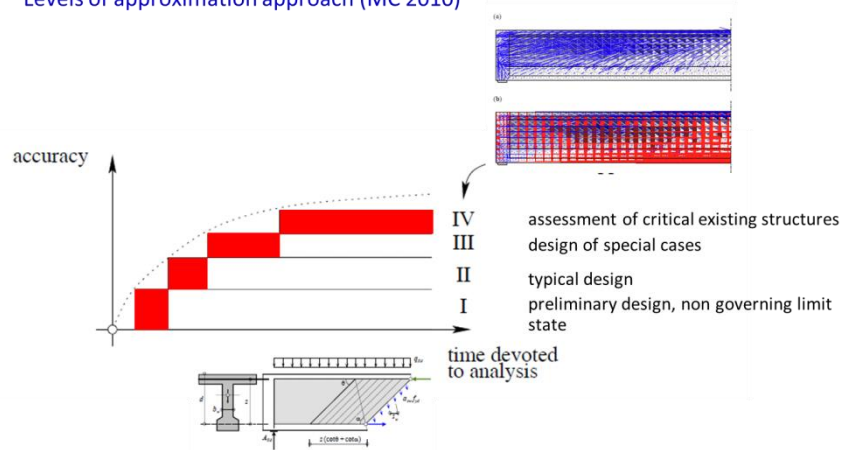


Figure 16. Different levels of Aproximations. Figure presented by Prof Aurelio Muttoni at the first workshop on Model Code 2020, held at The Hague on June 2015 [2]

Model Code 2020 will recognize the needs of engineering communities around the world. MC 2020 has to be a real International Code

From an open perspective there is no justification that structural engineering can be so different from some countries to others. Although, it is acceptable to think that there may be different environmental, or action or specific constraints in each region.

In reality there are very different problems to solve, very different traditions to solve them and very distinct social and economic conditions to approach them.

The fib the International Federation for Structural Concrete has set forth the need to collect information on this diversity and gather information on the needs of different regions. Therefore, it has programmed workshops in different continents that present the evolution of MC 2020 at the same time that local experts in different areas present their respective points of view and specific needs. This labor results in a more international character of the new MC 2020.

MC2020 Initiative – Global involvement



Figure 17. fib Model Code 2020 Workshops in different continents.

3 FINAL CONSIDERATIONS

The new version of MC 2020 has a solid starting point, MC 2010. It is a thorough document that shows many of the ideas that are needed in the new version and only require more or less development.

There has been a great discussion on what was needed for the future. The established criteria promise a MC 2020 that without a doubt will become a major reference in the future of structural engineer, just as it has happened with the previous versions. A MC for new and existing structures that aims for a single and consistent approach of problems. A MC that proposes, depending on the available knowledge, general and physical models that can be used indistinctly for new and existing structures. A MC that is practice-oriented. Finally, an international MC that represents the aspirations of fib that really is an international association formed by 45 countries from all of the continents.

It must a document that shows a new trend in the preparation of codes that has gradually become overwhelming.

The new MC must, in addition, serve to identify different fields where current knowledge is insufficient in order to, as much as possible, lead research in the direction where it is most needed.

REFERENCES

- Danton; S. Presentation made at the first workshop on Model Code 2020, held at The Hague on June 2015 [1]
Muttoni; A. Presentation made at the first workshop on Model Code 2020, held at The Hague on June 2015 [2]
fib. Model Code for Concrete Structures 2010. 28 October 2013. ISBN:9783433030615 [3]
fib Bulletin No. 80. Partial factor methods for existing concrete structures. 2016. Pages: 129. ISBN: 978-2-88394-120-5 [4]

New improvements in the 2018 Turkish Seismic Code

Haluk Sucuoğlu¹

¹ Professor, Middle East Technical University, Ankara, Turkey

ABSTRACT: Turkey has official Seismic Code since 1940's, which is updated regularly in conformance with the new developments in earthquake engineering, as well as the changing societal needs. The 2018 Seismic Code (AFAD 2018) has improved the 2007 Seismic Code (Ministry 2007) with an expanded content. The main improvements are on the definition of site-specific design ground motions, and on the seismic design of tall buildings, base isolated buildings and pile foundations. Nonlinear analysis procedures are included as mandatory in particular cases, however advised for performance evaluation for the non-standard practices. From the administrative point of view, a new "Design Review and Supervision" system is established on the non-standard practices, which is a peer review process administered with a central, official public body.

1 INTRODUCTION

The 2018 Turkish Seismic Code will be officially enforced as of January 1, 2019. However, it is already effective for the new parts that do not exist in the previous 2007 version of the code. AFAD (Disaster and Emergency Management Directorate of Turkey) is in charge of publishing and revising the Seismic Code, whereas The Ministry of Environment and Urbanization is in charge of its implementation and supervision. Turkish Seismic Code has the official powers of a By-Law, which is the main annex of Disaster Law.

The new improvements in the 2018 Code are presented in line with their order in the Code. Most of these improvements or revisions are in conformance with the major seismic codes in the World (Eurocode 2004, ASCE 2010). This paper covers seismic hazard maps, general design rules for buildings, fundamental aspects of force-based design and deformation based evaluation, seismic evaluation of existing buildings, and the design of tall and base isolated buildings.

2 SEISMIC HAZARD MAPS

The previous Seismic Hazard Map of Turkey (1996) was a seismic zonation map, which divides the country into 5 hazard zones. It was based on the PGA values on very stiff soil, with a return period of 475 years. These zones were quite wide, 100's of kilometers in many geographical regions, and hence representing hazard with a single PGA parameter was of course insufficient. AFAD has established a project study in early 2000 for updating both the active fault map of Turkey and Seismic Map of Turkey, which eventually became the main instrument of the Seismic Code for defining seismic hazard.

The new Seismic Hazard Map is not a seismic zonation map, but it is a contour map based on the geographical coordinates. Seismic hazard is not expressed in terms of PGA, but in terms of spectral acceleration. Site-specific spectral acceleration maps at $T=0.2$ s and $T=1$ s are developed for stiff soil sites, and for return periods of 2475, 475, 72 and 43 years. A PGA contour map is also developed. All maps are accessible for public use, through the web site "<https://tdth.afad.gov.tr/>".

A comparison of the 1996 Seismic Zones Map and the 2018 Seismic Hazard Map, both 475-year PGA based, are presented in Figure 1. The mean PGA value in Zone 1 (red zone) of the 1996 map

is 0.4g. The total area of the $PGA > 0.4g$ regions is seemingly less in the 2018 map, especially in the Aegean West and along the Eastern Iranian border.

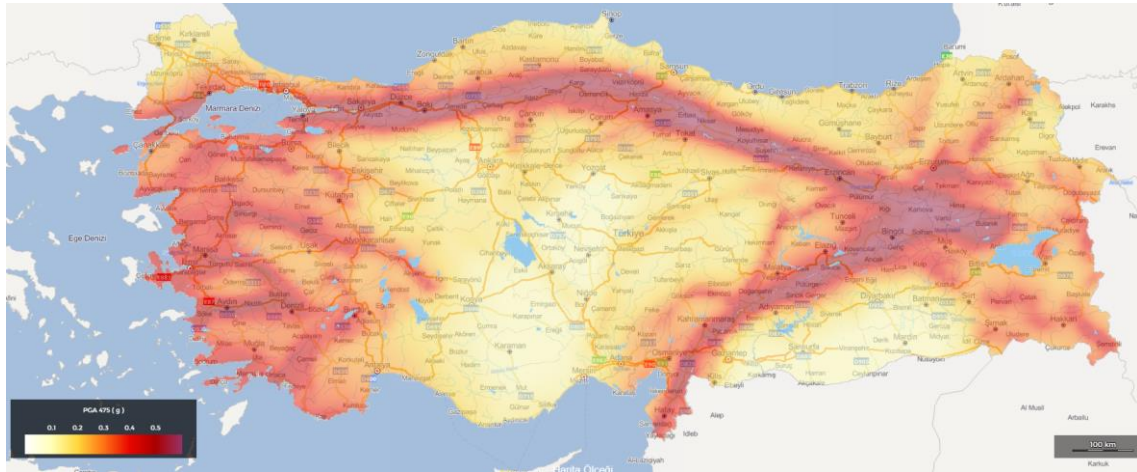
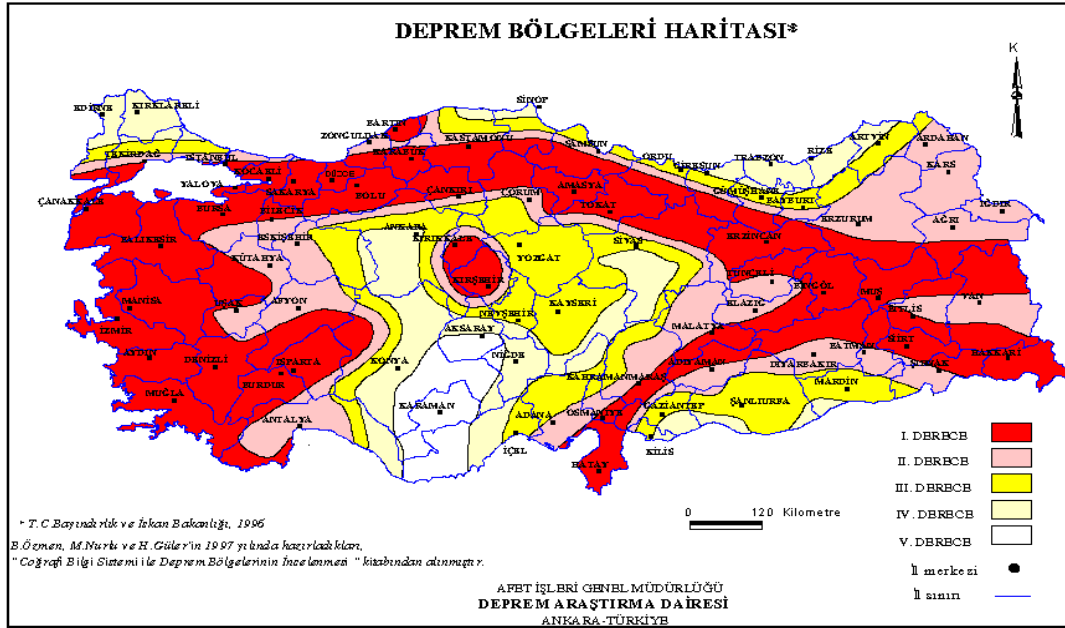


Figure 1. 1996 Seismic Zones Map (top) and 2018 Seismic Hazard Map (bottom). Both are based on 475-year PGA on very stiff soil.

Spectral acceleration values S_s and S_1 at $T=0.2$ and 1.0 seconds, respectively are obtained from the associated hazard maps prepared for reference stiff soil sites. Then they are modified with respect to the soil conditions at the project site in order to obtain the design spectral accelerations S_{Ds} and S_{D1} . Finally the design spectrum is constructed as illustrated in Figure 2. The corner periods T_A and T_B are obtained from the associated ratios of S_{Ds} and S_{D1} .

2.1 Earthquake ground motion levels

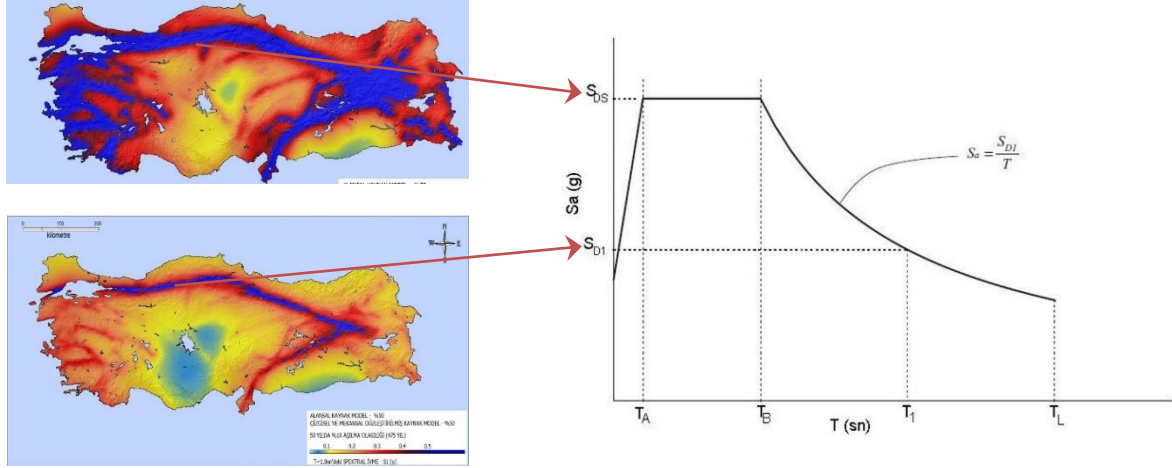
Four different levels of earthquake ground motion are specified in the 2018 Seismic Code different performance targets. These are defined in return periods, and the corresponding probabilities of exceeding the associated ground motion level.

DD-1: 2% probability of exceeding in 50 years, corresponding to a return period of 2475 years. It is the “maximum expected earthquake ground motion level”.

DD-2: 10% probability of exceeding in 50 years, corresponding to a return period of 475 years. It is the “standard design earthquake ground motion level”.

DD-3: 50% probability of exceeding in 50 years, corresponding to a return period of 72 years. It is the “frequently expected earthquake ground motion level”.

DD-4: 50% probability of exceeding in 30 years, corresponding to a return period of 43 years. It is the “service level earthquake ground motion”.



Contour maps for $T=0.2$ s and 1.0 s (S_s and S_1 , 475 years)

475-year design spectrum (5% damping)

Figure 2. Construction of the 475-year design spectrum from the 2018 Seismic Hazard Map.

3 GENERAL RULES FOR SEISMIC DESIGN OF BUILDING STRUCTURES

3.1 Building categories

Several classifications guide seismic design in the 2018 Code. These are the building use category with respect to the importance assigned to the building, seismic design category with respect to the seismic intensity at the design site, and building height category as related to the building height above the foundation or the rigid basement. They are summarized in Figure 3.

Building Use Categories (BKS)		Building Height Categories (BYS)																																									
I=1.5	: BKS=1	<table border="1"> <thead> <tr> <th rowspan="2">Bina Yükseklik Sınıfı</th> <th colspan="3">Bina Yükseklik Sınıfları ve Deprem Tasarım Sınıflarına Göre Tanımlanan Bina Yükseklik Aralıkları [m]</th> </tr> <tr> <th>DTS = 1, 1a, 2, 2a</th> <th>DTS = 3, 3a</th> <th>DTS = 4, 4a</th> </tr> </thead> <tbody> <tr> <td>BYS = 1</td> <td>$H_N > 70$</td> <td>$H_N > 91$</td> <td>$H_N > 105$</td> </tr> <tr> <td>BYS = 2</td> <td>$56 < H_N \leq 70$</td> <td>$70 < H_N \leq 91$</td> <td>$91 < H_N \leq 105$</td> </tr> <tr> <td>BYS = 3</td> <td>$42 < H_N \leq 56$</td> <td>$56 < H_N \leq 70$</td> <td>$56 < H_N \leq 91$</td> </tr> <tr> <td>BYS = 4</td> <td>$28 < H_N \leq 42$</td> <td colspan="2">$42 < H_N \leq 56$</td> </tr> <tr> <td>BYS = 5</td> <td>$17.5 < H_N \leq 28$</td> <td colspan="2">$28 < H_N \leq 42$</td> </tr> <tr> <td>BYS = 6</td> <td>$10.5 < H_N \leq 17.5$</td> <td colspan="2">$17.5 < H_N \leq 28$</td> </tr> <tr> <td>BYS = 7</td> <td>$7 < H_N \leq 10.5$</td> <td colspan="2">$10.5 < H_N \leq 17.5$</td> </tr> <tr> <td>BYS = 8</td> <td>$H_N \leq 7$</td> <td colspan="2">$H_N \leq 10.5$</td> </tr> </tbody> </table>			Bina Yükseklik Sınıfı	Bina Yükseklik Sınıfları ve Deprem Tasarım Sınıflarına Göre Tanımlanan Bina Yükseklik Aralıkları [m]			DTS = 1, 1a, 2, 2a	DTS = 3, 3a	DTS = 4, 4a	BYS = 1	$H_N > 70$	$H_N > 91$	$H_N > 105$	BYS = 2	$56 < H_N \leq 70$	$70 < H_N \leq 91$	$91 < H_N \leq 105$	BYS = 3	$42 < H_N \leq 56$	$56 < H_N \leq 70$	$56 < H_N \leq 91$	BYS = 4	$28 < H_N \leq 42$	$42 < H_N \leq 56$		BYS = 5	$17.5 < H_N \leq 28$	$28 < H_N \leq 42$		BYS = 6	$10.5 < H_N \leq 17.5$	$17.5 < H_N \leq 28$		BYS = 7	$7 < H_N \leq 10.5$	$10.5 < H_N \leq 17.5$		BYS = 8	$H_N \leq 7$	$H_N \leq 10.5$	
Bina Yükseklik Sınıfı	Bina Yükseklik Sınıfları ve Deprem Tasarım Sınıflarına Göre Tanımlanan Bina Yükseklik Aralıkları [m]																																										
	DTS = 1, 1a, 2, 2a				DTS = 3, 3a	DTS = 4, 4a																																					
BYS = 1	$H_N > 70$	$H_N > 91$	$H_N > 105$																																								
BYS = 2	$56 < H_N \leq 70$	$70 < H_N \leq 91$	$91 < H_N \leq 105$																																								
BYS = 3	$42 < H_N \leq 56$	$56 < H_N \leq 70$	$56 < H_N \leq 91$																																								
BYS = 4	$28 < H_N \leq 42$	$42 < H_N \leq 56$																																									
BYS = 5	$17.5 < H_N \leq 28$	$28 < H_N \leq 42$																																									
BYS = 6	$10.5 < H_N \leq 17.5$	$17.5 < H_N \leq 28$																																									
BYS = 7	$7 < H_N \leq 10.5$	$10.5 < H_N \leq 17.5$																																									
BYS = 8	$H_N \leq 7$	$H_N \leq 10.5$																																									
I=1.2	: BKS=2																																										
I=1.0	: BKS=3																																										
Seismic Design Categories (DTS)																																											
S_{D2} (g)	BKS=1	BKS=2, 3																																									
< 0.33	4a	4																																									
0.33-0.50	3a	3																																									
0.50-0.75	2a	2																																									
> 0.75	1a	1																																									

Figure 3. Building use, building height and seismic design categories

Building use is categorized according to the importance assigned to the building. BKS=1 is for critical facilities including hospitals and emergency facilities, schools, museums, toxic facilities, etc. BKS=2 is for buildings housing large populations temporarily, such as concert halls, stadiums, shopping centers. BKS=3 is for all other buildings.

Seismic design category is assigned in accordance with the short period spectral acceleration, which is an indication of PGA at the site as well when divided by 2.5. The difference between X and X_a in the table is for imposing additional requirements in the design of critical facilities.

Building height categories are employed in selecting the design procedure.

3.2 *Building performance levels*

Although the basic design procedure is force-based in the 2018 Code, building performance levels are defined explicitly for specifying the design targets clearly. They are summarized below.

Continued Operation Performance (CO): Damage in structural members are negligible (hairline cracks in concrete)

Limited Damage Performance (LD): Limited damage in structural components leading to very limited inelastic behavior.

Controlled Damage Performance (CD): Damage in structural components are significant, but possible to repair.

Collapse Prevention Performance (CP): Damage in structural components is severe, however partial or total collapse of the building is prevented.

3.3 *Building design targets and the associated design procedures*

Building design targets are associated with the combinations of target performances and the ground motion levels considered in design. Then a design procedure is mandated, either the conventional Force-Based Design (FBD), or the Performance-Based Assessment and re-Design (PBD) when necessary.

For all buildings which are not classified as a tall building, an ordinary performance target is set which is “Controlled Damage” under DD-2, or the 475-year design ground motion. However if the building has a DTS of 1a or 2a (critical buildings under high intensity GM’s), then an “advanced” target performance is set. Performance based procedures are employed for assessing the building performance under DD-1 and DD-3 whereas a force-based preliminary design is suggested under the DD-2 design spectra. The advanced performance targets are Limited Damage under the service earthquake DD-3 (43-year) and Controlled Damage under the maximum expected earthquake DD-1 (2475-year). The associated relations between the ground motion level, target performance and the must-use design procedure are given in Table 1(a).

When a building is classified as a tall building (BYS=1) from the category table in Figure 3 according to its height and the seismic design category, then it has a dual ordinary performance target. The tall building should remain linear elastic under the service earthquake DD-3 (43-year), and satisfy the collapse prevention limit state under the maximum expected earthquake DD-1 (2475-year). The service level performance can be assessed by a force-based analysis whereas the collapse prevention performance should be assessed by a performance based procedure which require nonlinear time history analysis. These relations are given in Table 1(b).

The initial design can be force-based with a controlled damage target under the 475 year design earthquake as advised in Table 1(b) below, however this design is usually controlled by architectural constraints and dimensions accepted in practice. Tall building designers mostly prefer conducting an initial design with the design forces obtained from the 43 year, DD-4 service earthquake spectrum rather than employing the 475 year earthquake and reducing the resulting forces with *R* factors that are hardly justifiable for tall buildings.

Table 1. Performance targets and design procedures for new buildings.

(a) Cast-in-place reinforced concrete, precast concrete and steel buildings

EQ GM Level	DTS = 1, 1a ⁽¹⁾ , 2, 2a ⁽¹⁾ , 3, 3a, 4, 4a		DTS = 1a ⁽²⁾ , 2a ⁽²⁾	
	Ordinary Performance Target	Design Procedure	Advanced Performance Target	Design Procedure
DD-3	—	—	LD	PBD
DD-2	CD	FBD	CD	FBD ⁽³⁾
DD-1	—	—	CD	PBD

(b) Tall Buildings (BYS = 1)

EQ GM Level	DTS = 1, 2, 3, 3a, 4, 4a		DTS = 1a, 2a	
	Ordinary Performance Target	Design Procedure	Advanced Performance Target	Design Procedure
DD-4	CO	FBD	—	—
DD-3	—	—	LD	PBD
DD-2	CD	FBD ⁽³⁾	CD	FBD ⁽³⁾
DD-1	CP	PBD	CD	PBD

⁽¹⁾ BYS > 3 ⁽²⁾ BYS = 2, 3 ⁽³⁾ Preliminary design

Advanced performance target is hardly applicable to tall buildings.

Similar performance tables are given in the 2018 Seismic Code for the existing buildings where the ordinary performance target is controlled damage (CD) under the 475 year DD-2 earthquake, and the assessment/design procedure is performance based. A new displacement-based linear elastic procedure is developed for existing buildings.

4 FORCE-BASED DESIGN OF BUILDINGS

Conventional force-based analysis procedures are valid for all new buildings except the performance assessment of tall buildings for collapse limit state, and the isolation level of seismically isolated buildings. When advanced performance is preferred for a building, then a performance-based assessment should be carried out. These are mostly exceptional cases.

Forced-based analysis and design procedures implemented with the capacity design principles are similar to the provisions of the 2007 Seismic Code, with notable improvement however in the definition of force reduction factors (R) and the overstrength factors (D). These factors are presented in Table 2 for cast-in-place reinforced concrete buildings. Similar tables are also provided for precast concrete, steel, masonry and timber structures.

The R factor employed in design is in fact the product of a ductility reduction factor, R_μ and the overstrength factor D . Hence, the ductility reduction factor for a particular system can be indirectly calculated from the R and D values given in Table 2, from the relation

$$R_\mu = R / D \quad (1)$$

A simple example for a frame with enhanced ductility yields $R_\mu = 8 / 3 = 2.67$, whereas it is 2.8 for a coupled shear wall with enhanced ductility. The actual values are difficult to calculate directly, but can be calculated through pushover analysis on an inelastic model schematized in Figure 4 from the obtained capacity curve (base shear versus roof displacement).

Table 2. Response reduction factors (R), overstrength factors (D) and permitted height categories (BYS) for building structural systems.

Structural system	R	D	BYS
A. CAST-IN-PLACE REINFORCED CONCRETE FRAMES			
A1. Building Frames with Enhanced Ductility			
A11. Moment resisting frames	8	3	BYS ≥ 3
A12. Coupled shear wall buildings	7	2.5	BYS ≥ 2
A13. Shear wall buildings	6	2.5	BYS ≥ 2
A14. Frame-coupled wall systems	8	2.5	BYS ≥ 2
A15. Frame-wall systems	7	2.5	BYS ≥ 2
A16. Single story buildings shorter than 12 m, with columns pinned at the ceiling level	3	2	–
A2. Building Frames with Mixed Ductility			
A21. EQ forces resisted together with ordinary frames and special coupled shear walls	6	2.5	BYS ≥ 4
A22. EQ forces resisted together with ordinary frames and special shear walls	5	2.5	BYS ≥ 4
A23. EQ forces resisted together with ordinary frames with joist slabs, and special coupled shear walls	6	2.5	BYS ≥ 6
A24. EQ forces resisted together with ordinary frames with joist slabs, and special shear walls	5	2.5	BYS ≥ 6
A3. Building Frames with Ordinary Ductility			
A31. Moment resisting frames	4	2.5	BYS ≥ 7
A32. Shear wall buildings	4	2	BYS ≥ 6
A33. Frame-wall systems	4	2	BYS ≥ 6

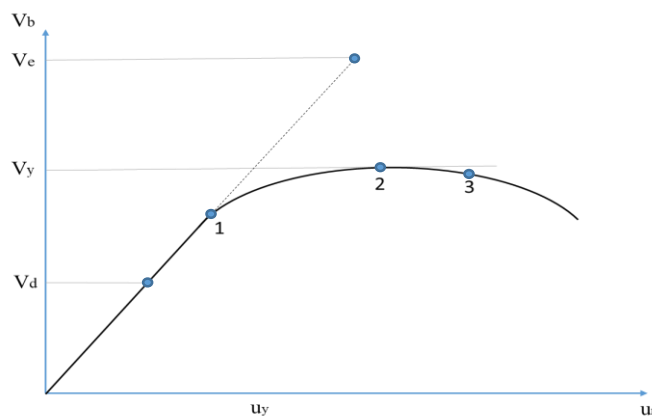


Figure 4. Pushover capacity curve for a typical building frame

4.1 Overstrength in design

Several force levels are indicated on the capacity curve in Figure 4. V_e is the linear elastic force demand, V_y is the realized yield strength and V_d is the reduced design force demand ($V_d = V_e / R$). Accordingly, $D = V_y / V_d$. The probable causes of overstrength in design are the minimum section dimensions and minimum reinforcement ratios, characteristic material strength lower than the

expected strength and material factors, and gravity load design in lower intensity seismic regions. It may be interesting to note that gravity design may control vertical member dimensions in tall buildings.

The main purpose of providing D factors in seismic codes is for the design of brittle, force-controlled members. Their design force demands V_e can only be reduced by the D factor, but not by the R factor. On the other hand, obtaining the associated $R\mu$ factor from Eq. (1) gives insight on the expected plastic deformations in the designed system under design earthquake since $R\mu$ is approximately equal to the ductility factor $\mu = u_{max}/u_y$ in elasto-plastic systems at moderate and long periods. These relations are transparently expressed in the new 2018 Seismic Code by providing the D factors explicitly for different systems.

4.2 Effective section stiffnesses for concrete members

Reinforced concrete members crack even under low levels of flexural effects, leading to significant reductions in their stiffness. If these reduced stiffnesses can be accounted for in linear elastic analysis by introducing effective stiffnesses, then more realistic internal force distributions can be obtained from analysis. However a larger gain would be in the deformations. Deformation distribution in the system can be represented much more realistically by employing effective stiffnesses of concrete members. The suggested effective stiffnesses in the 2018 Seismic Code is given in Table 3.

Table 3. Effective stiffness of concrete members

Concrete Member	Effective Stiffness Multiplier	
	Axial	Shear
Wall – Slab (In-plane)		
Shear Wall	0.50	0.50
Basement wall	0.80	0.50
Slab	0.25	0.25
Wall – Slab (Out-of-plane)	Flexure	Shear
Shear Wall	0.25	1.00
Basement wall	0.50	1.00
Slab	0.25	1.00
Frame member	Flexure	Shear
Coupling beam	0.15	1.00
Frame beam	0.35	1.00
Frame column	0.70	1.00
Wall (equivalent strut)	0.50	0.50

4.3 Limitation of interstory drift

Limitation of interstory drift is required for protecting the fragile non-structural components from lateral deformations imposed by the structural frame. Cracking or damaging of non-structural components, particularly the masonry infills reduce apparent performance of the entire building dramatically even when no damage occurs to the ductile frame members. A flexible separation between infill and frame may prevent such damage. Developing such interface connections is encouraged in the 2018 Seismic Code by imposing higher drift limits to flexible infill-frame connections and lower limits to connections with direct contact. The Code approach is explained in Figure 5.

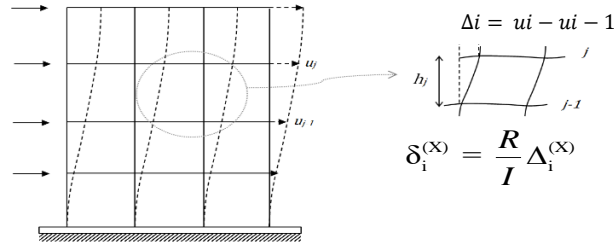


Figure 5. Interstory drift in a frame, and effective interstory drift δ_i at the i 'th story

The interstory drift limits in the 2018 Seismic Code are described below:

Infills rigidly connected to the frame:
$$\lambda \frac{\delta_{i,\max}^{(X)}}{h_i} \leq 0.008 \kappa$$

Infills with flexible connections to frame:
$$\lambda \frac{\delta_{i,\max}^{(X)}}{h_i} \leq 0.016 \kappa$$

Here, λ is the spectral acceleration ratio of DD-3 to DD-2, which is usually in the 0.4-0.5 range. κ is 1.0 for concrete, and 0.5 for steel buildings.

It should be noted here that interstory drift limit may control design rather than design forces in flexible, long period frames.

5 NONLINEAR PROCEDURES

Nonlinear analysis procedures are employed mainly in the seismic assessment of tall buildings. 2018 Code suggests using fiber elements in modeling the core walls. The basic modeling features of fiber elements are shown in Figure 6.

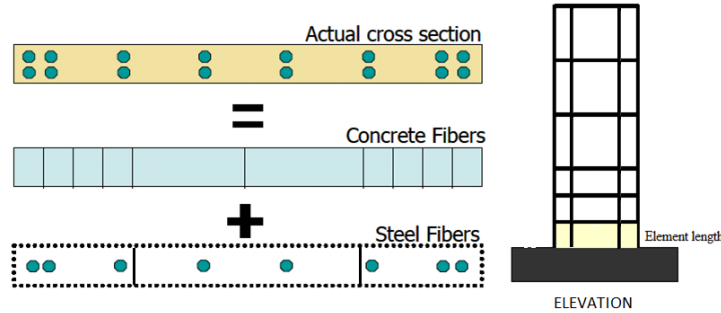


Figure 6. Fiber modeling of reinforced concrete wall sections.

Expected strengths are used rather than the characteristic strengths. Time history analysis is conducted under 11 pairs of horizontal bi-axial ground motions, selected by using the seismological features of the construction site and scaled to the design spectrum along the dominant period range of the building. Mean of the maximum absolute response quantities are used in performance evaluation. The performance limits in terms of plastic rotations are presented below.

Collapse prevention:
$$\theta_p^{(G\ddot{O})} = \frac{2}{3} \left[(\phi_u - \phi_y) L_p \left(1 - 0.5 \frac{L_p}{L_s} \right) + 4.5 \phi_u d_b \right]$$

Damage Control:
$$\theta_p^{(KH)} = 0.75 \theta_p^{(G\ddot{O})}$$

Damage Limitation:
$$\theta_p^{(SH)} = 0$$

6 CONCLUSIONS

The 2018 Turkish Seismic Code has been expanded to twice the size of 2007 Code. This is the usual trend of codes, especially when the revision comes after a decade. Only a brief summary of the revisions are presented in this paper.

Nonlinear analysis procedures are gaining wider acceptance as performance based earthquake engineering is increasing its popularity. Although their use is fairly limited in practice, their implementation will perhaps increase in the future. The 2018 Turkish Seismic Code made a courageous effort by including them in an earlier stage, hence preparing the practitioners for their prospective use in the next decade.

References

- American Society of Civil Engineers (ASCE). 2010. *Minimum Design Loads for Buildings and Other Structures, ASCE/SEI 7-10*.
- European Committee for Standardization. 2004. EN 1998-1 Eurocode 8: *Design of structures for earthquake resistance*.
- Turkish Ministry of Construction and Settlement. 2007. *Design Code for Buildings in Seismic Regions*, Ankara.
- Directorate of Emergency Management (AFAD). 2018. *Design Code for Buildings in Seismic Regions*, Ankara.

Collapse assessment of building columns through multi-axis hybrid simulation

Riadh Al-Mahaidi¹, M. Javad Hashemi², Hamidreza A. Yazdi³, Yassamin Al-Ogaidi⁴

¹ Professor, Swinburne University of Technology, Melbourne, Australia

² Lecturer, Swinburne University of Technology, Melbourne, Australia

³ PhD student, Swinburne University of Technology, Melbourne, Australia

⁴ Lecturer, University of Duhok, Duhok, Iraq

ABSTRACT: One of the major challenges in collapse assessment of building columns has been the lack of realistic data obtained from reliable experiments. Numerous experimental studies have been performed to examine the behavior of building columns under either pure axial or combined axial-lateral loads, which are not adequate to accurately capture the actual response of a collapsing column in real earthquake events. Hybrid simulation (HS) can be considered as an attractive alternative to realistically simulate more complex boundary conditions and improve response prediction of a structure from elastic range to collapse. In hybrid simulation, the flexibility and cost-effectiveness of computer simulation are combined with the realism of large-scale experimental testing to provide a powerful tool for investigating the effects of extreme loads on structures. The key advantage is that only the critical components of a structure that are difficult to model numerically are sub-structured for testing in the laboratory, while the remainder of the structure with more predictable behaviour is computer simulated using finite-element analysis software. A state-of-the-art loading system, referred to as the Multi-Axis Substructure Testing (MAST) system, has been designed and assembled at Swinburne University of Technology, Melbourne, Australia to expand the capabilities of hybrid testing to include three-dimensional responses of structures through switched/mixed load/deformation control of six-degrees-of-freedom (6-DOF) boundary conditions. This paper presents a series of large-scale quasi-static cyclic and hybrid simulation experiments on reinforced concrete (RC) and concrete-filled steel tube (CFT) columns. The results of this study provide significant insight into the response of these columns from initial linear-elastic range to the state of complete collapse.

1 INTRODUCTION

Structures are usually designed under a wide range of uncertainties, regarding the extreme loads that they are required to sustain during their service life. One of the major challenges facing structural engineers, today, is to develop creative ways to reduce the risk of catastrophic damage due to these extreme loads, and to enhance the resiliency of urban infrastructure. However, this requires the prediction of the structural response from the linear-elastic range to levels approaching collapse and thus poses significant challenges. Although there has been much advancement in the mathematical models employed in computational methods, study of structure's behavior is still a difficult task since the accuracy of the results depends on the assumptions made in the characterization of member properties. Therefore, experimental validation is still essential to examine the underlying assumptions made by these numerical models, especially considering the existence of highly nonlinear elements under extreme dynamic loading.

Experimental testing of the entire structure, although an excellent option at first glance, is very complex, very expensive, and potentially dangerous. Building structures are massive, and it is difficult to fabricate and load them in the laboratory, while small-scale models are known to fail to duplicate real structures behavior due to the lack of similitude. These limitations in the majority of the testing facilities combined with the cost of testing complete full-scale structures have motivated alternative large-scale testing methods. Evolved from pseudo-dynamic testing (Takanashi et al. 1975), hybrid simulation is an innovative cyber-physical testing technique that combines the flexibility and cost-effectiveness of computer simulation with the realism of experimental testing to provide a powerful and versatile platform for large-scale testing of structures (Hashemi et al. 2016).

Hybrid simulation is based on splitting the structure into numerical and physical models. Typically, the physical/experimental substructures are critical elements of the structure, which are difficult to model numerically, while analytical/numerical substructures represent structural components with more predictable behavior. The response of the hybrid model to extreme loads is computed by solving the equations of motion of the entire hybrid model using a time-stepping integration process. Computer control software and the specimen actuation and sensing system maintain the deformation-compatibility and force-equilibrium conditions at the interfaces between the numerical and physical portions of the hybrid model. For example, in collapse study of a three-span bridge subjected to earthquake and tsunami loads (see Figure 1), the deck can be modeled numerically in the computer as it is expected to behave linear or slightly nonlinear and therefore does not have to be physically present in the lab. The bridge pier(s) with larger demands and severe nonlinear behavior can be accommodated in the laboratory for experimental testing.

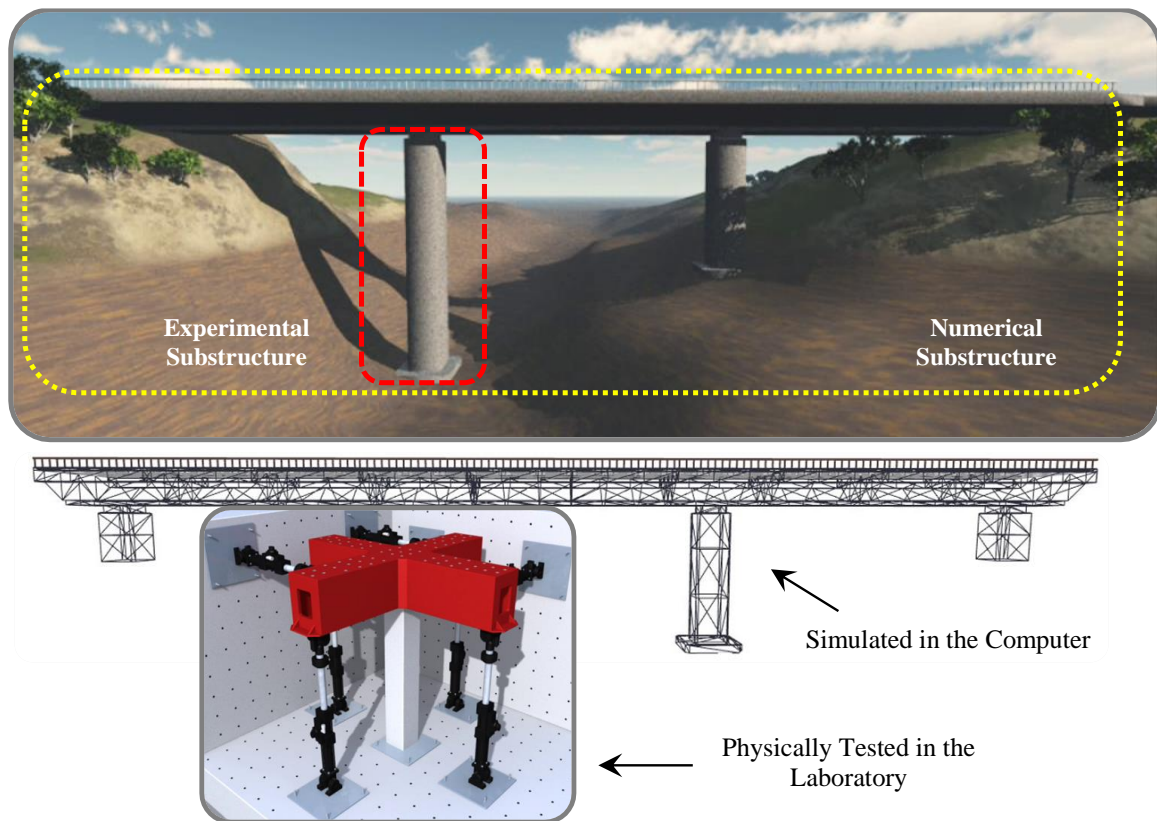


Figure 1. Hybrid simulation of a three-span bridge subjected to earthquake and tsunami loads

2 STATE-OF-THE-ART SYSTEM FOR HYBRID SIMULATION AT SWINBURNE

A state-of-the-art loading system, referred to as the Multi-Axis Substructure Testing (MAST) system, has been designed, assembled and validated at Swinburne University of Technology to expand the capabilities of hybrid testing to include three-dimensional responses of structures under extreme loads (Hashemi et al. 2015). The cutting-edge facility is located in the Smart Structures Laboratory (SSL), which is a major three-dimensional testing facility developed for large-scale testing of civil, mechanical, aerospace, offshore and mining engineering components and systems and the only one of its type available in Australia. An overview of the MAST system and the actuators assembly is shown in Figure 2. The actuators capacity and non-concurrent capacity of the MAST system in each DOF domain is also presented in Table 1. The key components of the 6-DOF hybrid testing facility (MAST system) are:

- 1) Four $\pm 1\text{MN}$ vertical hydraulic actuators and two pairs of $\pm 500\text{ kN}$ horizontal actuators in orthogonal directions. Auxiliary actuators are also available for additional loading configurations on the specimen (Figure 2 and Table 1).
- 2) A 9.5 tonne steel crosshead that transfers the 6-DOF forces from the actuators to the specimen. The test area under the crosshead is approximately $3\times 3\text{ m}$ in plan and 3.2 m high.
- 3) A reaction system comprising an L-shaped strong-wall (5 m tall \times 1 m thick) and a 1 m thick strong-floor.
- 4) An advanced servo-hydraulic control system capable of imposing simultaneous 6-DOF states of deformation and load in switched/mixed mode control. In addition, the Centre of Rotation (CoR) (i.e. the fixed point around which the 6-DOF movements of the control point occurs) can be relocated and/or reoriented by assigning the desired values.
- 5) An advanced three-loop hybrid simulation architecture including: the servo-control loop that contains the MTS FlexTest controller (inner-most loop), the predictor-corrector loop running on the xPC-Target real-time digital signal processor (middle-loop) and the integrator loop running on the xPC-Host (the outer loop).
- 6) Additional high-precision draw-wire absolute encoders with the resolution of 25 microns that can be directly fed back to the controller.

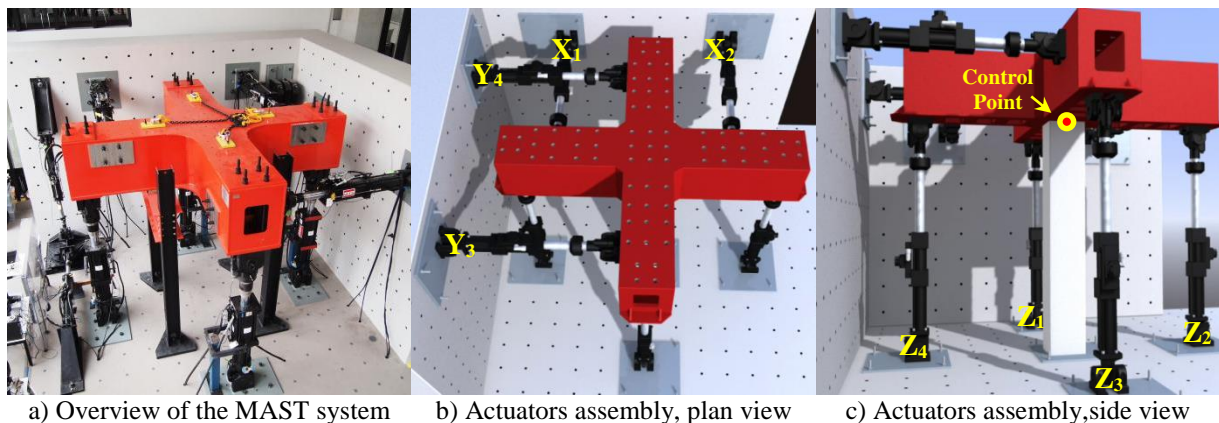


Figure 2. Overview and actuator assemblies of the MAST system

Table 1. Actuators and DOF specifications

MAST Actuator Capacity			
Actuator	Vertical	Horizontal	Auxiliary
Model	MTS 244.51	MTS 244.41	2 (MN) (Qty. 1)
Quantity	4 (Z ₁ , Z ₂ , Z ₃ , Z ₄)	4 (X ₁ , X ₂ , Y ₃ , Y ₄)	250 (kN) (Qty. 4)
Force Stall Capacity	± 1,000 (kN)	± 500 (kN)	100 (kN) (Qty. 3)
Static	± 250 (mm)	± 250 (mm)	25 (kN) (Qty. 3)
Servo-valve flow	114 (lpm)	57 (lpm)	10 (kN) (Qty. 1)

MAST DOFs Capacity (non-concurrent)			
DOF	Load	Deformation	Specimen Dimension
X (Lateral)	1 (MN)	± 250 (mm)	3.00 (m)
Y (Longitudinal)	1 (MN)	± 250 (mm)	3.00 (m)
Z (Axial/Vertical)	4 (MN)	± 250 (mm)	3.25 (m)
Rx (Bending/Roll)	4.5 (MN.m)	± 7 (degree)	
Ry (Bending/Pitch)	4.5 (MN.m)	± 7 (degree)	
Rz (Torsion/Yaw)	3.5 (MN.m)	± 7 (degree)	

3 HYBRID SIMULATION TO CAPTURE COLLAPSE OF RC COLUMNS

A comparative study was conducted to investigate the use of quasi-static (QS) versus hybrid simulation (HS) for collapse assessment of RC columns. For this purpose, two identical limited-ductility RC columns were tested with the respective experimental techniques. The specimens were 2.5 m high, had square 250×250 mm cross-sections and were reinforced with 4 longitudinal bars of N16 (reinforcement ratio = 1.28%) and tied with R6 stirrups spaced at 175 mm with 30 mm cover thickness. The specimens were attached to the strong floor from the base and to the crosshead from the top through rigid concrete pedestals. The first experiment conducted on the RC column was a three-dimensional mixed-mode QS cyclic test. The loading protocol consisted of simultaneously applying a constant gravity load, equal to 8% of ultimate compressive load capacity in force control, while imposing bidirectional lateral deformation reversals in displacement control, following the hexagonal orbital pattern suggested in FEMA 461. The failure of the specimen occurred when the specimen was subjected to the maximum of 7.0% and 3.5% drift ratios in Y and X axes, respectively. These are large drifts for a limited-ductility column, but effective of the relatively low axial loads applied to the column (Wibowo et al. 2014).

The second experiment conducted was a three-dimensional hybrid simulation of a half-scale symmetrical 5-storey (height of first storey $h_1=2.5$ m, height of other stories $h_{typ}=2.0$ m) 5×5 bay (column spacing $b=4.2$ m) RC ordinary moment frame building. The physical specimen served as the first-storey corner-column of the building, considered as the critical element of the structure due to dynamic overturning effects and the influence of axial load variation. The rest of the structural elements, inertial and damping forces, gravity and dynamic loads and second-order effects were modelled numerically in the computer. The structure's beams and columns were modelled using beam-with-hinges elements, where the non-linear behaviour is assumed to occur within a finite length at both ends based on the distributed-plasticity concept (Hashemi et al. 2014; Scott and Fenves 2006). The plasticity model follows a peak-ordinated hysteresis response based on the Modified Ibarra-Medina-Krawinkler (IMK) deterioration model of flexural behaviour (Ibarra et al. 2005; Zhong 2005). For the HS test, the two horizontal components of the 1979 Imperial Valley earthquake ground motions recorded at El Centro station with peak ground acceleration of 0.15g were used. Based on incremental dynamic analysis, four levels of intensity were considered to capture the full range of structural response from linear-elastic range to collapse. The selected scale factors were 0.6, 4.0, 8.0 and 9.0, which pushed the structure to nearly

0.25% (elastic), 2%, 4% and 6% inter-storey drift ratios, respectively. Prior to conducting the actual HS test with the physical sub-assembly in the laboratory, a series of FE-coupled numerical simulations (Schellenberg 2008) was conducted to evaluate the integration scheme parameters for the actual experiments. Accordingly, generalized Alpha-OS (Schellenberg et al. 2009) was used as the integration scheme and the integration time-step was optimized to preserve the accuracy and stability of the simulation, while allowing the completion of the entire test during the regular operational hours of the laboratory. 5% Rayleigh damping was specified to the first and third modes of vibration. Additional damping was also assigned to free vibration time intervals between the forced vibrations in order to quickly bring the structure to rest.

The hybrid simulation was started by applying the gravity load on the specimen, using a ramp function, followed by sequential ground motions. The entire sequence of loading was performed and automated using OpenSees. Considering the 117 milliseconds delay in the hydraulic system, 500 milliseconds was specified as the simulation time-step in xPC-Target predictor-corrector to provide sufficient time for integration computation, communication, actuator motions and data acquisition. This scaled the 60sec of sequential ground motions to 6 hours in laboratory time.

Figure 3 compares the responses of RC columns including hysteresis in X and Y axes and the axial force time history in Z-axis for the QS and the HS tests. The maximum time-varying axial load applied on the specimen was 553 kN in compression and 161 kN in tension. Figure 4 compares the biaxial lateral drifts in X- and Y-axes, and biaxial moment interactions at the top of the columns. By comparing the hysteresis plots from the HS test, it can be seen that the column was damaged as the structure progressively moved in one direction, while in the QS test the pattern of damage was symmetrical due to load reversals in cyclic deformations.

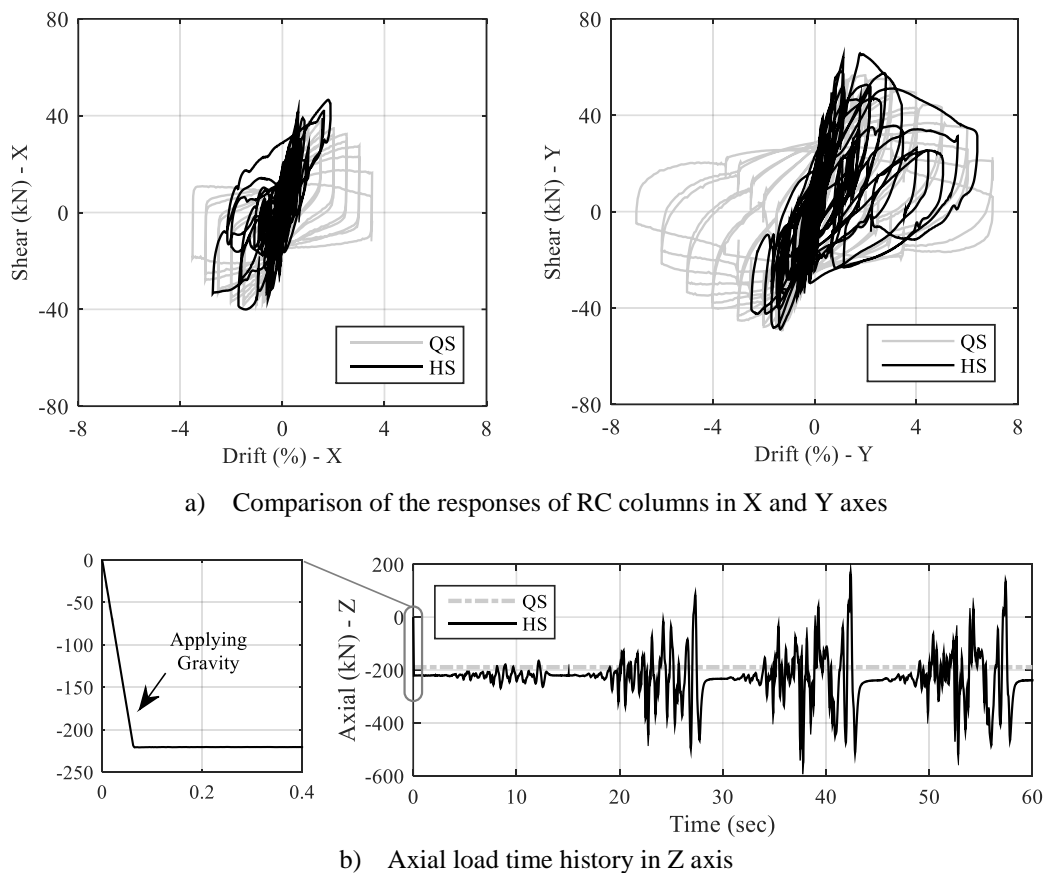


Figure 3. Response of the RC columns and applied axial load in QS and HS tests

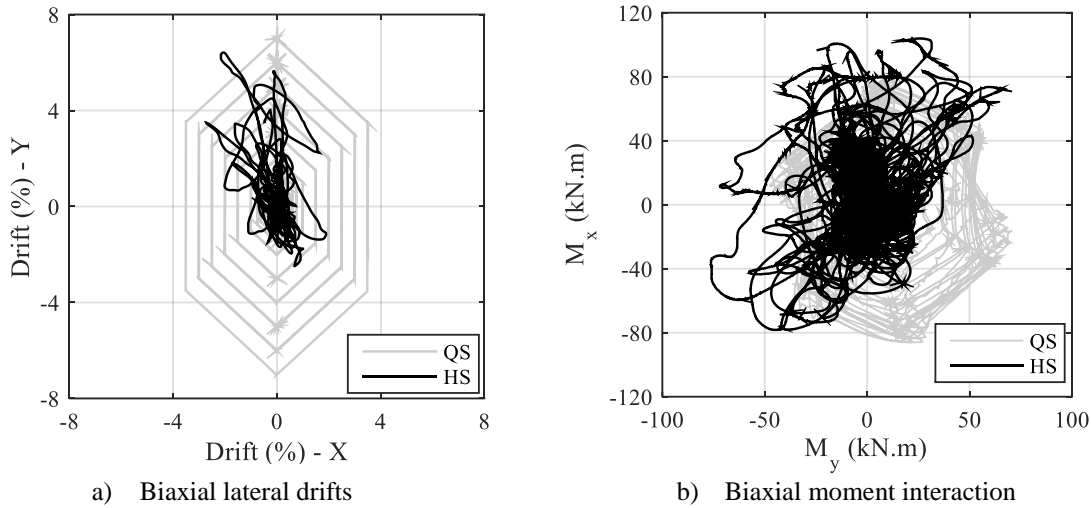


Figure 4. Biaxial lateral drifts and moment interactions of the RC columns in QS and HS test

4 HYBRID SIMULATION TO CAPTURE COLLAPSE OF CFT COLUMNS

Another project recently conducted using the MAST system was a comparative study to investigate the collapse assessment of square and circular CFT (SCFT and CCFT) columns under complex time-varying realistic boundary forces for large-scale QS cyclic and HS experiments. Table 2 provides an overview of the selected cross sections material and geometric properties were measured for the CFT column specimens. The stress-strain results were developed using the data obtained from associated coupon tests. Regarding the concrete infill, concrete with compressive design strengths of 50 MPa was used in this study.

Table 2. Geometry and material properties of test specimens

Steel Tubes								
Specimen	Section	D(mm)	t(mm)	As(mm ²)	Ac(mm ²)	Fy(MPa)	Fu(MPa)	Es(MPa)
CCFT	CHS	219.1	8.2	5433	32270	412	499	197000
SCFT	SHS	200	9	6597	32967	352	471	210000

The first set of experiments conducted on the CFT columns were three-dimensional mixed-mode quasi-static cyclic tests. The loading protocol consisted of applying a variable force-controlled gravity load (equal to 14% of ultimate compressive load capacity at balance point) while imposing displacement-controlled bidirectional lateral deformation reversals that follow the hexagonal orbital pattern similar to the one used in RC column QS test. The bidirectional hexagonal orbital lateral protocol reaches a maximum drift ratio of 4% (X-loading direction) and 8% (Y-loading direction) at the column's top. The axial load was varied around the gravity load value and proportional to the lateral drift acting on the column. The average of 571 kN (0.14 Py) compression load was considered to represent the initial gravity load on the column at balance point. According to the adopted axial variation protocol, the maximum time-varying axial load applied on the specimen was 874 kN in compression (0.2 Py: the target load).

The second set of experiments were two three-dimensional hybrid simulation tests that included the physical CCFT and SCFT column elements identical to the previously tested CFT columns in the quasi-static cyclic tests. For this purpose, two half-scale symmetrical five-story (height of first story $h_1 = 2$ m; height of other stories $h_{typ} = 1.75$ m) five-by-five-bay (column spacing $b = 4.2$ m) steel frame buildings with critical column were considered as the prototype buildings. The first and second frames were designed with CCFT and SCFT columns, respectively. The physical

specimen served as the first-story interior column of the building, considered as the critical element of the structure. The rest of the structural elements were modelled numerically using OpenSees. It is important to note that, in order to get a better understanding of the realistic behaviour and ultimate flexural capacity of the selected columns, soft story collapse mechanism was assumed in designing and modelling of the prototype steel buildings. Therefore, all energy dissipations are concentrated at columns ends in the first floor. The steel building's columns were modelled using beam-with-hinges elements and the plasticity model follows a bilin hysteresis response based on the IMK deterioration model of flexural behavior.

For these HS tests, the columns experiencing the same loading conditions in the previous hybrid test with the RC column. The intensity levels in hybrid tests were 0.25, 1.9, 3.4, and 4.0 for CCFT HS test and 0.25, 2.0, 3.7 and 4.3 for SCFT HS test which pushed the structure to nearly 0.5%, 1.5%, 5%, and 8% interstory drift ratios in Y-axis, respectively. Similar to the RC column hybrid test, 5% Rayleigh damping was specified to the first and third modes of vibration. Figure 5 compares the biaxial deformations in terms of lateral drifts in the X- and Y-axes, and biaxial moment interactions in the Rx- and Ry-axes.

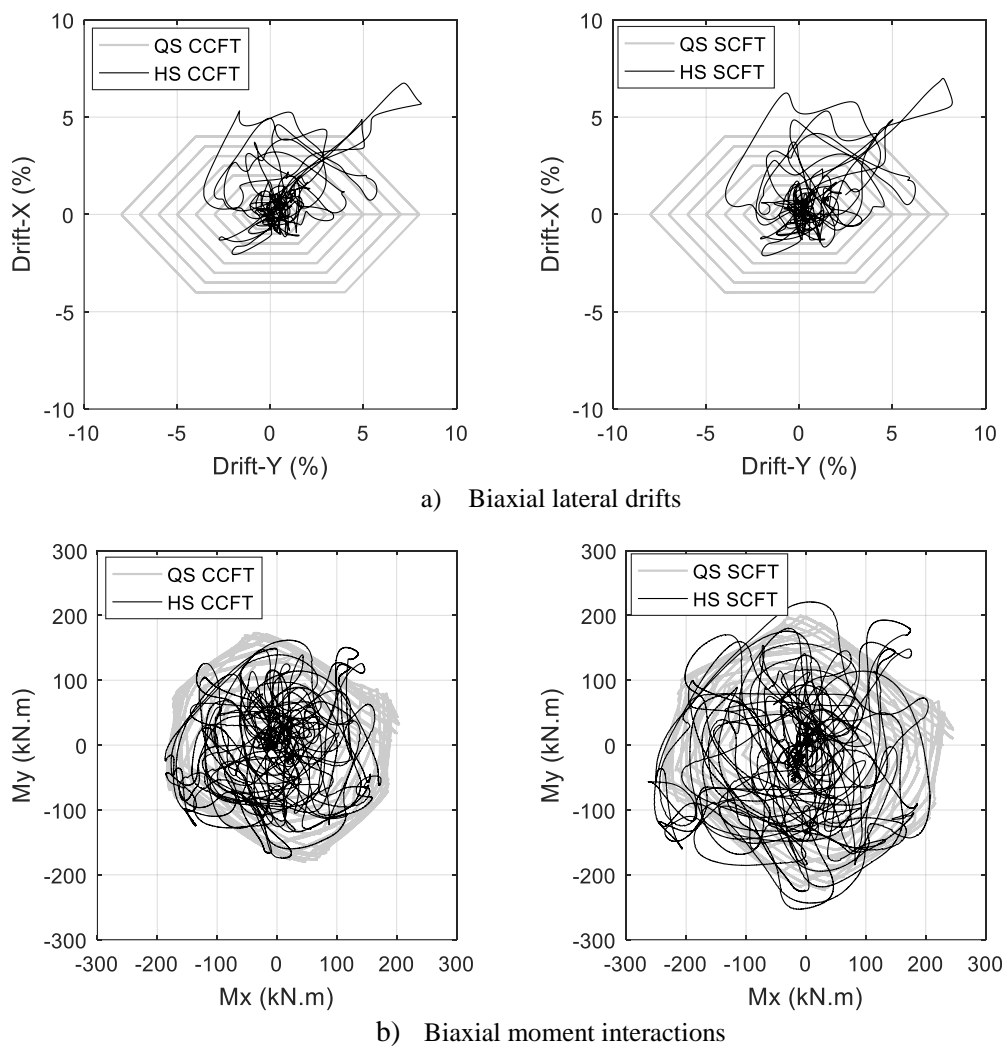


Figure 5. Comparison of biaxial drifts and moment interactions in QS and HS tests of CFT columns

Figure 6 compares the shear-drift responses of CCFT and SCFT columns in the QS and HS tests, including hysteresis in the X- and Y-axes. By comparing the hysteresis plots from the HS test, it can be seen that the columns suffered damage as the structure progressively moved in one direction, while in the QS test, the pattern of damage was symmetrical due to load reversals in

cyclic deformations. Figure 7 shows the flexural failure of columns for QS and HS tests by comparing the plastic hinges developed at the top and the base of the columns.

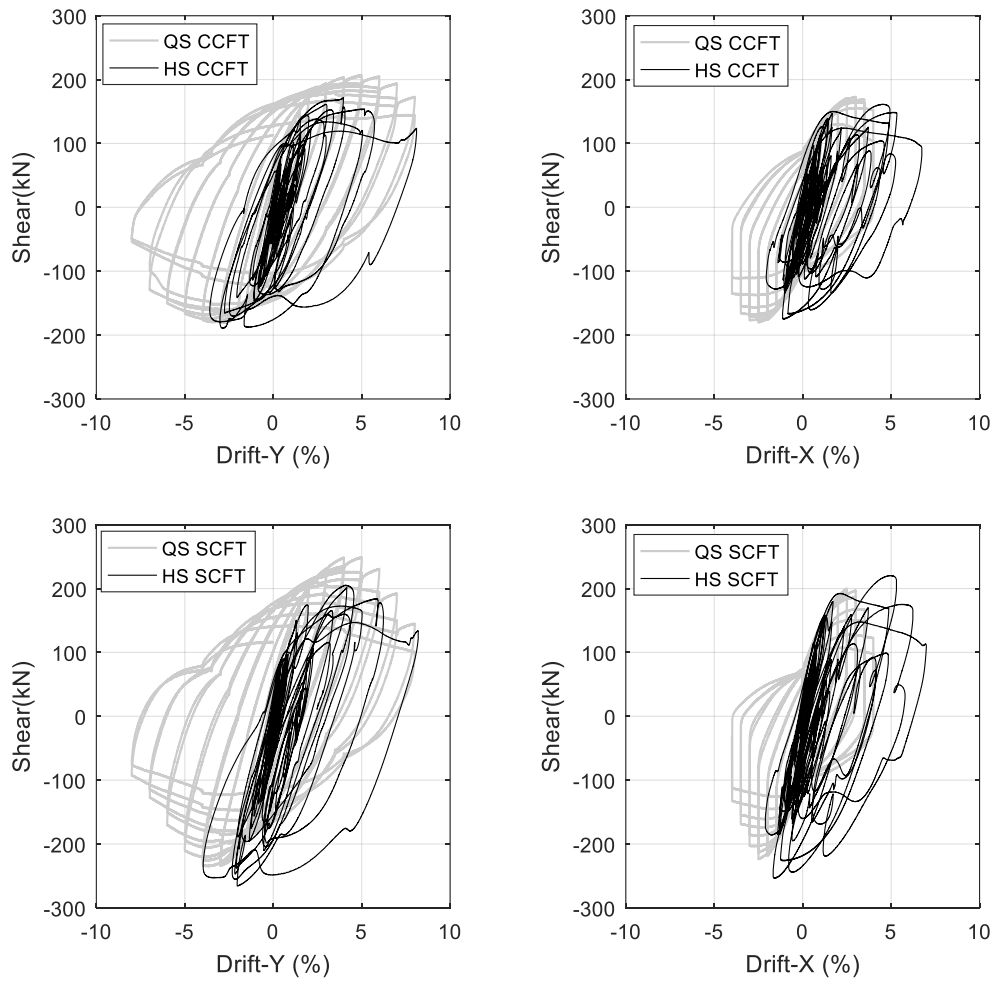


Figure 6. Comparison of the QS and HS response of columns in Y- and X-directions

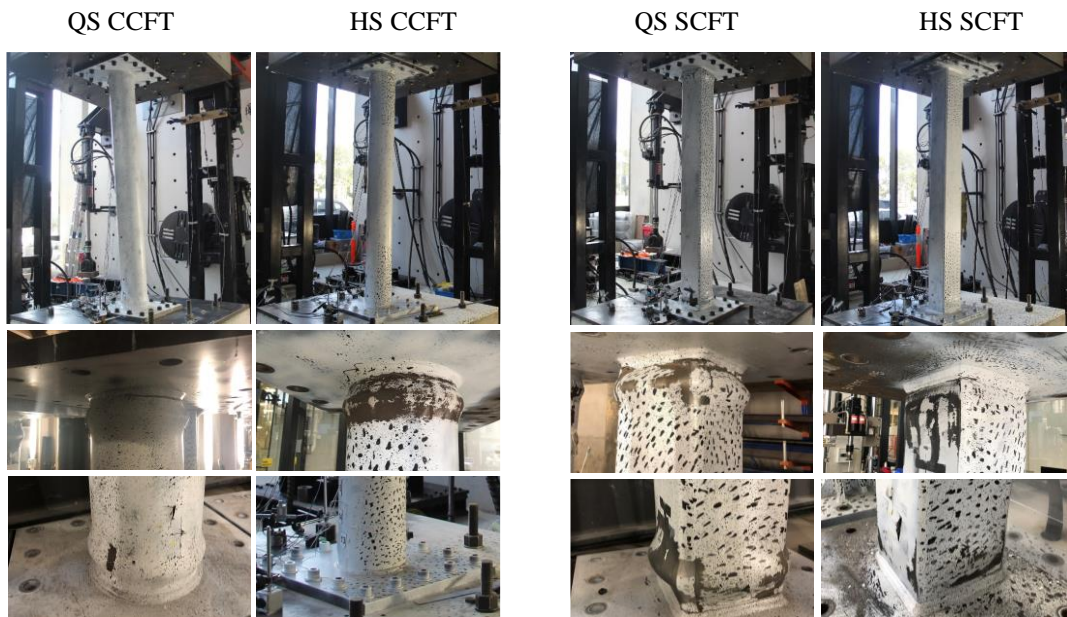


Figure 7. Comparison of plastic hinges in QS and HS tests

5 CONCLUSION

Hybrid simulation is a novel cyber-physical testing method for large-scale experimental testing of structures undergoing extreme events. This paper introduced Australia's first hybrid testing facility, referred to as the Multi-Axis Substructure Testing (MAST) system, for cost-effective large-scale testing of structural components. The system was used in application for comparative seismic performance assessment of RC and CFT columns through quasi-static cyclic and hybrid simulation tests. The results showed significant differences, which emphasizes that the credibility of collapse assessment results relies to a great extent on the application of correct boundary interface on the building columns.

ACKNOWLEDGEMENTS

The authors gratefully acknowledge the contribution of the Australian Research Council (Grants LE110100052, DP140103350, and DP1096753) and 11 partner universities for their assistance with the establishment of the 6-DOF hybrid testing facility. The authors would like to acknowledge the support of Prof John Wilson and the personnel of the Smart Structures Laboratory at Swinburne University of Technology.

REFERENCES

- Hashemi, M. J., Al-Mahaidi, R., Kalfat, R., and Burnett, G. (2015). "Development and validation of multi-axis substructure testing system for full-scale experiments." *Australian Journal of Structural Engineering*, 16(4), 302-315.
- Hashemi, M. J., Mosqueda, G., Lignos, D. G., Medina, R. A., and Miranda, E. (2016). "Assessment of Numerical and Experimental Errors in Hybrid Simulation of Framed Structural Systems through Collapse." *J Earthq Eng*, 20(6), 885-909.
- Hashemi, M. J., Tsang, H.-H., Menegon, S., Rajeev, P., and Wilson, J. (2014). "Modelling 3D Limited-Ductile RC Frame Structures for Collapse Risk Assessment." *Australian Earthquake Engineering Society Conference Lorne, Australia*.
- Ibarra, L. F., Medina, R. A., and Krawinkler, H. (2005). "Hysteretic models that incorporate strength and stiffness deterioration." *Earthquake Eng Struct Dyn*, 34(12), 1489-1511.
- Schellenberg, A., Huang, Y., and Mahin, S. A. "Structural FE-Software Coupling through the Experimental Software Framework, OpenFresco." *Proc., 14th World Conference on Earthquake Engineering* Beijing, China.
- Schellenberg, A. H., Mahin, S. A., and Fenves, G. L. (2009). "Advanced implementation of hybrid simulation." Pacific Earthquake Engineering Research Center, University of California, Berkeley, U.S.
- Scott, M. H., and Fenves, G. L. (2006). "Plastic hinge integration methods for force-based beam-column elements." *J Struct Eng*, 132(2), 244-252.
- Takanashi, K., Udagawa, K., Seki, M., Okada, T., and Tanaka, H. (1975). "Nonlinear earthquake response analysis of structures by a computer-actuator on-line system." Bulletin of Earthquake Resistant Structure Research Centre, No. 8, Institute of Industrial Science, University of Tokyo, Japan.
- Wibowo, A., Wilson, J. L., Lam, N. T. K., and Gad, E. F. (2014). "Drift performance of lightly reinforced concrete columns." *Eng Struct*, 59, 522-535.
- Zhong, W. (2005). "Fast hybrid test system for substructure evaluation." PhD Dissertation, University of Colorado Boulder, U.S.

Advanced pre-cast concrete system and innovative steel fibre reinforced concrete structural system in Japan

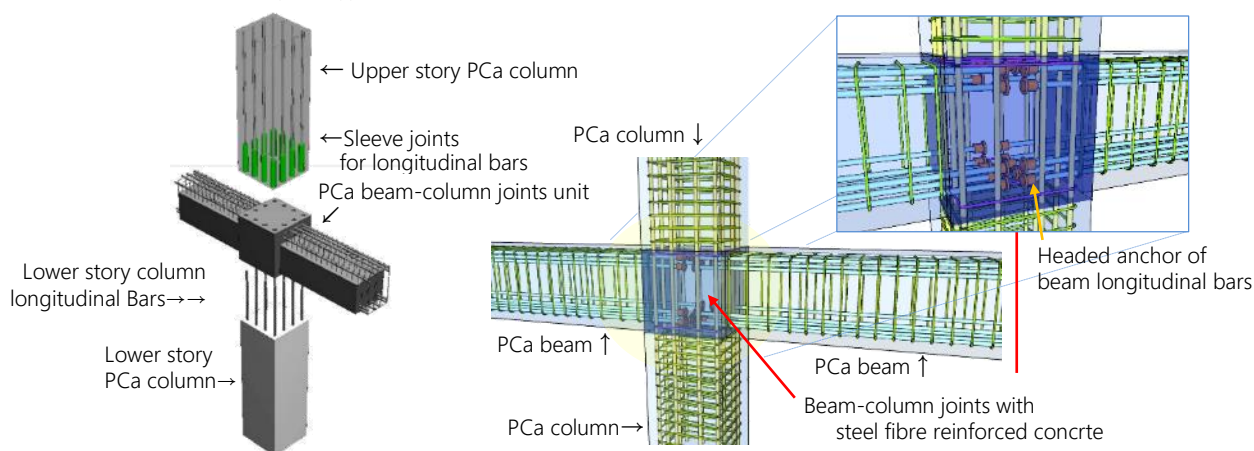
Yuji Ishikawa¹

¹ Shibaura Institute of Technology, College of System Engineering and Science, Saitama, Japan

ABSTRACT: This paper discusses an advanced precast system and an innovative steel fibre reinforced concrete structural system, developed to streamline the works of reinforcing for R/C interior joints. 1) Advanced precast system: The feature of the system uses precast beam-column joints unit which have integrated beam and beam-column joints. Column longitudinal bars in the precast concrete columns of lower stories pass through ducts in the precast beam-column joint unit and have sleeve joint connections to the column longitudinal bars of the upper story. 2) Innovative steel fibre reinforced concrete structural system: Beam longitudinal bars on opposite sides of interior joints are neither lapped nor connected within the joints and anchored with head anchors using steel fibre concrete. The headed bars are anchored around the middle section of the joints. Steel fibres are added to plain concrete to enhance the joints' shear strength and anchor load capacity of the headed bars without joint shear reinforcement. At present, the innovative structural system has been put to practical use for two projects in Japan. In addition, this paper introduces the historical trend of high-rise RC buildings and latest utilization of high strength steel fibre reinforced concrete.

1 INTRODUCTION

As it is well known, Japan sits on a high-density seismicity area and has experienced several earthquake disasters. Thus, seismic design has evolved after repeated disasters. These disasters' lessons have led to sophisticated seismic design practices in Japan. Japanese seismic design requires that structures should have sufficient horizontal stiffness and horizontal capacity to sustain frequent and large earthquakes. On the other hand, the concentration of populations into urban areas in Japan has meant a need for high-rise residential buildings despite the high seismic hazards. Until now, we have solved these problems for high-rise RC buildings using high strength concrete and steel bars and several precast systems. This paper introduces how to reach the advanced system for high-rise RC buildings at present (refer to Figure1(a), Ishikawa(2017)). Recently, innovative steel fibre reinforced concrete structural system was developed and has been put to practical use for two projects in Japan (refer to Figure1(b), Ishikawa et.al.(2012)).



(a) Advanced precast system (b) Innovative steel fibre reinforced concrete structural system
 Figure 1. Advanced precast system and Innovative steel fibre reinforced concrete structural system

2 ADVANCED PRECAST SYSTEM AND HISTORICAL TREND OF HIGH-RISE RC BUILDINGS IN JAPAN

2.1 Positioning of high-rise buildings in Japan

High rise buildings are defined “Super high-rise buildings” as per Building Standard Law as shown in Table 1. High rise buildings are defined as being over 45 meters high, or over 31 meters high for irregular buildings with special features. Building Standard Law, in 1963 removed the 31-meter height limitation for buildings, and also set out that those high-rise buildings need time history analysis design. The two reasons were that the base shear coefficient of high-rise buildings used was less than ordinary buildings based on the law, and the law described that special usage of materials and building design have to be evaluated for safety. As a result, the Ministry of Construction (present Ministry of Land, Infrastructure and Transport) installed a council for high rise building structures in 1963, and subsequent approval for the establishment of the Building Center of Japan (BCJ) in 1965. Also, technical appraisal councils were established for such high-rise structures and fire safety performance. Only the BCJ evaluated high-rise structures’ designs until 2000 and the council is composed of academic professors, researchers and experienced structural designers. After the introduction of new seismic design methods in 1981, high rise buildings were re-defined as being over 60 meters high and expected to be influenced by higher mode effects which will cause different story drift angles on each floor. As a result, high rise buildings have to utilize more technical structural calculation methods such as a time history analysis to estimate force and deformation of the building. After 2000, the BCJ, the General Building Research Corporation of Japan (GBRC) and JAPAN ERI CO., LTD began to carry out performance evaluations under the amended Building Standard Law as an organization designated by the Minister of Land, Infrastructure and Transport. At present, 16 designated facilities are able to review high-rise buildings.

Table 1. Definition and history of judgment of high rise building in Japan

Year	since 1963	since 1965
The Building standard law	Amended in 1963	---
Description	Removal the limitation of 31 meters high	---
Designated certificate organization	the Ministry of Construction	Building Center of Japan (BCJ)
Name	The council for high rise building structure	The rating of high rise buildings structures
Subjected buildings	more than 45 meters high and special buildings over 31 meters	
Year	since 1981	since 2000
The Building standard law	Amended in 1981	Amended in 2000
concept	New seismic design method	Performance Evaluation Design Concept
Designated certificate organization	Building Center of Japan (BCJ)	Building Center of Japan (BCJ)
		General Building Research Corporation of Japan (GBRC)
		JAPAN ERI CO.,LTD
		13 other designated certificate
Name	The rating of high rise buildings structures	The evaluation of super high rise buildings structures
Subjected buildings	more than 60 meters high	more than 60 meters high

2.2 Historical trends of high-rise buildings in Japan

Table 2 shows the historical trends of high-rise RC buildings in relation to the political environment and economy, social trends, international research, and Building standard law. It can be seen that the building standards law were amended after several disasters. As a result, the technical standard manual for the amended building standard law were published for structural designers. After the great Hanshin-Awaji great disaster in 1995, response-controlled structures with dampers and base-isolated structures have increased, and concrete and steel bars used in high-rise RC buildings have gotten remarkably stronger compared to the 1970’s. It can be seen that the development of several technologies for seismic design and construction of high-rise

RC buildings in JAPAN has occurred. Figure 2 also shows the structural design records for high rise RC buildings using the total number of buildings and comparison between structural types where it can be seen that the birth of high-rise RC building occurred in 1972. In the 1980's, under 10 buildings were designed each year. From 1990 to 1994, about 10 buildings were designed each year, and after 1995, the number of high-rise RC buildings increased rapidly. Up to now more than 600 high rise RC buildings have been designed.

Table 2. Historical trends of high-rise RC buildings

Year	1960	1965	1970	1975	1980	1985	1990	1995	1996	1997	1998	1999	2000-2004	2005-2010	2011-2015	
S: Showa era, H: Heisei	S35	S40	S45	S50	S55	S60	H2	H7	H8	H9	H10	H11	H12-H16	H17-H20	H17-H20	
Political Economy Social trend	• 1960 Doubling national income plan	• 1970 Expo in Osaka	• 1964 Tokyo Olympics	• 1972-1976 New seismic design method project	• 1982 Jyoetsu, Tohoku Shinkansen	• 1985 Expo in Tsukuba	• 1982 Jyoetsu, Tohoku Shinkansen	• 1995 Launch of Windows95	• 1992 Yamagata Shinkansen	• 1993 Launch of internet usage, digital mobile phone	• 1994 Kansai International Airport	• 1998 Nagano Olympics	• 2002 FIFA World Cup Korea/Japan	• 2005 New Nagoya International Airport	• 2014 Tokyo would host the 2020 Olympic	
Earthquake			• 1963 Tokachi earthquake	• 1978 Miyagi earthquake	• 1995 Kobe earthquake										• 2011 The Great Eastern Japan Earthquake (Long-period earthquake, Tsunami)	
The Building Standard Law	• 1963 Removed limitation of 31 meters high				• 1981 Amended the building standard law (New seismic design method)								• 2000 Amended the building standard law (Performance based concept)			
National Research Project	• 1964 The council for high rise building structure in Ministry of Construction				• 1982-1993 NewRC Project								• 2006 Amended Promotion of Seismic Retrofit		• 2013 Amended Promotion of Seismic Retro	
RC-related standard and guideline by Architectural Institute of Japan	• 1964 Technical guideline for high rise buildings				• 1976 Standard for Structural Calculation of RC Structures amended in 1971								• 1999 Standard for Structural Calculation of RC Structures (Based on Allowable Stress Concept)	• 2010 Standard for Structural Calculation of RC Structures (Based on Allowable Stress Concept)	• 2015 Technical standard manual of 2014 building standard law	
International Situation	• 1965 Alaska earthquake				• 1976 Tangshan earthquake	• 1985 Mexico earthquake	• 1989 Loma Prieta earthquake	• 1989 Berlin Wall	• 1997 Kyoto Protocol	• 1999 Turkey earthquake	• 2001 The Terrorist Attacks in the US				• 2011 Christchurch earthquake	
High rise RC building (Seismic structures)	• 1963 Hotel New Otani SRC17				• 1972 Shina-machi apartment	• 1986 Grand Heights Hikarigaoka D-5	• 1996 JR-Sakai ekimae (RC43F)								• 2011 Christchurch earthquake	
*SRC, Steel Reinforced Concrete structures	• 1965 Mitsui Kasumigaseki building				• 1988 MKO mansion RC41F (Tube structure)								• 2002 Royal Arc Tsurumi Tower (RC31F)	• 2011 Toranomon Hills (Controlled, CFT52F, H-247m)		
High rise RC building (Response controlled st.) (Seismic Isolated st.)					• 1982 Sagami-hara heights (RC25F)	• 1993 The scene Jyouchoku (RC45F)								• 2016 Toranomon Residential Tower (Controlled, RC54F, Fc120, H-215m)		
					• 1990 Kamogawa ground tower (33F)									• 2011 ARK Hills Sengokuyama Mori Tower (Controlled 47F, H-228m)		
					• 1997 R-H Capital tower (Isolation, 21F)									• 2012 Nishi-Tomiku redevelopment tower (Controlled 53F, Fc200)		
					• 1998 Shuginami-wada A building (Isolation 28F)									• 2015 The Park house NAKANOSHIMA (isolated 55F, H=193m)		
The maximum record each year or a few years	Story	20F	-	25F	30F	41F	39F	45F	43F	43F	43F	47F	56F	59F	60F	
	Concrete	Fc30	-	Fc36	Fc42	Fc48	Fc60	Fc60	Fc100	Fc70	Fc100	Fc80	Fc100	Fc120	Fc150	Fc200
	Steel bars	SD390	-	SD390	SD390	SD390	SD490	SD685*	SD685	SD685*	SD685	SD685	SD685	SD685	SD685	SD685
	Shear reinf.	SD295	-	SD295	*1275	*1275	*1275	*1275	*1275	*1275	*1275	*1275	*1275	*1275	*1275	*1275

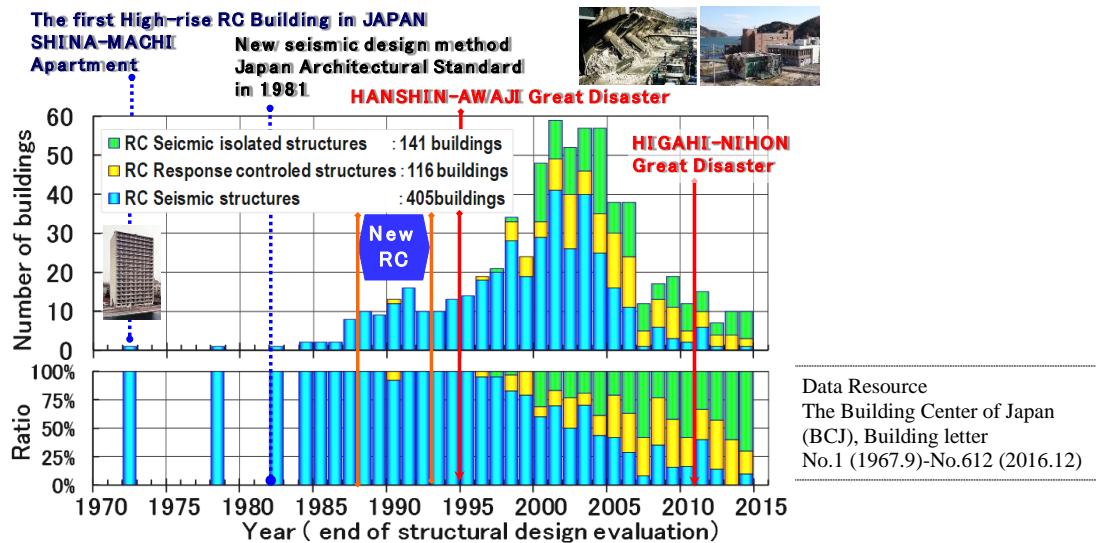


Figure 2. Structural design records for high rise RC buildings by Ishikawa (2017).

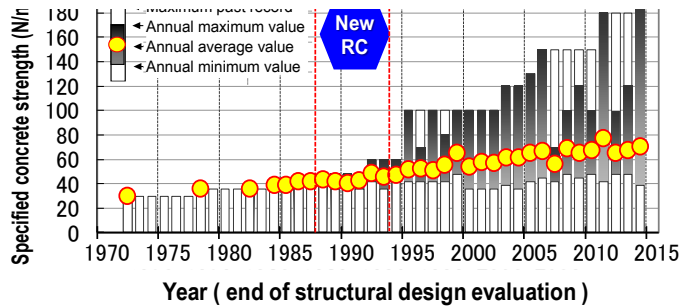
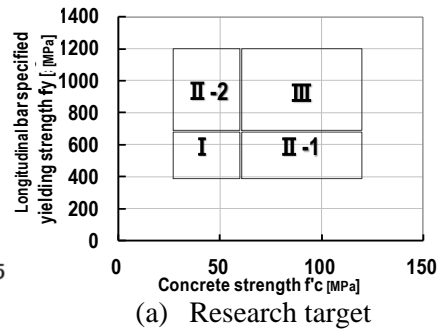
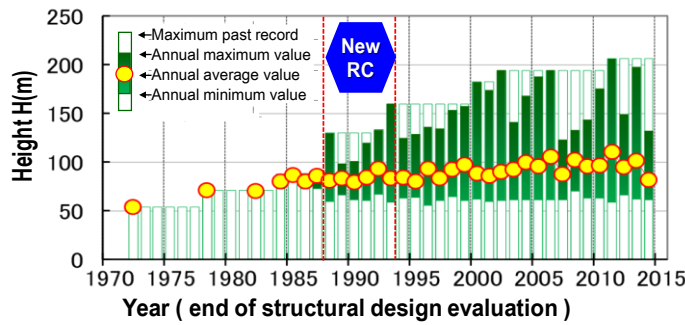


Figure 3. Transition in specified design concrete strength and height of high-rise RC buildings by Ishikawa(2017)

(b) High strength concrete column test by Aoyama (1999)

High-rise RC buildings in Japan have become taller than ever before. One of the reasons for these trends is because of high-strength concrete technology in Japan. Figure 3 shows the transition of height of high-rise RC buildings and utilization of high strength concrete. This historical trend was promoted by the national research project (New RC) from 1988 to 1993 by Aoyama(1999). The New RC research project had expanded the possibilities of usage of high strength materials by means of industry-government-academic collaboration (refer to Figure 4.). The director of the New RC research project was Professor Emeritus Hiroyuki Aoyama from University of Tokyo. It can be seen that material strengths for high rise RC buildings grew rapidly after 1995 and that high strength materials were put to practical use as a result of the New RC project. At present, the highest and average specified design strength of concrete for high-rise RC buildings has reached 200MPa and more than 60MPa, respectively.

2.3 Historical trends of construction methods for high rise buildings in Japan

In the early 1980's, 30 story 100-meter-high residential towers were developed by each of the big general contractors around the suburbs of big cities (refer to Figure 5, Courtesy of TAKENAKA Corporation). By the 1980's, construction of high-rise RC buildings adopted pre-formed reinforcing cages to rationalize working and lifting construction materials on the construction floor. Also, hollow core slabs and other half precast slabs were adopted for high rise RC building construction. Column longitudinal bars were connected by special welding methods as shown Figure 5. At that stage, the construction time per floor was about 8 to 10 days. Figure 6. (Courtesy of TAKENAKA Corporation) shows the Shiodome H-block super high-rise tower which was designed in 2000. It was famous as being the first RC high rise building over 50-stories built in Japan where previously most designers had applied CFT(Concrete Filled steel Tube) structures for high-rise structures over 50-stories. High strength materials were used – concrete with a design specified strength of 100 MPa and high strength SD685 steel bars with a yield stress of more than 685 MPa. The building was constructed from precast columns, beams, slabs and insitu beam-column joints as shown Figure 6. The figure shows the construction site ground floor being used for the manufacture of the precast members. This was convenient in the case where the high-rise building has regular spans and floor plans. Because lap joints for column longitudinal bars at column bases are prohibited in Japan, Japanese precast systems use sleeve joints and mechanical joints. This is one of the most significant differences between Japanese construction and construction practices overseas.

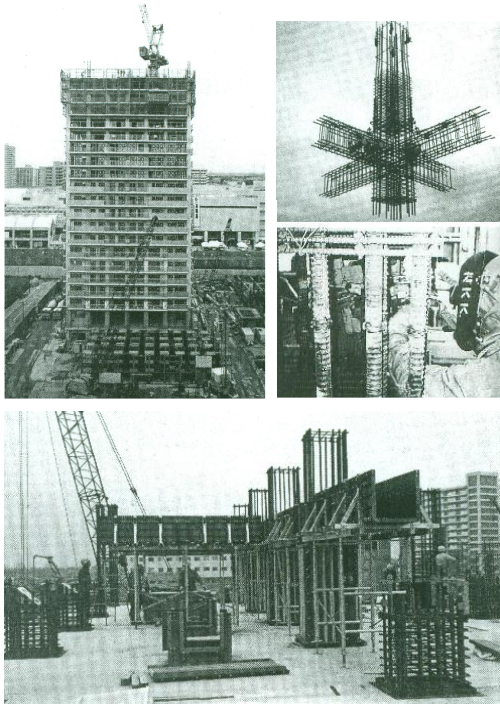


Figure 5. 1980' cast-in -place Construction



Figure 6. 2000' Precast concrete system (Site PCa)



Figure 7. Park city Musashi Kosugi (59F,47F, 2006) using advanced pre-cast concrete system

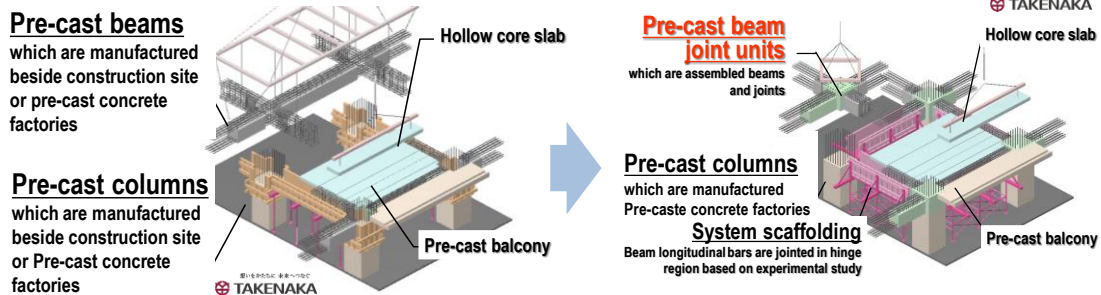
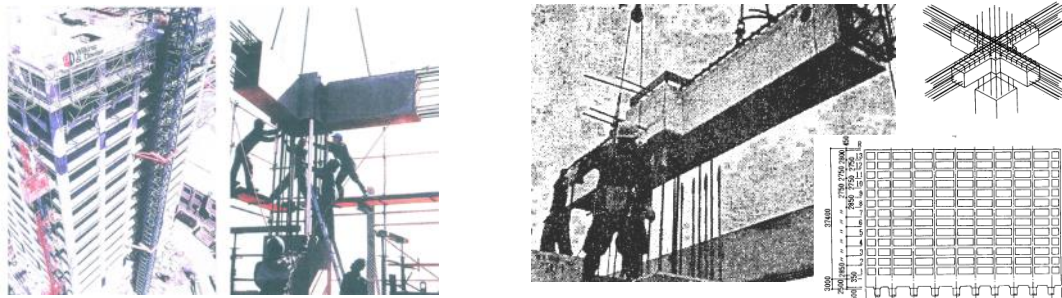


Figure 8. Comparison of previous Pre-cast system and the advanced pre-cast concrete system

2.4 Advanced pre-cast concrete system

In 2006, Park city Musashi Kosugi used the advanced precast concrete system to realize 59 and 47 story high-rise RC residential towers as shown Figure 7 (Courtesy of TAKENAKA Corporation). The feature of the system used precast beam-column joint units which integrated the beams and beam-column joints. Column longitudinal bars in precast concrete columns of the lower story passed through ducts in the precast beam-column joint units and were connected using sleeve joints to the column longitudinal bars of the upper story. In Japan, it is prohibited

to use lap joints for columns longitudinal bars. The system simplifies the beam-to-beam connections and has major advantages of shortened construction times despite the large scale of projects. Figure 8 (Courtesy of TAKENAKA Corporation) shows the comparison of previous Pre-cast system and the advanced pre-cast concrete system. On the construction floor, the lifting plan for construction materials and parts is very important to realize shortened construction times. The advanced precast concrete system is immediately able to put on upper floor precast columns after the precast beam and joint units. After that, precast column longitudinal bars are connected using sleeve joints to the upper story precast column reinforcement. In fact, the advanced precast sleeve concrete system was previously applied in New Zealand and Japan as shown Figure 9(a) by Wilkinson(1997) and Figure 9(b) by Nagahara et.al(1986). Nevertheless, both of the projects could not use mortar sleeve joints for steel bars as shown in Figure 10 (Courtesy of Splice Sleeve Japan). Each project used cast-in place columns and lap joints and pressure welding joint for columns longitudinal bars which was difficult to keep dimensional precision. The technology did not apply for many subsequent projects in New Zealand and Japan. After the 1990's, NMB splice sleeve and other companies have accomplished to put into practical application. As a result, the advanced precast concrete system has supported for use in Japan. In 2015, The advanced precast concrete system was applied for the Capital Green project in Singapore using NMB mortar sleeve joints for steel bars as shown Figure 11 (Courtesy of TAKENAKA Corporation)). At present, the system has expanded for RC buildings less than 10 story to resolve the social challenge of decreasing numbers of construction workers and continued control of high quality.



(a) Price Waterhouse-Coopers building(1989) Christchurch, New Zealand, RC20F, H=76m
 (b) Precast beam and joints unit system(1986) RC13F,H=37.4m, Japan, OBAYASHI
 Figure 9. Previous precast concrete system (Both of the system used cast-in-place columns)

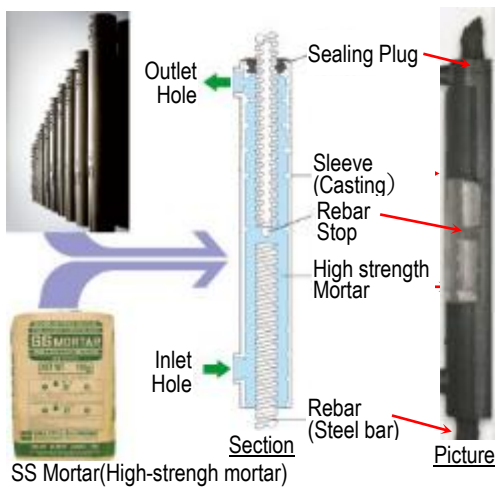


Figure 10. NMB sleeve joints for steel bar



Figure 11. Capital Green (H=250m,Singapore)

3 INNOVATIVE STEEL FIBRE REINFORCED CONCRETE STRUCTURAL SYSTEM

Recently, the innovative steel fibre reinforced concrete structural system was put in practical use in Japan. The research results was published by Ishikawa et.al.(2012). In this paper, the outline of the system using steel fiber concrete and implementation projects is introduced.

3.1 Description of the innovative steel fibre reinforced concrete structural system

In this system, beam longitudinal bars on opposite sides of interior beam-column joints are neither lapped nor connected within the joints, but provided with head anchors using steel fibre concrete of which the volumetric ratio to concrete of steel fibre is 1.0%. The headed bars are anchored around the middle section of the joints as shown in Figure 12. The effect of using steel fibre reinforced concrete of which rough two tests. Pull-out tests of single headed bars and seismic structural performance tests of the proposed interior joints were carried out by Ishikawa et.al (2012). These experimental tests have proven that 1.0% ratio steel fibre are added to plain concrete to enhance the joints' shear strength and anchor load capacity of the headed bars without joint shear reinforcement.

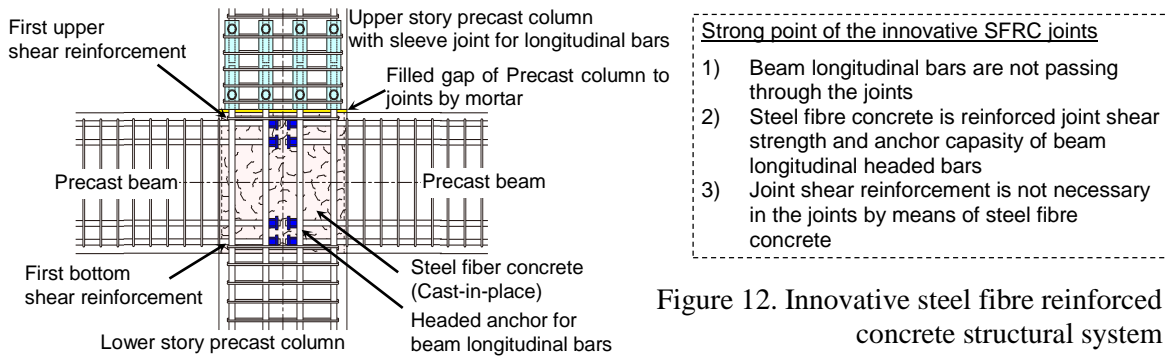
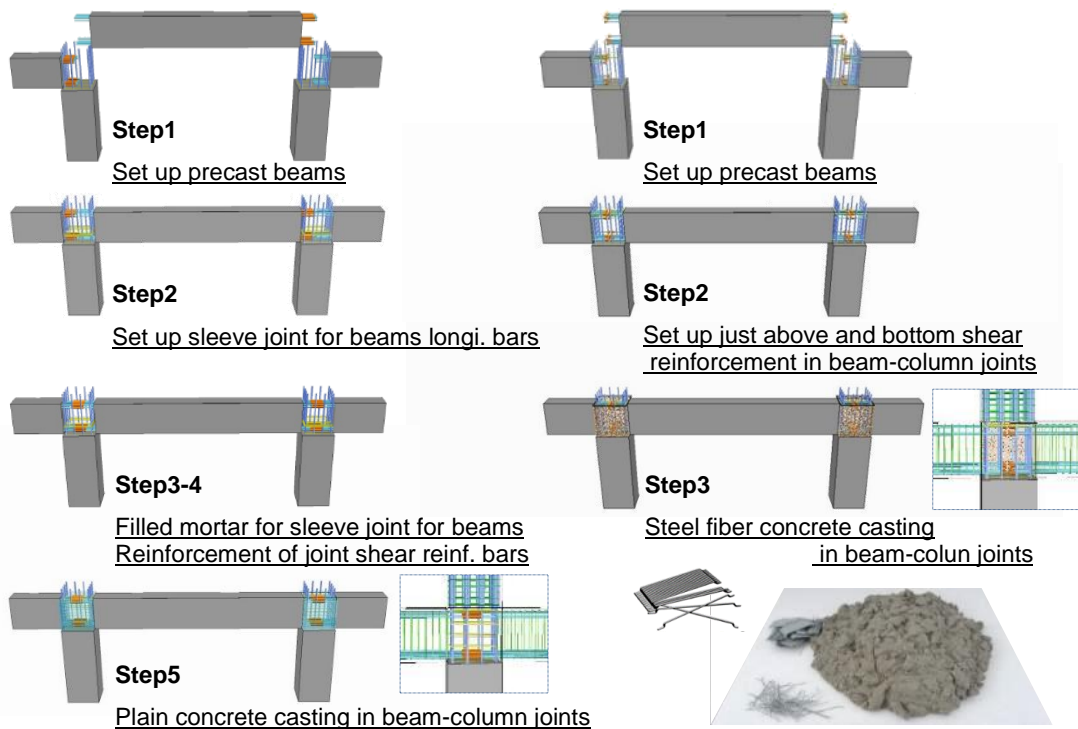


Figure 12. Innovative steel fibre reinforced concrete structural system



(a) Previous precast beams and columns system (b) The innovative SFRC system
Figure 13. Construction sequences using the ordinary precast and the innovative SFRC system

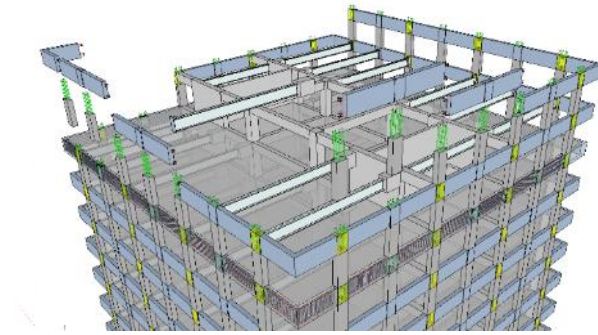


Figure 14. Construction sequence image of RC building applied the innovative precast concrete system for outer frame (Courtesy by TAKENAKA corporation)

*Inner core and outer RC frame are connected the hybrid RC-Steel long span beams

3.2 Research target of the innovative steel fibre reinforced concrete structural system

The innovative SFRC system was developed to accomplish a rationalized precast concrete system. Figure 13(a) shows the ordinary precast system using precast beams, precast columns and casting plain concrete in beam-column joints. In this case, beam longitudinal bars have to be connected and joint shear reinforcement in beam-column joints installed. This construction sequence has a heavily congested beam column joint area and is often difficult and time-consuming to construct. On the other hand, with the innovative SFRC system it is not necessary to connect beam longitudinal bars in the beam-column joints and install joint shear reinforcement. The system realizes the reasonable construction sequences as shown Figure 13(b) by means of the steel fibre concrete. Figure 14. shows construction sequences image of a RC building realizing the research and development goal of applying the innovative precast concrete system for an outer frame. The example RC building is composed of an outer frame using the innovative SFRC system and an inner RC frame. The outer frame is connected by RC-Steel hybrid long-span beams.

3.3 Beam-column joint test of the innovative steel fibre reinforced concrete structural system

This experimental study was carried out with the two main objectives. First, to understand the structural performance of the innovative SFRC system as shown Figure 15, and second to make a design equation and find out the stress transfer mechanism in the joints. To accomplish these objectives, it was necessary to obtain different failure modes of the joints. Two specimens, half size of the intended actual elements, were prefabricated in a similar way as in the actual case and then tested as shown Table 3. and Figure 15. Both of two specimens' beam-column joints were casted steel fiber reinforced concrete of which volumetric ratio was 1.0%. Specimen No.1, designated as “Design standard”, was to simulate the actual beam column joints and flexural yielding of beam longitudinal bars without joint shear failure was expected to occur.

Table 3. Description of test specimens

Specimen		No.1	No.2
key-word		Beam yielding type	Joint failure type
Joints	Concrete strength, f'_c (second modulus : Ec)	Steel Fiber concrete 75.3 (3.89×10^4 MPa) ^{*1}	
	First upper and bottom shear reinforcement (Grade)	2-D6 (SD685) ^{*2}	
Section : B×D [mm]		225×450	
Beam	Concrete strength, f'_c (second modulus : Ec)	Plain concrete 38.4 (3.05×10^4 MPa)	
	Longitudinal Bars (Grade) , [pt]	4+2-D16 (SD390) ^{*3} [1.34%]	3+2-D22 (SD490) ^{*4} [2.21%]
	Shear reinforcement (Grade), [pw]	2-D6@60 (SD685) ^{*1} , [0.47%]	
Section : B×D [mm]		400×400	
Column	Concrete strength, f'_c (second modulus : Ec)	Plain concrete 38.4 (3.05×10^4 MPa)	
	Longitudinal Bars (Grade) , [pt]	12-D19 (SD490) ^{*5} [1.91%]	
	Shear reinforcement (Grade), [pw]	4-D6@60 (SD685) ^{*2} , [0.53%]	
Notation pt : tensile reinforcement ratio, pw : shear reinforcement ratio			
Steel bars information Cross-sectional Area D22: 387.1mm ² , D16: 199mm ² , D6: 32mm ²			
*1 Steel fibre volume ratio $\rho = 1.0\%$.			
*2 Yield strength $f_y=757$ MPa. Modulus of elasticity $E_s=1.99 \times 10^5$ MPa			
*3 Yield strength $f_y=448$ MPa. Modulus of elasticity $E_s=1.93 \times 10^5$ MPa			
*4 Yield strength $f_y=522$ MPa. Modulus of elasticity $E_s=1.94 \times 10^5$ MPa			
*5 Yield strength $f_y=496$ MPa. Modulus of elasticity $E_s=2.03 \times 10^5$ MPa			

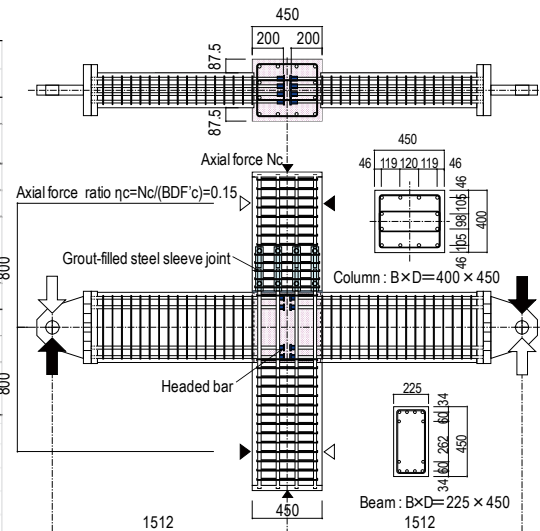


Figure 15. Outline of specimens No.1

Specimen No.2 was designed to experience a joint shear failure by using high strength steel (SD490) for its beam longitudinal bars. While the tensile reinforcement ratio of this specimen was 1.64 times that of No.1 to increase the joint shear stress, the other details were similar. Figure 16 shows the relationships of story shear force to interior story drift angle and the cracking pattern at 40×10^{-3} rad. The beam longitudinal bars of specimen No.1 reached their yielding strength level at the story drift angle $R=5.9 \times 10^{-3}$ rad and then plastic hinges formed at the ends of the beams at the cycle of $R=7.5 \times 10^{-3}$ rad owing to the radiating cracks developed under cyclic loadings without joint shear failure. Afterwards, the story shear force decreased beyond $R=40 \times 10^{-3}$ rad after beam yielding due to the sliding shear failure at the beam ends. The beam flexural strength of specimen No.2 did not reach the calculated flexural yielding strength. The specimens showed joint shear failure occurred. These results derived the mechanism of shear and moment transfer in beam-column joints under seismic loading as shown Figure 17, with the double strut model shown in Figure 18 used for the design equation.

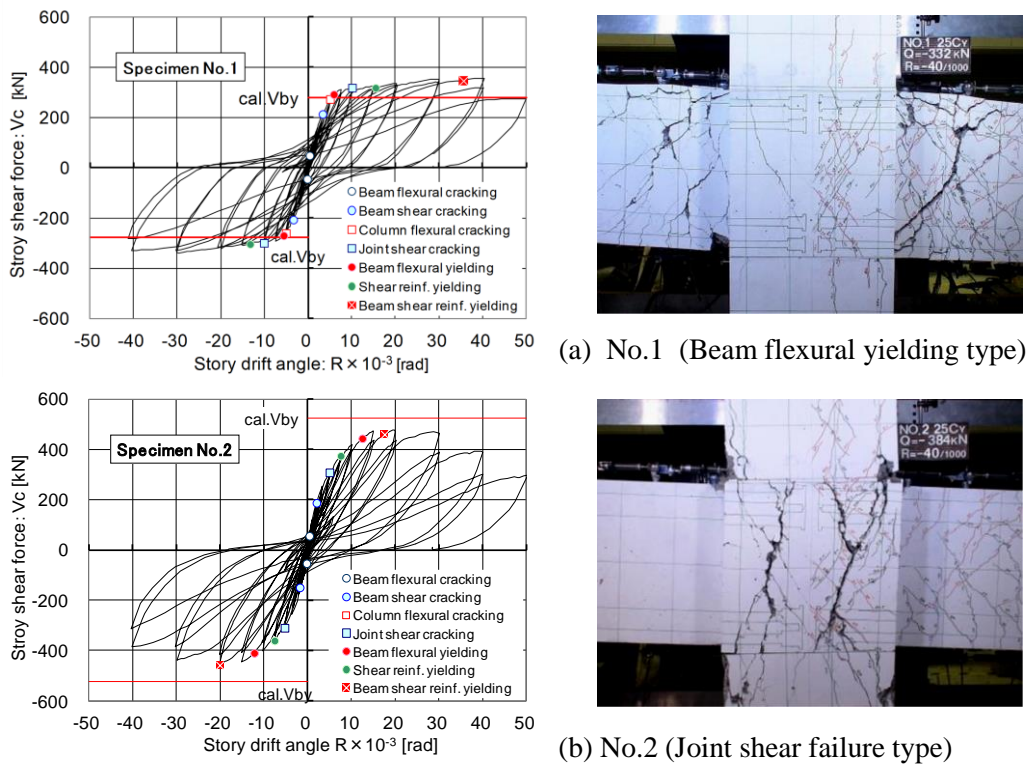


Figure 16. Story shear force- story drift angle relationship and crack patterns at $R=40 \times 10^{-3}$ rad.

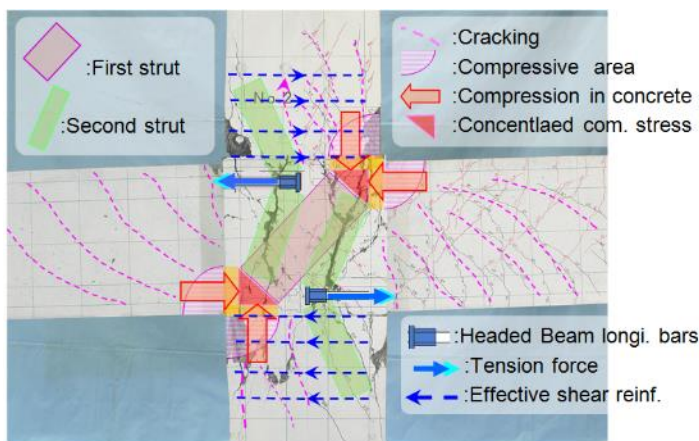


Figure 17. Stress transfer mechanism

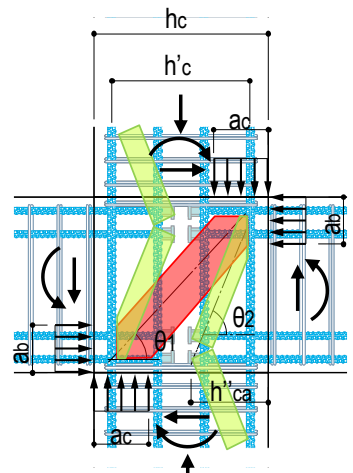


Figure 18. Proposed model for joint shear design

Under seismic loading, the resulting moments and shear forces of beams and columns acted as external loading on beam column joints. The stresses of diametrically opposed compression areas as well as the reaction force of the beam longitudinal headed bars are mutually balanced. Because beam longitudinal bars are not passing through the joints, a second compressive strut arises between the beam longitudinal anchors and the compressive area at beam ends. The innovative SFRC joints system was assessed as evaluation technology of structural design guideline by GBRC in 2006. The first project to apply the innovative SFRC system in 2015 is as shown in Figure 19 (Courtesy by TAKENAKA corporation). The four-story RC building uses the system for 12 beam-column joints using the merits of steel fibre concrete based on the evaluated structural design guideline. In 2018, the innovative SFRC structural system was installed in a second project which is an international sporting arena in Tokyo.

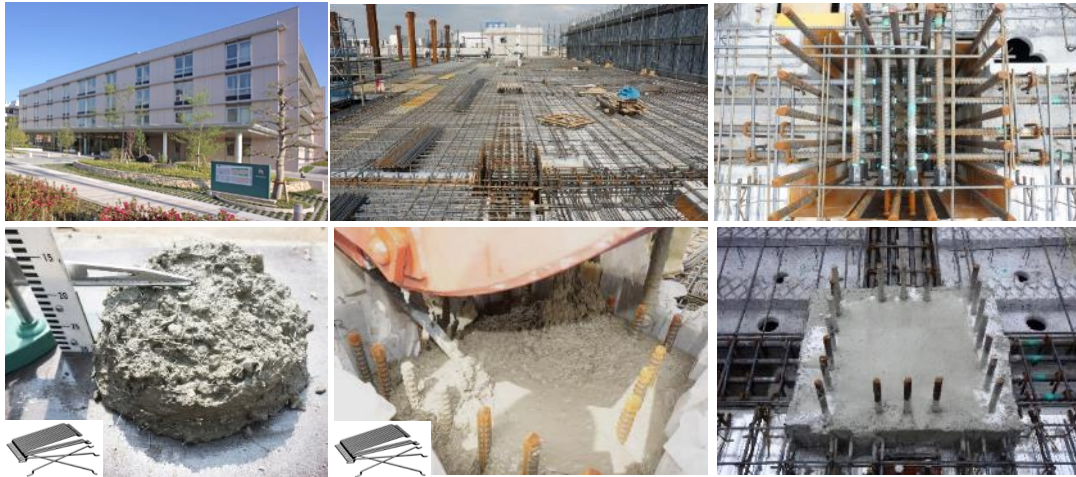


Figure 19. First project applied the innovative SFRC system (Nagoya, Japan, 2015)

4 SUMMARY AND FURTHER DEVELOPMENTS

This paper has described two new structural technologies in Japan:

- 1) The advanced precast system: a system using precast beam-column joint units with integrated beam and beam-column joints. At present, the technology has expanded into Singapore.
- 2) The innovative steel fibre reinforced concrete structural system: beam longitudinal bars on opposite sides of interior joints are neither lapped nor connected within the joints and provided with headed anchors using steel fibre concrete. The headed bars are anchored around the middle section of the joints. At present, the innovative structural system has been put to practical use for two projects in Japan.

Recently, steel fibre is being applied for 300MPa high-strength concrete to protect spalling of the concrete cover under severe fire conditions. The ductility of steel fibre reinforced concrete has been successfully investigated for 150MPa high strength concrete columns for high-rise RC residential tower to minimize damage to RC columns under severe earthquake loading.

REFERENCES

- Yuji Ishikawa, Advanced precast technology in Japan, Materials Science and Technology in Engineering Conference, The Hong Kong Institution of Engineering, 2017
- Yuji Ishikawa, et.al, Steel fibre reinforced interior beam-column joints without shear reinforcement and beam bars passing through joint, 8th RILEM International Symposium on Fibre Reinforced Concrete, 2012
- Hiroyuki Aoyama; Development of High-rise Concrete Construction in Seismic Countries, George Winter Commemorative Lecture 1999 ACI Fall Convention, 1999
- R.G. Wilkinson; Precast concrete structural frames and wall panels -Design and detail-, NZSC, 1997
- Katsumi Nagahara et al; Experimental study on the full-scale beam-column joint sub assemblages adopting precast member of beam and beam-column connection, AIJ, 1986 (in Japanese)

Evolution of bridge construction in Japan

Akio KASUGA¹

¹ Sumitomo Mitsui Construction, Tokyo, Japan

ABSTRACT: A new type of bridge called “Butterfly Web Bridge” has been constructed in Japan. In a butterfly web bridge, the panels used as the web are cut so as to appear pinched in the centre, giving a butterfly-wing shape. 80MPa steel fibre reinforced concrete is used for the butterfly shaped web made of precast panels with a thickness of 150 mm. In this paper, three projects of expressway bridges using this new technology will be shown. By simplified construction process, construction time can be reduced. Then possibility of much longer concrete bridges with butterfly webs will be proposed in the last part of this paper. The butterfly web technology will greatly affect bridge design and construction in the near future.

1 INTRODUCTION

One of the recent innovations in bridge technology is the composite bridge. A variety of ideas have been applied in this area, including the use of steel members in the web, and attempts to find an effective method for utilizing the prestressing forces in the concrete members used for the deck slab and bottom slab. Examples include corrugated steel web bridges and composite truss bridges. In Japan, over 150 corrugated steel web bridges have been constructed since the first in 1993. The composite truss approach was first adopted in 2003, and there are now 8 composite truss bridges in service. These composite bridges achieve reductions in girder weight of 10% to 15% compared to conventional concrete bridges, and the weight reduction has given them an advantage in Japan, where earthquakes are frequent.

In a corrugated steel web bridge, the joints between the web and the concrete slabs run continuously along the longitudinal direction of the bridge, enabling the structural details of the joint to be simplified. However, fabricating the corrugated steel web requires folding of the steel sheets using a press, and the individual corrugated steel webs need to be welded together at the construction site. These processes can detract from economy and ease of construction. In contrast, composite truss bridges use conventional materials such as steel pipes that do not need to be joined on site, but because nodes are used for the joints with the concrete slabs, substantial forces concentrate at the nodes. Moreover, joint details become more complex for longer spans. These factors make it more difficult to achieve economy and ease of construction, and that is probably why there are still few examples of composite truss bridges around the world.

Being involved in the design and construction of such bridges, the author had long thought about the potential for structures that combine the benefits of these two types of composite bridge, and eventually produced the “butterfly web bridge” [Kasuga et al. (2006)] (Figure 1) described in this paper. A butterfly web bridge, which uses butterfly-shaped panels instead of a double warren truss, is a new structure that has both the corrugated steel web bridge’s advantage of being able to simplify the joints with the concrete slabs, and the truss bridge’s advantage of not needing on-site work to make joints between the butterfly-shaped panels that carry the shear forces.

This paper describes the butterfly web bridge, presenting examples of its use in actual projects and introducing prospects for the future.



Figure 1. Butterfly web bridge

2 STRUCTURAL FEATURES OF THE BUTTERFLY WEB

The butterfly web is a new structure with butterfly-shaped web members having the following characteristics.

- (1) The web is configured with butterfly-shaped panels placed independently and not joined continuously. The shape limits the orientation of compression and tension in the panel due to shear forces, meaning that the structure is similar to a double warren truss (Figure 2).
- (2) The butterfly web uses 80 MPa steel fiber reinforced concrete and has prestressing steel oriented in the direction that tensile forces act (Figure 3), limiting the occurrence of cracks. It does not use steel reinforcements, relying instead on steel fibers and prestressing to achieve the required strength.
- (3) Transmission of shear forces between the butterfly web and deck slabs is achieved by the joint between the slab concrete and dowels embedded in the panel.

Many corrugated steel web bridges and steel truss web bridges have been built. These bridges had rational structures and excellent structural characteristics, but at the same time, they required complex machining of steel members, on-site welding, or other special skills for fabrication or construction. In contrast, as the butterfly web is a precast product, all that is needed to construct a girder is to combine the web with the slabs on site. The prestressing steel oriented in the same direction as the tensile forces in the web is pre-tensioned at the factory, so there is no need to work on the butterfly web at the construction site. The potential weight reduction of the main girder is similar to that of a corrugated steel web bridge, achieving about a 10% to 15% reduction compared to a conventional box girder section. Consequently, the length of segments that can be constructed using a form traveler can be 50% longer because of light weight of the girder. Then light weight structures have big advantages in earthquake prone area, like Japan.

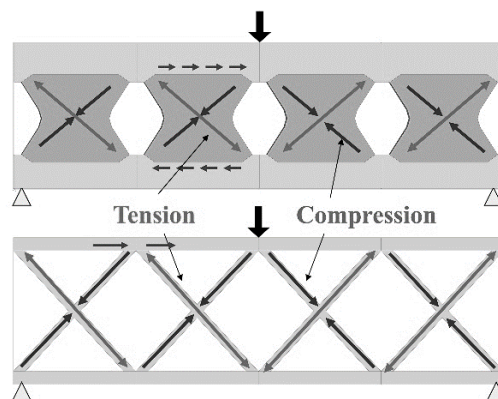


Figure 2. Structural characteristics of butterfly web

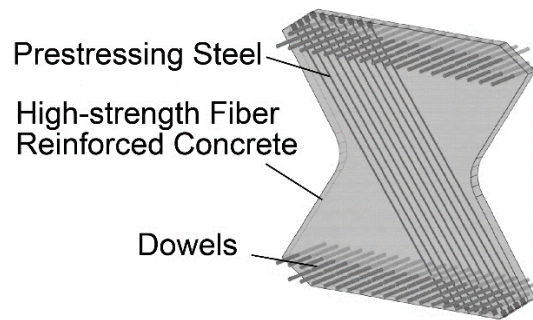


Figure 3. Butterfly web panel

3 PROJECTS USING BUTTERFLY WEB

The three projects using butterfly web technology described below are all expressway bridges. In Japan, the company handling construction of this sort of project is also responsible for detailed design. For these bridges, the basic design was performed by a consultant, and in each case, a conventional box girder design was stipulated. This was then changed to a butterfly web bridge at the detail design stage, and the necessary testing was performed to ensure the appropriateness of the design.

3.1 *Takubogawa Bridge*

Takubogawa Bridge [Ashizuka et al. (2012)] (Figures 4 and 5) is located in the city of Hyuga, Miyazaki, Japan. This bridge has 10 spans, with a maximum span length of 87.5m. A section of the main girder for the Takubogawa Bridge is shown in Figure 6. Based on the main girder height and the size of the indentations that make the butterfly shape, the butterfly web panels were designed to be 2.9 m long and were installed at a 3.0 m pitch (Figure 7). The area of tensile stress is reinforced by prestressing strands, with the number of strands determined such that there is no tensile stress intensity under dead load, and such that no cracking occurs under design live load. Web panel thickness is 150 mm, a thickness designed to be sufficient for the necessary number of prestressing strands as described above, and to be able to resist the compressive force acting on the compression side under ultimate load. The panels incorporate dowels in order to join them to the upper and lower cast-in-situ deck slabs.

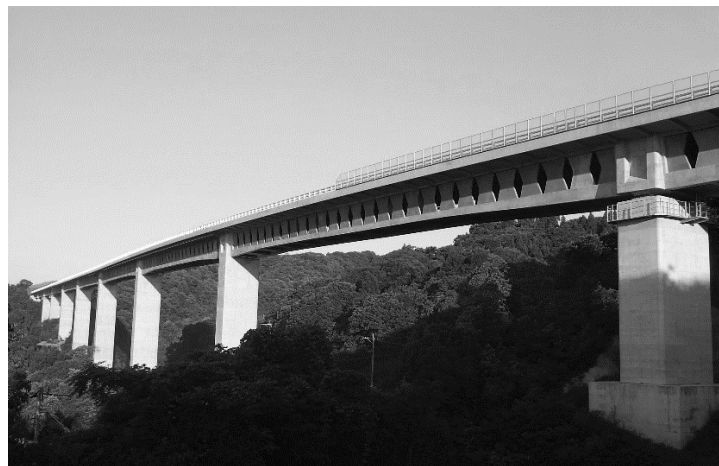


Figure 4. Takubogawa Bridge

The butterfly web panels are fabricated at a plant situated 270 km away from the bridge construction site and transported to the site by truck. In total, the bridge requires 444 web panels, and although external shape and thickness are standardized, panels used at different points in the

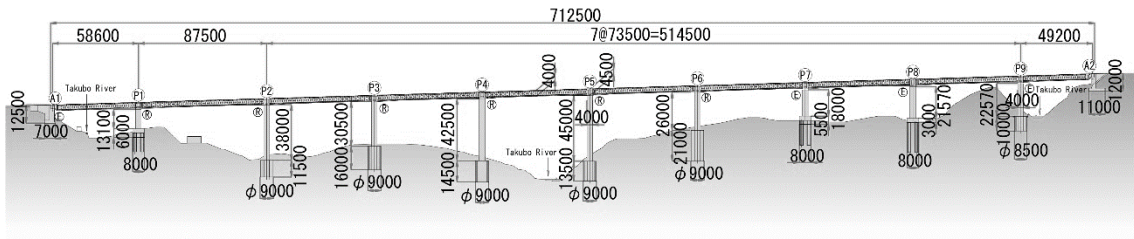


Figure 5. General view

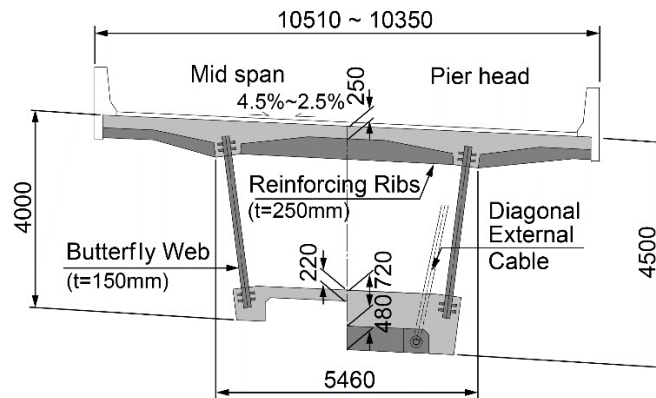


Figure 6. Cross section

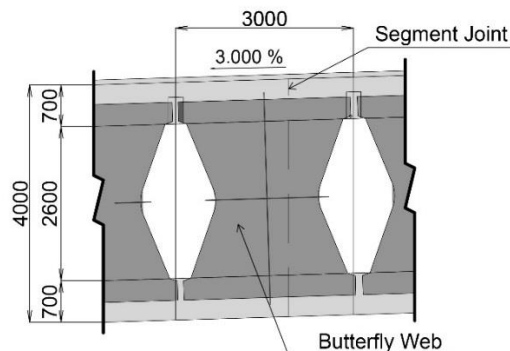


Figure 7. Arrangement of butterfly web.

design require different amounts of prestressing strands and dowels (Figure 8). In all, 13 different types of panel are fabricated. At the inflection point, tensile force also acts counter to the orientation of the pre-tensioning steel. Post-tensioning steel is therefore used to bear stress in excess of the steel fiber reinforced concrete's allowable tensile stress.

The cantilever construction is used for the Takubogawa Bridge. Each butterfly web panel weighs approximately 3.25 tons, enabling construction of a main girder lighter than would be possible with an ordinary concrete web. Consequently, a segment length of 6.0 m could be used, equivalent to the length of two butterfly web panels on each side of the bridge. As a result, whereas constructing each span of this bridge with ordinary concrete box girder sections would have required 8 segments, the butterfly web enables construction with only 5 segments. With fewer segments required, the construction period can be substantially shortened. The concrete for the upper and lower deck slabs is placed to construct the main girder. Figure 9 is a photograph taken inside the completed girder. It is very bright inside, which makes inspection easy. Furthermore, it is possible to inspect for girder deformation inside the girder, which is normally difficult for an expressway bridge in service. This feature makes maintenance easier. The Takubogawa Bridge was completed in 2013.

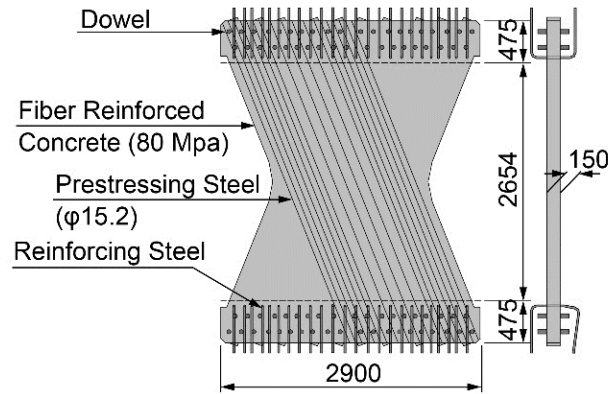


Figure 8. Detail of butterfly web

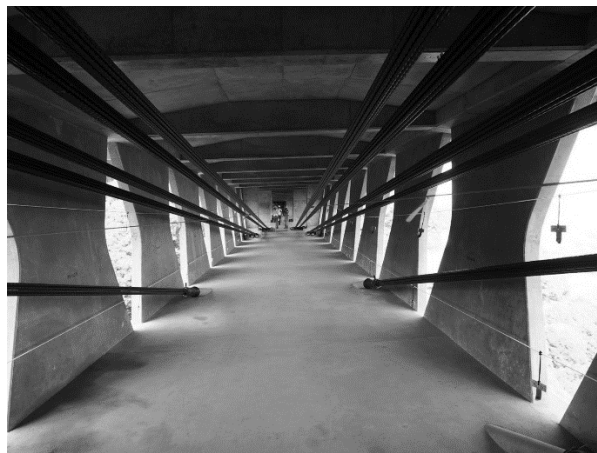


Figure 9. Inside view of the girder

3.2 Okegawa Viaduct

The Okegawa Viaduct [Homma et al. (2015)] has a total length of 3089 m, with 45 m spans (Figures 10 and 11). In order to complete construction, including detail design, within a very short period of one and a half years, precast segment construction was adopted. Altogether, the viaduct used 900 segments, and 2,372 butterfly panels. The segments were fabricated at factories about 100 km from the erection site, so it was necessary to lower the weight of the main girder in order to reduce the number of segments. For that reason, a butterfly web design was selected, and, as can be seen in Figure 12, the segments had a special U-shaped design that permitted the upper deck slab to be casted later. This approach enabled the viaduct to be constructed with only 60% of the number of segments than would have been required with a conventional segment shape. The butterfly panels for the Okegawa Viaduct were fabricated at the same factory, which was not the same as the factories used for the other projects described above. Sumitomo Mitsui Construction has four concrete factories within Japan and can produce the materials required for the butterfly web at any of the plants.

Segment fabrication proceeded by standing the butterfly panels in the segment mold, then casting the horizontal ribs and bottom slab to complete the segment. Even the pier head and girder end sections were precast as segments in the same way. At the erection site, the U-shaped segments were erected first of all, and then the primary external cables were tensioned to make the structure independent. Afterwards, the deck slab was constructed with cast-in-situ concrete, and the secondary external cables were then tensioned to complete the bridge. The Okegawa Viaduct is due to be completed in December 2014.



Figure 10. Okegawa viaduct

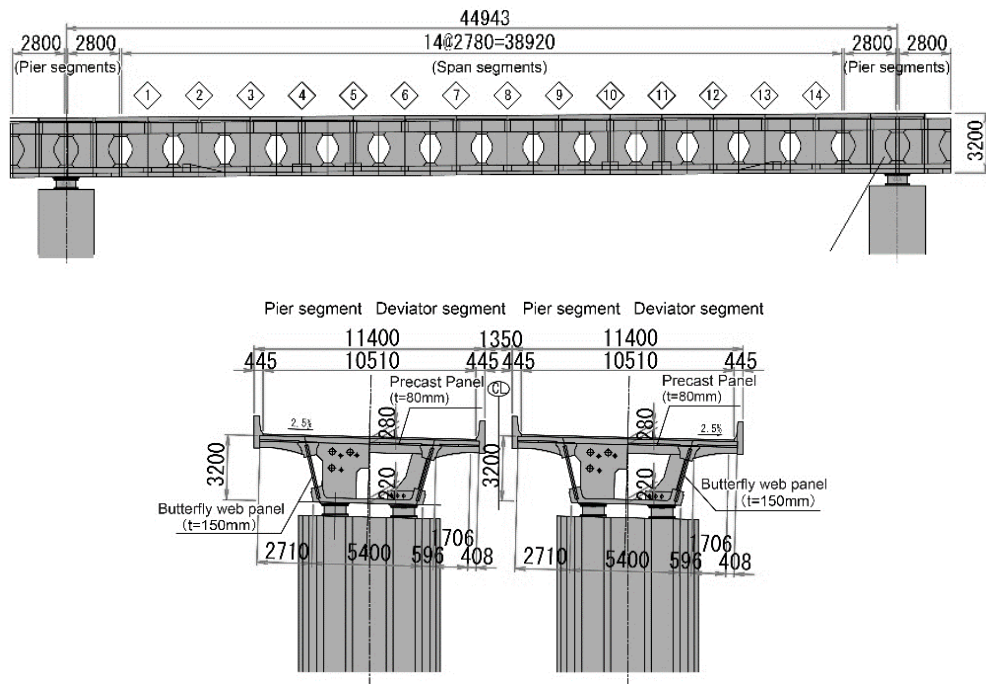


Figure 11. General view



Figure 12. U-shaped segment

3.3 Mukogawa Bridge

3.3.1 Structural features

The Mukogawa Bridge, shown in Figures 13 and 14 is an extradosed bridge [Samizo et al. (2015)] using butterfly web technology and located in the city of Kobe, Hyogo, Japan. This is a 5-span continuous rigid frame bridge with a span length of 100 m. The tallest pier is 81 m, and they were designed for rapid construction, including the use of some precast sections (Figure 15). The cross-section incorporates four butterfly webs, and the extradosed cables are located in the center of the cross-section. The main girder is constructed by the free cantilevering method, with individual segments having a length of 6.0 m and incorporating two butterfly web panels parallel to the axis of the bridge. After installation of butterfly webs into the form traveler, the concrete deck is cast in place. The reduction in superstructure weight achieved enables a substantial reduction, approximately 50%, in pier thickness and the size of foundations. Furthermore, the extradosed cables for the Mukogawa Bridge use high-strength strands [Kido et al. (2010)] that are 30% stronger than regular strands.



Figure 13. Mukogawa Bridge

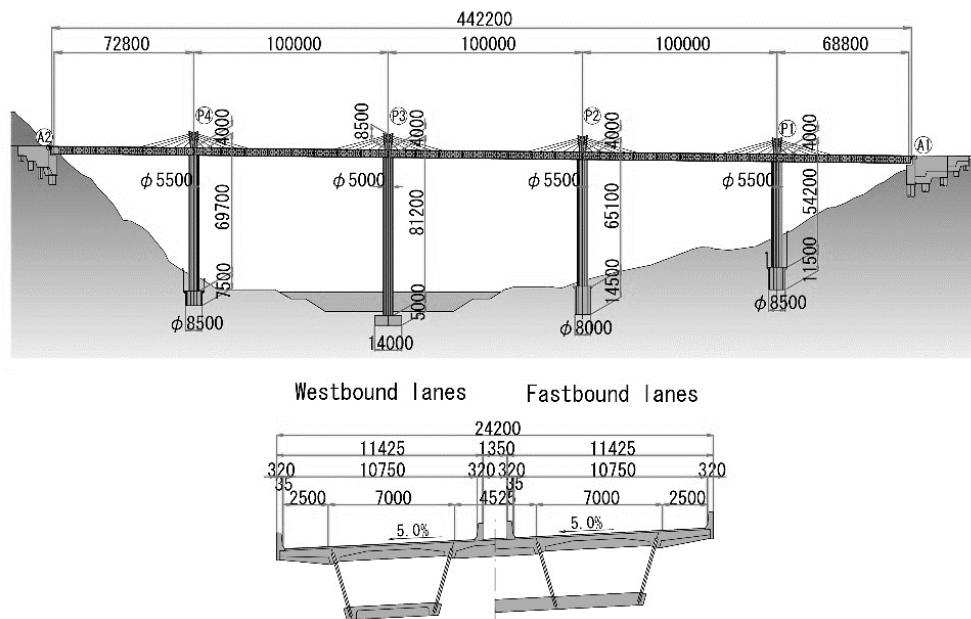


Figure 14. General view



Figure 15. Precast construction of piers

The pylons stand 8 m above the deck. They are installed in the median strip, but because only a narrow space is available, special considerations applied to the cable anchorages. As can be seen in Figure 16, the pylon structure has 100 mm thick steel plates in the center to carry the horizontal components of the forces of the cables anchored to both sides. Loading tests were performed on this new structure to confirm the appropriateness of the design. Mukogawa Bridge is scheduled to be completed in June 2016.



Figure 16. Extradosed cable anchorage of pylon

3.3.2 Advantages in seismic design

The highest pier located in the middle of the river is designed to have a cylindrical hollow cross section with a diameter of 5.0 m in consideration of the obstruction ratio of the pier width to the channel width. Other piers are originally planned to have a square hollow cross section of 6.5 to 7.0 m. Among the piers, 81.2 m is the tallest, and 54.2 m is the shortest. A concern is raised about the higher rigidity of three piers which may cause localization of seismic inertia force on the shortest pier. In the detail design, three piers are changed to a hollow cylinder with a diameter of 5.5 m to reduce their rigidity and equalize the rigidity levels between all piers. With this change in design, seismic inertia force is expected to be distributed properly and also reduced significantly by the extended natural periods. Table 1 shows natural periods of the bridge and Figure 17 shows the response values at the bottom of the piers.

Adequate bearing capacity was ensured by using high strength reinforcing steel (SD490) for the longitudinal reinforcement and concrete having a strength of 40 or 50 N/mm² for the piers. The total weight of superstructure and substructure in the detail design was about 35% smaller than that in the basic design. Figure 18 shows a comparison of structural dimensions between the basic plan and the detail design.

Table 1. Comparison of natural period

Natural period	Basic plan (s)	Detail design (s)
Longitudinal (temporary)	1.59	2.29
Transverse (temporary)	2.90	3.82

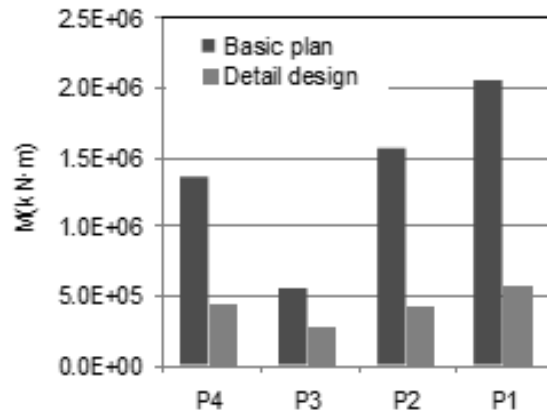


Figure 17. Bending moments at the bottom of piers

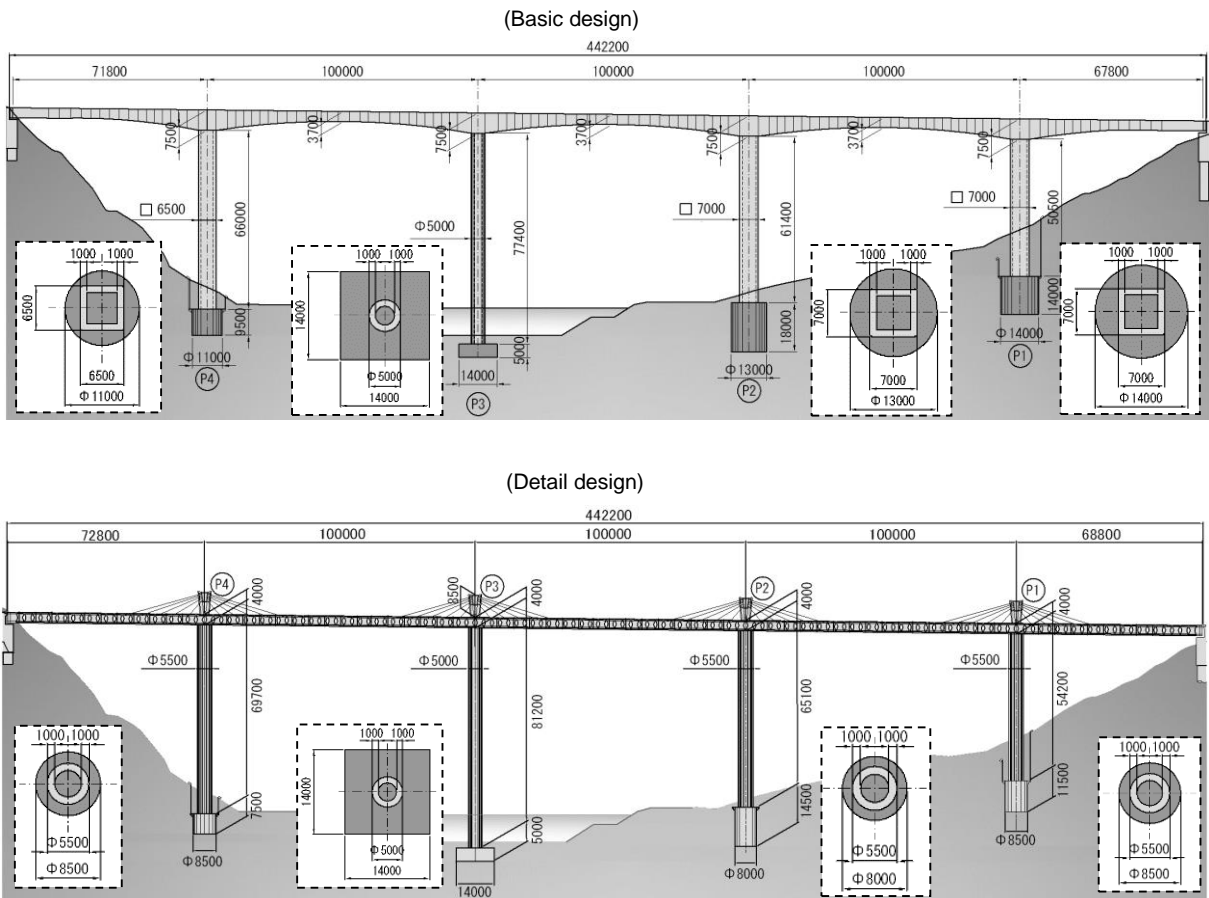


Figure 18. Comparison of structural dimensions

4 FURTHER POSSIBILITIES OF BUTTERFLY WEB BRIDGES

Extradosed bridges have become popular structures for spans of 150m-250m, taking a place between conventional girder bridges and longer cable-stayed bridges. However, it is useful to consider whether using extradosed bridges for longer spans would be structurally and economically feasible. Consequently, investigation whether the technologies for producing lighter main girders described above have the potential to enable the construction of longer spans will be discussed here.

4.1 Long span extradosed bridges

4.1.1 Structural features

Here a cable-stayed bridge with a central span of 435m as shown in Figure 19 is considered, and it is compared with an extradosed bridge having the same span length but with shorter main towers, about 60% of the height of the towers for the cable-stayed bridge. The girder cross-section is 3.5m deep in the cable-stayed type bridge, and 6.0m in the extradosed type, using a single plane of stay cables and struts inside the box girder [Kasuga et al. (2015)] (Figure 20). The cable-stayed bridge uses a conventional box girder, but the extradosed bridge uses a butterfly web to counter the increase in weight due to the larger girder height. Consequently, the superstructure weight is unchanged, but the stiffness of the main girder is doubled. Figure 21 shows the variation in stay tension due to live loads. The JPCI Code in Japan [JPCI (2000)] (Figure 22) permit a maximum allowable stress of 0.6fpu for stay cables, even for this sort of long span extradosed bridge. The number of cables required is about 20% more than for the cable-stayed bridge, but because the weight reduction technology has produced a stiffer main girder without an increase in weight, the pylons can be shorter, which makes this structure very competitive in earthquake-prone Japan. Table 2 shows a comparison of the material quantities for the two configurations. The amount of concrete for the extradosed bridge using butterfly webs is almost the same, despite having a deeper girder. And because the safety factor can be lowered with the use of an extradosed bridge, the weight of stay cables is similar to that of the cable-stayed bridge, even with a shorter pylon. This demonstrates that a long span extradosed bridge with reduced weight main girder is feasible.

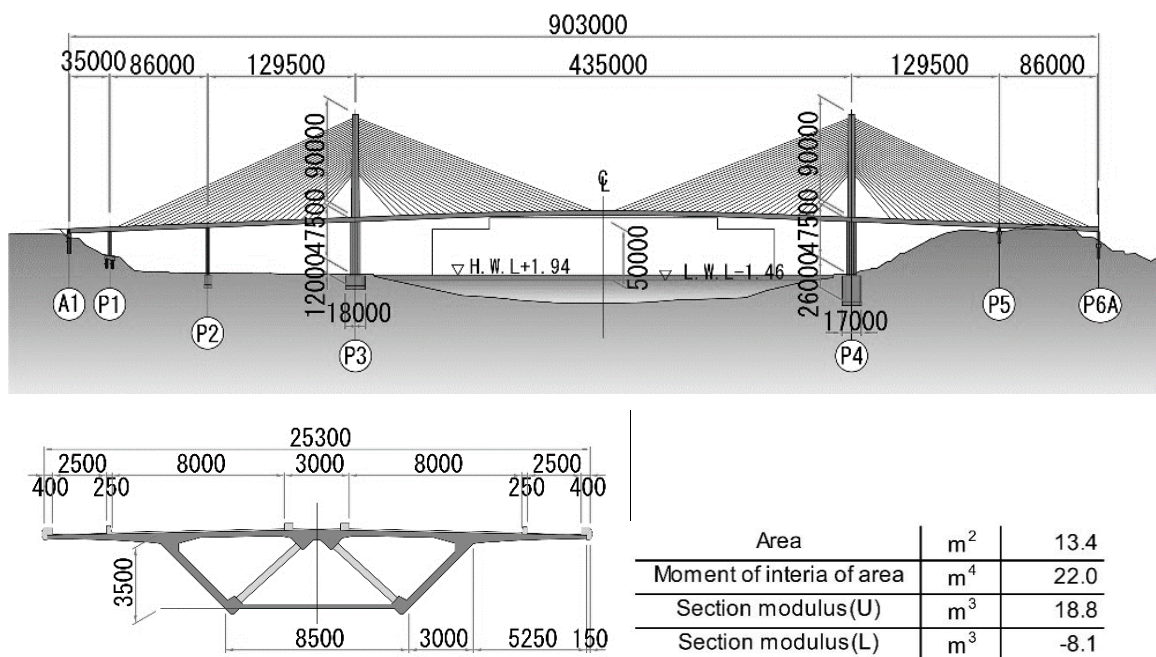


Figure 19. General view and section data of Cable-stayed type (Bai-Chai Bridge, 2006)

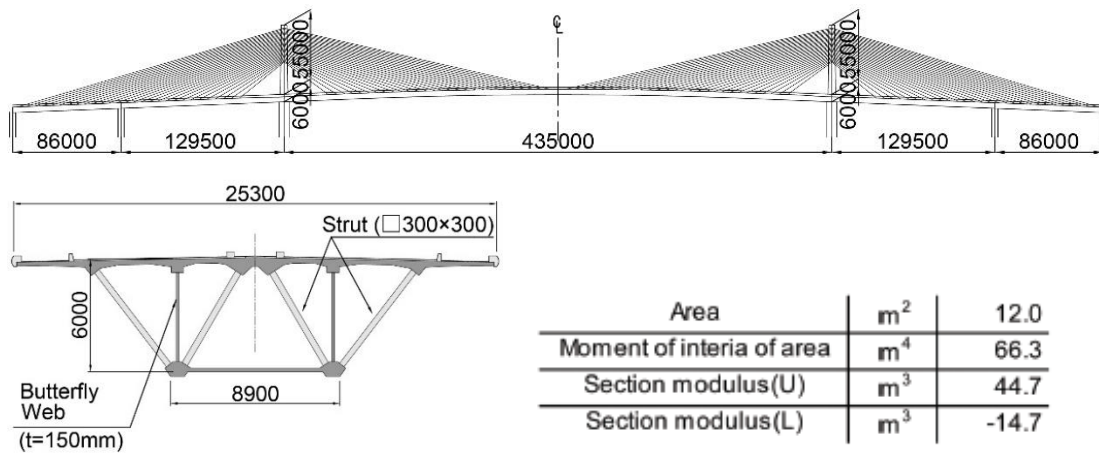


Figure 20. General view and section data of extradosed type

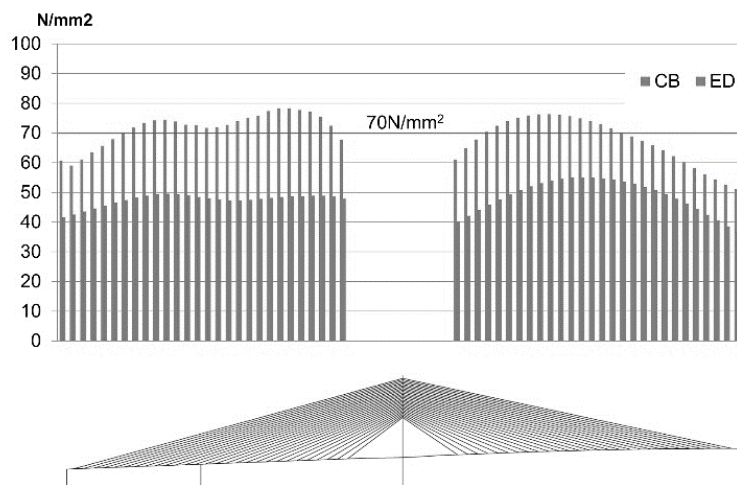


Figure 21. Stay cable stress change due to live load

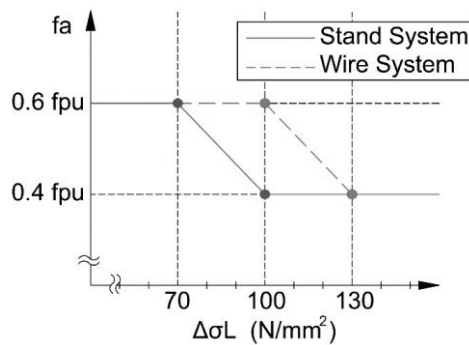


Figure 22. Allowable stay cable stress versus stress change owing to live loads.

Table 2. Comparison of material quantities (three spans)

			CSB	EDB
Concrete	Girder	m ³	13200	13400
	Pylon	m ³	2200	1400
Rebar		ton	3190	2751
Prestressing steel		ton	220	195
Stay cable		ton	1040	1042

4.1.2 Advantages in seismic design

In verifying dynamic behavior under seismic loading, it is interesting to examine the differences between cable-stayed bridges with their tall main towers and flexible girders, and extradosed bridges with short main towers and stiff main girders. Seismic response analysis was performed using the acceleration response spectrum (Figure 23) for soft soil sites as stipulated by Japanese seismic design specifications, assuming a rigid connection between main tower and main girder. The natural periods for each of these bridge types are shown in Table 3, and the maximum bending moments are shown in Figure 24. The extradosed bridge has a longer natural period for the 1st mode. The response value of the extradosed bridge is definitely smaller than that of the cable-stayed bridge, but because the stays are at a shallower angle, they resist horizontal movement of the main girder and generate flexure in the main towers. As a result, the difference in response values was surprisingly small. For long span bridges, adoption of an extradosed bridge with a light main girder instead of a cable-stayed bridge was found to be advantageous in regions prone to earthquakes.

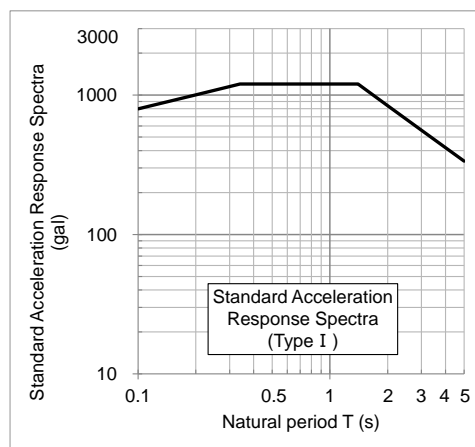


Figure 23. Acceleration response spectra

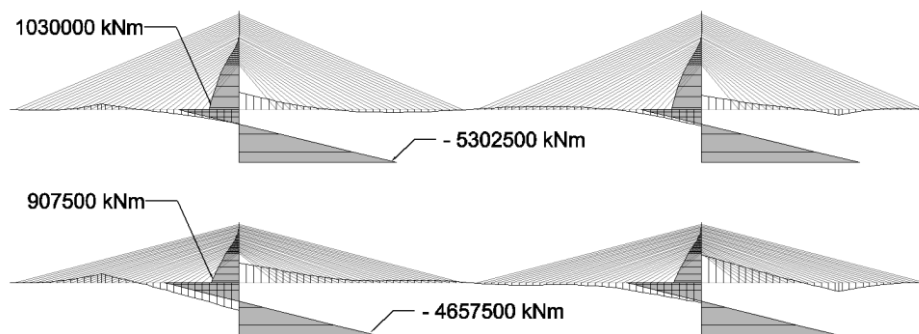


Figure 24. Maximum bending moment

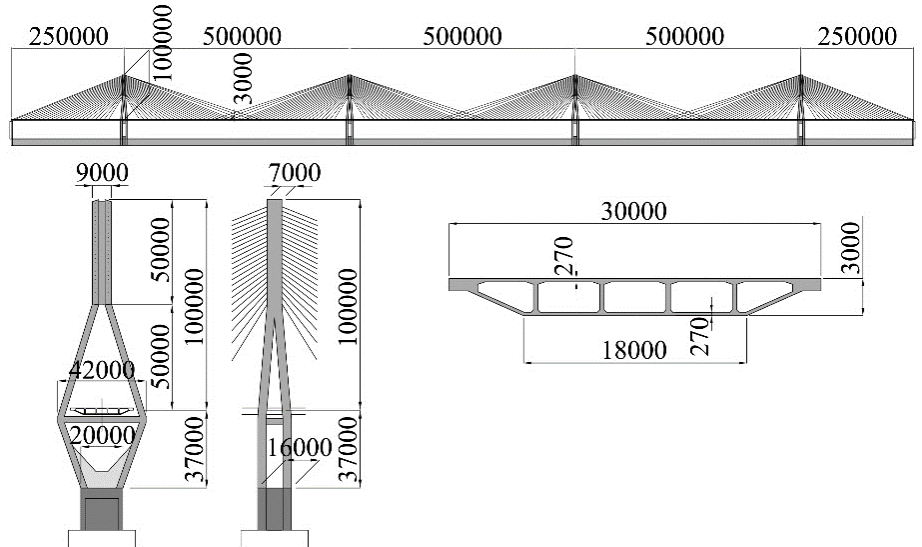
Table 3. Natural frequency

	(sec)		
	1st	2nd	3rd
CBD	3.47	2.65	1.98
EDB	4.12	2.38	1.68

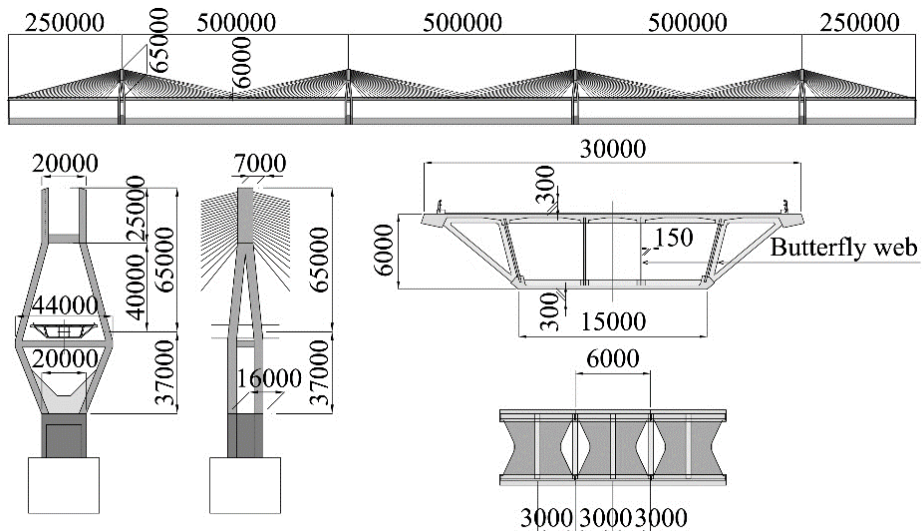
4.2 Multi-Span Large extradosed bridge

4.2.1 Structural features

The models used for this comparative study are a cable-stayed bridge and an extradosed bridge composed of five continuous spans with a central span of 500 m (Figure 25). In order to raise the overall stiffness of the multi-span cable supported structure, overlapping cables are distributed at the middle of the span, and the stiffness of the bridge piers and pylons is increased. Moreover, highly stiff butterfly webs with a 6.0 m depth are used for the extradosed bridge. Using these two structures, stay cable stress variations at the serviceability limit state and, as well as the behavior under aerodynamic vibrations, were compared, and the structural feasibility of the proposed continuous long span extradosed bridge is verified [Kasuga (2015)].



(a) Cable-stayed type (CSB)



(b) Extradosed type (EDB)

Figure 25. The 500-m five-span bridge. (a) Cable-stayed type and (b) extradosed type

Figure 26 shows a comparison of the stress variations in stay cables due to live loads. According to the JPCI code of Japan (Figure 22), up to 0.6fpu, the limit value for stay cable tension, is allowed for road bridges as long as the stay cable stress variation is 70 N/mm² or less. However, it was confirmed that almost all of the cable stress variations exceed 70 N/mm² except some

cables of the side span because multi-span structures are very flexible. Table 4 shows a comparison of the material quantities for the two configurations. The amount of concrete for the extradosed bridge using butterfly webs is lighter, despite having a deeper girder. Moreover, the material required for the pylons was reduced. However, there is no big difference of the weight of stay cables in the multi-span structures.

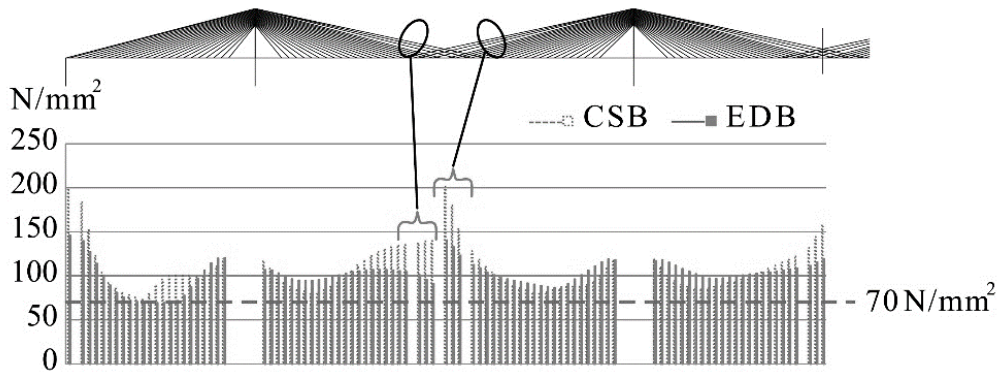


Figure 26. Stay cable stress variations owing to live loads

Table 4. Comparison of material quantities (five spans)

			CSB	EDB
Concrete	Girder	m ³	48900	43700
	Pylon	m ³	18500	14400
Rebar		ton	15960	13410
Prestressing steel		ton	259	261
Stay cables		ton	6030	6300

4.2.2 Advantages in seismic design

In verifying dynamic behavior under seismic loading, it is interesting to examine the differences between cable-stayed bridges with their tall main towers and flexible girders, and extra-dosed bridges with short main towers and stiff main girders. Seismic response analysis was performed using the wave of Japanese seismic specifications (Figure 27) for soft soil sites. The natural periods for each of these bridge types are shown in Table 5, and the maximum bending moments of girders and pylons are shown in Figure 28. The response value of the extra-dosed bridge girder is larger than that of the cable-stayed bridge, but the bending moment of pylons has no large difference. For long span bridges, adoption of an extradosed bridge with a light main girder instead of a cable-stayed bridge was found to be advantageous in regions prone to earthquakes.

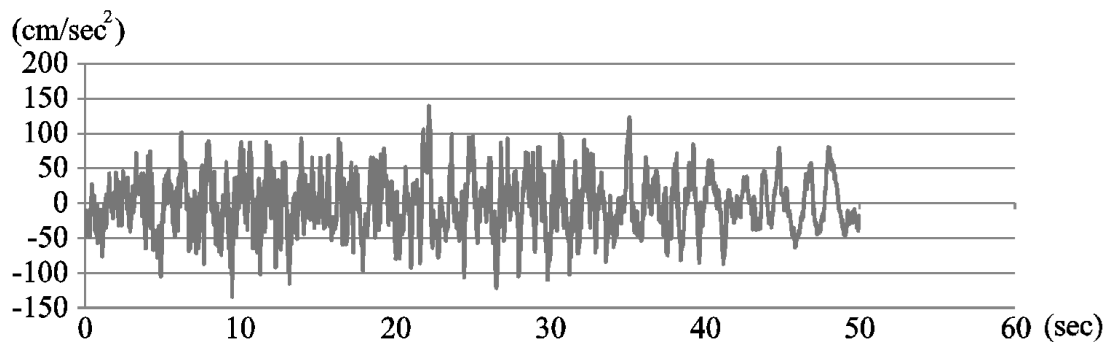


Figure 27. Wave of Japanese seismic specifications

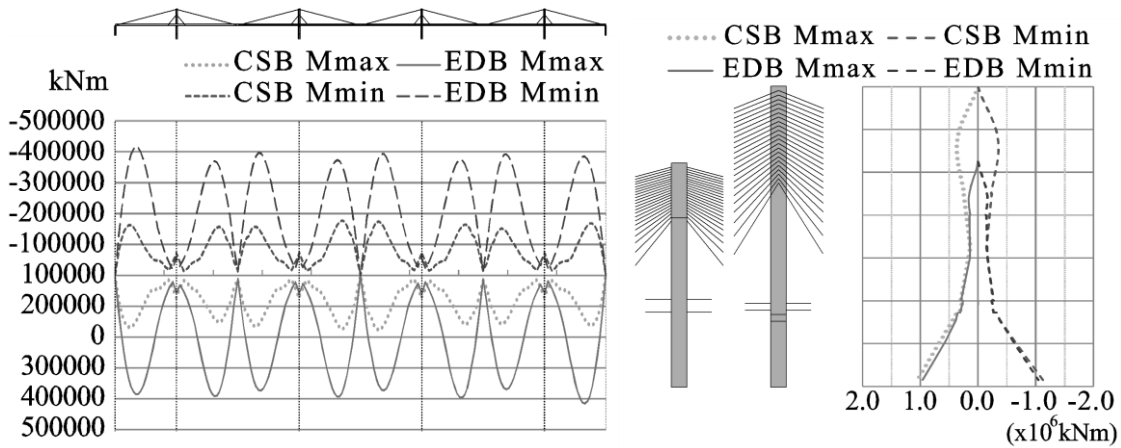


Figure 28. Girder and pylon bending moment

Table 5. Natural Period

	1st	2nd	3rd
CSB	7.92	5.14	4.17
EBD	8.00	5.38	3.99

5 LARGE SPAN HYBRID DESIGN FOR FUTURE GENERATIONS OF BRIDGES

The first idea of hybrid structure in the Brooklyn Bridge which combines the suspension system with the stays to achieve more efficient structural system has been noticed [Gimsing (2016)]. However, these hybrid structures are generally adopted with higher towers, which consequently, the angular change of the main suspension cable at the tower saddle could be larger and causes increasing secondary stress in the main cable to lead the cable becomes more critical in fatigue. Therefore, to deal with the secondary stress in main suspension cable and as well as to enhance the aerodynamic stability of the hybrid structure, the new structural system is developed for a long span concrete box girder bridge which is a hybrid between an extradosed structure and a suspension structure. By applying a deeper girder, the hybrid structure is expected to be stiffer and at the same time, the angular change of the main suspension cable will be smaller due to their short towers.

Furthermore, in order to reduce the weight of the girder, the butterfly web girder in which the webs are replaced by thin panels with a butterfly-wing shaped is adopted. In past studies, butterfly web has an open section of around 30% and can reduce the weight of the superstructure from 10% to 20%. Then its wind resistance is desirable, due to its special openings [Kasuga (2015)], and also maintenance is easier because of brightness in the girder.

As a case study, a hybrid of extradosed and suspension bridge with 800 m span of concrete butterfly web girder is suggested (Figure 29) [Salpisoth et al. (2017)]. The bridge basically consists of a main span 800 m long and effective width of 30 m wide respectively. Stiffening girder is a structural element subjected directly to the live load and transfer the vertical load globally to the main tower through the cable system. For the extradosed bridge, by making the girder deeper, the stiffness of the girder increases so that the load distribution ratio for the cable is smaller and makes the material consumption effectively. The towers are considered to be 100 m in height as well as the girder is set to 7 m deep with 150mm butterfly web.

In a hybrid structure system, some important issues have been raised, such as the discontinuity of the system and how to optimize the span of the extradosed area to achieve an economical efficiency as well. The hybrid systems with three different extradosed-to-span ratios, 79%, 61% and 43% respectively, are examined and investigated their structural behaviors. Herein, the extradosed-to-span ratio is the ratio of extradosed span (L_{ED}) to main span (L). After parametric study, it was confirmed that this new type structure of hybrid bridge is able to be soundly

designed. Moreover, it was found that the system with extradosed-to-span ratio of 61% used the least materials than the other ratios. Table 6 shows the difference between two design methods. Case 1 is the ordinal design method and the rational design method introduced by JPCI is applied to case 3 [JPCI (2000)]. Tremendous reduction of material quantities can be derived because of higher rigidity of concrete structure. Therefore, it is too conservative to apply the ordinal design method to the proposed structure [Uchibori et al. (2018)].

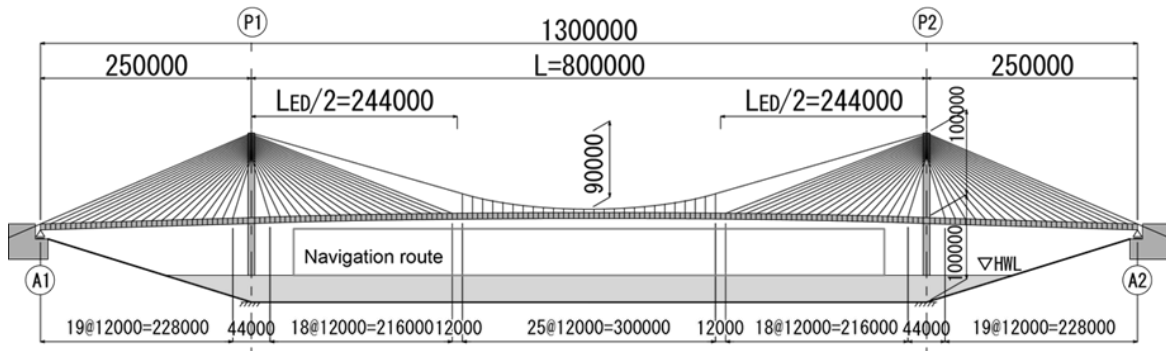


Figure 29. Hybrid of Extradosed and Suspension Bridge with 800m Span

Table 6. Comparison of material quantities (three spans)

	Unit	Case 1	Case 3
Stay Cable	t	2,873	2,536
Main Cable	t	11,170	5,639
Hanger	t	55	29
PC tendon	t	541	505
Total	t	14,639	8,709

6 CONCLUSIONS

The following conclusions could be drawn from this paper.

1. The bridges using a butterfly web presented in this paper are structures that are as lightweight as composite bridges such as corrugated steel web bridges. This gives them a significant advantage in Japan, where earthquakes are frequent. Also, since they do not have the steel members of composite bridges, they are advantageous in terms of maintenance performance. In particular, with the materials used in the butterfly web projects described here, strength is produced by prestressing steel and steel fibers, so there is no need to use reinforcing steel.
2. A design for extradosed bridges with span lengths of the 500 m range is proposed and the structural characteristics on the basis of a comparison with cable-stayed bridges are examined. Studies revealed that a long-span extradosed bridge using butterfly webs is structurally feasible.
3. Use of butterfly webs enables a lighter main girder, making it possible to increase the depth of the girder without increasing weight. This counteracts the larger bending moment of the main girder resulting from shorter main towers, and as there is less stress variation of the stay cables due to live load, it also becomes possible to reduce the factor of safety for the stay cables. The quantities of stay cables is similar to that of a cable-stayed bridge.
4. A bridge of a hybrid between an extradosed bridge and a suspension bridge with a central span of 800m is examined. This study shows the feasibility of rational design involving separate safety factors for individual cables in accordance with variable stress due to live load. And this design method leads to tremendous reduction of material quantities.

REFERENCES

- Ashizuka, K., Miyamoto, K., Kata, K. and Kasuga, A. 2012 Construction of a Butterfly Web Bridge, *Proceedings of fib Symposium Stockholm*.
- Gimsing, N. J. et al. 2012, Cable supported bridges, John-Wiley, West Sussex, UK.
- Homma, A., Kojima, T., Kasuga, A. and Nakatsumi, K. 2015 Design and Construction of Okegawa Viaduct which has precast segmental U-Shaped Butterfly Web Girders, *Proceedings of fib Symposium Copenhagen*.
- JPCI, 2000 *Specifications for Design and Construction of Prestressed Concrete Cable-Stayed Bridges and Extra dosed Bridges*, Japan Prestressed Concrete Institute.
- Kasuga, A., Kata, K., Nakatsumi, K. and Takaki, Y. 2006, New Concept of Composite Bridges, *Proceedings of 2nd fib Congress*.
- Kasuga, A. 2015 Multi-span Extradosed Bridges, *Multi-Span Large Bridges International Conference Porto*.
- Kasuga, A., Nagamoto, N., Kata, K. and Ishii, Y. 2015 Study on 500m span extradosed bridges, *fib Symposium Copenhagen*.
- Kido, T. and Hoshino, Y. 2010 Recent Development of External Tendon System Using Ultra High Strength Prestressing Strand with Epoxy Coating, *3rd fib International Congress, Washington DC*.
- Salpisoth, H. Kasuga, A. Uchibori, H. 2017, Study on the design of an extradosed and suspension hybrid bridge with 800m span of butterfly web girder, *fib Symposium, Maastricht*.
- Samizo, J., Fukuda, M., Kasuga, A. and Mizuno, K. 2015 Design and Construction of the Mukogawa Bridge, *Proceedings of fib Symposium Copenhagen*.
- Uchibori, H. Kasuga, A. Salpisoth, H. 2018 Study on Cable Design Method of an Extradosed and Suspension Hybrid Bridge with 800m Span, *5th fib International Congress, Melbourne*.

Raising the bar in earthquake risk reduction: integrated low-damage building systems to enhance community resilience

Stefano Pampanin¹

¹ University of Rome “La Sapienza, Italy; University of Canterbury, Christchurch, New Zealand

ABSTRACT: The severe socio-economical impact of recent earthquake events have further highlighted, on one hand, the severe mismatch between societal expectations over the reality of seismic performance of modern buildings, while confirming, on the other hand, the crucial need for a coordinated seismic risk reduction plans at a national level.

A paradigm shift in performance-based design criteria and objective towards damage-control or low-damage design philosophy and technologies is urgently required.

In particular, the Canterbury earthquake sequence in 2010-2011 has represented an unfortunate but fundamental trigger for a fundamental step-change in the high-level policy approach as well as in the community awareness and openness towards the implementation of a new and proactive approach for seismic risk reduction.

This paper and associated keynote presentation will provide an overview of recent advances towards the development and implementation of: a) an integrated (skeleton + non-structural elements) low-damage building system and b) a national-wide mandatory long-term program to assess the seismic vulnerability/capacity of the whole building stock and implement adequate retrofit solutions.

1 A PARADIGM SHIFT: FROM LIFE-SAFETY TO LOW-DAMAGE AND LOSSES

The excessive socio-economic impacts of the recent earthquake events in developed countries have clearly and critically highlighted the mismatch between the societal expectations over the reality of engineered buildings' seismic performance.

The engineering concept and code-approach to define an earthquake-resistant building, e.g. a structure capable of sustaining a design level earthquake with extensive (often non-repairable) damage in both structural and non-structural component with the main target being the Life Safety of the occupants, is apparently far from the understanding of the general public who would prefer to talk about an “earthquake-proof” building.

The overall performance of the modern building stock, represented in a schematic in Figure 1 below, where structural, non-structural and soil-structure interactions aspects are summarized, has come with a shocking surprise to the general population.

On one hand, a better communication between technical and non-technical could help clarifying and disclosing to the wide public what are the accepted/targeted performance levels built in a design code, itself to be considered a ‘minimum’ (not a maximum) standard.

On the other hand, the Earthquake Engineering community is challenged with the complex task to **“raise the bar”**, by shifting the targeted performance goals from the typically accepted Life-Safety level, to a more appropriate and needed Damage-Control level (see performance matrix in Figure 2), all this without increasing (significantly) the cost of constructions.

These increased expectations would require a significant **paradigm shift** in terms of performance-based design, which can be accomplished by the development and/or further refinement of design methodologies as well as of high seismic-performance, whilst cost-effective, technologies.

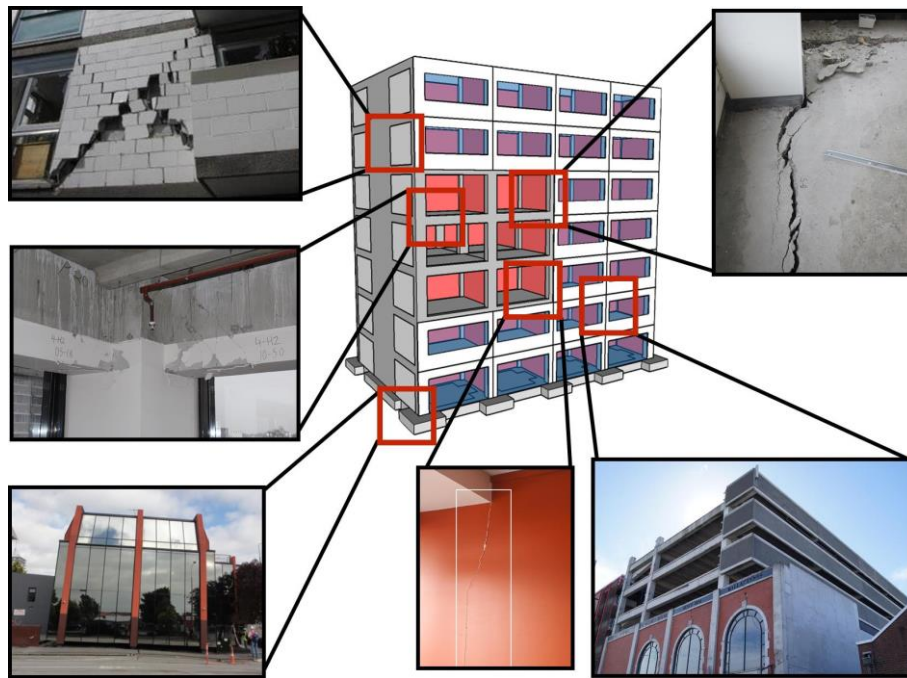


Figure 1. Holistic representation of damage/performance to a modern building, including structural skeleton (frame system, floor diaphragm), non-structural components (lightweight partitions, heavy brick infills and precast concrete facades) and foundation system (significant settlement and residual tilting) (modified after Johnston et al., 2014)

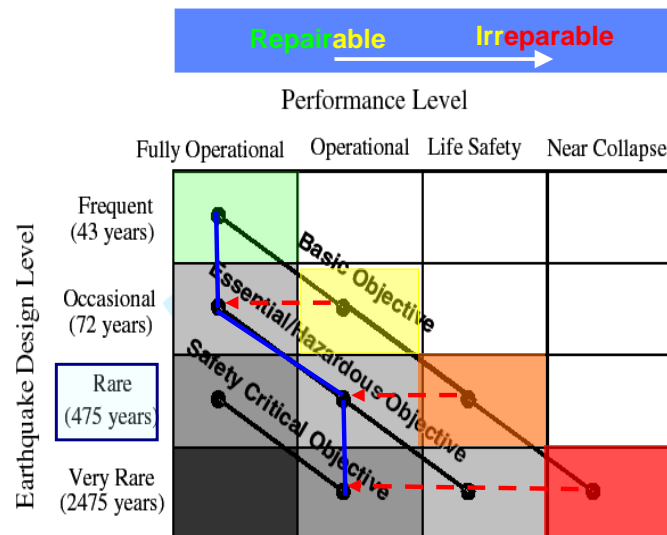


Figure 2. Seismic Performance Design Objective Matrix as defined by SEAOC Vision 2000 PBSE Guidelines, herein rearranged to match building tagging, and proposed/required modification of the Basic-Objective curve towards a damage-control approach (blue line, modified after Pampanin, 2010, Kam et al., 2011)

When considering the existing building stock, the urgency of a medium-long-term plan for seismic retrofit and risk reduction strategy at a national scale is becoming increasingly evident in most of the seismic-prone countries worldwide.

With no doubt the assessment of the seismic vulnerability of existing buildings and the definition of appropriate solutions – i.e. structurally effective, easy to apply, cost-effective, possibly reversible and respectful of the architectural, heritage and cultural conservation requirements – hide a level of significantly higher complexity than designing new structures. Moreover, as if the technical complexity was not a sufficient deterrent, the constraint of economic resources for a national scale implementation and the lack of a prioritization plan based on risk considerations and cost-benefit analyses are often referred to, or blamed as, primary obstacles to the practical implementation of such a bold and ambitious project. Yet, studies and comparative evaluations of the effectiveness of a seismic prevention strategy when opposite to a post-event reaction/repair/reconstruction approach clearly show its long-term and national benefits.

To tackle this delicate issue, it is necessary to improve and standardize the tools and procedures ('protocols') for the 'diagnosis' and 'prognosis' of the seismic vulnerability and of the expected performance of existing buildings. Such procedures should be based on state-of-the-art but simplified methodologies (analytical rather than numerical approaches) that could highlight the structural weaknesses of the building system, while ensuring consistency of results and proper level of independence from the operators. Similarly, suitable "therapeutic pathways" or appropriate retrofit strategies can be defined by comparing alternative options through a cost-benefit approach.

2 ENHANCING COMMUNITY RESILIENCE

Building safer and more resilient communities should be and is eventually being recognized as the overarching goal of risk reduction policies and practices.

The concept of resilience, more commonly used in other disciplines such as psychology, sociology, economics as well as material engineering is generally related to the capacity to "bounce back" within a recovery time after absorbing the impact of an external event (Figure 3). When referring to seismic resilience, the concept is much wider than the evaluation of the seismic response/performance of a single/individual building, through the evaluation of drift/acceleration parameters etc, and yet goes beyond and broader than the evaluation of direct and indirect losses (in accordance to the Performance-Based Earthquake Engineering Framework by Cornell et al.).

A general framework to define, quantitatively measure and enhance the seismic resilience of communities has been recently proposed by Bruneau et al. (2008), in an attempt to support decision makers to assess the progresses made, via alternative top-down or bottom-up practices and policies, towards this ultimate goal of risk reduction. According to Bruneau et al., '*Seismic resilience can be achieved by enhancing the ability of a community's infrastructure (e.g., lifelines, structures) to perform during and after an earthquake, as well as through emergency response and strategies that effectively cope with and contain losses and recovery strategies that enable communities to return to levels of predisaster functioning (or other acceptable levels) as rapidly as possible*'. It becomes evident that targeting a more damage-resistant or impact-resilient built environment, including structures and infrastructures, would represent a key and now more tangible step towards the goal of building community resilience as it would score highly against two out of these three measures of resilience, namely "Reduced Failure Probability" and "Reduced time to Recovery", whilst the "Reduced Consequences" from failures would be more related to the overall structure/infrastructure/organization system and associated intra and inter-dependencies.

Considering the unsustainable socio-economic consequences of the typical "passive" and "reactive" approaches adopted in most seismic-prone countries around the world, a

comprehensive and coordinated national plan for both the new design and the assessment/ retrofit of buildings, structures and infrastructures should become one of the highest government priority.

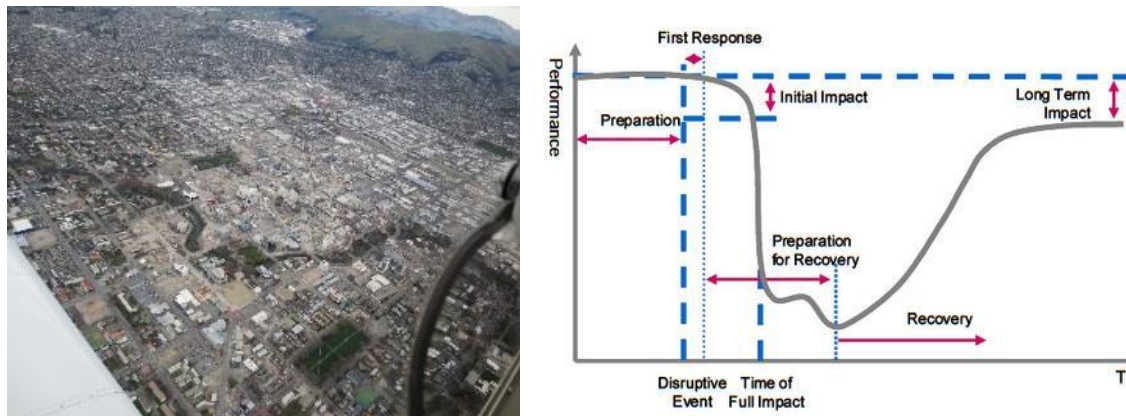


Figure 3. Left: Aerial view of Central Building District (CBD) in Christchurch in the aftermath of the 2010-2011 Earthquake Sequence with entire lots demolished and “cleaned up” (Photo courtesy of Kam Weng and Umut Akguzel); Right: Concept of Resilience (Source: Yossi Sheffi & James B. Rice Jr., MIT Sloan Management Review, 2005)

3 THE NEXT GENERATION OF INTEGRATED LOW-DAMAGE BUILDING SYSTEMS

Within the aforementioned overall framework of risk reduction and enhancement of seismic resilience of community, the next crucial step in performance-based seismic design should more explicitly focus towards the development of an integrated approach, involving, in a holistic view, all aspects of the design framework, design procedures and tools and technological solutions for engineers and stakeholders to control the performance/damage of the building system as a whole, thus including superstructure, non-structural elements and soil/foundation system (Figure 4).

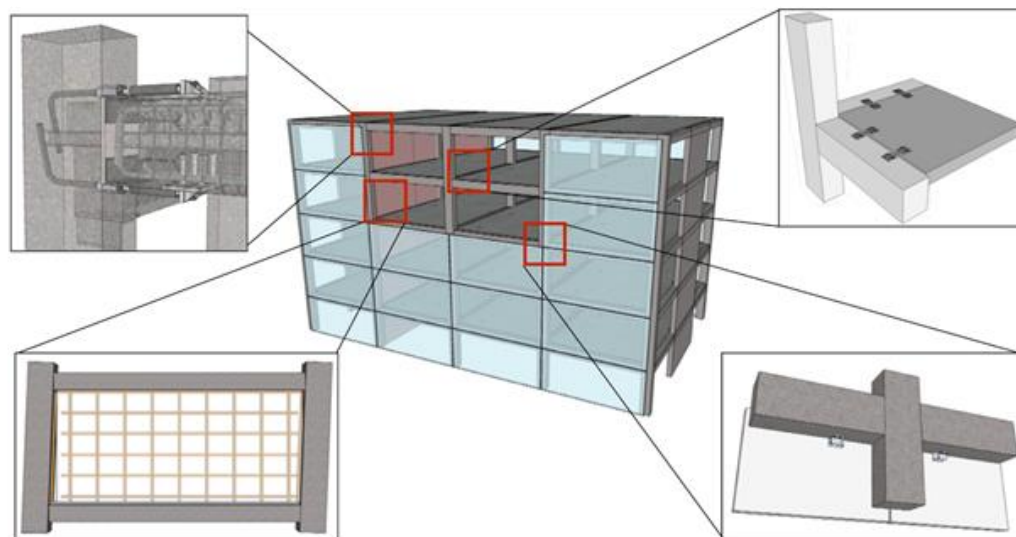


Figure 4. Concept of integrated (structure/skeleton including floor/diaphragms, and non-structural/envelope) low-damage building system (after Johnston et al., 2014)

3.1 A low-damage structural skeleton

In addition to, or better complementary and integrative of, more “traditional” damage-control technology such as base isolation and dissipative braces, which are experiencing a resurgence in New Zealand after the Canterbury earthquake sequence, particular interest is being received by alternative and more recently developed “low-damage” systems, based on (unbonded) post-tensioned rocking & dissipative mechanisms, see Fig. 5, for either concrete, timber and steel

structures (Priestley, 1991, Stanton et al., 1997, Priestley et al., 1999, Pampanin, 2005, Palermo et al., 2006, NZCS, 2010).

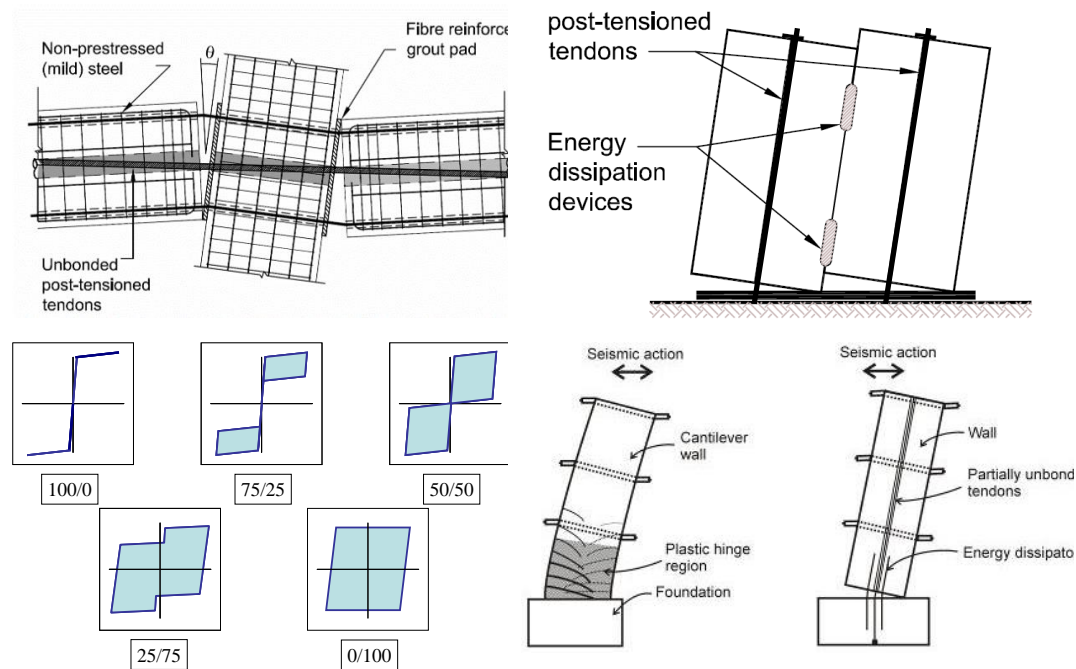


Figure 5. Top: Jointed precast “hybrid” frame and wall connections developed in the US PRESSS-Program (fib, 2003; NZS3101:2006, NZCS2010. Bottom: flag-shape hysteresis loop for a hybrid system when varying the ratio between re-centering vs. dissipative contribution (modified after Nakaki and Stanton 1999) and comparative response of a traditional monolithic system (damage in the plastic hinge and residual deformations) and a jointed precast (hybrid) solution (rocking mechanism with negligible damage and negligible residual deformations, fib, 2003)

During the earthquake shaking, the inelastic demand is accommodated within the connection itself (beam-column, column to foundation or wall-to-foundation critical interface), through the opening and closing of an existing gap. This controlled rocking (dissipative and re-centering) mechanism acts as a fuse or “internal isolation system” with negligible or no damage accumulating in the structural elements, when compared to a traditional “plastic hinge”.

3.1.1 Replaceable fuse-dissipaters: “Plug&Play”

Cost-efficient external and replaceable dissipaters, referred to as “Plug&Play”, for their easy access, inspection and if needed, replacement after an earthquake, have been conceived and developed (Pampanin, 2005; Marriott et al., 2008, NZCS, 2010; Sarti et al., 2013).

They consist for example of axial, tension-compression yielding mild steel short-bar-elements, machined down to the desired “fuse” dimension (thus acting as the “weakest link of the chain” according to capacity design principles) and inserted and grouted (or epoxied) in a steel tube acting as anti-buckling restrainer have been developed and extensively tested within several subassemblies configurations, e.g. beam-column joint connections, wall systems, column (or bridge pier)-to-foundation connections (Fig. 6).

Either metallic and/or other advanced materials (e.g. shape memory alloys, visco-elastic systems) can be used and implemented to provide alternative type of dissipation mechanisms (elasto-plastic due to axial or flexural yielding, friction, visco-elastic). A second generation of self-centering/dissipative high-performance systems, referred to as advanced flag-shape systems (AFS) has been proposed, tested and implemented in real practice (Kam et al., 2006, Marriott et al. 2008, Latham et al., 2013). AFS systems combine alternative forms of displacement-proportional and velocity-proportional energy dissipation (i.e. yielding, friction or viscous

damping) in series and/or in parallel with the main source of re-centering capacity (unbonded post-tensioned tendons, mechanical springs or Shape Memory Alloys (SMA) with super-elastic behaviour). As a result, an enhanced and very robust seismic performance, under either far field and near field events (high velocity pulse) can be achieved, as proven by numerical investigations (Kam et al. 2006) as well as shake table testing (Marriott et al. 2008).

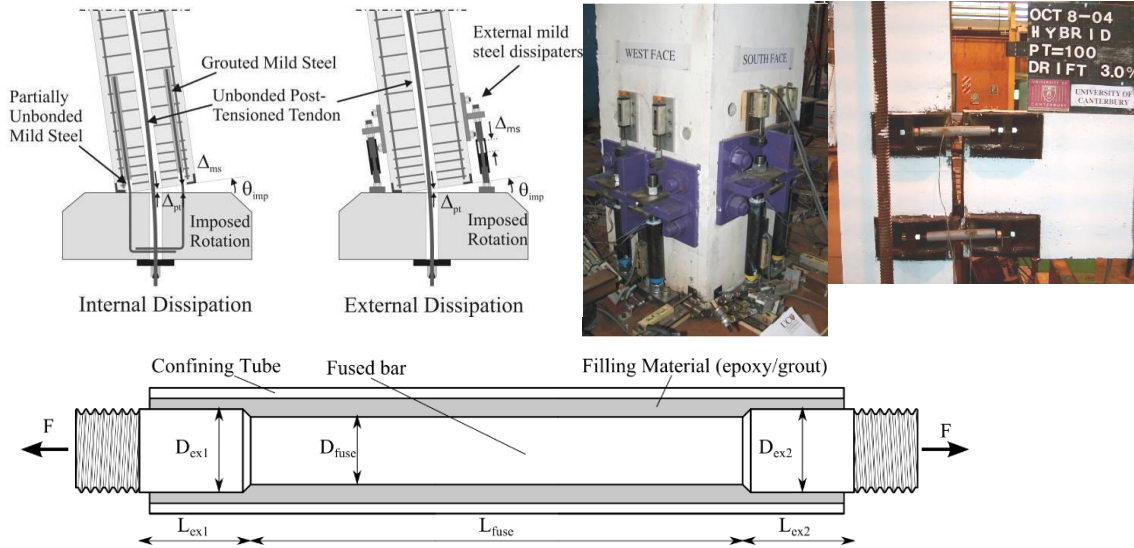


Figure 6. Top: Internal vs. external replaceable (Plug&Play) dissipaters/fuses in a column/pier and beam-column connections (Marriott et al., 2008, 2010) Bottom: Schematic of geometry and element composition (Sarti et al., 2013)

3.2 Low-damage multi-storey timber buildings: the Pres-Lam system

The concept of post-tensioned hybrid (recentering&dissipating) system has been in the past decade successfully extended from precast concrete to timber (engineered wood) frames and walls (Palermo et al., 2005; Pampanin et al., 2006). Since 2004, a series of experimental tests, including quasi-static cyclic, pseudo-dynamic and shake-table, have been carried out on several subassemblies or larger scale structural systems at the University of Canterbury to develop different arrangements of connections for unbonded post-tensioned timber frame and walls (Fig. 7). Any type of engineered wood product such a Laminated Veneer Lumber (LVL), Glulam or Cross-lam (X-lam or CLT) can be adopted as shown by recent experimental tests and numerical analyses on both materials (Smith et al., 2014; Dunbar et al. 2014).

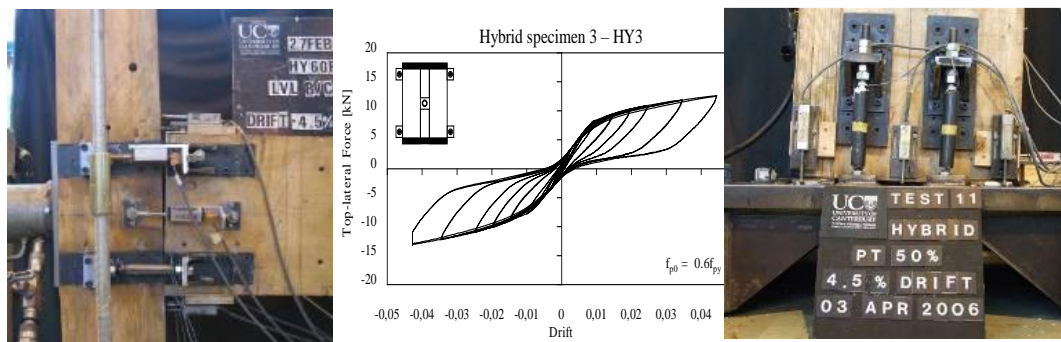


Figure 7 Testing of hybrid post-tensioned timber (Pres-Lam) beam-column joints and column-to-foundation connections (Palermo et al., 2005,2006) and typical flag-shape hysteresis loop.

The extensive experimental and numerical campaign has provided very satisfactory results and confirmation of the high potential of this new construction system, referred to as a Pres-Lam system (acronym for Prestressed Laminated timber) and has opened new opportunities for much greater use of timber and engineered wood products in multi-storey and large buildings, using innovative technologies for creating high quality buildings with large open spaces, excellent living and working environments, and resistance to hazards such as earthquakes, fires and extreme weather events (Buchanan et al., 2009).

3.3 A low-damage diaphragm system: jointed articulated floor

The peculiarity of a jointed ductile connection, consisting of an “articulated” assembly of precast elements can be further exploited and extended to the design of floor-to-lateral-load-resisting-system connections in order to minimize and control the damage to the diaphragms, as observed in recent earthquakes. Alternative innovative solutions have been recently developed and proposed in literature to minimize the damage to the floor system due to displacement incompatibilities with the response of the seismic resisting frame, while guaranteeing a reliable diaphragm action. One proposal, developed from the original concept of discrete X-plate mechanical connectors implemented in the Five-Storey PRESS Building tested at UCSD (Priestley et al., 1999, Fig. 8 left), is based on the concept of an articulated or “jointed” floor system to be combined with precast rocking/dissipative frames (Amaris et al., 2007). The floor (hollowcore in this case) units are connected to the beams by mechanical connectors, acting as shear keys when the floor moves orthogonal to the beam and as sliders when the floor moves parallel to the beam (Fig.8).

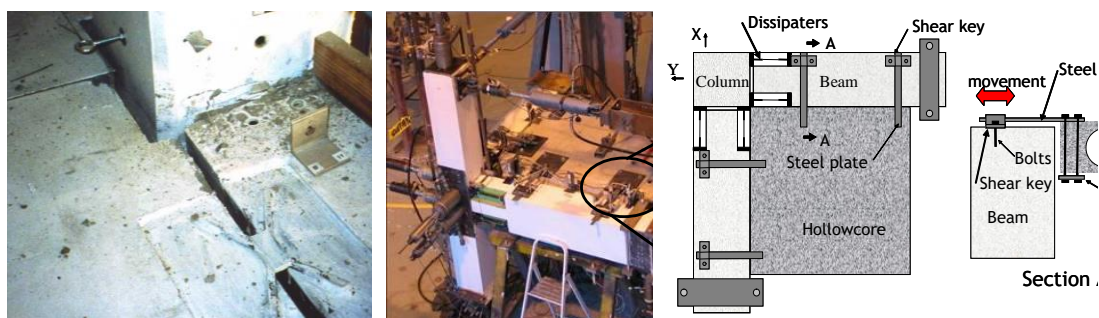


Figure 8. Left: “X-connectors between precast floor (pre-topped double-tee) units and frames as implemented in the PRESS Five Storey Building (Priestley et al., 1999). Centre and right: “Articulated floor” system - concept, connection details (Amaris et al., 2007)

3.4 A low-damage envelope: solutions for non-structural elements

In parallel to the refinements of low-damage structural systems, a substantial effort has been dedicated at the University of Canterbury since 2009 (thus well before the main earthquake event) to the development of low-damage non-structural components (Palermo, Pampanin et al., 2010), with focus on either vertical elements, e.g. infills/partitions (Tasligedik et al., 2012) and façades (Baird et al., 2011), or horizontal, e.g. ceilings (Dhawal et al., 2014).

In the case of infilled walls, either being lightweight partitions (drywalls) or “heavy” concrete or clay brick infills (more typical of the European Construction practice), the conceptual solution for a low-damage system is based once again on the possibility to create an articulated mechanism or jointed system, so to accommodate the interstorey drift demand through a sort of internal rocking mechanism of smaller panels with concentrated inelastic behaviour in few discrete locations, between adjacent panels and between panel and surrounding frame (Figs. 9 and 10). Full details of the experimental campaign and suggested construction details can be found in Tasligedik 2014 and Tasligedik et al., 2015.

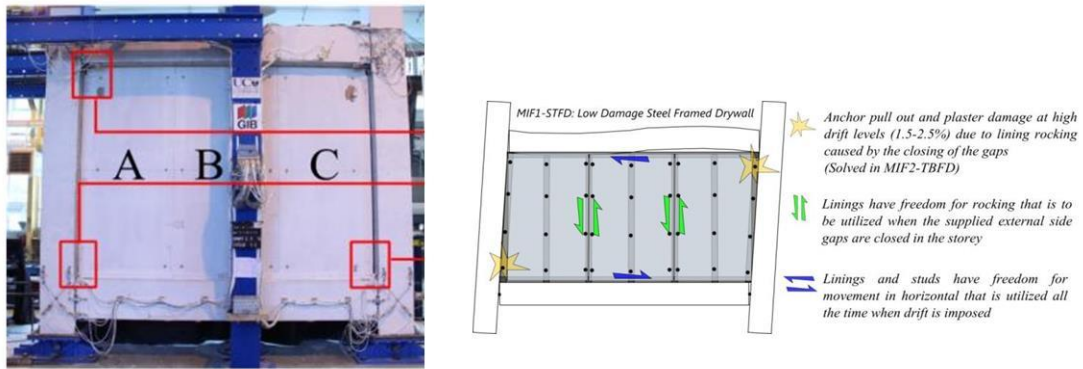


Figure 9. Low-damage solution for infilled walls: general concept (after Tasligedik et al., 2014, 2015)

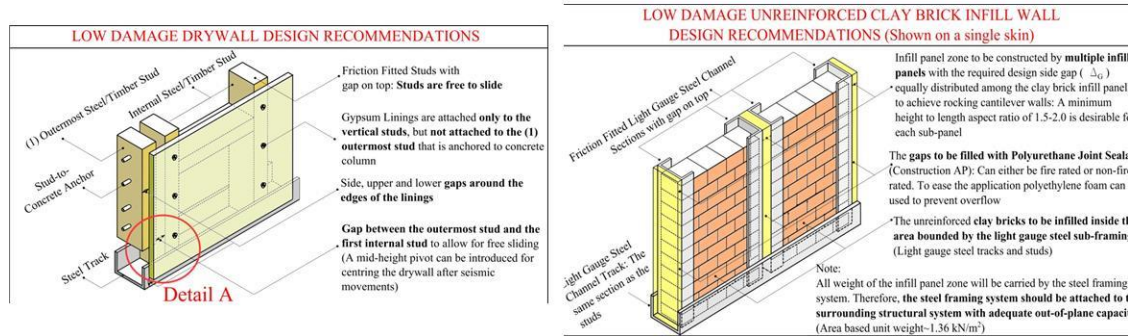


Figure 10. Low-damage solution for infilled walls/partitions: technology details of (after Tasligedik et al., 2014, 2015)

In the case of precast concrete facades/claddings, a number of connection solutions and detailing has been tested, ranging from traditional ones relying upon rods of different length, to slotted-bolted connections, to innovative solution with dissipative U-shape Flexural Plates (Skinner et al, 1972; Priestley et al., 1999), widely adopted in PRESSS or Pres-Lam structures as dissipative coupling systems for rocking walls. The target strategy could be either a full disconnection between the façade and the bare structures or a controlled disconnection with additional dissipation capability provided by ad-hoc designed elements (i.e., UFP). For detailed information the reader is referred to Baird, 2014 and Baird et al. 2014 (Fig. 11).

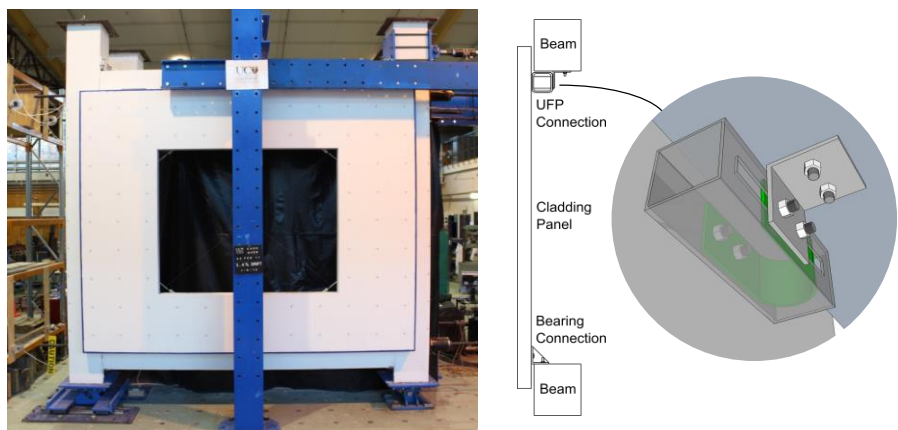


Figure 11 Low-damage solution for precast concrete facades with UFP connectors (after Baird et al., 2014)

4 SHAKE TABLE TESTS ON INTEGRATED LOW-DAMAGE BUILDING SYSTEMS

The next challenge towards the development of an integrated low-damage resisting building system is to investigate the feasibility and seismic performance of a building system prototype combining the aforementioned low-damage solutions for both skeleton and envelope

With this scope, a shake table tests of a two storey, $\frac{1}{2}$ scale, concrete frame building consisting of a post-tensioned rocking hybrid frame and incorporating an articulated floor solution (with U-shape Flexural Plates), low damage drywall infills and façades (Fig. 12) have been carried out at the University of Canterbury (Johnston et al., 2014). The test building was tested under different configurations and subjected to over 400 earthquakes of different intensity levels, with no evident level of structural and non-structural damage.

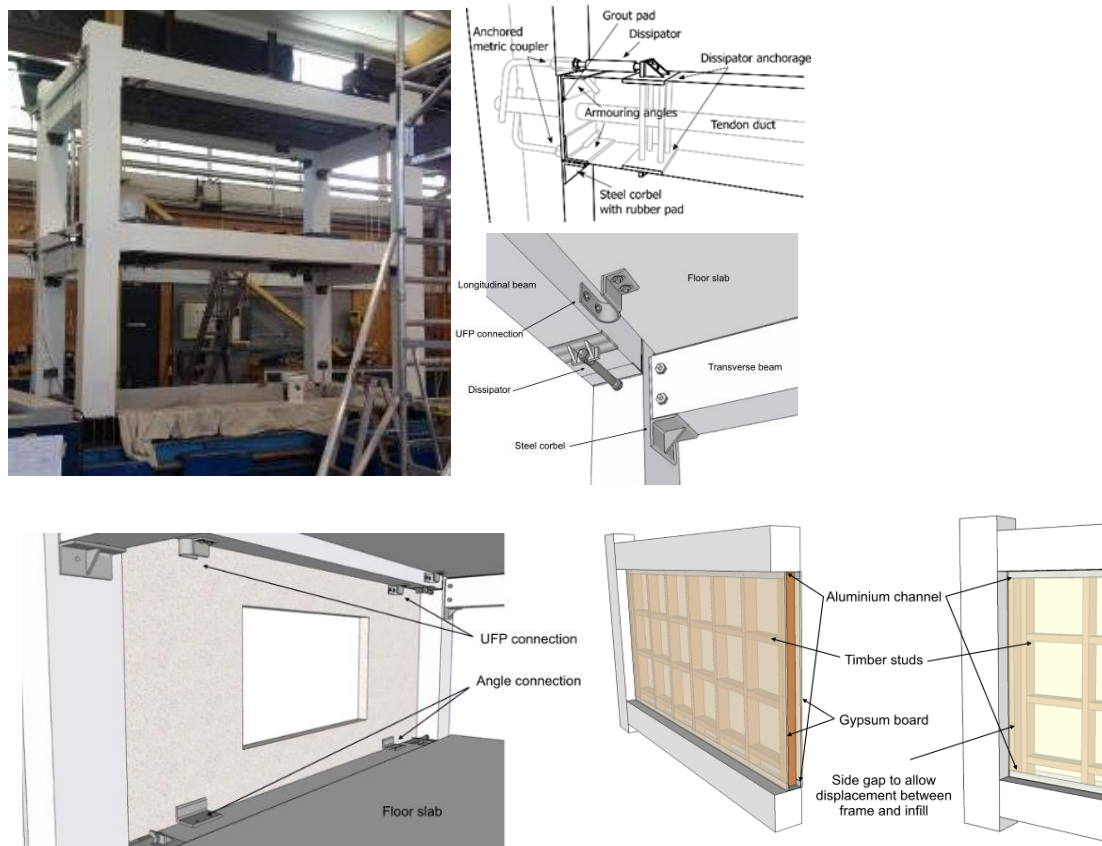


Figure 12. Low-Damage concrete test-building, $\frac{1}{2}$ scale two-storey one-bay, under shake-table tests (after Johnston et al., 2014)

More recently, as part of a Horizon 2020 European-funded project SERA (Seismology and Earthquake Engineering Research Infrastructure Alliance for Europe Project), titled “(Towards the) Ultimate Earthquake proof Building System: development and testing of integrated low-damage technologies for structural and non-structural elements and coordinated by the University of Rome “La Sapienza” (Pampanin et al., 2017), shake table tests on a 1:2 scale two storey building (Fig. 13) implementing an integrated low-damage structural skeleton and envelope are under preparation at the LNEC in Lisbon (testing planned in 2019).

The structural system comprise of unbonded post-tensioned hybrid frames in the longitudinal directions, consisting of precast concrete columns and laminated timber post-tensioned beams, and unbonded post-tensioned rocking-dissipative walls in the transverse direction. Various type of envelope elements (and solutions, either low-damage or traditional) are implemented and will be tested, including glazing, precast concrete, unreinforced masonry, partitions, ceilings.

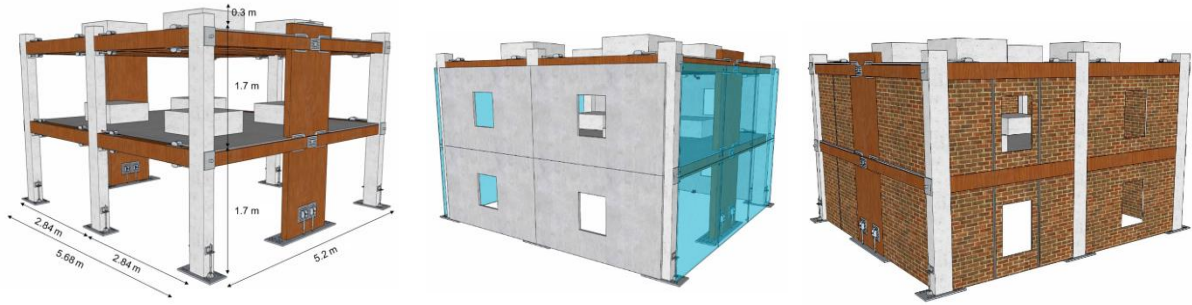


Figure 13. Low-Damage Concrete-Timber Test Building, 1/2 scale two storey two-bays, under shake-table tests at LNEC, Lisbon (SERA Project, Pampanin et al., 2017)

5 SEISMIC LOSS ESTIMATION OF INTEGRATED BUILDING SYSTEMS

A cost/performance-based evaluation of an integrated building systems, implementing either traditional or low-damage technology for the structural skeleton and/or the building envelope has been carried out by Bianchi et al., 2018.

With reference to a five-storey reinforced concrete building prototype three damage-resistant solutions were studied: a) a low-damage building consisting of hybrid post-tensioned dissipative connections with traditional non-structural elements; b) a monolithic structure with low-damage non-structural components; c) an integrated structural/non-structural low-damage system and compared with a traditional cast-in-situ building system (Fig. 14).

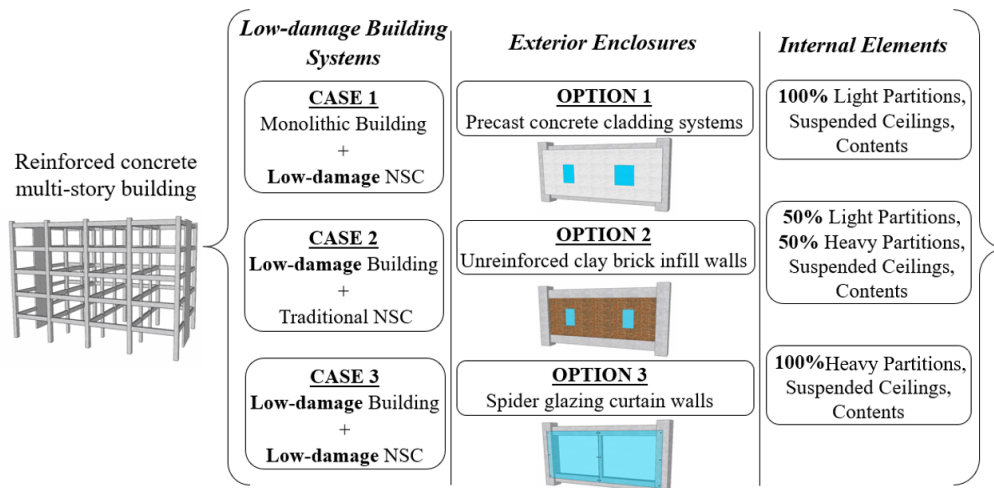


Figure 14. Integrated Building System Configurations (Bianchi et al., 2018)

Non-linear static analyses (pushover) were carried out (and later supported by non-linear time-history analysis) to determine the seismic performance of the building system within Acceleration-displacement Response spectrum domain for different demand intensity levels. Damage states and fragility curves for each component were derived from numerical or experimental data.

The loss assessment analyses, carried out using the tool PACT from FEMA P-58, highlighted the significant benefits - in terms of expected annual losses (EAL) - of adopting an integrated structural/non-structural low-damage system (Fig. 15). Worth noting that, the simple implementation of low-damage non-structural components in combination with traditional structural skeletons, would lead to a considerable reduction of repair costs, especially for heavy infill walls.

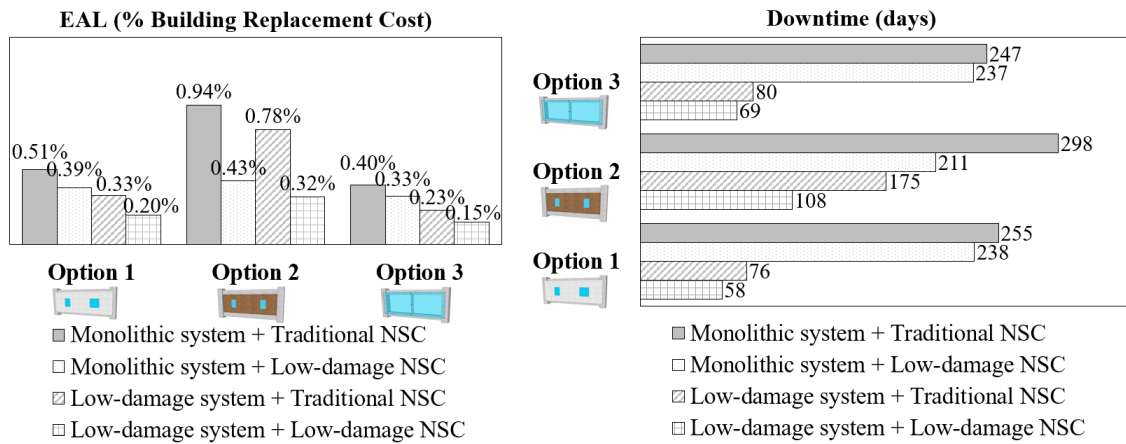


Figure 15. Comparison of Expected Annual Losses (EAL) values and Downtime for the case of Light partitions (Bianchi et al., 2018)

6 INNOVATIVE SOLUTIONS FOR THE NEXT GENERATION OF EARTHQUAKE RESISTANT FASTENERS

Within the context of performance-based design philosophy and damage-control, the enhanced seismic design of fasteners used to anchor non-structural components (NSC) or part of the retrofit strategy (i.e. post-installed anchors) represent a crucial and further step.

Following a comprehensive experimental (shake-table tests) and numerical research campaign, the concept of a new generation of high performance fasteners – referred to as EQ-Rod - capable to guarantee full protection to the connected objects in single and/or multi-storey buildings in seismic regions has been recently proposed in literature (Quintana-Gallo et al., 2018, Fig. 16).

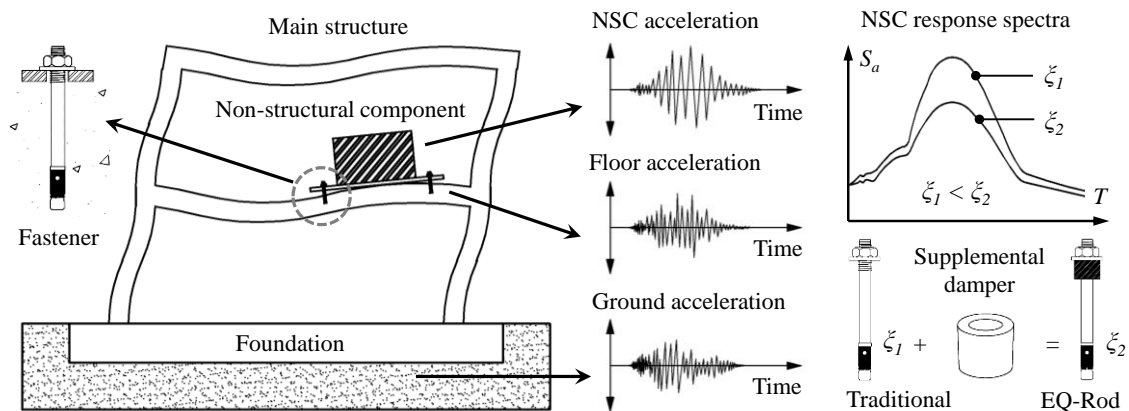


Figure 16. Schematic of demand on fastener & Non-structural Component (Quintana-Gallo et al., 2018)

The innovative solution relies upon the combination of alternative types of supplemental damping, based on viscous and/or hysteretic mechanisms, added to a traditional fastener in series or in parallel, to reduce the acceleration demand to the NSC. The results showed that, in general, the EQ-Rod was able to improve the seismic response of the system when compared to traditional fasteners. The findings indicate that the concept of a dissipative fastener incorporating supplemental damping constitutes a promising solution for higher seismic protection of non-structural elements, thus in line with the overall target of “moving towards an earthquake proof-building”.

7 ON-SITE IMPLEMENTATION OF LOW-DAMAGE BUILDING SYSTEMS

The continuous and rapid developments of jointed ductile connections using PRESSS and PRES-LAM for seismic resisting systems have resulted in a wide range of alternative arrangements currently available to designers and contractors for practical applications. On site implementations have occurred in different seismic-prone countries around the world, e.g. U.S., Central and South America, Europe and New Zealand. Overviews of research and developments, design criteria and examples of on-site implementations can be found for concrete structures in Pampanin et al., (2005) and in the PRESSS Design Handbook (2010). In the following Figures 17-25 a brief overview of implementations in New Zealand of such low-damage structural systems in concrete, timber and steel will be given.



Figure 17. First multi-storey PRESSS-concrete building in New Zealand. Post-tensioned frames with external Plug&Play dissipaters in one direction; Post-tensioned walls coupled with steel beams in the other (Structural Engineers: Dunning Thornton Consultants; Cattanaach and Pampanin, 2008).

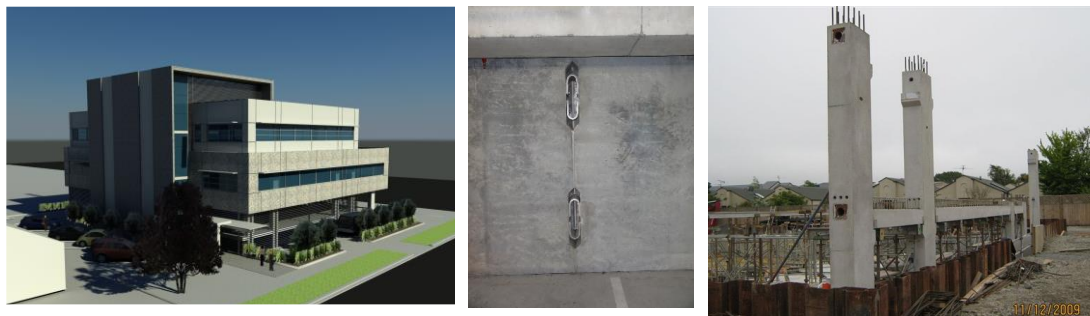


Figure 18. Southern Cross Hospital Endoscopy Building, Christchurc. Post-tensioned frames with internal (top-only) mild steel in one direction: Post-tensioned UFPs coupled walls in the other. Rendering, U-shape Flexural Plate dissipaters and construction of the frame (Structural Engineers: Structex Metro, Pampanin et al., 2011).



Figure 19. Police Station in Rotorua. Post-tensioned concrete (PRESSS) walls with external & replaceable dissipaters in both directions (Structural Engineers: Spiere)



Figure 20. World First Pres-Lam Building. Nelson Marlborough Institute of Technology, (NMIT), Nelson, New Zealand. Post-tensioned timber (Pres-Lam) walls coupled with U-shape Flexural Plates (UFPs) (Structural Engineers Aurecon; Architects Irving-Smith-Jack, Devereux et al., 2011)



Figure 21. College of Creating Arts - MacDiarmid Building, Massey University, Wellington, New Zealand. Post-tensioned timber (Pres-Lam) frames with draped tendons in the transverse directions with horizontal U-Shape flexural plate dissipaters on the first floor and Post-tensioned concrete (PRESSS) walls in the longitudinal direction (Structural Engineers: Dunning Thornton Consultants)



Figure 22. Trimble Building , Christchurch. Two storey office building (more than 6,000m²) consisting of post-tensioned timber (Pres-Lam) frames with external replaceable dissipaters at the beam-column connections and at the column-to-foundation connection and Pres-Lam coupled (with UFP, U-shape Flexural Plates) walls with external dissipaters at the base-connections. (Architecture and Structures by Opus International; Construction by Mainzeal/ City Care)



Figure 23. Merritt Building, Victoria Street, Christchurch. Three Storey commercial Building consisting of Post-tensioned timber (Pres-Lam) frames with Plug&Play external dissipaters in the transverse direction and cast-in-situ reinforced concrete wall in the longitudinal direction. (Structural Engineers: Kirk and Roberts; Architects: Sheppard and Rout)



Figure 24 Former 'St Elmo Courts' Building, Christchurch. Five storey building, combining base-isolation and two-ways post-tensioned frames in the superstructure with timber beams and concrete columns (Architect: Ricky Proko, Structural Engineers: Ruamoko Solutions)

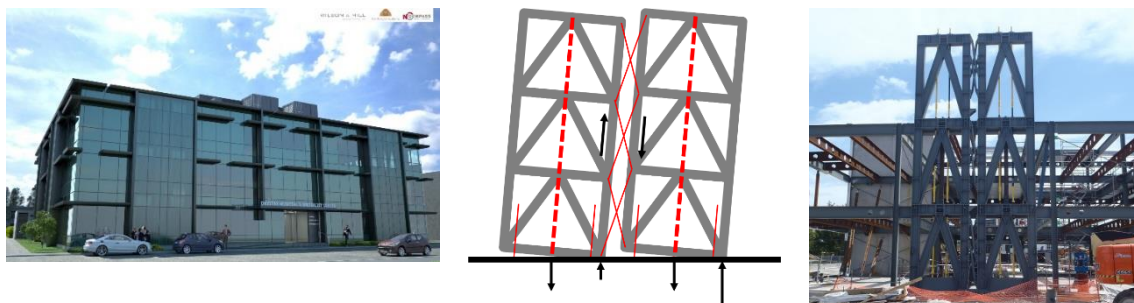


Figure 25. Forté Health Medical Centre, three storey building with over 5000m² of specialist medical facilities. Post-tensioned steel rocking coupled 'walls' (or braced-frames) in both directions, combining hysteretic and viscous dampers in parallel for "an advanced flag-shape" system (World first).

8 THE NEW NATIONAL PLAN FOR SEISMIC RISK REDUCTION IN NEW ZEALAND

In the aftermath of the Canterbury Earthquake Sequence and following the recommendation from the 'Canterbury Earthquake Royal Commission of inquiry' (CERC, 2012), the New Zealand Government decided to radically "change gear" in terms of seismic risk reduction strategies and policies, moving from a "passive" approach to an "active" and mandatory one at a national level.

The Building (Earthquake Prone Buildings) Amendment Act 2016, taking effects from 1 July 2017, introduced major step-changes to the way earthquake prone buildings are identified and managed under the Building Act, under a new national plan for managing buildings in New Zealand. Explicit intent of this national policy framework is to ensure a more consistent and homogeneous approach across the country in the management of the seismic risk for private and

public buildings, trying to achieve a balance e between: 1- Life safety; 2- Cost of strengthening/retrofitting or removing buildings; 3- Considerations on Heritage Buildings

The new Building Act categorises New Zealand into three seismic risk areas- high, medium and low – corresponding to peak ground acceleration, PGA, or Z (seismic coefficient in accordance to the NZS1170.5 Loading Standard) of $PGA < 0.15$; $0.15 \leq PGA < 0.3$; $PGA \geq 0.30$, respectively, as shown in Figure 26. Timeframes are set for each seismic areas for identifying earthquake-prone buildings (seismic assessment, within 5-10-15 years respectively) and taking action on them (retrofit or demolition, 15-25-25 years, respectively). A special category of ‘priority buildings’ is introduced, in high and medium seismic areas, to recognize buildings that are considered higher risk because of their construction, type, use or location. For this category, the timeframe for both assessment and, if need be, remediation is half the time allowed for other buildings in the area.

Important to highlight that the owners should bear the costs for these seismic evaluation and remediation actions. No specific financial incentives, as for example implemented in the recent Italian Guidelines for the classification of the seismic risk (Giovinazzi and Pampanin, 2017), have been introduced at this stage nor are envisaged in the near future for ordinary buildings in New Zealand. Discussions are taking place in some local municipality to address the issue of preservation of heritage buildings, often owned by private people, but with a non-tangible value for the overall community.

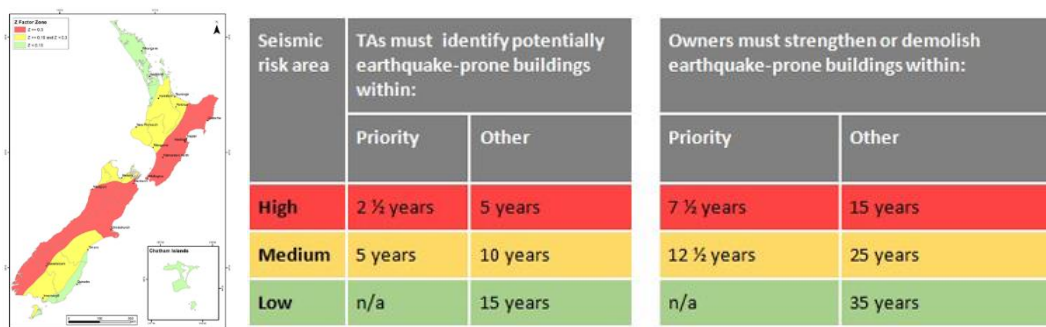


Figure 26. National risk reduction plan in New Zealand (taking effect from 1 July 2017): timeframe for the identification and the remediation (strengthening/retrofit or demolition) of Earthquake Prone Buildings depending on the level of seismicity (low-medium-high seismic areas - $PGA < 0.15g$; $0.15g \leq PGA < 0.3g$; $PGA \geq 0.30g$) – MBIE 2016

8.1 NZSEE2017 Guidelines on seismic assessment of existing buildings

As part of the new national risk reduction plan, the Ministry for Business, Innovation and Economy (MBIE) was in charge of the development of new guidelines for the Seismic Assessment, and Rating, of Existing Buildings, with particular focus on a consistent procedure to be used on a daily based by practitioner engineer and Territorial Authorities (TAs) to identify Earthquake Prone Buildings. Following a major multi-year effort of the selected committee, which actually started in 2014 following the CERC Recommendations, the older version of the NZSEE2006 was significantly rewritten and integrated with the more recent lessons and know-how from earthquake events and the national and international state-of-art and latest research findings. As it stands, the new NZSEE2017 guidelines “The Seismic Assessment of Existing Buildings” represents the key tool for the actual implementation of the national risk reduction plan. An overview of the motivations, scope and methodology can be found in Pampanin, 2017, with design example and numerical studies in Del Vecchio et al., 2017, 2018 and Gentile et al., 2017, respectively.

8.1.1 The SLaMA – Simple Lateral Mechanism Analysis - Methodology

In line with the Park, Paulay and Priestley ‘School’, in the new NZSEE2017 guidelines and specifically at the Detailed Seismic Assessment (DSA) level (Tier 2), particular attention has been given to the development of an advanced, reliable while simplified methodology, referred to as SLaMA (Simple Lateral Mechanism Analysis), based on an analytical and mechanical approach, i.e. basically “by hand” or using a spreadsheet, rather than and prior to a numerical (i.e. finite element and computer-based).

The SLaMA procedure for the assessment of the seismic vulnerability/safety and seismic rating (Fig. 27) develops from the identifications of the expected critical structural weaknesses through the evaluation of:

- Step 1a): the flexural and shear capacity (in terms of both forces and displacements) of the structural elements;
- Step 1b): the hierarchy of strength and sequence of events of the connections and beam-column subassemblies (according to Pampanin et al., 2007)
- Step 1c): the local and global collapse mechanisms of the seismic-resisting systems and, finally, the global capacity curve

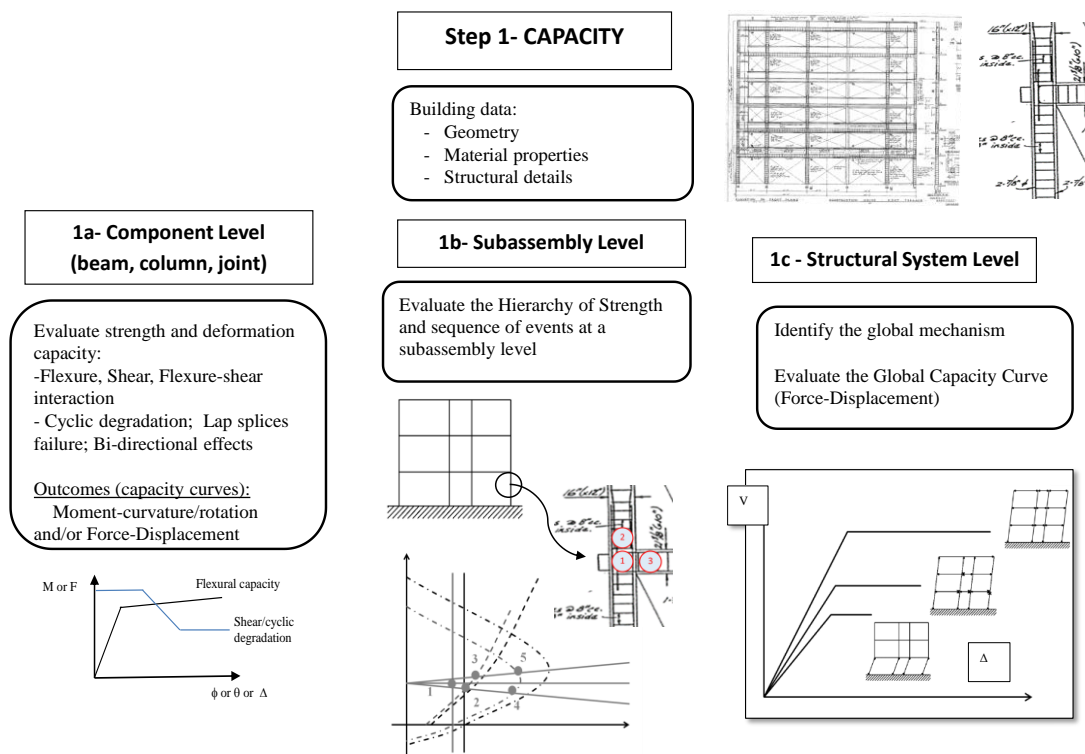


Figure 27. Key steps of the SLaMa analytical procedure according to the NZSEE2017 guidelines (Pampanin, 2017) to derive the capacity curve of a building: 1a) evaluation of the strength and deformation capacity for flexure and shear of structural components; 1b) evaluation of the hierarchy of strength and sequence of events in the beam-column systems and 1c) identification of the global mechanism and evaluation of the global force-displacement capacity curve

By comparing the Capacity curve of the structure (in terms of analytical force-displacement non-linear curve) and the Demand (in terms of acceleration-displacement response spectra, ADRS, in line with the capacity spectrum or similar approaches), the expected performance of the building under different level of shaking intensity (i.e. earthquake return period), can be evaluated with a relatively simple approach and good level of approximations (Fig. 28).

Such an analytical approach allows to evaluate the level of ‘relative’ safety when compared to a newly built structure, by means of the % NBS (New Building Standard, a capacity-demand ratio) index and to associate a seismic risk rating or class (from A to E, with indicative ranges of collapse probabilities when compared to a brand-new structures).

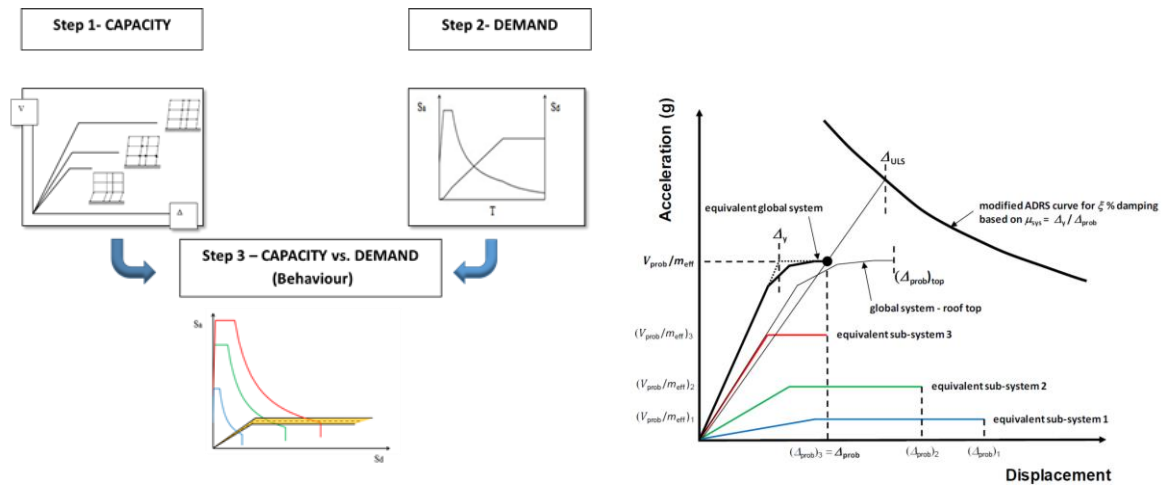


Figure 28. Left: Evaluation of the seismic performance at different level of intensity by intersecting the Capacity (force-displacement) curve with the Demand (ADRS – Acceleration-Displacement Response Spectra). Right: evaluation of the %NBS as Capacity/Demand ratio, (modified after NZSEE2006-2017)

Following the same approach, by intersecting the capacity curve with various intensity levels, the return periods (intensity) corresponding to the exceedance of a given set of limit states (i.e. Operation, Damage Control, Life Safety and Collapse Prevention) can be analytically evaluated, thus defining the Fragility Curves for a given limit state and the Expected Annual Losses.

As demonstrated in a series of analytical-numerical comparisons (Del Vecchio et al., 2017,2018; Gentile et al., 2017), the SLaMa analytical procedure provide quite reliable results, particularly satisfactory if considering the simplicity of the method. Refinement of the results can be obtained by preparing a non-linear numerical lumped plasticity model, ‘informed’ by the hierarchy of strength and local mechanism predicted by SLaMA, and running a pushover analysis.

8.2 Selection of retrofit strategies and techniques

The SLaMa method can be used for a relatively quick (when compared to what required by detailed non-linear pushover end time-history analyses) estimation of the expected behavior and performance of the building (or a class or buildings) before and after a retrofit/strengthening intervention, thus becoming a fundamental supporting tool for the implementation of a medium-long term strategy of seismic-risk reduction at national scale.

In fact, as part of the analytical evaluation of the force-displacement capacity curve of the system, the sequence of local and global mechanisms can be captured, (i.e. what happens at what stage). More specifically, as shown in Figure 29, the values of chord rotation, interstorey drift, (top floor or effective height) displacements corresponding to each event (i.e. achievement of ULS shear or flexure in a beam, column or joint), can be identified and clearly visualized in a Force-Displacement or ADRS domain.

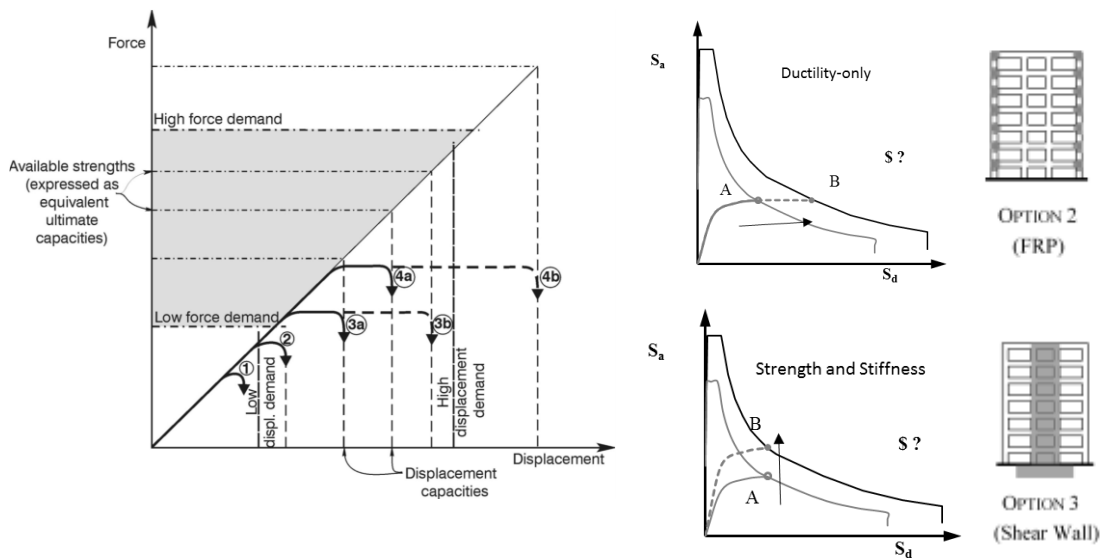


Figure 29. Left: use of SLaMA method to capture the sequence of events/mechanisms within an analytically-derived pushover capacity curve. Right: selection of alternative retrofit strategies and techniques to achieve the targeted performance (Ligabue et al., 2015).

9 CONCLUSIONS

The increased awareness by the general public/tenants, building owners, territorial authorities as well as insurers/reinsurers, of the severe economic impacts in terms of damage/dollars/downtime of moderate-strong earthquakes has indeed stimulated and facilitated the wider acceptance and implementation of cost-efficient damage-control, also referred to as low-damage, technologies in New Zealand, based on concrete, timber, steel or combination of the above material.

From an earthquake engineering community prospective, the challenge is still significant:

- on one hand, maintaining and support this (local and temporary) renewed appetite for seismic protection for both new buildings and existing ones (retrofit);
- on the other hand, pushing towards a wider internationally dissemination and acceptance of damage-resisting technologies according to current best know-how and practice

Somehow the target goal has not changed but the societal expectations (the ‘bar’) are higher and the allowed time frame shorter: to develop, at comparable costs, what the general public would referred to as the “ultimate earthquake-proof” building system (including skeleton, non-structural components/contents and foundation systems) capable as a whole of sustaining the shaking of a severe earthquake basically unscathed, thus structural skeleton, non-structural components/contents and the soil-foundation system.

Similar approach should be used to deal with the existing building stock and promote a national plan for a medium-long term implementation of assessment and retrofit. Extensive effort and resources have been dedicated in the past few decades in the area of seismic assessment and retrofit of existing buildings. Significant advances have been achieved not only in the development of simplified assessment methodology potentially valuable (cost-effective) retrofit techniques along with the estimation through seismic risk analyses of the (possible reduction of) socio-economical impact (losses).

Eight years ago the author wrote (Pampanin, 2010): “*On the negative side, the actual implementation of seismic upgrading intervention at a large scale still appear as an exception than as a practical rule, often being initiated as part post-earthquake repairing reconstruction process rather than as a prevention strategy. The actual lack of immediate financial resources to complete the whole task is too often perceived and considered the main obstacle to justify a*

passive approach (reaction-only). Certainly, and from a different perspective, the implementation, at the higher levels, thus beyond the restricted scientific community, of ad-hoc regulations and incentives capable of enforcing while favouring such actions, based on prioritization strategy within realistic multi-year intervention plans would be most welcome”

In the aftermath of the Canterbury earthquake sequence 2010-2011, significant step-change have occurred in New Zealand with the introduction of a national policy for seismic risk reduction with a mandatory active approach for the seismic assessment and retrofit of the entire building stock within given timeframe.

This paper has provided an overview of the motivations, objectives and, more importantly, the implementation plan of what we hope will be the first of a long list of high-level initiatives in other major seismic prone countries for the mitigation of the seismic risk at international level.

ACKNOWLEDGEMENTS

The research, development and implementation of innovative solutions for low-damage earthquake resistant building, assessment procedures and retrofit strategies described in this paper are the results of the exceptional support and collaborative effort between a great number of individuals and organizations from academia, the wider industry, governmental and funding agencies, at national and international level, a list of whom would be practically impossible to prepare. Nevertheless, the author wishes to acknowledge and sincerely thank all those involved in this extended and extraordinary “research team”. The financial support provided by the Foundation of Research, Science and Technology (FRST) and by the Natural Hazard Research Platform through a series of projects, e.g. Retrofit Solutions, “SAFER Concrete Technologies and “Advancements in Engineering Guidelines and Standards” and by the research Consortium STIC (Structural Timber Innovation Company) Ltd, is gratefully acknowledged.

REFERENCES

- Akguzel, U. and Pampanin, S., 2012. Assessment and Design Procedure for the Seismic Retrofit of Reinforced Concrete Beam-Column Joints using FRP Composite Materials. *ASCE Journal of Composites for Construction*, vol. 16, p. 21-34, doi: 10.1061/(ASCE)CC.1943-5614.0000242
- Amaris, A.D., Pampanin, S., Bull, D.K., Carr, A.J., 2008 Solutions to control and minimize floor damage in precast concrete buildings under severe earthquake loading, NZ Concrete Industry Conference, Rotorua, 2-4 October
- Baird, A., Tasligedik, A., S., Palermo, A., Pampanin, S., 2014 “Seismic Performance of Vertical Non-Structural Components in the 22nd February 2011 Christchurch Earthquake”
- Bianchi, S., Ciurlanti, J., Pampanin, S., 2018 A Cost/Performance-Based Evaluation of Low-Damage Building Systems, 16th European Conference of Earthquake Engineering, Thessaloniki, 18-21 June
- Buchanan, A.H., Pampanin, S., Newcombe, M., Palermo, A., (2009) “Non-Conventional Multi-Storey Timber Buildings using post-tensioning”, 11th International Conference on Non-Conventional Materials and Technologies (NOCMAT), 6-9 Sept, University of Bath
- Building Act 2004. Department of Building and Housing-Te Tari Kaupapa Whare, *Ministry of Economic Development*, New Zealand Government, Wellington, New Zealand.
- Brown, A., Lester, J., Pampanin, S., Pietra, D. 2012. Rebuilding Timber Navigation’s Offices using a Damage-Limiting Seismic System, World Conference on Timber Engineering, Quebec City
- Cattanach A., and Pampanin, S., 2008. 21st Century Precast: the Detailing and Manufacture of NZ's First Multi-Storey PRESSS-Building, NZ Concrete Industry Conf., Rotorua
- CERC, 2012 Canterbury Earthquake Royal Commission, <http://canterbury.royalcommission.govt.nz>.
- Del Vecchio, C., Gentile, R., Pampanin, S., 2017. The Simple Lateral Mechanism Analysis (SLaMA) for the seismic performance assessment of a case study building damaged in the 2011 Christchurch earthquake. University of Canterbury Department of Civil and Natural Resources Engineering, *Research Report 2016-02*, New Zealand, ISSN 1172-9511
- Del Vecchio, C., Gentile, R., Di Ludovico, M., Uva, G., Pampanin, S., 2018, Implementation and Validation of the Simple Lateral Mechanism Analysis (SLaMA) for the Seismic Performance

- Assessment of a Damaged Case Study Building, *Journal of Earthquake Engineering*, doi/full/10.1080/13632469.2018.1483278
- Devereux, C.P., Holden, T.J., Buchanan, A.H., Pampanin, S., 2011. NMIT Arts & Media Building - Damage Mitigation Using Post-tensioned Timber Walls, *Proceedings of the Ninth Pacific Conference on Earthquake Engineering*, "Building an Earthquake-Resilient Society", 14-16 April, Auckland, New Zealand, paper 90
- Dhakal, R.P., Pampanin, S., Palermo, A., MacRae, G., Pourali, A., Tasligedik, S., Yeow, T., Baird, A., 2014. Seismic Performance of Non-Structural Components and Contents in Buildings: An Overview of NZ Research, *International Workshop in Non-Structural Element*, China, Sept
- Dunbar, A., Moroder, D., Pampanin, S., Buchanan, A., 2014. Timber Core-Walls for Lateral Load resistance of Multi-storey Timber Buildings, *World Conference of Timber Engin.*, Quebec City
- Earthquake Engineering Research Institute (EERI) – 2014. 2010-2011 Canterbury Earthquake Sequence Special Issue, *Earthquake Spectra* Vol. 30 (1)
- fib*, 2003, International Federation for Structural Concrete. *Seismic Design of Precast Concrete Building Structures*. Bulletin No. 27, Lausanne, 254 pp.
- Gentile, R., Del Vecchio, C., Uva, G., Pampanin, S., 2017. Seismic Assessment of A RC Case Study Building Using the Simple Lateral Mechanism Analysis, SLaMA, Method, *Proceedings of Computational Methods in Structural Dynamics and Earthquake Engineering, Compdyn 2017*, Rhodes Island, Greece, 15-17 June
- Giovinazzi S., Pampanin, S., Lagomarsino, S. 2006, Vulnerability Models and Damage Scenarios for Pre-1970 R.C. Buildings Before and After Alternative Retrofit Strategies, *Proceedings of the 1st European Conference in Earthquake Engineering and Seismology (ECEES)*, Geneva, Switzerland, Sept 3-8
- Giovinazzi, S., Pampanin, S., 2017, Simplified Approaches for the Seismic Risk Rating of Reinforced Concrete Buildings and the Selection of Retrofit Strategies, XVII ANIDIS, Italian Association for Earthquake Engineering, Pistoia, 17-22 Sept
- Johnston, H., Watson, C., Pampanin, S., Palermo, A., 2014. Shake Table Testing of an Integrated Low Damage Building System, *2nd European Conference in Earthquake Engineering and Seismology*, Istanbul 25-29 Aug
- Kam W.Y., Pampanin S., Palermo A., Carr A. 2010. Self-centering structural systems with combination of hysteretic and viscous energy dissipations. *EESD*. Aug 2010; 39:10, 1083-1108.
- Kam, W.Y., Pampanin, S., Elwood, K., 2011. Seismic Performance of Reinforced Concrete Buildings in the 22 February Christchurch (Lyttleton) Earthquake, Special Issue, *Bulletin of the New Zealand Society of Earthquake Engineering*, Vol. 44(4), 239-279, ISSN 1174-9875
- Kelly, J. M., Skinner, R. I. and Heine, A. J., 1972. "Mechanisms of energy absorption in special devices for use in earthquake resistant structures. *Bulletin of NZSEE*, 5(3), 63-88.
- Kurama, Y. C., 2001. Seismic Design of Unbonded Post-Tensioned Precast Concrete Walls with Supplementary Viscous Damping. *ACI Structural Journal*, 97(4): 648-658.
- Kurama, Y. and Shen, Q., 2004. Posttensioned hybrid coupled walls under lateral loads." *Journal of Structural Engineering ASCE*, 130(2), 2004, 297-309.
- Ligabue, V., Savoia, M., Pampanin, S., 2015. Repairing/Retrofitting vs. Replacing? Evaluating the Cost-Effectiveness of alternative options to support decision making, *NZSEE Conference*, Rotorua
- Marriott, D., Pampanin, S., Palermo A., 2008 Quasi-static and Pseudo-Dynamic testing of Unbonded Post-tensioned Rocking Bridge Piers with External Replaceable Dissipaters, *Earthquake Engineering and Structural Dynamics*, 38(3):331-354, March
- Marriott, D., Pampanin, S., Bull, D., Palermo A., 2008. Dynamic Testing of Precast, Post-Tensioned Rocking Wall Systems with Alternative Dissipating Solutions, *Bulletin of the NZ Society for Earthquake Engineering*, 41(2): 90-103
- MBIE, 2016 – Building (Earthquake prone Buildings) Amendment Act, 2016, Ministry of Business, Innovation and Employment, NZ. *Portal 'Managing Earthquake Prone Buildings'*, <https://www.building.govt.nz/managing-buildings/managing-earthquake-prone-buildings/>
- NZCS, 2010 "PRESSSS Deign Handbook" (Editor: S. Pampanin), NZ Concrete Society, Wellington
- NZSEE 2006. Assessment and Improvement of the Seismic Performance of Existing Buildings, *New Zealand Society of Earthquake Engineering*, Wellington, <http://www.nzsee.org.nz/publications/assessment-and-improvement-of-the-structural-performance-of-buildings-in-earthquake/>
- New Zealand Society for Earthquake Engineering (NZSEE), 2011. Special Issue on the Christchurch Earthquake 22 February 2011, *NZSEE Bulletin* B44 (4)

- NZSEE 2017. The Seismic Assessment of Existing Buildings (the Guidelines), New Zealand Society of Earthquake Engineering, Wellington, Version October 2016, <http://www.eq-assess.org.nz/>
- Palermo, A., Pampanin, S., Buchanan, A.H., and Newcombe, M.P., 2005. Seismic Design of Multi-storey Buildings using Laminated Veneer Lumber (LVL), Proceedings, New Zealand Society for Earthquake Engineering Conference, Wairakei.
- Palermo, A., Pampanin, S., Buchanan, A., 2006. Experimental Investigations on LVL Seismic Resistant Wall and Frame Subassemblies, 1st ECEES, Geneva, Sept 3-8, paper n. 983.
- Pampanin, S., Pagani, C., Zambelli, S., 2004. Cable-stayed and suspended post-tensioned solutions for precast concrete frames: The Brooklyn System. NZ Concrete Industry Conference, Queenstown
- Pampanin S., (2005). Emerging Solutions for High Seismic Performance of Precast -Prestressed Concrete Buildings, *J. of Advanced Concrete Technology*, invited paper, 3(2), 202-222.
- Pampanin, 2009. Alternative Performance-Based Retrofit Strategies and Solutions for Existing R.C. Buildings, *Chapter 13, Book "Seismic Risk Assessment and Retrofitting - with special emphasis on existing low rise structures"* - (Editors: A. Ilki, F. Karadogan, S. Pala and E. Yuksel) Publisher Springer, pp. 267-295
- Pampanin, S., 2012. Reality-check and Renewed challenges in Earthquake Engineering: Implementing low-damage structural Systems – from theory to practice, *Bulletin of the New Zealand Society for Earthquake Engineering*, 45(4), pp. 137-160, December, ISSN 1174-9875, Keynote Lecture at the 12th World Conference on Earthquake Engineering, Lisbon 2012.
- Pampanin, S., Palermo, A., Buchanan, A.H., Fragiacommo, M., Deam, B.L. 2006. Code Provisions for Seismic Design of Multi-Storey Post-tensioned Timber Buildings, CIB W18, Florence, August
- Pampanin, S., Kam W., Haverland, G., Gardiner, S., 2011. Expectation Meets Reality: Seismic Performance of Post-Tensioned Precast Concrete Southern Cross Endoscopy Building During the 22nd Feb 2011 Christchurch Earthquake, NZ Concrete Industry Conference, Rotorua, August
- Pampanin, S., 2012. Reality-check and Renewed challenges in Earthquake Engineering: Implementing low-damage structural Systems – from theory to practice, *Bulletin of the New Zealand Society for Earthquake Engineering*, 45(4), pp. 137-160, December, ISSN 1174-9875
- Pampanin, S., 2017 Towards the practical implementation of performance-based assessment and retrofit strategies for RC buildings: challenges and solutions, SMAR2017- Fourth conference on Smart Monitoring, Assessment and Rehabilitation of Structures, Keynote Lecture, 13-15 Sept, Zurich, Switzerland
- Priestley, M.J.N., 1991. Overview of the PRESSS Research Programme, *PCI Journal*, 36(4), pp.50-57.
- Priestley, 1996. The PRESSS Program Current Status and Proposed Plans for Phase III, *PCI Journal*, Vol. 41, No. 2, pp. 22-40
- Priestley, M. J. N., Sritharan, S., Conley, J. R. and Pampanin, S., 1999. Preliminary results and conclusions from the PRESSS five-story precast concrete test building. *PCI Journal*, 44(6), 42-67.
- Quintana Gallo, P., Moghaddasi, M., Pampanin, S., Bergemeister, K., 2018, Shake Table Tests of Post-Installed Anchors with Supplemental Damping, *ACI Structural Journal* 115(3)- 595-606.
- Sarti, F., Smith, T., Palermo, A., Pampanin, S. Bonardi, D., Carradine, D.M. 2013. Experimental and analytical study of replaceable Buckling-Restrained Fused-type (BRF) mild steel dissipaters, NZSEE Conference, Wellington, 26-28 April
- SEAOC Vision 2000 Committee, 1995. Performance-Based Seismic Engineering, Structural Engineers Association of California, Sacramento, California.
- Smith, T., Pampanin, S., Buchanan M., 2009. Post-tensioned timber building, construction, costs and business case study, ANIDIS Bologna 28 June – 2 July

Fastenings in seismic environment

Ulrich Bourgund¹, Roberto Piccinin²

¹ Hilti Corporation, Schaan, Liechtenstein

² Hilti Corporation, Schaan, Liechtenstein

ABSTRACT: Seismic events can occur almost anywhere in the world and, thanks to the increased number of seismic stations, many more are reported nowadays than in the past. While this is related to the improvement in instrumentation rather than an increase in the number of events, earthquakes represent a continuous threat when considering the high correlation between population density and seismic hazard. Engineers around the world try to cope with this reality by developing and providing adequate solutions to overcome or prevent, when possible, the problems related to structural and nonstructural seismic-related failures. Part of their daily struggles is a proper seismic design of cast-in and post-installed anchors for structural and nonstructural applications. Failure of anchors, in fact, is reflected not only in risk to life safety, but on property loss and business interruption as well.

Avoiding (or limiting) anchor failures means providing a complete fastening solution that encompasses the use of proper products and ends with on-site testing, passing through proper drilling, anchor selection, anchor qualification and assessment, proper design (and software), and proper installation training.

The intent of this paper is to highlight the importance of safe fastening solutions and the key role that research and, ultimately, proper product qualification and design requirements play in their development.

1 INTRODUCTION

Over the centuries, cities and countries around the World have been struck by earthquakes and seismic-related events (e.g., tsunamis, landslides, land liquefaction, etc.). In many cases, multiple events have occurred in the same area with a certain frequency (e.g., California, Italy, Japan, Mexico, Chile, China, New Zealand, etc.). It was in 1992 that the United Nations International Decade for Natural Disaster Reduction (UN/IDNDR) launched the Global Seismic Hazard Assessment Program (GSHAP) to provide evidence of the impacts and risks associated with earthquakes in our daily lives. In addition to this, the fact that high population densities are combined with areas of high seismic hazards magnifies the potential impact of future events.

Besides the high likelihood of loss of lives, higher risk of seismic exposure means higher exposure to potential damage to buildings and structures, nonstructural systems and components, equipment, anchorages, etc. The three fundamental consequences of seismic-related structural and nonstructural damage are (1) deaths or casualties (risk to life safety), (2) property loss (direct economic impact), and (3) business interruption (downtime).

High risk and population density are, however, not the only factor to influence the scale of impact of a seismic event. Other important factors are the magnitude of the event, its recurrence and frequency, and the state of development of a country. While this last factor might be considered controversial, it is obvious that using proper building and construction materials and products, and, above all, having good quality building codes and regulations in place could help reducing

the impact of seismic events and allow, potentially, faster recovery or no need for recovery (the so-called resilience of structural and nonstructural systems that is nowadays pursued worldwide).

2 FASTENINGS

An essential component of building and construction products is represented by fastenings used to connect different building components. Nowadays, two are the main fastening methods commonly used in construction: cast-in place and post-installed systems.

While cast-in place connections have been used widely in the past and have the advantage to be accommodated in the design of the (reinforced) concrete members because the location of the anticipated external loads is known, post-installed anchors have become very popular in recent years because of their flexibility of installation and use, the possibility of being installed in locations different than the ones originally planned, and their versatility in performance (e.g., static loading, seismic loading, sustained loading, high temperatures, low temperatures, etc.).

Post-installed anchors are typically used to connect steel elements to existing concrete members and can be classified as mechanical anchors and bonded anchors. Mechanical anchors are placed into pre-drilled holes and anchored within the concrete by mechanical means. They can be classified based on their functioning principle as displacement-controlled expansion anchors, torque-controlled expansion anchors, undercut anchors, and screw anchors).

Bonded anchors consist of steel elements (e.g., threaded rods, rebars, etc.) inserted into pre-drilled holes filled with resin (typically, epoxy-, polyester-, vinylester-based) and anchored within the concrete by bond or adhesion. In general, these products can be classified as capsule systems (glass capsules, foil pouch) or injection systems (cartridges, bulk).

Post-installed anchors are broadly used or considered as an optimal solution by structural engineers, contractors, and installers worldwide.

Applications involving post-installed anchors can be classified in structural and non-structural applications. Typical structural applications are represented by connections between steel beams/columns to concrete (e.g., retrofitting of braced frames, shear collectors) as shown in Figure 1(a).

Beyond post-installed anchors, a very common solution for structural applications are post-installed rebars. In this case, the connection is between two concrete members, one existing and one cast at a later stage. Post-installed rebars are installed similarly to bonded anchors (rebars in pre-drilled holes filled with resin), but are required to be designed as structural reinforcing bars (e.g., reinforced concrete design) and not as anchors. Typical applications with post-installed rebars are, for example, concrete-to-concrete beam-to-column connections, column-to-foundation connections, or wall-extensions as shown in Figure 1(b).

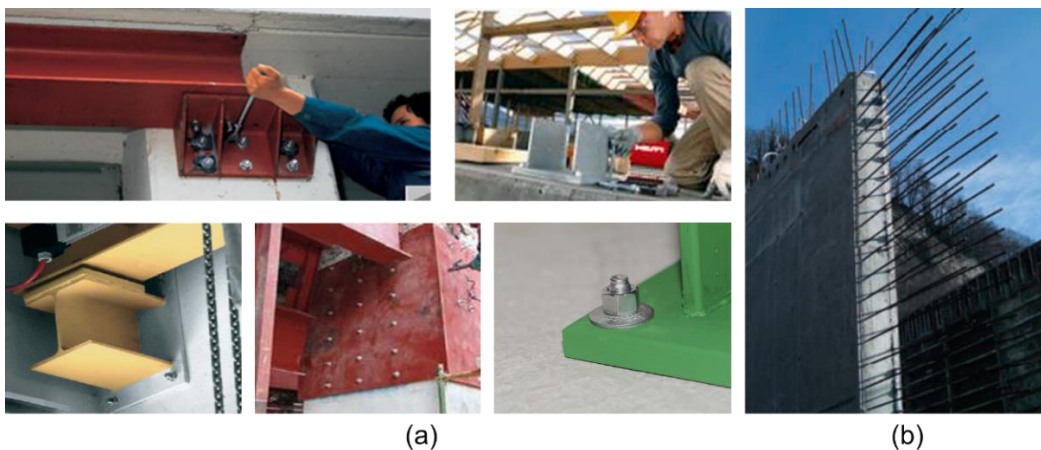


Figure 1. Typical structural applications for (a) post-installed anchors, and (b) post-installed rebars

Nonstructural applications represent about 70% of the applications involving the use of post-installed anchors and can span from anchorage of pipe hanging and sprinkler systems, facades, elevator rails, cabinets and racks, electric equipment, traffic signs, balconies, stairs, etc. Only a few examples can be provided here and are shown in Figure 2.



Figure 2. Examples on anchorage of nonstructural components applications

When consider the broad use of post-installed anchor connections, the correlation with seismic hazard and possibility of failures is inevitable. In fact, because of their critical function, failures of post-installed anchors or rebars and the elements that they are used in conjunction with have typically a significant impact in one of the three key dimensions mentioned above: deaths or casualties, property loss, and downtime. Figure 3 shows some of the failures related to anchorage of nonstructural components after seismic events.

It has to be noted that failures of structural and nonstructural components or connections can occur under static or quasi-static loading conditions as well (not necessarily under seismic loads, that is). Among many cases, the very well-known “big dig” (Boston) and the Sasago tunnel (Japan) failures are still impressed in the memory of engineers and the community.

This is to highlight the fact that safe fastening solutions are not something to take lightly and are related to the product performance but, more importantly, to the proper product selection, proper design assumption, correct installation, etc.



Figure 3. Examples on anchor failures (nonstructural)

3 THE KEY ELEMENTS OF SAFE FASTENINGS

Post-installed fastening in concrete is a relatively young discipline in civil and structural engineering and, while now provisions are going to be included in design and building codes, engineers rely heavily on product-specific guidelines, product qualification, and product-specific approvals. Given the large spectrum of products available and the variety of applications they could be used for, manufacturers and engineers are confronted with their daily (or continuous) task to balance between safety and economics. In the European Community, in the U.S., and in other countries around the world, this balance is provided by (1) proper testing and assessment of product performance, and (2) proper selection and design of the product.

Overall, the key elements of a safe fastening solution are provided by a full set of key elements: drilling hardware, anchor hardware, installation instructions, third party and product evaluation/assessment, proper design method and software, installation training, and onsite testing (Figure 4).



Figure 4. Key elements required to provide safe fastening solutions

4 RESEARCH ON FASTENING SYSTEMS

Two of the key elements for a safe fastening solution are the selection of suitable products and proper design. These two elements require a proper test program and assessment criteria, the former, and accurate and easy to implement design methods, the latter. To the authors' experience, this is may be possible with strong scientific background and evidence that can be provided only with extensive but well-tailored research activities.

4.1 Research on fastenings for structural applications

4.1.1 Post-installed rebars (PIR) under seismic loading

PIR consist of the installation of deformed reinforcing bars in holes drilled in concrete and filled with injectable polymer grouts, and are generally used to construct concrete-to-concrete connections where new concrete is placed against existing concrete. By necessity, the portion of the reinforcing bars installed in existing concrete is straight, while the portion embedded in new concrete can be straight or hooked.

PIR are often used to construct and extend existing reinforced concrete structural elements or to strengthen and rehabilitate them. In contrast to steel-to-concrete anchoring applications, concrete-to-concrete connections using post-installed reinforcing bars often involve relatively small edge and corner distances as dictated by cover requirements (in this case, concrete splitting governs the strength of the connection and is anticipated in the expressions for required bar embedment).

Currently, the use of adhesive systems for the realization of connections with PIR is limited to qualified products according to the existing qualification guidelines (in Europe: EOTA TR 023,

to be replaced by the EAD 330087; in USA according to AC308). The qualification procedures given in the existing guidelines are based on extensive research work carried out in past years, e.g. Spieth for static and Simons for seismic applications, and revolve around the concept of equivalence of performance between cast-in and PIR.

Two main aspects need to be considered when testing and designing PIR: *bond failure*, understood as extraction of the bars from the concrete without significant concrete breakout, and *splitting failure*, which is typically characterized as cracking and spalling of the concrete cover. Bond failure occurs when sufficient confinement (e.g. large concrete cover) is provided to the bar, while splitting failure occurs when the concrete tensile resistance associated with the cover thickness is not sufficient to reach the load corresponding to bond failure.

One of the significant differences between AC308 (U.S.) and EAD 330087 (Europe) is that the former includes procedures to qualify products for seismic loading focusing only on bond failure, while no provisions are available in the latter.

The lack of a seismic solution for European engineers, back in 2013, was the motivation for the initiation of a research project to allow the development of seismic qualification requirements for PIR. The main issue to resolve was that, while for static loading the main qualification documents consider that the splitting resistance for different systems can be assumed to be equivalent or superior compared to corresponding cast-in systems, no information on the splitting behavior of PIR under cyclic loading was available.

Based on this consideration, a new test specimen was developed (Beam-End Test, BET specimen) to allow to test and assess the cyclic (seismic) performance of PIR in cases where splitting failure is governing (Figure 5). The loading protocol most suitable for cyclically loading PIR testing using BET specimens was identified in ACI 374.1.

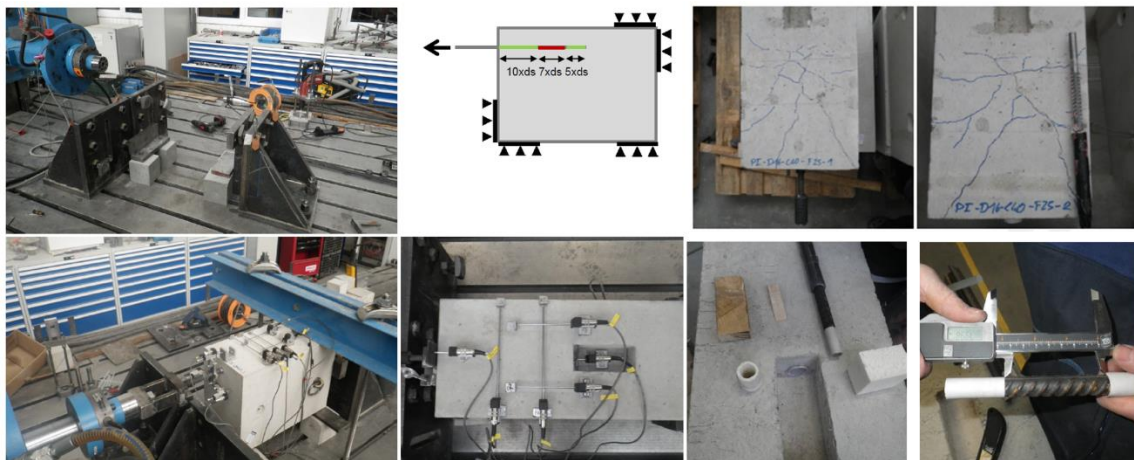


Figure 5. BET to identify the splitting behavior of PIR under cyclic loading

4.1.2 Yielding-anchor structural connections

Seismic design requirements as per ACI 318 or, equivalently, EOTA TR045, allow engineers to opt for multiple options when designing their fastening solution: (1) the connection can be designed such that failure is governed by ductile steel failure of the anchors, or (2) the connection can be designed such that failure is governed by yielding of the attached element, yielding of the fixture, or the maximum capacity of a non-yielding attached element, or (3) the connection can be designed such that a non-ductile failure (concrete cone) of the anchor is prevented by applying an extra (over-strength) load factor.

Option 1 (yielding-anchor connections) stems from observations from the 2010 Chilean Earthquake (Maule) where it was observed that yielding anchors with a well-defined stretch-length promoted desirable connection and, in some cases, system-level performance. Ultimately,

these were the premises for changes in ACI 318 (and EOTA TR045 afterwards) stretch length requirements (minimum 8 times the diameter of the anchor).

When the option to design connections using yielding-anchor was introduced, engineers were both skeptical about the requirements (an 8d stretch length might be quite cumbersome to achieve) and lacking the knowledge required to detail structural connections accordingly. This was the motivation that lead to start a research program to understand the load-bearing behavior of structural baseplate connections under seismic (cyclic) loading. The research program consisted of multiple phases, from the basic material testing of anchor bolts and threaded rods to system-type (scaled building) shake table tests.

The key findings of this research investigations were:

- Material tests; Steel type and processing (cold-forming, hot-rolling, annealing, etc.) have a pronounced effect on the overall anchor behavior (ductile, non-ductile)
- Base connection tests; An increase in stretch length and/ or material ductility improves the overall behavior of the baseplate connection (larger rotation and displacements before failure)
- System tests; For moment frame structures, the total base shear for uplifting configurations (yielding-anchor connections) was generally found to be slightly less than non-uplifting configurations, with some exceptions. Though the reductions in base shear were found to be motion-dependent. Reductions of over 20% were observed in the test program
- System tests; Maximum roof drifts were observed to be similar for uplifting-column and fixed-base moment frames. However, residual drifts were drastically reduced in the uplifting column configurations

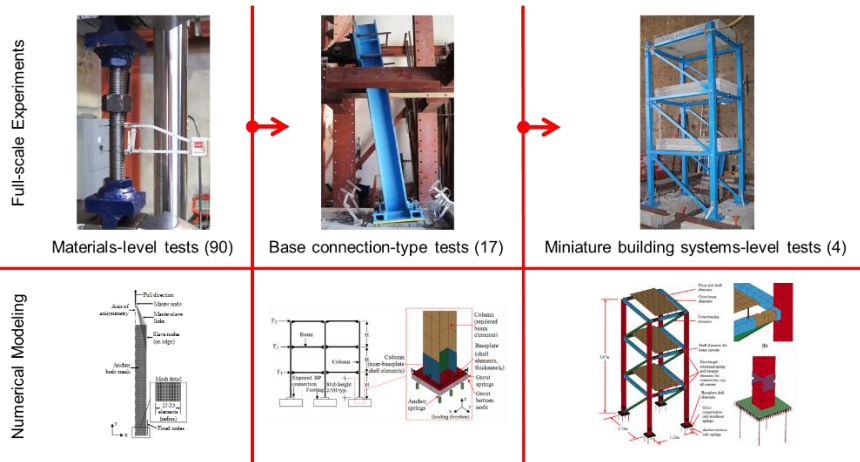


Figure 6. Framework of research program to understand the load-bearing behavior of structural baseplate connections under seismic (cyclic) loading

4.1.3 Moment transfer tests

Seismic design of moment transfer connections (e.g., beam-to-column or column-to-foundation connections) requires a thorough understanding of all potential failures modes that could occur, including concrete cone breakout in tension. ACI 318 suggests, however, that this failure mode can be precluded by anchoring headed bars a distance greater than $d/1.5$, with d being the effective depth of the beam connected to a column as shown in Figure 7a.

With the intent to verify whether this assumption is sound and safe, a research program has been focusing on testing moment transfer connections and observing their failure mode. One of the test setup used for the tests is shown in Figure 7b.

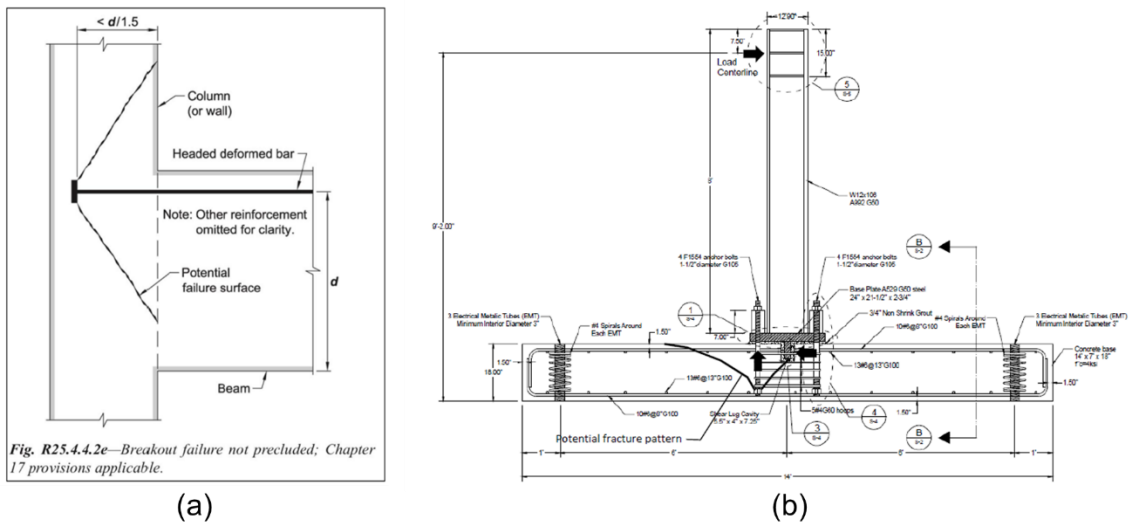


Figure 7. (a) Commentary to ACI 318-14 and (b) column-to-foundation test specimen

For this specific test, concrete breakout occurred at a load level corresponding to almost half of the expected failure load determined in accordance with ACI 352R-02 and the failure mode was concrete cone breakout rather than panel shear zone failure.

This result is extremely useful in that it contradicts code provisions or commentaries and shed light on the importance of properly considering anchorage failure modes, regardless of the complexity of the design calculations or their presumed high level of conservativeness, in the hierarchy strength approach typically adopted for seismic design of reinforced concrete structures.

4.2 Research on fastenings for nonstructural applications

4.2.1 The BNCS project and WALLE

The Building Nonstructural Component Systems (BNCS) project in 2012 revolved around the shake table tests of a full scale reinforced concrete frame building at the University of California, San Diego (UCSD). The 5-story building under investigation was fully equipped externally (cladding systems, water tank and chiller unit on the roof) and internally (stairs, doors, nonstructural components, a typical hospital OR, etc.). The shake table test plan was split in two phases: building base-isolated first, and building non-isolated second. Among the several objectives of the investigations, the ones relevant for fastenings were: 1- observe anchor behavior during a seismic event (loading and displacement); 2- observe concrete cracking and damage during a seismic event; 3- demonstrate that anchor cannot be installed in regions where large plastic deformations occur (e.g., plastic hinges); 4- observe performance of all structural and nonstructural components installed in the building in relation to their fastening method and design (e.g., cladding, stairs, and pipe hanging systems displacements).

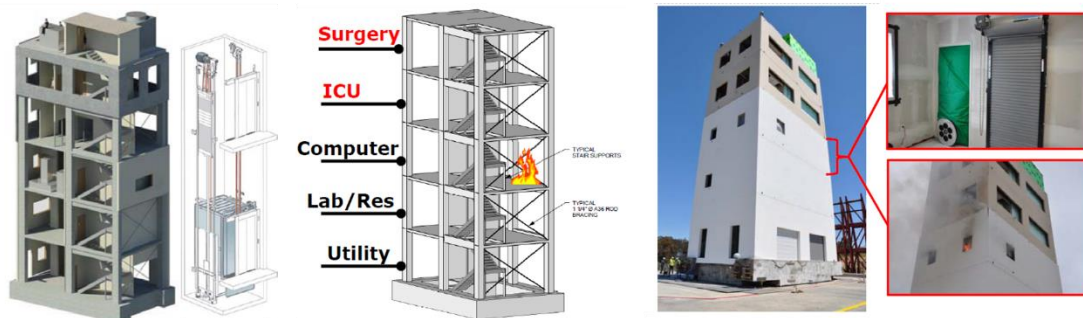


Figure 8. Five-story building shake table and post-earthquake fire tests

Following the shake table tests, fire tests were performed to identify the fire safety measures with the given damage from motion tests, and to assess the potential for fire and smoke spread from the collected data. The test outcomes could also serve as a base data set for seismic design of fire safety products and building components.

The main conclusions for the study were:

- Structural system: the building performed as expected except for the final motion, where some longitudinal bars fractured in the frame beams and punching shear mechanism was observed in the slab at the second floor
- Nonstructural components: elevators remained functional with throughout most of the tests, until the last two, strongest, events. After these, elevator doors became non-operational. Steel stairs detached, fractured (connection plates) or collapsed at very low drift levels, highlighting the need for changing design requirements in the codes. Cladding showed some damage, but no collapse.
- With regards to the fire tests: most mechanically undamaged fire protection system from the earthquake motions such as automatic sprinkler system and fire door functioned well in fire tests. Furthermore, most fire stop sealants and devices were activated and prevented fire and smoke spread. Potential concerns, however, were raised with regards to the performance of fire stop sealants for pipe penetration.

Testing nonstructural components and seismic anchorage of nonstructural components to simulate real earthquake conditions could be a challenging task due to the variability in geometry, weight, and other geometric parameters of real nonstructural components. In the early 2000s, a model nonstructural component named WALLE, Weighted Anchor Laboratory Loading Equipment, was developed to specifically understand the behavior of a certain spectrum of nonstructural components, forces acting on the anchors, and the response of the overall system nonstructural component and anchors to seismic events. Investigations of seismic anchorage of nonstructural components are important in that (1) many nonstructural components and systems are anchored overhead and, therefore, anchors might be interested by flexural cracks crossing through their load bearing area, and (2) anchors can typically only be designed as nonductile elements, thus being affected by over-strength factors applied to the horizontal component of the seismic force to protect them from potential brittle failure modes. This increase in demand, together with the condition that anchors might be located in concrete cracks, makes the seismic design of anchorage of nonstructural components difficult, especially when concrete members or slabs are of limited thickness. As part of his doctoral studies, Tim Johnson (2017) and Philipp Mahrenholtz (2012) performed shake table tests with WALLE focusing on the measurement of anchor forces, the former, and on anchor forces and their correlation with crack width, the latter.

Key findings from testing involving WALLE were:

- Seismic anchorage forces need to account for an amplification of the horizontal component of the seismic design load, but this factor could be lower compared to the values currently included in the design codes
- Correlation between anchor load and crack width during shake table tests with simultaneous crack width cycles showed to be low in general. Furthermore, the correlation factor seems to be independent of the maximum anchor load and crack width during shaking and depends primarily on the fundamental period of the NCS

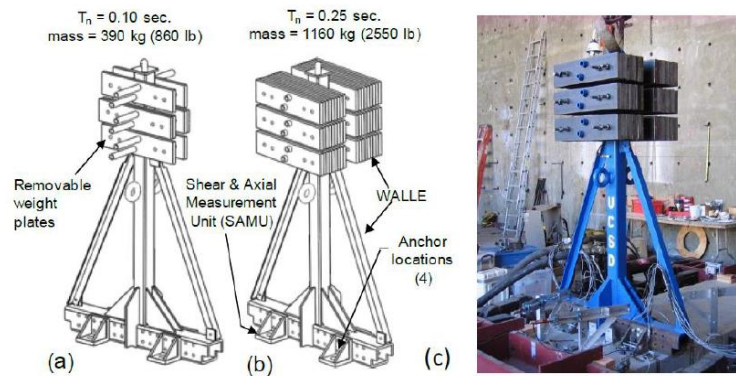


Figure 9. Weighted Anchor Laboratory Loading Equipment - WALLE models. (a) stiff configuration; (b) flexible configuration; (c) photograph of flexible configuration

5 IMPLEMENTATION OF RESEARCH RESULTS

Extensive research on fastenings under seismic loading conditions have lead in recent years to the development or amendment of several design and qualification documents in Europe and in the U.S.

Based on the research results on structural and nonstructural components (BNCS, WALLE), the efforts of manufacturers and Technical Assessment (formerly, Approval) Bodies (TAB) in Europe has lead in 2013 to the development and adoption of EOTA TR045 and ETAG 001 Annex E (Now EOTA TR049) for the design and seismic qualification of post-installed anchor products. Figure 10 highlights the subdivision of the European countries in high and moderate seismicity levels that require the use of appropriately qualified anchors (Category C1 and C2).

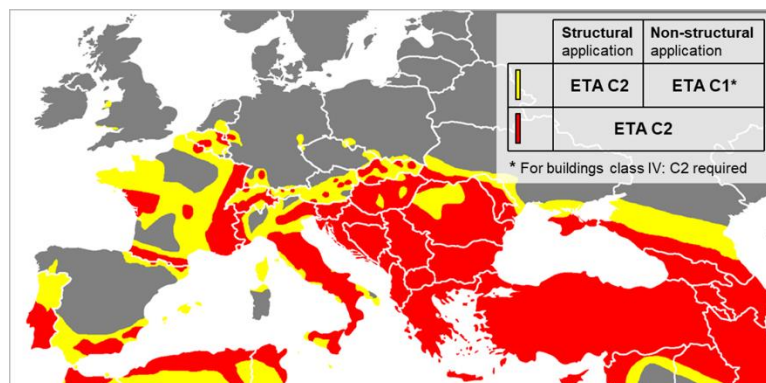


Figure 10. ETAG 001 Annex E and EOTA TR045 recommendations for seismic anchorage (from Countries seismic acceleration maps)

In June of 2018, the first two ETAs for PIR seismic were published in Europe based on the new qualification procedures (EAD 331522) revolving around the newly developed BET.

Based on the results of the BNCS and WALLE tests, furthermore, in recent years the requirements of ASCE 7 for the seismic anchorage of nonstructural components have been modified and tailored to the outcomes of the research results.

6 CONCLUSIONS

Seismic events and anchorage failures can have a significant impact on lives, structures, and nonstructural components and the only way to mitigate these effects is to foster a culture of safe, or safer, fastening solutions.

The two key components that, among others, can make fastening solutions safer are the selection of suitable products and their proper design. The only means to achieve this is to try to provide

full understanding and information on anchors, their safe use, their qualification requirements, and their design with state-of-the-art research programs.

These research programs should be tailored to the need to advance the knowledge in fastening technology and foster a proper understanding of the important details and complexities revolving around fastenings and their behavior.

REFERENCES

- ACI 318-14: Building Code Requirements of Structural Concrete (ACI 318-14) and Commentary, *American Concrete Institute*, 2014
- ACI 352R-02: Recommendation for Design of Beam-Column Connections in Monolithic Reinforced Concrete Structures, *American Concrete Institute*, 2002
- ASCE 7-10: Minimum Design Loads and Associated Criteria for Buildings and Other Structures, *American Society of Civil Engineers*, 2010
- Eligehausen, R., Mallè, R., and Silva, J.: Anchorage in Concrete Construction, *Ernst and Sohn* (A Wiley Company), Berlin, 2006
- EOTA EAD 330087: Systems for Post-Installed Rebar Connections with Mortar, in preparation.
- EOTA EAD 331522: Post-Installed Rebar with Mortar under Seismic Action, in preparation.
- EOTA TR 023: Assessment of post-installed rebar connections, November 2006.
- EOTA TR 045: Design of metal anchors for use in concrete under seismic actions, 2013
- EOTA TR 049 (former ETAG 001 Annex E): Post-Installed fasteners in concrete under seismic action, May 2016
- Global Seismic Hazard Assessment Program (GSHAP), global hazard maps, information and reports, <http://www.seismo.ethz.ch/static/GSHAP/index.html>
- Hutchinson, T., Conte, J., Restrepo, J., Astroza, R., Chen, M., Ebrahimian, H., Mintz, S., Pantoli, E., Wang, X., : Building System Performance during Earthquakes and Post-Earthquake Fire, BNCS project, University of California, San Diego, 2012
- Genesio, G., Piccinin, R., and Silva, J.: Qualification of a system for post-installed reinforcing bars under the rules established by EOTA and ICC-ES, proceedings of ConSC 2017, Stuttgart, 2017
- ICC-ES AC 308: Acceptance criteria for post-installed adhesive anchors in concrete elements, June 2016.
- Johnson, P., T.: Evaluation of Seismic Overstrength Factors for Anchorage into Concrete of Nonstructural Components, PhD Thesis, University of California, San Diego, 2017
- Mahrenholtz, P.: Experimental Performance and Recommendations for Qualification of Post-Installed Anchors for Seismic Applications, PhD Thesis, University of Stuttgart, 2012
- Park, H., Brian J. Meacham, B., J., Kim, J.: Fire Performance of Full-Scale Building Subjected to Earthquake Motions: Fire Test Program and Outcomes, Fire Safety Science – Proceedings of the 11th International Symposium, 2014
- Silva, J.: Post-Installed Reinforcing Bar Guide, Hilti North America, 2015
- Simons, I.: Verbundverhalten von eingemörtelten Bewehrungsstäben unter zyklischer Beanspruchung (Bond behavior of post-installed reinforcing bars subjected to cyclic loading), PhD Thesis, University of Stuttgart, 2007.
- Soules, J., Bachman, R., and Silva, J.: Chile Earthquake of 2010 – Assessment of Industrial Facilities around Concepcion, American Society of Civil Engineers, Reston, VA, 2016
- Spieth, H.: Tragverhalten und Bemessung von eingemörtelten Bewehrungsstäben (Behaviour and design of post-installed reinforcing bars), PhD Thesis, University of Stuttgart, 2002
- Trautner, A., C.: Steel Baseplate Connections with Ductile Anchors for the Improved Seismic Performance of Structural Systems, University of California, San Diego, 2016

Shear behaviour of interfaces within repaired/strengthened RC elements subjected to cyclic actions

Elizabeth Vintzileou¹, Vasiliki Palieraki¹, Giovacchino Genesio², Roberto Piccinin²

¹ National Technical University of Athens, Athens, Greece

² Hilti Corporation, Schaan, Liechtenstein

ABSTRACT: In this paper, the efficiency of the fib Model Code 2010 (MC10) formula in predicting the shear resistance of RC interfaces within repaired/strengthened elements is checked against experimental results. The shortcomings of the formula are identified and adequate modifications are proposed to account for the specific characteristics of interfaces reinforced using post-installed reinforcement. The improved efficiency of the modified formula is proven through comparison to both published and recently obtained experimental data. Furthermore, based on recent results, additional checks are provided to cover adverse failure modes that may occur, in case of reinforcement of limited embedment length, typical for interventions to existing reinforced concrete (RC) structures. Thus, a set of equations is proposed, adequate for safe prediction of the shear resistance of interfaces within repaired/strengthened elements (i.e. between existing and added concrete) crossed by post-installed reinforcement.

1 INTRODUCTION

Interventions to existing RC structures is a field of growing significance worldwide: the decay and ageing of the building stock, the need to make existing buildings compliant to current Design Codes or adequate for new use, as well as damages due to natural hazards lead to increasing need for design guidelines able to provide a basis for rational, safe, and economic interventions. Furthermore, the international economical environment makes the option of intervening on existing structures more attractive than that of demolition and re-building. Thus, increasing effort (both in research and in Code-making) is dedicated to repair and strengthening of existing RC structures.

The behaviour of interfaces between existing and added concrete, crossed by post-installed reinforcement (re-bars or industrial anchors) and, indeed, their design are of major significance for the efficiency of numerous intervention techniques. Actually, strengthened elements (e.g. jacketed RC columns, spans of existing RC frames filled with RC walls, etc.) are assumed to behave monolithically. Such a monolithic behaviour being to be ensured by adequately designed interfaces, one would expect current Codes [e.g. EN 1998-3 (2005)] to provide relevant design models. It seems though that this is not the case, for the time being.

On the other hand, Design Codes [such as fib Model Code for Concrete Structures 2010 (2013) and ACI 318-14 (2014)] do include formulae for the calculation of the shear resistance of interfaces within RC elements. In an effort to check the efficiency of Code formulae, as well as of formulae proposed by several investigators, the selected equations were applied to the database (including the worldwide published results of more than 600 tests on interfaces), created at NTUA, Palieraki (2014). That work is presented in detail in Palieraki et al. (2014).

The present paper concentrates on the fib MC10 formula. Its efficiency is checked against results obtained from testing concrete interfaces crossed by post-installed reinforcement (reinforcing bars). After having identified the shortcomings of the Code formula, the authors of this paper suggest adequate modifications. The improved performance of the modified formula is confirmed by recent test results obtained by the authors and presented herein.

2 THE MAXIMUM RESISTANCE OF RC INTERFACES

Although several relationships were proposed by investigators [e.g. Loov et al. (1994), Mattock (2001), Tassios et al. (2003), Mansur et al. (2008), Harries et al. (2012)] or were included in current Codes [e.g. fib Model Code for Concrete Structures 2010 (2013) and ACI 318-14 (2014)] for the calculation of the maximum shear resistance of concrete interfaces crossed by reinforcement, most of them are not adequate for interfaces between old and new concrete in repaired/strengthened elements because of the specific characteristics of the latter: the quality and the strength of the new and the old concretes may differ significantly, the surface of the old concrete may be smooth or artificially roughened, the reinforcement crossing the interface may be anchored to the old concrete by means of resins or by mechanical means while in the new concrete the anchorage of the reinforcement is achieved by bond, the dimensions of both the existing and the added portion of concrete may be limited, not allowing for full anchorage of the reinforcement or/and for sufficient edge distance of the reinforcement crossing the interface.

Among the available equations, the one included in fib Model Code for Concrete Structures 2010 (2013), is selected for further investigation (§7.3.3.6 “Shear at the interface between concrete cast at different times”), as this formula is assumed to be adequate for interfaces within repaired/strengthened RC elements as well. The design shear resistance, τ_{Rdi} , of an interface intersected either by reinforcing bars or by post-installed reinforcement is calculated as follows:

$$\tau_{Rdi} = c_r \cdot f_{ck}^{1/3} + \mu \cdot \sigma_n + k_1 \cdot \rho \cdot f_{yd} (\mu \cdot \sin a + \cos a) + k_2 \cdot \rho \cdot \sqrt{f_{yd} \cdot f_{cd}} \leq \beta_c \cdot v \cdot f_{cd} \quad (1)$$

where, strength values are in N/mm² and:

c_r is the coefficient for aggregate interlock effects at rough interfaces;

k_1 is the interaction coefficient for tensile force activated in the reinforcement or the dowels;

k_2 is the interaction coefficient for flexural resistance;

μ is the friction coefficient;

ρ is the reinforcement ratio of the reinforcing steel crossing the interface, having a yield strength equal to f_{yd} ;

σ_n is the (lowest expected) compressive stress resulting from an eventual normal force acting on the interface;

f_{ck} and f_{cd} is the compressive strength of concrete (characteristic and design value, respectively);

a is the inclination of the reinforcement crossing the interface;

β_c is the coefficient for the strength of the compression strut; and

$$v = 0.55 \left(\frac{30}{f_{ck}} \right)^{1/3} < 0.55$$

The values of coefficients (depending on the roughness of interfaces reinforced with dowels or re-bars) are listed in Table 1. The roughness of a concrete surface can be measured in various ways. According to the Model Code 2010 (2013), an appropriate way is the sand patch method, as described by Kaufmann (1971). It is noted, that under fatigue or dynamic loads, the values for τ_{Rdi} according to Equation (1) are reduced to 40%.

In Figure 1a, the values of maximum shear resistance, calculated on the basis of Equation (1) and Table 1, are compared to experimental values. For the comparison between calculated and experimental values to be possible, mean values of the mechanical properties of concrete and steel (as measured by the respective researchers) are inserted in Equation (1). The data plotted in Figure 1a show that the fib MC10 formula largely underestimates most of the experimental

results, with the exception though of the recent experimental results presented in this paper. This discrepancy will be discussed upon in Section 3.

Table 1: Factors for the calculation of the interface resistance, according to the interface roughness (CEB-fib Model Code 10, 2013).

Surface Roughness	c_r	k_1	k_2	β_c	μ	
					$f_{ck} \geq 20$	$f_{ck} \geq 35$
Very rough, $R_f \geq 3.0\text{mm}$ (valid also for shear keys)	0.2	0.5	0.9	0.5	0.8	1.0
Rough, $R_f \geq 1.5\text{mm}$	0.1	0.5	0.9	0.5	0.7	
Smooth	0.0	0.5	1.1	0.4	0.6	
Very smooth	0.0	0.0	1.5	0.3	0.5	

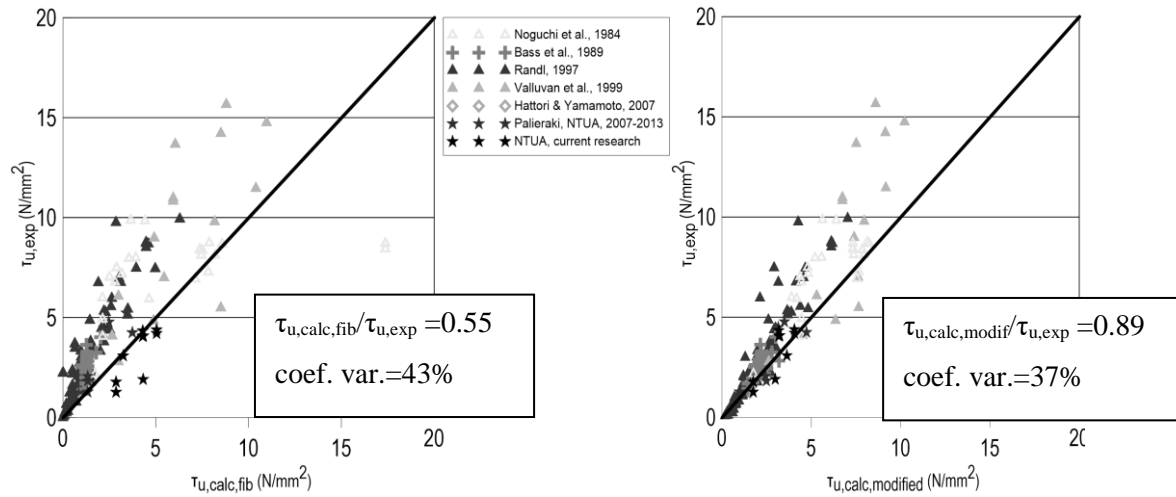


Figure 1. Interfaces crossed by post-installed re-bars or anchors; Comparison between experimental shear resistance and values calculated based on (a) the fib Model Code formula and (b) the modified formula.

Although an alternative relationship, developed by Palieraki (2014), proves to be quite accurate in predicting the shear resistance of interfaces, an effort is made to adequately modify the fib formula and to set minimum requirements with the purpose of improving its performance and covering in an adequate way interfaces crossed by post-installed reinforcement:

$$\tau_{Rdi} = \mu \cdot \sigma_n + k_1 \cdot \rho \cdot \sigma_s \cdot (\mu \cdot \sin a + \cos a) + k_2 \cdot \rho \cdot \sqrt{f_{yd} \cdot f_{cd}} \leq \beta_c \cdot v \cdot f_{cd} \quad (2)$$

The modifications, based on the Mechanics of interfaces, are described herein:

(a) The first term of Equation (1) is referred to in two locations within the fib MC10: In Equation 7.3-51, where it is attributed to aggregate interlock and in Equation 6.3-8, where it is attributed to adhesion along the interface. The second definition is adopted, as aggregate interlock and friction are terms referring to the same mechanism (according to the international Literature), whereas, in Equation (1), there is already a term calculating the contribution of friction. If this is so, it is reasonable to neglect adhesion, since this mechanism (of chemical nature) is mobilized under practically zero slip along the interface, whereas the mobilization of friction and dowel action necessitates the occurrence of slip. This is more so, in case of interfaces under cyclic actions. Furthermore,

(b) The friction coefficient, μ , is not expressed by a constant value. Actually, it is well known that the friction coefficient is a function of the ratio between the normal stress on the interface and the compressive strength of the weaker concrete. Thus, the following Equation (3) applies:

$$\mu = 0.33 \cdot \sqrt[3]{\left(\frac{f_c}{(\sigma_c + \sigma_n)}\right)^2} \quad (3)$$

(c) Another modification is related to the factors expressing the contribution of each mechanism to the shear resistance of the interface, k_1 and k_2 . On the basis of the evaluation of the NTUA database, the values included in the following Tables 2 and 3 (valid both for cast-in and post-installed reinforcement) should apply. The different contribution factor values for cyclic actions are justified by the effect of the magnitude of the imposed cyclic shear slip, as well as by the effect of cycling on the mobilized shear resistance of the interface.

Table 2: Interfaces between old and new concrete – cast-in/post-installed re-bars: contribution factors for the friction mechanism (k_1).

Interface Characteristics	k_1			
	Monotonic Loading	Cyclic Loading, Maximum Resistance		Maximum Resistance
		$l_{emb} > 12d$	$6d < l_{emb} \leq 12d$	
Mechanically roughened (1/4-in. amplitude), normal strength concrete	0.60	0.60	0.40	0.20
Mechanically roughened (1/4-in. amplitude) lightweight concrete or high strength concrete (> C50/60)	0.40	0.40	0.20	0.20
Smooth Interface	0.40	N/A	0.20	0.20
Very Smooth Interface, steel formed	0.20	N/A	N/A	N/A
Smooth Interface, lightweight concrete	0.20	N/A	N/A	N/A
Smooth Interface, no cohesion	0.10	N/A	N/A	N/A
Rough Interface, external compressive stress	0.70	0.70	0.70	0.70
Smooth Interface, external compressive stress	0.50	N/A	0.50	N/A
Interface with Shear Keys	0.80	0.40	N/A	N/A

N/A applies for cases in which no experimental results are available.

Table 3: Interfaces between old and new concrete – cast-in/post-installed re-bars: contribution factors for dowel action.

Normalized embedment depth	k_2
$l_{emb}/d > 8$	0.70
$6 \leq l_{emb}/d \leq 8$	$0.525 = 0.70 * 0.75$

(d) The validity of Equation (2) depends on the anchorage conditions of the reinforcement crossing the interface, on the basis of the available data, some minimum requirements are set, as follows:

(i) When a bar is anchored to the concrete by bond (usually in the new concrete) and its embedment length, l_{emb} , is smaller than the required for full anchorage, the maximum tensile stress, σ_s , to be developed (obviously, smaller than the yield strength of the bar) can be calculated and translated into compressive stress on the concrete, σ_c . The following Equation (4) applies:

$$\sigma_c = \frac{l_{emb} f_y A_s}{A_c 0.80 l_b} = \rho \cdot \sigma_s \quad (\text{N, mm}) \quad (4)$$

where, l_b denotes the anchorage length, according to EN 1992 (2009): $l_b = (f_{yd} \Phi) / 4 \tau_{Rd}$ (N, mm). As the majority of the available experimental results have shown [tests at NTUA-Vintzileou and Palieraki (2007), Palieraki and Vintzileou (2009), Palieraki et al. (2012)-and database evaluated in Palieraki (2014)], the embedment length needed for the bars to develop their yield strength is equal to $0.80 l_b$. Thus, the tensile stress, σ_s , of the bars (to be inserted in Equation (4)) is calculated as $\sigma_s = 4 \tau_{Rd} l_{emb} / 0.8 \Phi$ (N, mm).

(ii) In case of post-installed reinforcement, the value of τ_{Rd} (bond strength) provided by the manufacturer (for the resin used for the installation of the reinforcement) is applied. The state of concrete (uncracked and cracked) as well the loading type (static or seismic) should be taken into account while choosing the value τ_{Rd} of a specific resin to be used in the design.

(e) Interfaces reinforced with (bonded by means of resins) post-installed reinforcing bars, embedded in the old concrete to a limited depth (6 to 8 times the bar diameter), exhibited quite frequently brittle failures, namely, concrete cone breakout and pry-out failure [Bass et al. (1989), Randl (1997), Valluvan et al. (1999), Hattori et al. (2007)]. Thus, to predict the (reduced) bearing capacity of interfaces crossed by short post-installed bars (embedment length between $6d$ and $8d$), an additional check (on top of Equation (2)) of the verification of concrete cone breakout capacity seems to be generally required (according to EN/TS 1992-4-5 (2009) or ETA: Design of Bonded Anchors, TR 029 (2010)).

The modified fib Model Code 2010 (2013) formula [Equation (2)], along with the additional limitations and verifications (§§ (a) to (e)) were applied to interfaces reinforced with post-installed re-bars. As in the case of application of Equation (1), Figure 1a, mean values of mechanical properties were taken into account. As shown in Figure 1b, the performance of the modified formula is significantly improved. The average value of the calculated values divided by the experimental ones is improved, while also the coefficient of variation is smaller in the case of the modified formula.

3 EXPERIMENTAL PROGRAM

3.1 Introduction

Although the international Literature is rich in results of testing plain or reinforced concrete interfaces, simulating construction joints, connections between precast elements, natural cracks, etc., the data on the behaviour of reinforced interfaces simulating the interfaces between old and new concrete in repaired/strengthened elements subjected to cyclic shear slip are still limited in number. The experimental results presented herein are part of the research in-progress at NTUA, aiming at providing reliable information on the cyclic behaviour of interfaces between old and new concrete in repaired or strengthened elements as well as focusing the behavior of the connectors in the case of short embedment.

The geometry of the specimens, the test setup and the testing procedure valid for previous tests performed at NTUA were selected, to ensure direct comparison with available experimental results. Due to space limitations, only the absolutely necessary information is provided herein. For detailed description of the test setup and procedure, the Reader may refer to Palieraki et al. (2012).

3.2 Specimens, Test set-up and Testing procedures

The geometry of the specimens, designed to allow for cyclically imposed shear slips without any eccentricity, is shown in Figure 2a. The dimensions of the interface are equal to 500x200 [mm]. The interface is crossed by three reinforcing bars, 16mm in diameter.

The specimens were constructed in two phases. The first portion, simulating the existing concrete (mean compressive strength, between 24MPa and 38MPa at the age of testing) was cast first. The reinforcing bars were installed at mid-width of the section, after the artificial roughening of the interface using a pickaxe (Figure 2b). Their bond with the existing concrete was ensured using a Hilti post-installed injection system, whereas the installation instructions and setting operations, specified by the Manufacturer were followed. The post-installed reinforcing bars were protruding to sufficient length (350mm and with a hook at their far end) to ensure their full anchorage to the portion of the specimen simulating the new added concrete (mean compressive strength, 31 MPa to 41MPa at the age of testing), cast approximately one month after the portion simulating the existing concrete. Thus, the behaviour of the interface is governed by the part of the bars that is installed in the existing concrete. The mean yield stress of the re-bars is equal to 550MPa, whereas their ultimate stress is equal to 627-693MPa.

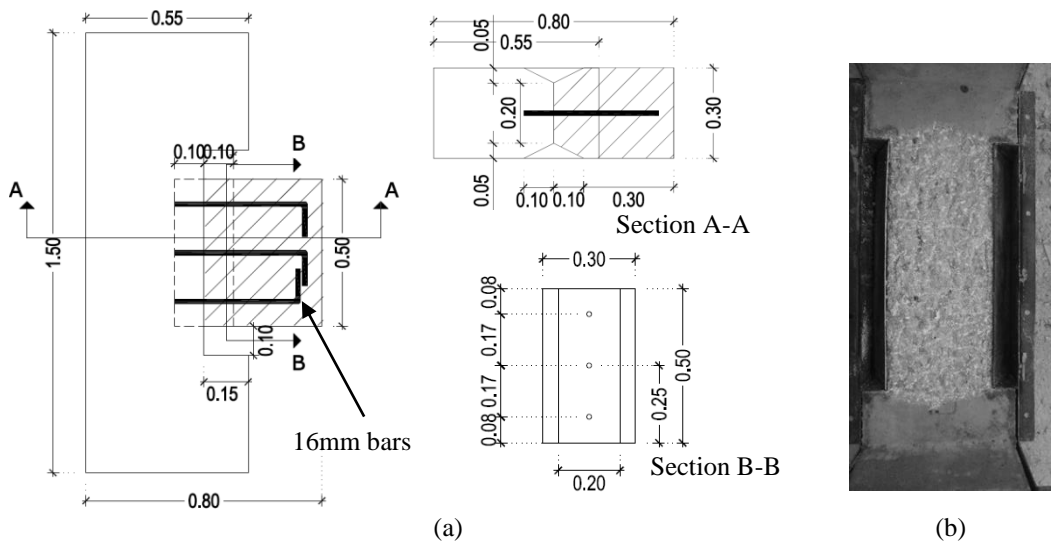


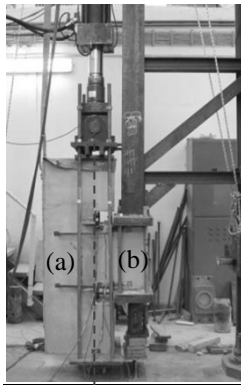
Figure 2. (a) Geometry of the specimens, (b) The surface of the part simulating the old concrete, after its artificial roughening.

Among the available data, the results of six tests are presented herein. The investigated parameter is the embedment length of the post-installed portion of the reinforcing bars, equal to 6d, 8d or 10d (d being the diameter of the bars). The embedment length values are smaller than prescribed by HILTI for seismic applications ($min.l_{emb}=12d$) [Hilti Post-Installed rebar guide (2015)]. However, those values were selected as representative of strengthening applications, where the available thickness of the RC elements may be limited. In one specimen, an external compressive stress, equal to 0.50MPa was imposed to the interface. Three more specimens, not included in this paper, were tested monotonically to failure.

The test setup [Figure 3 and Palieraki et al. (2012)] is designed to allow for application of shear along the interface, under zero eccentricity. The tests are performed under displacement-controlled conditions, using an actuator of max. capacity +/-500kN. The imposed shear slip and the opening of the crack along the interface were measured using eight (8) LVDTs, whereas strain gauges were

positioned on the bars, close to the interface, to measure their strains.

The loading history consists in sets of three full displacement reversals at gradually increasing maximum displacement along the interface. The first set of cycles was $\pm 0.10\text{mm}$ or $\pm 0.20\text{mm}$. Each test was completed after significant force-response degradation or after the occurrence of cracks away of the interface, as explained in the following Section 4.



(a) Movable (old concrete)
(b) Immovable (new concrete)

Figure 3. Test setup and instrumentation (the axis of the actuator coincides with interface).

4 EXPERIMENTAL RESULTS

4.1 General observations

In all specimens a crack opened along the interface between the two concrete blocks and it was visible even for an imposed shear slip as small as 0.10mm . In case of specimens with shallow bars ($l_{\text{emb}}=6d$), a second crack, almost parallel to the interface occurred at a distance practically equal to the embedment length of the post-installed bars. This second crack, that occurred at a shear slip value approximately equal to 0.20mm , increased in width during testing and, finally, led to the failure of the specimen (Figure 4). It is interesting to observe that, in the specimen subjected to an external compressive stress (Table 4), the opening of the crack was significantly delayed. Similar cracks occurred to the specimens where larger embedment lengths were provided to the bars ($8d$ or $10d$). However, those cracks occurred at significantly larger shear slip values (Table 4). It seems, therefore, that for small embedment lengths, a concrete cone failure may be imminent or it may not be excluded.



Figure 4. Formation of a second crack, parallel to the interface. The crack occurs close to the back end of the (short) reinforcing bars. Observe the formation of concrete cones.

4.2 Hysteresis loops and maximum shear resistance

The hysteresis loops for the six specimens, presented in Figure 5, show typical shear sensitive behaviour, namely, pinching effect and, hence, limited area of the loops and force-response degradation due to cycling. Those characteristics are more pronounced for smaller re-bar embedment lengths. In general, limited asymmetry of the loops in the two loading directions is observed. As shown in Table 4, the maximum shear resistance increases with increasing embedment length of the bars, whereas the positive effect of the normal compressive stress on the interface is also evident. The shear slip values corresponding to the maximum resistance are rather scattered, with the larger values recorded for the longer embedment lengths, as well as in the specimen subjected to external compressive stress.

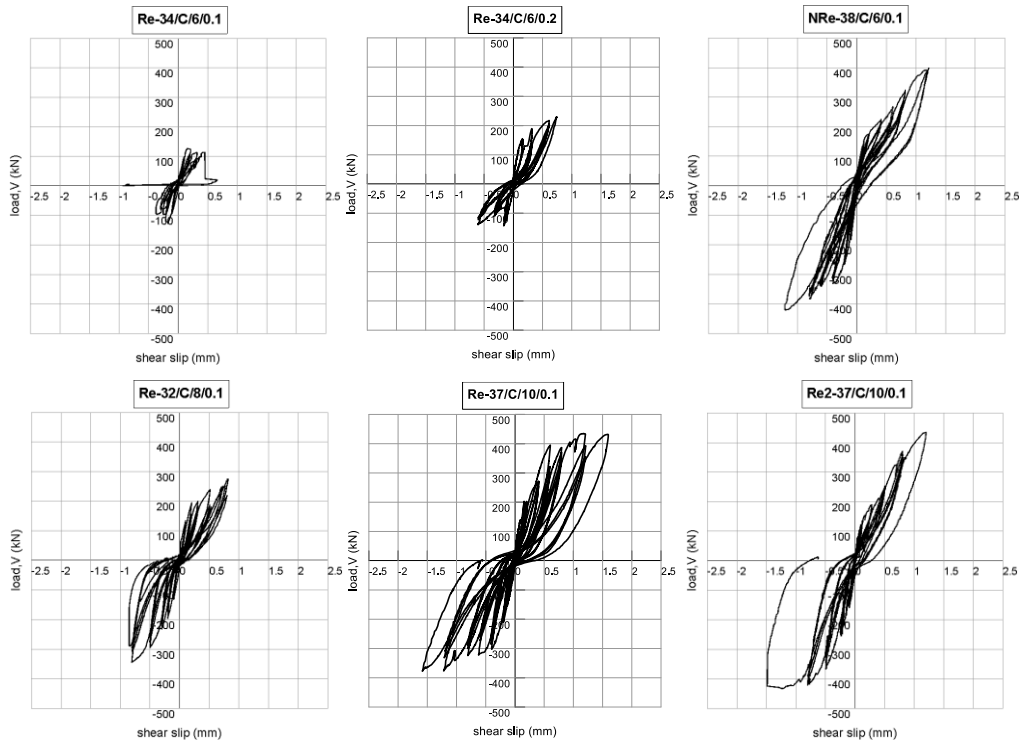


Figure 5. Hysteresis loops for specimens reinforced with 6d, 8d and 10d embedment length of the bars.

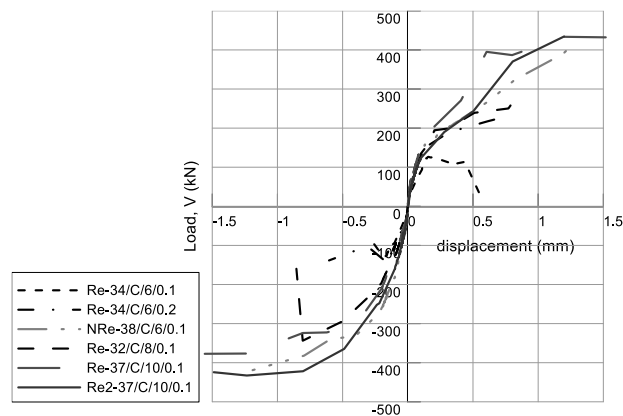


Figure 6. Hysteresis loop envelopes, first loading cycle

The effect of the embedment length on the shear behaviour of the interfaces is apparent in the hysteresis loops envelopes (Figure 6): As the embedment length increases, the resistance increases, the interface may sustain larger displacements, whereas its behaviour is more stable, after the attainment of the maximum resistance.

The values of maximum resistance obtained from testing the specimens subjected to cyclic shear, as well as those for the three reference tests (monotonically tested) are included in Figure 1. It is clear that the fib MC10 (2013) formula overestimates the shear resistance of the specimens (see tests “NTUA current research”, black stars in the diagrams). The overestimation of the resistance is more significant, in case the failure is due to the failure of concrete and not the yielding of the connector. On the contrary, the formula modified according to Section 2 of the present paper, is able to predict quite accurately the shear capacity measured experimentally. This is a further confirmation of the validity of the proposed modifications.

Table 4: Summary of experimental results

Specimen	Reinforcement/ Embedment length	τ_{\max} (MPa)	Crack Parallel to the interface, at s (mm)	Slip at maximum resistance (mm)
Re-34/C/6/0.1	3 Φ 16/6d	1.27	0.20	0.20/-0.20
Re-34/C/6/0.2	3 Φ 16/6d	1.78	0.20	0.70/-0.60
NRe-38/C/6/0.1	3 Φ 16/6d/N	4.09	0.40	1.00/-1.20
Re-32/C/8/0.1	3 Φ 16/8d	3.09	0.50	0.80/-0.80
Re-37/C/10/0.1	3 Φ 16/10d	4.06	0.60	1.20/-1.20
Re2-37/C/10/0.1	3 Φ 16/10d	4.34	0.50	1.20/-1.20

Re: anchorage by means of epoxy resins, N: Normal force on the interface (compressive stress =0.50 MPa).

The first number indicates the compressive strength of the weaker concrete (in MPa).

C: Three bars, 16 mm in diameter.

The second number indicates the embedment depth normalized to the bar diameter.

The third number indicates the maximum slip for the first set of cycles (in mm).

5 CONCLUSIONS

On the basis of the work presented in this paper, the following conclusions can be drawn:

1. The shear resistance of interfaces within repaired/strengthened RC elements subjected to cyclic actions cannot be accurately predicted by the fib MC10 (2013) formula. Several modifications are needed to account for the specific characteristics of those interfaces.
2. The modifications proposed in this paper proved to improve the accuracy of the Code formula. Actually, the modified formula is able to predict quite accurately the shear resistance even in the case of post-installed reinforcing bars embedded to a small depth in the existing RC element. This is mainly attributed to the fact that, a small embedment length may cause a concrete cone failure and, hence, lead to reduced shear capacity.
3. This feature is confirmed by the tests presented in this paper: An embedment length equal to six times the bar diameter (6d), is acceptable for interfaces under static conditions; it seems though that it may not be acceptable for interfaces subjected to seismic actions, as a premature concrete cone failure occurs at small imposed shear slip.
4. The check of the validity of the modified formula is herein limited to the tested post-installed rebar system. A re-evaluation of the available results of cyclic tests on interfaces is in course, along with further experimental work, with the purpose to set a safe minimum value for the embedment length of post-installed reinforcing bars. The

limited number of tests presented in this paper show that an embedment length equal to 10d leads to significantly improved behaviour. Nonetheless, the occurrence of secondary cracks at the far end of the embedded bars cannot be excluded and the verification of the resistance of the connectors is crucial in the overall design of the interface.

ACKNOWLEDGMENTS

The research presented in this paper was sponsored by Hilti Corporation. The support of this organization is gratefully acknowledged. Findings, opinions, and conclusions are those of the authors and do not necessarily reflect those of the sponsoring organization.

REFERENCES

- ACI Committee 318. 2014. *Building Code Requirements for Structural Concrete (ACI 318-14) and Commentary*. American Concrete Institute, Farmington Hills, Mich. 519 pp.
- Bass, R.A., Carraquillo, R.L., and Jirsa, J.O. 1989. Shear Transfer across New and Existing Concrete Interfaces, *ACI Structural Journal*, 86(4): 383-393.
- EN 1992-1. 2009. Eurocode 2. *Design of concrete structures*, Brussels: European Committee for Standardization.
- EN 1992-4-5. 2009. Eurocode 2. *Design of fastenings for use in concrete - Part 4-5: Post-installed fasteners - Chemical systems*, Brussels: European Committee for Standardization.
- EN 1998-3. 2005. Eurocode 8. *Design of structures for earthquake resistance - Part 3: Assessment and retrofitting of buildings*, Brussels: European Committee for Standardization.
- EOTA Technical Report TR 29. 2010. *Design of bonded anchors*, European Organisation for Technical Assessment.
- fib Bulletin No. 65. 2013. *Model Code 2010. Final draft, Vol. 1*, International Federation for Structural Concrete, Lausanne, Switzerland, 350 pp.
- Harries, K.A., Zeno, G., and Shahrooz, B. 2012. Toward an Improved Understanding of Shear-Friction Behavior, *ACI Structural Journal*, 109(6): 835-844.
- Hattori, Y. and Yamamoto, Y. 2007. Shear Transfer Mechanism to bonded Anchors for Exterior Seismic Retrofitting, *Proceedings of the 2nd International Symposium on Connections between Steel and Concrete*, Stuttgart, Germany, Vol. 2: 759-769.
- Hilti AG. 2015. *Post-installed reinforcing bar Guide*, 69 pp.
- Kaufmann, N. 1971. Das Sandflächenverfahren, *Strassenbautechnik*, 24(3): 131-135.
- Loov, R.E., and Patnaik, A.K. 1994. Horizontal Shear Strength of Composite Concrete Beams with a Rough Interface, *PCI Journal*, 39(1): 48-69.
- Mansur, M.A., Vinayagam, T., and Tan, K.W. 2008. Shear Transfer across a Crack in Reinforced High-Strength Concrete, *Journal of Materials in Civil Engineering, ASCE*, 20(4): 294-302.
- Mattock, A.H. 2001. Shear Friction and High-Strength Concrete, *ACI Structural Journal*, 98(S5): 50-59.
- Noguchi, H., Ochiai, M., Izhuka, S. 1984. Sliding Shear in Cracked Reinforced Concrete Shear Walls Subjected to Reversed Cyclic Shear, *Proceedings of the 8th World Conference on Earthquake Engineering*, San Francisco, California, Vol. 6: 331-338.
- Palieraki, V. 2014. Seismic Behavior of Reinforced Interfaces in Repaired/ Strengthened Reinforced Concrete Elements. *Ph.D. Thesis, National Technical University of Athens, Greece*, 578 pp (in Greek).
- Palieraki, V., and Vintzileou, E. 2009. Cyclic Behaviour of Interfaces in Repaired/Strengthened RC Elements, *"Architecture - Civil Engineering - Environment ACEE" Journal*, 2: 97-108.
- Palieraki, V., Vintzileou, E., and Trezos K., 2014, Shear Transfer along Interfaces: Constitutive Laws, *Proceedings of the Second European Conference on Earthquake Engineering and Seismology*, Istanbul, Turkey (electronic source).
- Palieraki, V., Vintzileou, E., and Zeris, Ch. 2012. Behaviour of interfaces in repaired/strengthened RC elements subjected to cyclic actions: Experiments and Modelling, *Proceedings 3rd International Symposium on Life-Cycle Civil Engineering (IALCCE 2012)*, Vienna, Austria (electronic source).
- Randl, N. 1997. Untersuchungen zur Kraftübertragung zwischen Alt- und Neubeton bei unterschiedlichen Fugenrauigkeiten, *Ph.D. Thesis, Universität Innsbruck, Austria*, 379 pp (in German).

- Tassios, T.P., and Vassilopoulou, I. 2003. Shear transfer capacity along a RC crack, under cyclic sliding, *Proceedings of fib Symposium on Concrete Structures in Seismic Regions*, Athens, Greece (electronic source).
- Valluvan, R., Kreger, M.E., and Jirsa, J.O. 1999. Evaluation of ACI 318-95 Shear-Friction Provisions, *ACI Structural Journal*, 96(4): 473-481.
- Vintzileou, E. and Palieraki, V. 2007. Shear Transfer along Interfaces in Repaired/Strengthened RC Elements subjected to Cyclic Actions, *Special Edition "Beton- und Stahlbetonbau"*, 102: 60-65.

Performance Based Mix Design of Steel Fiber Reinforced Concretes – Recent Advances in Applications

Mehmet Ali Taşdemir

Istanbul Technical University, Civil Engineering Faculty, İstanbul, Turkey

ABSTRACT: Steel fiber reinforced concrete (SFRC) has a wide range of applications such as; pavements and overlays, industrial floors, precast elements, hydraulic and marine structures, repairing and retrofitting of reinforced concrete structures, tunnel linings and slope stabilization works. Recent advances in concrete technology and the increasing emphasis on ductility of concrete structures have brought on the development of new type of materials which are generally named as the High Performance Fiber Reinforced Cementitious Composites (HPFRCCs). Those composite materials, that display a typical tensile strain hardening behavior, have received significant research attention in the last three decades. This paper mainly summarizes the mechanical properties and fracture energies of conventional and high performance steel fiber reinforced concretes. Load-crack width and load-deflection curves exhibit significant ductile behavior if the strengths of both the steel fibers and the concrete are high. Mixtures containing high strength steel fibers have higher residual strength and fracture energy values than mixtures with normal strength steel fibers. Performance of steel fiber reinforced concrete for a given concrete class; depends on the strength, content and aspect ratio of the steel fibers. Some examples from the applications of steel fiber reinforced concrete and self-compacting concrete with fibers are also presented.

1 INTRODUCTION

In the 1970's, any concrete mixture that showed 40MPa or more 28-day compressive strength was classified as high strength concrete. Such a concrete is nowadays considered quite low strength when compared to the very high strength concretes with cube compressive strengths between 200 MPa and 800 MPa, flexural strengths between 25 MPa and 150 MPa, and fracture energies of about 30000J/m² (Richard and Cheyrezy., 1995; Dugat et al., 1996; Bonneau al., 1997; Taşdemir, 2010).

In recent years, a number of specific developments have occurred in parallel to the evolution of what is commonly described as high performance concretes. Such concretes have high strength combined with highly enhanced durability. The brittleness of concrete, however, increases with an increase in its strength (Taşdemir et al., 1998). In other words, the higher the strength of concrete, the lower is its ductility. Although HSC has high modulus of elasticity, reduced creep, high abrasion resistance and high tensile strain capacity against risk of cracking before peak stress, there are some disadvantages of high strength concrete such as brittleness, high heat of hydration, high autogeneous deformation, and high risk of early age cracking. On the other hand, due to their low water to cementitious materials ratio, HSCs require special curing conditions. The inverse relation between strength and ductility is a serious drawback and limits the use of high strength concrete (Balaguru et al., 1992). Their potential use is yet to be established and more work is required, in particular, to evaluate their long-term performance. In recent years, High Performance Fiber Reinforced Cementitious Composites (HPFRCCs), that display a tensile strain hardening

behavior in the pre-peak region, have received significant research attention in recent years. The fracture energies of Reactive Powder Concretes (RPCs), are about 300 times that of normal strength concrete or even 1350 times in case of Slurry Infiltrated Fiber Reinforced Concrete (Fritz, 1991).

In order to control micro and macro cracks, the use of hybrid fibers (i.e., short and long discrete steel fibers) play important role in the mechanical behavior of SFRCs. The use of short discrete fibers prevents the formation and propagation of micro-cracks and also increases the concrete tensile strength before macro-cracks are formed while they are pulled out. Long steel fibers affect the post peak response part of the cracking process and increase both the fracture energy and ultimate strength of the concrete (Betterman et al., 1995; Akçay and Taşdemir, 2012).

This paper mainly focuses on residual strengths used in the design of conventional fiber reinforced concretes. In addition, the mechanical behavior of some advanced cement based materials such as HPFRCCs, Normal and Self Compacting Concretes with and without steel fibers are summarized. Some typical applications of these composites are also presented.

2 CLASSIFICATION OF CEMENTITIOUS COMPOSITES

From the strength point of view, the classification of high strength concretes can be made as: i) normal strength concrete (NSC) up to grade 60 MPa, ii) high strength concrete (HSC), grades 60-90 MPa, iii) very high strength concrete (VHSC), grades 90-130 MPa, iv) reactive powder concrete (RPC), grades 200-800 MPa, and v) high performance lightweight concrete (HPLWC) greater than 55 MPa (Taşdemir et al. 2008; Taşdemir et al., 2010).

From the mechanical behavior point of view, SFRCs can be divided into two categories based on their performances: i) conventional SFRCs, and ii) HPFRCCs such as RPCs. The conventional SFRCs exhibit ductile behavior compared to the brittle matrix, but their flexural and tensile strengths are not very high, and especially the compressive strengths of these materials do not practically change with the fiber volume fraction. The HPFRCCs, however, exhibit large strain hardening before peak stress, and their tensile and compressive strengths are very high compared to those of conventional SFRCs (Alaee, 2002). Ductile Fiber Reinforced Cementitious Composites (DFRCCs) or Strain Hardening Cementitious Composites (SHCCs) show hardening deflection and multiple cracking in bending with significant ductility in tension and compression. DFRCC (or SHCC) is a class of Fiber Reinforced Cementitious Composite (FRCC) that exhibits multiple cracking. Multiple cracking leads to improvement in properties such as ductility, toughness, fracture energy, and strain capacity under tension, compression, and bending. DFRCC is a broader class of materials than HPFRCC. FRCC includes the entire class of FRCC, where DFRCC as well as other composites such as fiber reinforced concrete (FRC) and fiber reinforced mortar (FRM) are sub-sets (Kimita, 2000). Engineered Cementitious Composites (ECCs), make up a particular type of HPFRCC, whose composition is optimized in a cost-effective way on the basis of micromechanics. ECC typically has a tensile strain capacity of greater than 3%. Microstructure optimization limits the fiber content of ECC to be less than 2-3% (JCI-DFRCC Committee, 2003). HPFRCC also includes SIFCON and SIMCON (Slurry-Infiltrated Mat Concrete).

3 PERFORMANCE BASED DESIGN OF CONVENTIONAL SFRCs

In this part, the main objective is to explain the performance classes of SFRCs from the equivalent flexural tensile strength point of view. In order to obtain optimum solutions, equivalent flexural tensile strengths for both Serviceability Limit State (SLS) and Ultimate Limit State (ULS), splitting tensile strength and fracture energy were maximized, and fiber content and cost of the

mixture were minimized simultaneously. For the optimum mix design of SFRCs, three-level factorial experimental design and Response Surface Method (RSM) were used.

3.1 Design of conventional SFRCs considering small and large deflections

Effects of the aspect ratio (L/d) and volume fractions of steel fibers (V_f) on the fracture properties of normal and high strength concretes were investigated by Yalçın (2009) using three groups of experiments in bending by measuring the fracture energy and ductility. In the first group of the experiments, the effect of the same type of single hooked end steel fibers on the mechanical and performance properties of concrete having two different concrete classes was investigated. The normal strength steel fibers had the same aspect ratio ($L/d=80$), but four different volume fractions (V_f). Volume fractions of steel fibers were varied between 0.19% and 0.58%, in steps of 0.13%. Thus, in this group, mixtures including two control concretes with water-cement ratios of 0.45 and 0.65, and eight mixtures of SFRCs, therefore a total of ten mixtures were produced. In the second group, the effect of aspect ratio of the steel fiber on the mechanical and performance properties of steel fiber-reinforced concrete was investigated. The normal strength steel fibers having the aspect ratios of 80, 65 and 55 were utilized. In this group, nine concrete mixtures with steel fibers, and one control concrete were cast. In the third group of the experiments; the aspect ratio was 80 for all fibers. Lengths of these high strength steel fibers were; 60 mm, 40 mm and 30 mm, and they were added in hybrid form to the mixtures having water-cement ratios of 0.32, 0.44 and 0.75. Volume fractions of these high strength hybrid steel fibers were; 0.27%, 0.50% and 0.73%. Thus, twelve concrete mixtures were produced for this group. The load versus deflection curve for each beam was obtained by recording the average of three measurements taken at the mid span.

3.1.1 Test Procedure

Standard strength tests were conducted in accordance with European Standards (EN 206 and EN 12390). Four-point bending tests were performed on the beams of 150x150x750 mm size. For the plain concretes, the displacement rate at the mid-span of the beams was kept constant at 0.02 mm/min. The beams with steel fiber, however, were tested at the displacement rate of 0.05 mm/min up to a displacement of 0.5 mm, and then at 0.1 mm/min up to a 5 mm displacement. The load was applied by an Instron 5500R closed-loop testing machine of 100 kN capacity, and deflections were measured simultaneously by using three linear variable displacement transducers (LVDTs). The load versus displacement curve for each beam was obtained by recording the average of three measurements taken at the mid span. The load-displacement curves were used for evaluating the equivalent flexural strengths of both SLS and ULS. As seen in Figure 1, the area under the load versus displacement at mid span curve was described as a measure of the energy required for each displacement.

Characteristic equivalent flexural strength can be calculated as follows:

$$f_{eq} = \frac{T_i}{\delta_i} \frac{S}{bh^2} \quad (1)$$

Where, T_i is the area under load versus displacement curve for SLS or ULS, δ_i is the corresponding displacement for each limit state; b x h (150x150 mm) and S (600 mm) are the cross-section of the beam and the length of the span, respectively.

According to DBV (German Concrete Society), equivalent flexural strengths of steel fiber reinforced concrete are given as indicated in Table 1 (DBV, 1996). In this table and in Figure 1, δ_0 shows the displacement at the first crack.

Table 1. Deformation regions for SFRCs (DBV, 1996).

Deformation Region	Limit State	Displacement
I (small deformation, A)	SLS	$\delta_1 = \delta_0 + 0.65$
II (large deformation, A+B)	ULS	$\delta_2 = \delta_0 + 3.15$

The dimensions of the beams, prepared for four point bending tests, were 150x150x750 mm. At least four beam specimens from each concrete mixture were tested. For each mixture, three cylinders, 150 mm in diameter and 300 mm in height, were used for compressive strength and modulus of elasticity tests. Six disc specimens, 150 mm in diameter and 60 mm in height, were prepared for the splitting tests.

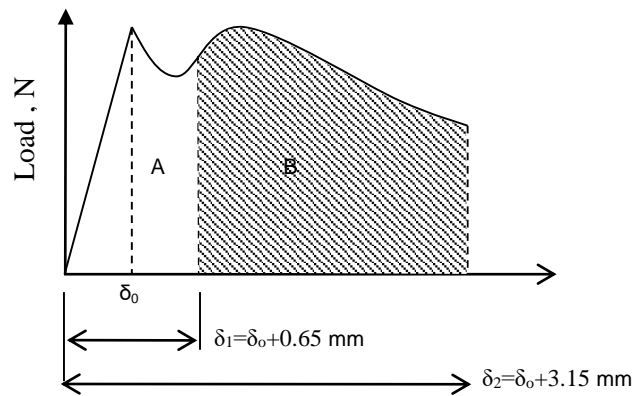


Figure 1. Specified deflections for the calculation of equivalent tensile strengths (DBV, 1996)

3.1.2 Complete load-displacement curves under bending

Based on the second group of Yalçın's experiments, as seen Figure 2a, the flexural strength can be expressed in terms of the fiber volume fraction and the aspect ratio. Typical load-displacement curves for the mixture containing fibers with the aspect ratio of 80 are shown in Figure 2b. These curves obtained in this study were used for evaluating the equivalent flexural strengths for both SLS and ULS. The area under each curve was indicated to be a measure of the fracture energy of the material. It can clearly be seen that fracture energy increases as the fiber volume fraction of steel fiber increases. As seen in Figure 2b, after the formation of the first crack, except the mixture with the steel fiber volume fraction of 0.32%, the progress of strain hardening in the ascending branch of the curve is a typical indication of high performance cement based composites. Similar results were obtained for the mixtures with the other aspect ratios (Yalçın, 2009).

One of the major roles of fiber in concrete is to provide an increase in the fracture energy. The results reported by Yalçın et al. (2009) here are also based on the area under the complete load-deflection curve up to a specified deflection. As seen in Table 1, the specified deflections for SLS and ULS are $\delta_0 + 0.65$ mm and $\delta_0 + 3.15$ mm, respectively. The cut-off point was chosen as 5mm deflection. The energy at this deflection (i.e. 5mm), however, is not totally dissipated. SFRCs allow obtaining high values of equivalent flexural strengths and high ductility, depending on their strengths and the volume fraction of fibers used. The increase in equivalent strengths for

both SLS and ULS due to the high energy of fiber pull-out and fiber debonding in the fracture process

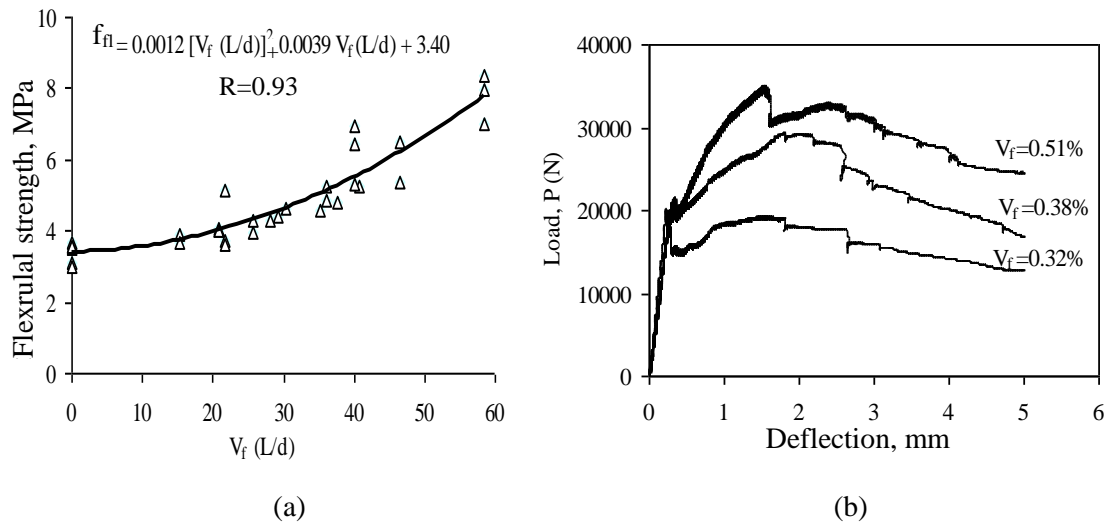


Figure 2. a) Flexural strength versus $V_f (L/d)$, b) Typical load versus displacement at the mid-span curves for the second group of mixtures containing fibers with the aspect ratio of 80 (Yalçın, 2009).

Figure 3 shows the effects of concrete strength and fiber content on the flexural strengths for the serviceability and ultimate limit states. For a certain volume fraction of hooked end steel fibers, the equivalent strength $(f_{eq})_I$ increases significantly as the water-cement ratio of SFRC decreases. However, in SFRCs with the water/cement ratio of 0.65, equivalent strength $(f_{eq})_{II}$ increases slightly with increasing the steel fiber volume fraction. It should be noted that these experimental results are valid for normal strength matrix and low carbon steel fiber; which has a yield strength of 1100 MPa. It can be concluded that the ability of the beam to absorb energy is substantial, even if the cut-off point is taken at the specified deflections of $\delta_0 + 0.65$ and $\delta_0 + 3.15$ mm. Hence, it can be concluded that the results obtained give a clear picture of how a quasi-brittle concrete transforms into a ductile composite with the addition of steel fibers (Bayramov et al., 2004a; Yalçın et al., 2007)

Based on the test results obtained by Yalçın et al. (2007), the performance classes of SFRCs for both small and large deformations (i.e. SLS and ULS), can be indicated. For example, the performance class of SFRC with water-cement ratio of 0.45 and fiber volume fraction of 0.19% can be expressed as, C 40/50 F 2.39/2.00. In this designation, after F the first and the second numbers show f_{eq-I} and f_{eq-II} , respectively. Similarly, for the mixture of SFRC with water/cement ratio 0.65 and $V_f = 0.19\%$, the performance class becomes C 30/37 F 2.01/2.25. In the second group of the experiments obtained by Yalçın (2009), the effect of aspect ratio of the steel fiber on the mechanical and performance properties of steel fiber-reinforced concrete was investigated. The normal strength steel fibers having the aspect ratios of 80, 65 and 55 were utilized. In this group, nine concrete series with steel fibers, and one control concrete were cast.

Figure 4 shows the effects of aspect ratio and fiber content on the equivalent strengths for SLS and ULS. For a certain volume fraction of hooked end steel fibers, the equivalent flexural strengths (f_{eq-I}, f_{eq-II}) increase significantly, as the aspect ratio of SFRC increases. In SFRCs with the aspect ratio of 80, f_{eq-II} increases rapidly with the increasing steel fiber volume fraction. It should be noted that these experimental results are valid for normal strength matrix and low carbon steel fiber; which has a yield strength of 1100 MPa.

It can be concluded that the capability of the beam to absorb energy is substantial, even if the cut-off point is taken at the specified deflections of $\delta_0 + 0.65$ and $\delta_0 + 3.15$ mm. Figures 4a and 4b show the effects of fiber content on the equivalent flexural tensile strengths for both SLS and ULS for three different aspect ratios. For a certain concrete class it is seen that, the fiber content and aspect ratio are the main variables in determining the performance classes of SFRCs (Falkner et al., 1995; Bayramov et al., 2002).

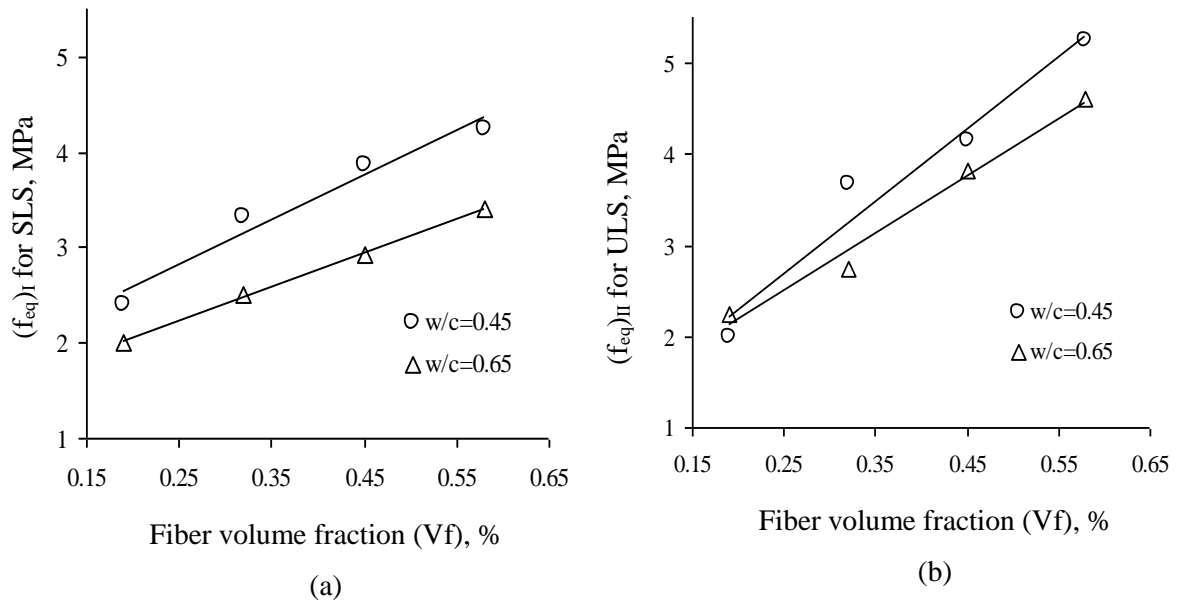


Figure 3. (a) Equivalent flexural strength versus fiber volume fraction curves for SLS, (b) Equivalent flexural strength versus fiber volume fraction curves for ULS (Yalçın, 2007).

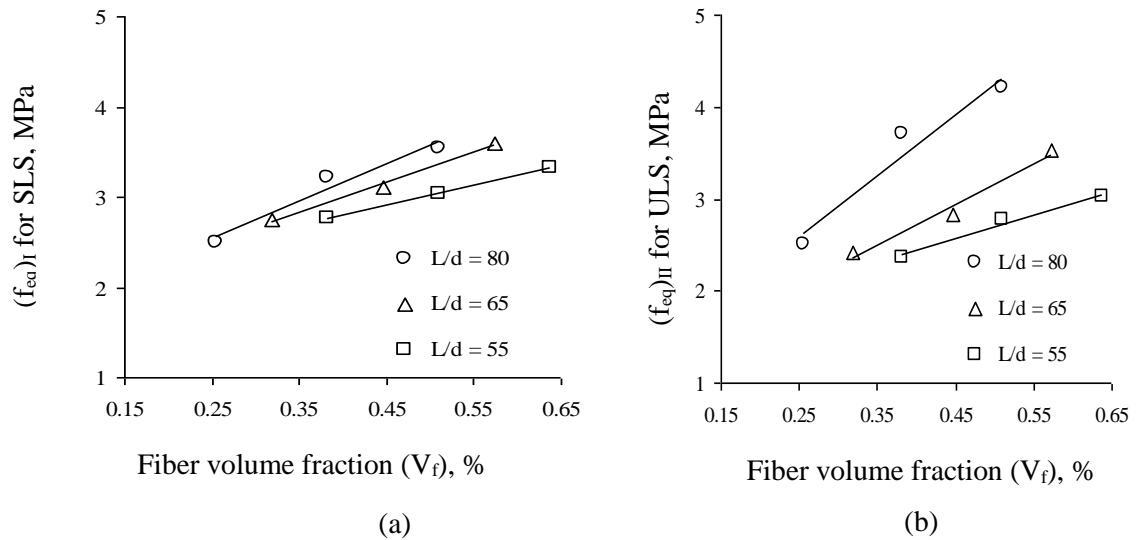


Figure 4. (a) Equivalent flexural strength versus fiber volume fraction curves for SLS, (b) equivalent flexural strength versus fiber volume fraction curves for ULS (w/c=0.55) (Yalçın, 2010).

Based on the test results obtained by Yalcin (2009), the performance classes of SFRCs for both small and large deformations (i.e. SLS and ULS) can be given. For example, the performance class of SFRC with water/cement ratio of 0.55, fiber volume fraction of 0.51% and aspect ratio of 80 can be denoted by C35/45 F 3.54/4.21. Similarly, the performance class of the mixture ($L/d = 65$, $V_f = 0.45\%$ and $w/c = 0.55$) can be said to be C35/45 F 3.11/2.82. It can be concluded that, depending on the concrete quality and the fiber content f_{eq-II} may be greater than f_{eq-I} due to the typical strain hardening behavior as in C35/45 F 3.54/4.21.

3.1.3 Optimization

For the optimum mix design, a multi-objective optimization method was used by using the single composite response (D), which is the geometric mean of the individual desirability function (Meyers and Montgomery, 1995; Bayramov et al., 2004b; Köksal et al., 2006).

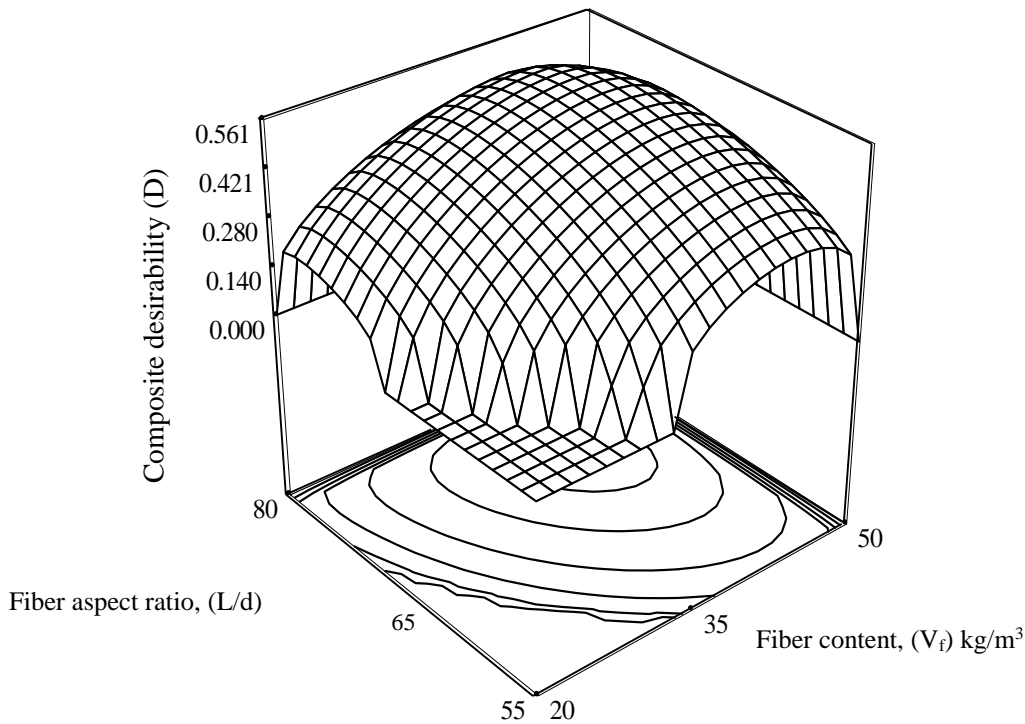


Figure 5. Response surface plot of the composite desirability (D) for group 2 when f_{eq-I} , f_{eq-II} , f_{sp} and G_f are maximized, fiber content (V_c) and cost of mixture are minimized simultaneously

After building the regression models, all independent variables are varied simultaneously and independently in order to optimize the objective functions (Bayramov et al., 2002). For the second group of experiments, composite desirability (D) for this multi objective optimization is shown in Figure 5. Here, the optimal values of design variables are $L/d=72.2$, $V_c=40.9 \text{ kg/m}^3$, and cost of mixture is 1.97 units.

The optimum values of the third group of experiments obtained by Yalçın (2009) are also shown in Table 2. In the third group of his experiments; the aspect ratio was 80 for all fibers. Lengths of these high strength steel fibers were: 60 mm, 40 mm and 30 mm, and they were added in hybrid form to the mixtures having water-cement ratios of 0.32, 0.44 and 0.75. Volume fractions of hybrid steel fibers were: 0.27%, 0.50% and 0.73%. Thus, twelve concrete mixtures were produced for this group.

In summary, based on the results obtained, it can be concluded that; 1) for a certain aspect ratio, as the steel fiber volume fraction increases, mixtures with lower water cement ratio give higher equivalent flexural strengths for both serviceability and ultimate limit states, 2) Response Surface Method (RSM) can be used to maximize mechanical properties and minimize the cost of SFRCs, 3) Performance classification of SFRCs can be made according to the parameters of concrete strength class, the volume fraction, strength and aspect ratio of steel fibers.

Table 2. Optimum values of three groups (Yalçın et al. 2010).

Factors and responses		1st group	2nd group	3rd group
Factors	Water/Cement ratio (%)	49,8	-	46.6
	L/d	-	72.24	-
	V_f , kg/m ³	32	40.92	41.23
Responses	Unit cost	1.83	1.97	2.73
	SLS, $f_{eq I}$, MPa	3.38	3.51	3.45
	ULS, $f_{eq II}$, MPa	3.81	3.80	4.96
	f_{sp} , MPa	5.05	4.6	6.33
	Fracture energy, kN/m	5	4.56	6.06
	Composite desirability (D)	0.463	0.561	0.502

3.1.4 Examples of performance classes for SFRCs

Based on the three groups of experiments and within the limits of the work, performance classes of SFRC can be determined according to both SLS and ULS. The two different examples are shown in Table 2. In case of high volume fractions and high aspect ratios of steel fibers as in Groups 1 and 2 and also in all concretes with hybrid high strength steel fibers, the values of equivalent flexural strength determined according to ULS are higher than those of SLSs. The reason for this is that, after the formation of the first crack, a typical strain hardening behavior is observed in these mixtures except the mixtures with low volume fractions and low aspect ratios, and also low strength plain concrete. Based on the test results obtained by Yalçın (2009), performance classes of SFRCs for both small and large deformations (SLS and ULS), can be given in Table 3. In this table, the concrete mixes were designated with the following codes; the first two digits show the aspect ratio of the fiber, V denotes the volume fraction of fibers, and the last two digits show volume fraction of fibers (i.e., %0.51 and % 0.45).

Table 3. Examples of performance classes for SFRCs (Yalçın et al. 2008)

Mix code	$(f_{eq})_I$ MPa	$(f_{eq})_{II}$ MPa	Performance class
80V51	3.54	4.21	C35/45 F 3.54/4.21-XC4
65V45	3.11	2.82	C35/45 F 3.11/2.82-XC4

If SFRCs are subjected to the exposure class of carbonation with wetting - drying cycle, XC4 in EN206-1 can be added to the designation shown in the last column of the above table.

3.2 Design of SFRCs using the residual strength concept containing crack width limits

The use of normal or high strength steel fibers in tunnel constructions, especially in TBM (Tunnel Boring Machine) segments is gaining acceptance with and/or without classical reinforcement. In recent years, energy based design approaches such as methods using toughness ratings and ultimate flexural strengths through the equivalent flexural strength obtained from a beam test were proposed (Yalçın et al., 2011). Crack width limits are also used in the design practice of SFRCs using the residual strength versus CMOD (Crack Mouth Opening Displacement) curve.

3.2.1 Experimental technique used

In the mix design of SFRC for a tunnel segment project, the main target was to obtain the residual strengths 3.44 MPa for CMOD of 0.05mm, and 2.70 MPa for CMOD of 3.50mm. Two different types of steel fibers with single hooked-ends were added to the mixtures of normal and high strength concretes but in the same volume fraction (0.32% of the total volume of concrete, i.e. 25 kg/m³). Both fibers had the same aspect ratio of 80. The normal and high strength concrete classes are C50 and C70, respectively. The tests were conducted according to EN 14651 “Test method for metallic fiber concrete - Measuring the flexural tensile strength (limit of proportionality (LOP), residual)”. The notched beam specimen tested is shown in Figure 6. A closed-loop testing machine capacity of 100 kN was used for the beam tests. The effective cross-section was reduced to 125x150 mm by means a saw cut. During the testing, the load and signals for displacements were recorded and stored by a computerized data acquisition system. The CMOD was used as a feedback control variable to obtain stable tests and deflections were measured simultaneously by means of a linear variable displacement transducer (LVDT) at mid-span. Thus, load versus CMOD and load versus deflection at the mid-span were obtained for each specimen.

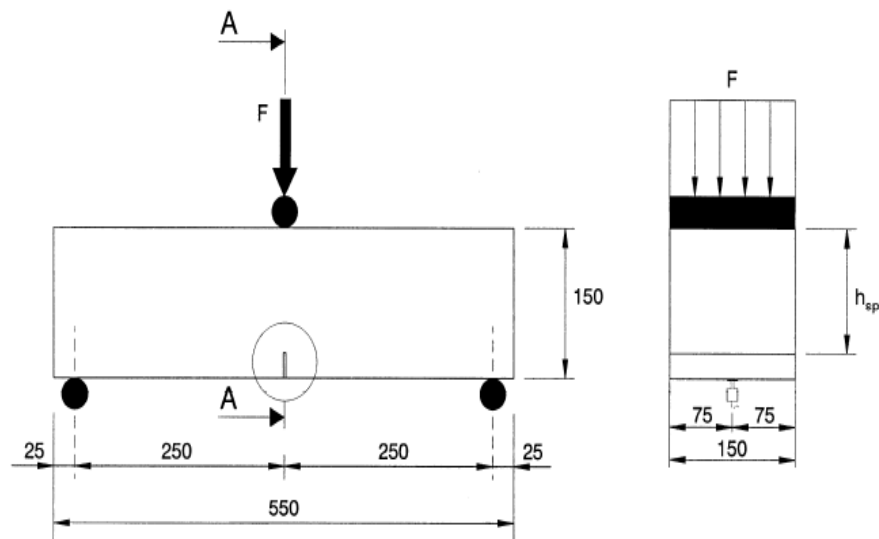


Figure 6. The dimensions of beam tested

3.2.2 Experimental results

Combined effects of steel fiber strength and concrete quality on the residual strength versus CMOD of SFRCs are shown in Figure 7. The curve at the bottom shows the mechanical behavior of C70 NSF (C70 as high strength concrete) with normal strength steel fiber. The tensile strength of this single hooked end steel fiber is 1100 MPa. The curve in the middle shows the response of C50 NSF beam containing the same amount of normal strength fiber. The upper curve shows the behavior of C50 HSF beam reinforced with the same amount of high strength steel fiber, but the tensile strength of the fiber is 1500 MPa. It can be concluded that both C50 NSF and C50 HSF

beams show the typical tensile strain hardening behavior, thus the fiber pull out mechanisms work in these two curves. As seen in the upper curve, for the same concrete quality (i.e., C50), high strength steel fibres significantly affect the post peak response part of the cracking process and increase both the fracture energy and ultimate strength of the concrete.

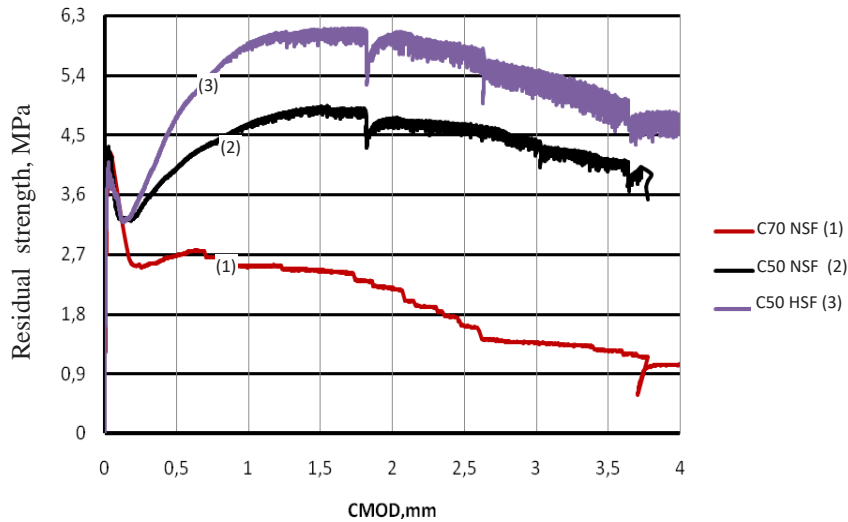


Figure 7. Typical Residual strength - CMOD curves.

As seen in Figure 7, the strengths of steel fibers and concrete have significant effects on the residual stresses in the post-peak response of SFRCs in bending. In high strength concrete (C70) with the same volume fraction of normal strength fibers 0.32% (i.e., 25 kg/m³), the cracks usually cut the fibers without pull out mechanism and thus, fracture tends to be less ductile. As a result, steeper gradients of the residual strength-crack width curve was obtained. In addition, it can be concluded that the normal strength concrete (C50) with high strength steel fibers shows significant ductile behavior in both load-crack width and load-displacement curves. Thus, using different fibers and different concretes, an optimized mix can be obtained as explained in Section 3.1.3

3.2.3 Equivalence between CMOD and deflection

As seen in Figure 8, there is a very strong correlation between the measured values and the linear equation given in Equation 2.

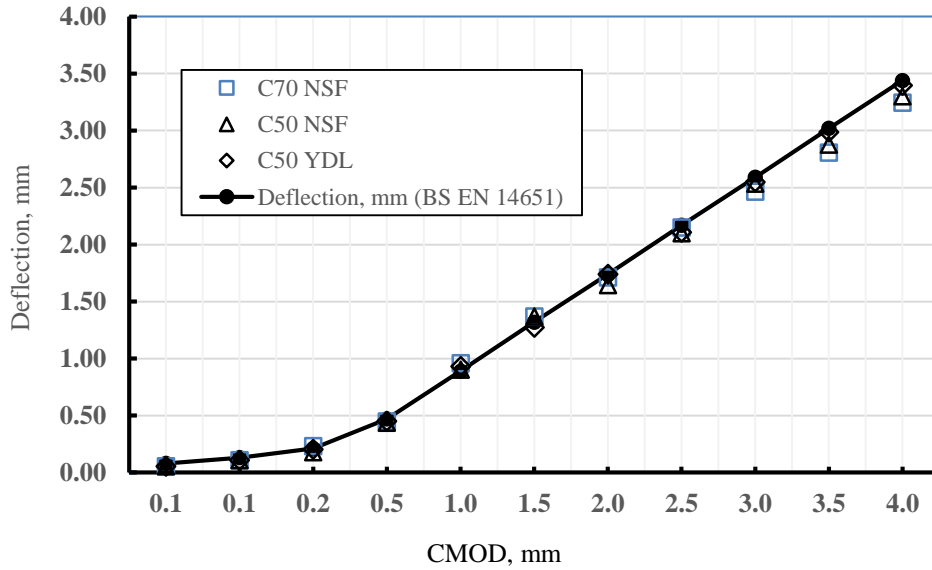


Figure 8. Comparison of the measured values and linear relation in EN 14651

According to EN 14651, the relation between CMOD and deflection can be written as;

$$\delta = 0.85\text{CMOD} + 0,04 , \text{ where } \delta \text{ is the deflection, in mm.} \quad (2)$$

3.2.4 Examples of performance classes for SFRC_S

According to EN 14651 the residual flexural tensile strength $f_{R,j}$ can be given as;

$$f_{R,j} = 3F_j l / 2bh^2_{sp} \quad (3)$$

where $f_{R,j}$ is the residual flexural tensile strength corresponding to $\text{CMOD} = \text{CMOD}_j$ or $\delta = \delta_j$ ($j = 1,2,3,4$), in MPa; as seen in Figure 9, F_j is the residual strength corresponding to $\text{CMOD} = \text{CMOD}_j$ or $\delta = \delta_j$ ($j = 1,2,3,4$), in ; l is the span length, in mm; b is the width of the specimen, in mm; h_{sp} is the distance between the tip of the notch and the top of the specimen, in mm.

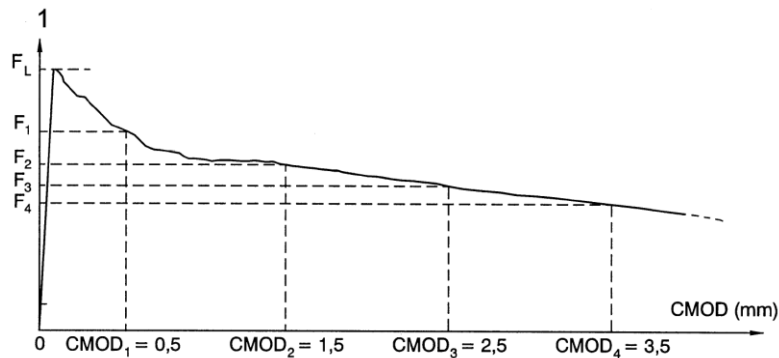


Figure 9. Residual strength, F_j ($j = 1, 2, 3, 4$) versus CMOD (EN 14651)

Based on the comparison of equivalent flexural strengths of SFRCs determined according to DBV (1996) and the residual strengths defined in EN 14651, it can be concluded that $(f_{eq})_I$ and $(f_{eq})_{II}$ are close to the residual flexural strengths $f_{R,1}$ and $f_{R,4}$. Accordingly, the following approximations can be made; $(f_{eq})_I \approx f_{R,1}$ and $(f_{eq})_{II} \approx f_{R,4}$. Thus, as seen in Table 4, within the limits of this work for these three groups, performance classes of SFRCs tested can be determined according to both SLS ($f_{R,1}$) and ULS($f_{R,4}$).

Table 4. According to the critical residual strengths, examples of performance classes of SFRCs

Mix code	$f_{R,1}$ MPa	$f_{R,4}$ MPa	Performance class
C70 NSF	2.7	1.3	C70/85 f 2.7/1.3-XC4
C50 NSF	4.0	4.1	C50/60 f 4.0/4.1-XC4
C50 HSF	4.8	4.9	C50/60 f 4.8/4.9-XC4

As seen in Table 4, since C50 NSF and C50 HSF beams show the typical tensile strain hardening behavior, SLS ($f_{R,1}$) and ULS ($f_{R,4}$) are very close to each other for each specimen. In C70 NSF beam, however, there is dramatic drop from $f_{R,1}$ to $f_{R,4}$ due to the sharp descending branch in the post-peak region of the residual strength versus CMOD. Similar results were also obtained for the load versus deflection curve. As mentioned earlier, if SFRCs are subjected to the exposure class of carbonation with wetting - drying cycles, XC4 in EN206 can be added to the designation shown in the last column of the above table.

As a summary, the design based critical residual stresses obtained in this study were compared with the equivalent flexural strengths based on both SLS and ULS using small and large deflection concepts. Similar trends were obtained for these design based critical stresses for the two approaches.

4 HPSFRCCs and SCCs WITH STEEL FIBERS

As the steel fibre hybridization, the use of a combination of short and long discrete steel fibres controls micro and macro cracks that affect the mechanical behaviour of SFRCs. In such a case, short discrete fibres prevent the formation and propagation of microcracks and also increases the concrete tensile strength before macrocracks are formed while they are pulled out. As summarized here, the amount and strength of steel fibres significantly affect the post peak response of both load versus CMOD and load versus deflection curves in the cracking process, and they increase both the fracture energy and ultimate strength of the concrete (Taşdemir, 2010; Aral et al., 2012).

4.1 Effects of Curing on the Mechanical Behavior of HPFRCCs

In the work of Özalp et al. (2007), effects of fiber strength and curing conditions on the mechanical behavior and fracture properties of high performance cement based composites with hybrid steel fibers were investigated. Depending on the curing temperature condition, concretes with hybrid steel fibers showed a behavior of enhanced toughness and ductility. Fracture energy of plain concrete increased up to 94 times when normal strength steel fibers were included, while in concretes with high strength steel fibers the increase in fracture energy due to steel fibers was 166 times. In their work, partial replacement of aggregate by steel fiber was based on one to one volume basis.

The test results of Özalp et al. (2007) have shown that the most significant effects of both the fiber addition and curing condition are observed on the fracture energy of composites. It was seen that the use of high strength steel fibers improves the mechanical performance and increases the fracture energy of the composite. Especially after the first crack, the formation of strain hardening in the ascending branch of the curve is a typical indication of high performance cementitious composites. The high temperature curing regimes activate pozzolanic reactions in the composites investigated; as a result, fracture energies of the composites increase significantly. The composites with normal strength hooked-end steel fibers have lower peak load and steeper gradients of the softening branch compared to the composites with high strength hooked end steel fibers and the highest fracture energies were obtained from these composites.

4.2 Mechanical Behavior of HPC with HS Short Steel Fibers

Some experimental results obtained by Güvensoy et al. (2004) are shown in Table 5. As seen in the table, the addition of steel fibers results in net bending strengths ranging between 22 and 54 MPa, splitting tensile strengths from 21 to 38 MPa, compressive strengths between 117 and 220 MPa, and fracture energies between 8560 J/m² and 23500 J/m². The measured average fracture energy in M1 was 23500 J/m² for HPFRCC and 108 J/m² for the conventional mortar. It can be concluded that the fracture energy of HPFRCC is almost 220 times that of the conventional mortar.

Table 5. Mechanical properties of HPFRCCs (Güvensoy et al., 2004)

Mechanical properties		M1	M2	M3	M4	M5
Compressive strength, f_c	MPa	162	156	117	146	220
Net bending strength, f_{net}	MPa	54	49	30	22	37
Splitting tensile strength, f_{st}	MPa	30	24	20	21	38
Fracture energy, G_F	J/m ²	23500	18740	9840	8560	17220

4.3 Degradation Properties of HPFRCCs

The determination of a unique focal point of stiffness degradation in concrete has been defined by Lee et al. (1995) for compression, and used by Taşdemir et al. (1999) for three point bending. In the later one, the first three unloading-reloading cycles have been used to locate the focal point; when the post-peak load dropped to about 40 percent of the maximum value, further cycles proved to be inappropriate to use. The normalized stiffness as a measure of degradation of stiffness and the focal point had been determined using unloading-reloading cycles in both the load-Crack Mouth Opening Displacement (CMOD) and the load-deflection curves. The normalized stiffness had been correlated to the normalized local fracture energy, to the normalized permanent CMOD and δ , and to the normalized load (strength degradation). Thus, the focal point has been employed as a measure of concrete brittleness (Taşdemir et al., 1999).

In the work of Güvensoy et al. (2004), load-mid span deflection curves obtained from the bending tests under cyclic loading on HPFRCC beams were studied. In this work, there was no significant loss in the initial compliance of HPFRCCs, the slopes of the unloading-reloading loops were almost same as the slope of the initial ascending part of the load-deflection curve. This is an evidence of the ductility of HPFRCCs. Although, the residual strength decreased after the peak stress, stiffness degradation in HPFRCCs was not significant. Under cyclic actions, steel fibers efficiently bridge the cracks and no significant loss of stiffness is observed even when high levels of deflections are reached. Similar results were obtained in conventional steel fiber reinforced concretes depending on the steel fiber volume fraction (V_f) and the aspect ratio (L/d) by Bayramov et al. (2004a), and also in steel fiber reinforced lightweight concretes depending on aggregate type by Campione et al. (2004).

4.4 SCCs with and without Steel Fibers

In a study, conducted at ITU, the mixture design, workability, mechanical properties and fracture behavior of Self Compacting Hybrid Steel Fiber Reinforced Concretes (SCHSFRC) were investigated. Three different types of steel fibers with and without hooked-ends were added to the mixtures to examine the effect of hybrid steel fibers and their strengths on the mechanical and fracture properties of these concretes. Two different volume fractions of fibers, 1.5 and 0.75% of the total volume of concrete, were used. The results have shown that increasing the fiber content

of the concretes slightly reduced the workability of HSFRCs. It has been shown that the effects of strength and the volume of the steel fibers on the mechanical behavior of the concretes were significant. It was seen that the use of hybrid steel fibers improved the mechanical performance and increased the fracture energy of the concretes. Especially after the formation of the first crack, the progress of strain hardening in the ascending branch of the curve was a typical indication of high performance cementitious concretes. The increase in the fiber content significantly increased the fracture energy of concretes. The short fibers had a limited effect on the post-peak response of load versus displacement at mid-span of the beam, while there was a substantial effect of long fibers on the post peak response part of the curve, which resulted in a high value of fracture energy. The concretes with normal strength hooked-end steel fibers had lower peak loads and steeper gradients of the softening branch compared to the concretes with high strength hooked-end steel fibers and the highest fracture energies were obtained from the latter concretes (Akçay et al., 2007).

The mixture design, fresh and hardened concrete properties of self-compacting concretes with and without steel fibers were studied by Yılmaz et al. (2007). In these mixtures, water/powder ratio was kept constant at the value of 0.52 by volume and, part of cement was replaced with siliceous powder by volume. Steel fiber volume fraction in self-compacting fiber reinforced concretes (SCFRCs) were kept constant at 1%. It was observed that both compressive strength and modulus of elasticity of SCCs and SCFRCs were not affected adversely although water to cement ratio was increased from 0.24 to 0.45 (i.e. cement to powder ratio decreased from 0.73 to 0.41), while the cement content was decreased from 850 kg/m³ to 440 kg/m³. The energy absorption capacity was increased by 13 to 48 times with the addition of fibers. It was also observed that the fiber reinforced concrete with water/cement ratio of 0.63 (i.e. cement/powder ratio of 0.30) did not show self-compacting ability.

5 ORIENTATIONS OF STEEL FIBERS

As mentioned above, the most important parameters affecting the mechanical properties and fracture energy in a properly placed SFRC are the strength of the concrete, the amount, strength and the aspect ratio of the steel fibers. Apart from these parameters, the orientation of the steel fibers is also important for both conventional and high performance steel fiber concretes.

5.1 *Examples for the fiber orientation in conventional SFRCs*

As seen in the Figure 10, an increasing trend was observed in the orientation number with an increase in FA/CA ratio for both types of fibers. The average orientation numbers of 30 mm ($l/d=55$) and 60 mm ($l/d=80$) long fibers are in the ranges of 0.72 – 0.75 and 0.75 – 0.80, respectively. It was found that, when the fiber aspect ratio (and also fiber length) increases, the orientation number also increases (Yardımcı et al., 2014).

Besides the number of fibers in the cross-section of a beam, the orientation of the fibers with respect to main tensile stress is also important. Grünwald (2004) showed that the longer the fibers are, the higher is the orientation number, therefore the performance of beams with longer fibers is more favorably affected by the orientation of the fibers, and suggested a single-parameter model for SFRC mixes. As seen in Figure 10, increasing the FA/CA ratio from 0.94 to 1.72 has resulted in an increase in the orientation number and correspondingly an increase in fracture energy for both types of fibers. Increasing the FA/CA ratio above this level increased the orientation number, however, could not increase the fracture energy anymore. Thus, it may be concluded that enhancement of the workability by increasing the FA/CA ratio may facilitate a more proper fiber orientation and as a consequence this enables a superior flexural performance. However, increasing the FA/CA ratio upon a certain limit may not be able to increase the fracture energy, even if it causes a higher (more favorable) fiber orientation.

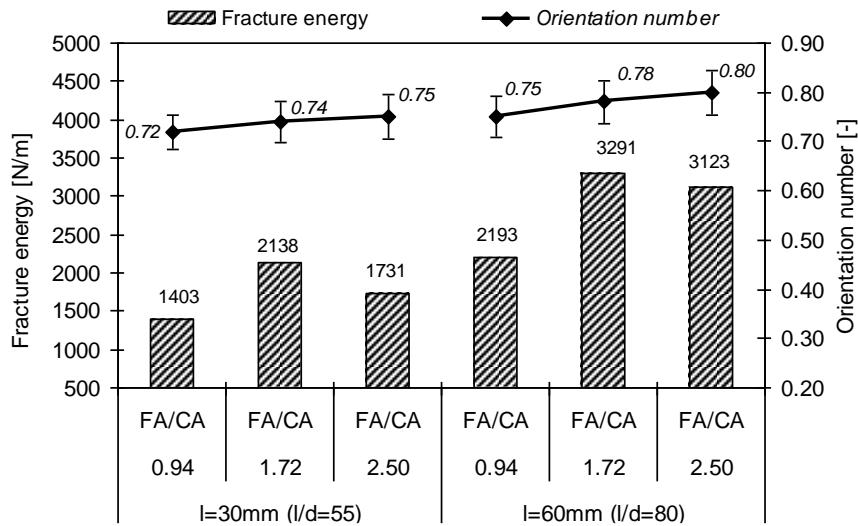


Figure 10. Fracture energy and orientation number of mixtures (Yardımcı et al., 2014)

5.2 Typical fiber orientations in hybrid steel fibre reinforced self-compacting concretes

Akçay and Taşdemir (2012) investigated mixture design, workability, fibre dispersion / orientation, mechanical properties and fracture behaviour of hybrid steel fibre reinforced self-compacting concretes (HSFRSCCs). Three different types of steel fibres with and without hooked-ends were added to the mixtures in two different volume fractions (0.75 and 1.5% of the total volume of concrete). The results have shown that increasing the fibre content of the concretes slightly reduced the workability of HSFRSCC, and the main influencing factor on flowability was the geometry of fibres. The addition of fibres, although did not change the final flowability, decreased the rate of flowability. The orientation and distribution of fibres in concrete have been investigated by image analysis. Since the particles in images are projectiles of fibres, the orientation angles could be obtained. When the orientation angle was 90° , fibres were perpendicularly orientated to loading directions and therefore, they could effectively perform in fracture plane. In contrast, when the orientation angle was 0° , fibres were parallel to the loading direction and thus they could not perform efficiently. It was observed that fibres dispersed homogeneously in all concrete series without any clumping. With increasing amount of fibres, the fibres were more vertically orientated relative to the bending direction, resulting in enhancement in the mechanical properties of concrete.

The results from the experimental tests showed that the flexural strengths increased slightly with increasing strength of long fibres, whereas the splitting tensile strength remained unchanged. The concretes with high strength, long steel fibres show behaviour of enhanced toughness and ductility compared to that with normal strength steel fibres. In this study, no extrusion technique was applied in producing HSFRSCCs. However, the orientations of fibres were almost in the desirable condition. This indicates an effective mixing procedure with superplasticizers and self-compaction during production. As shown in Figure 11, with increasing amount of fibres, the fibres become more vertically aligned relative to the loading direction, resulting in enhancement in the mechanical properties of concrete. Flexural strength and fracture energy of fibre reinforced concrete, in particular, can be enhanced with homogenous distribution of fibres orientated in angles functioning effectively.

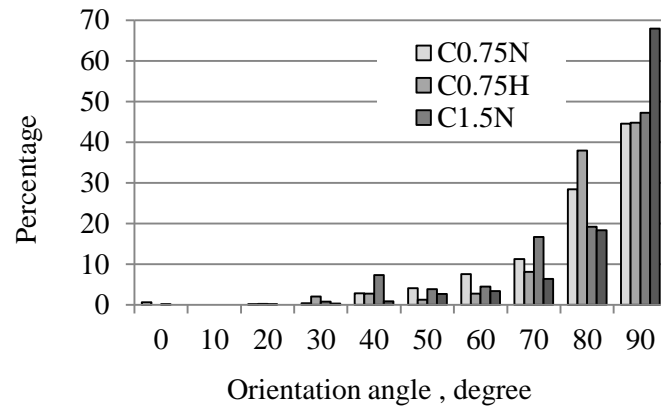


Figure 11. Percent distribution of orientation angles of long fibres (Akçay and Taşdemir , 2012)

6 RECENT ADVANCES IN APPLICATIONS AS ITU-INDUSTRY EXPERIENCES

As products of ITU-Industry collaborations, some recent applications such as industrial floors, precast elements for the city infrastructure made with conventional or high performance SFRCs, and HPRCC panels to be used as shelters against the weapon effects can be presented.

6.1 Full scale industrial floor tests

In the work of Gökalp et al. (2012), the full scale investigations were carried out on eight slabs with the dimensions of 3.0 x 3.0 x 0.15 m. Hooked end steel fibers with a minimum tensile strength of 1050 MPa were utilized. The fibers used in tests were 60 mm in length and 0.75 mm in diameter. In the production of SFRC ground slabs, three steel fiber volume fractions (0.19%, 0.26%, and 0.32%) and four types of elastic sub-base with different elasticity moduli were used. The properties of concrete, type and aspect ratio of steel fibers, and properties of sub ground were kept constant. To obtain different elastic sub-base moduli, different types of extruded polystyrene foam plates, and a rubber sheet in different thicknesses were used.

Specimens were instrumented to monitor both global and local behavior, and a data acquisition system was employed to capture the data. Slabs were loaded at the center with an hydraulic jack through a steel plate with dimensions of 150 mm x 150 mm. Load was applied in 10 kN increments. At every load step, deflections were collected at 16 points by linear variable differential transducers (LVDTs) with a precision of 1/1000 mm. LVDTs were attached to an aluminum frame, which was designed to measure the deflections without touching the specimen or the subgrade. As it is shown in Figure 12, four of the LVDTs (23, 24, 25 and 26) were used at the corners of the slab; another four of them were placed at the midpoint of the edges (19, 20, 21 and 22). To measure the center deflection, as shown in Figure 12, four of them (11, 12, 13 and 14) were used at the center and the rest of them (15, 16, 17 and 18) were distributed on the x and y axes.

Gökalp et al. (2012) have concluded that; i) Maximum observed crack widths were between 1.8 - 3.0 mm and increasing the fiber dosage decreased the crack widths. Therefore, steel fibers create a crack control mechanism and limit the crack width. For the same load level, when the steel fiber dosage rate was increased; the crack widths and the deflections decreased ii) First cracks occurred at between 100 kN and 110 kN, while the ultimate loads ranged between 302 kN and 671 kN. Thus, plates exhibited significant ductility and first cracking load was not an indicator of the ultimate load. iii) Increasing the modulus of the subgrade underneath the slab, increased the

failure load. For the same load level, when the modulus of subgrade reaction decreased; the crack widths and the deflections increased. Increasing the steel fiber dosage rate, increased the ultimate load. iv) Very good agreement was obtained between the experimental results and Finite element Analysis (Gökalp et al. 2012).

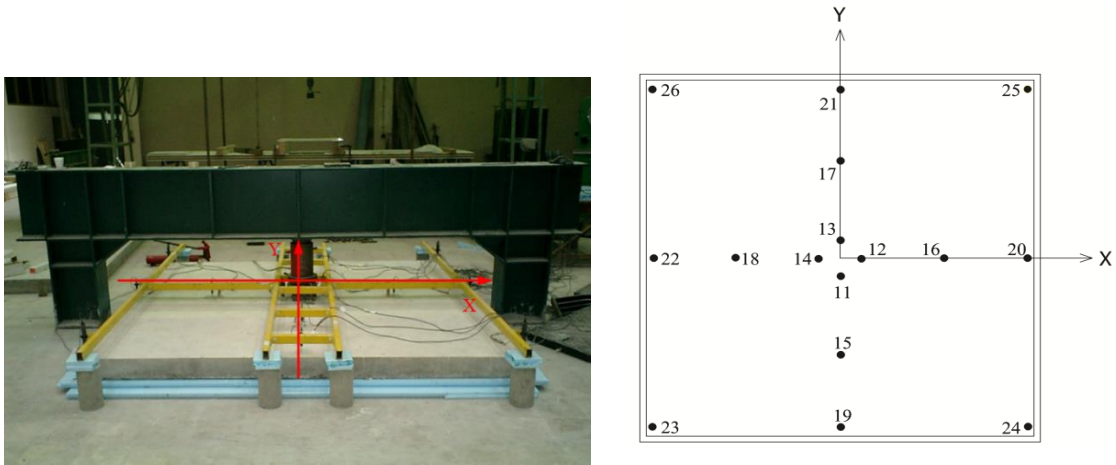


Figure 12. General view of the experimental setup and locations of the LVDTs (Gökalp et al. 2012)

6.2 Some prefabricated elements produced with RPC matrix

As seen in Figures 13 a and 13b, gully tops and manhole covers produced in İSTON, which is a company of Istanbul Metropolitan Municipality, can be used in roads and urban environment for rain water drainage. As seen in 14, the fiber optic cable canal cover was the other prefabricated element produced in the same company for the city infrastructure. In these structural elements containing classical reinforcing bars, ultra high performance steel fiber reinforced composites were used as the matrix. The strength of these matrices reached up to the compressive strength of 350 MPa. The average load carrying capacity of gully tops and manhole covers produced was 460 kN. This means that these productions can be classified to be D400, which is a load carrying ability indicated in EN 124. They are available in different sizes and with special designs such as square gully tops and circular manhole covers. Typical examples are shown in Figure 13 (Özalp et al., 2007).



(a) Circular manhole



(b) Gully tops

Figure 13. Examples of prefabricated elements produced in İSTON for the city infrastructure. In addition to classical reinforcement, reactive powder concrete was used as their matrix (Özalp et al., 2007; Taşdemir and Arslan, 2011)



Figure 14. Fiber optic cable canal cover

6.3 *Development of panels made with HPFRCC for protective structures*

The main objective of this study which was recently completed, is to investigate HPFRCC panels to be used as shelters against the weapon effects.

In this work, the effects of both small arms and anti-tank weapons on a protective system consisting of panels made of a combination of HPFRCCs having various compressive strengths and a wire steel mesh were presented. HPFRCC was employed as a matrix in the proposed protective panel system, which is a quite common application of fine steel fibers in protective elements such as detonation slabs, missile storage and telecom shelters. Small arms include ballistic weapons such as pistols, rifles, shotguns, and submachine guns up to 12.7 mm (0.50 caliber), while anti-tank weapons are limited to shoulder fired rockets such as different types of RPGs and M-72 type Light Anti-tank Weapons (LAWs). In addition to HPFRCC matrix, wire steel mesh reinforcements were welded together in different layers positioned at the various levels of the square panel mold depending on the applied ballistic weapons. Laminated panels, that were organized in a sequence, where either some space or weak materials were present in between them, were developed for demonstrating the ability of the system to absorb more impact energy.

It can be concluded that increasing both the fracture energy and the strength of HPFRCC enhances the penetration resistance of the panels tested regarding protective structures. It was also shown that the size of entrance crater was reduced in the tests where a high amount of fine fibers were used due to the increase in strength and ductility. Large volume fractions of both classical and fiber reinforcements reduced the penetration depth in this investigation. Especially the use of wire mesh steel layers enhanced the penetration resistance of HPFRCC panels by reducing the penetration depth and the front and rear face damages.

7 CONCLUSIONS

Based on the experimental studies realized at ITU and some experiences gained from ITU – Industry collaborations summarized in this paper, the main conclusions that can be drawn are as follows:

The design based critical residual strengths obtained in this study were compared with the equivalent flexural strengths for both SLS and ULS using the small and large deflection concepts in DBV. Equivalent flexural strengths defined in DBV as $(f_{eq})_I$ and $(f_{eq})_{II}$ are close to the residual

flexural strengths $f_{R,1}$ and $f_{R,4}$ in EN 14651. Hence, the following approximations can be made; $(f_{eq})_I \approx f_{R,1}$ and $(f_{eq})_{II} \approx f_{R,4}$.

The strengths of steel fibers and concrete quality have significant effects on the residual strengths in the pre-peak and post-peak responses of SFRCs. It is shown that the normal strength concrete with normal strength steel fibers (C50 NSF) exhibits strain hardening behavior in the pre-peak regions of both load-crack width and load-deflection curves. More substantial results were obtained in the same quality of concrete (C50) with especially high strength steel fibers (C50 HSF). Since C50 NSF and C50 HSF beams show the typical tensile strain hardening behavior, SLS ($f_{R,1}$) and ULS ($f_{R,4}$) are very close to each other for each specimen. In high strength concrete (C70) with the same volume fraction of normal strength fibers 0.32% (i.e., 25 kg/m³), however, the cracks usually cut the fibers without pull out mechanisms and thus, fracture tends to be less ductile. As a result, the decreasing branch of the residual strength-crack width curve is obtained. In this curve, just after the peak, a dramatic drop, i.e. a sharply descending residual strength versus CMOD plot, indicates the lack of pull-out mechanisms of fibers.

The composites with normal strength hooked-end steel fibers have lower peak load and decreasing trend in the softening branch of the load versus deflection curve in bending, compared to the composites with high strength hooked end steel fibers. Thus, the highest fracture energies were obtained from these composites. The measured average fracture energy was 23500 J/m² for HPFRCC and 108 J/m² for the conventional mortar. It can be concluded that the fracture energy of HPFRCC is almost 220 times that of the conventional mortar.

If the steel fiber volume fraction in fiber reinforced self-compacting concretes (SFRSCCs) is kept constant at 1%, it is observed that both compressive strength and modulus of elasticity of SCCs and SCFRCs are not affected adversely although water to cement ratio was increased from 0.24 to 0.45 (i.e. cement to powder ratio decreased from 0.73 to 0.41), while the cement content was decreased from 810 kg/m³ to 440 kg/m³. The energy absorption capacity is increased by 13 to 48 times with the addition of steel fibers.

In SCCs with hybrid steel fibers, it has been shown that with increasing the amount of fibers, the fibers become more vertically aligned relative to the loading direction, resulting in enhancement in the mechanical properties of concrete. Flexural strength and fracture energy of fiber reinforced concrete, in particular, can be enhanced with homogenous distribution of fibers orientated in angles functioning effectively.

Orientation of the steel fibers in laboratory-size beams can be evaluated by means of orientation number. Increasing the FA/CA (fine aggregate/coarse aggregate) ratio from 0.94 to 1.72 has resulted in an increase in the orientation number.

Curing regimes enhance the microstructure of the composite, as a result, the compressive strength, specific fracture energy, toughness and flexural strength can be greatly improved.

There is no significant loss in the initial compliance of HPFRCCs, the slopes of the unloading-reloading loops are almost the same as the slope of the initial ascending part of the load-deflection curve. In HSCs without steel fibers, the focal point defined can be taken as a measure of concrete brittleness and it is close to origin. In HPFRCCs, however, this point is far from the origin or does not exist, in contrast to that of HSCs without steel fibers. Although, the residual strength decreases gradually after the peak stress in HPFRCCs, the stiffness degradation is not significant under cyclic loading condition.

Full scale industrial floor test results show that steel fibers provide a crack control mechanisms and limit the crack width. For the same load level, when the steel fiber dosage rate is increased; the crack widths and the deflections decrease. Increasing the steel fiber dosage rate, increases the ultimate load. Very good agreement was obtained between the experimental results and finite element analysis.

In the production of gully tops and circular manhole covers, specially designed HPFRCC was used as the matrix. Compressive strength of this matrix was about 350 MPa. The load carrying capacity of these productions was 460 kN, which corresponds to a class D400 indicated in EN 134.

It can be concluded that increasing both the fracture energy and the strength of HPFRCC enhances the penetration resistance of the panels tested regarding protective structures. It was also shown that the size of entrance crater was reduced in the tests where a high amount of fine fibers were used due to the increase in strength and ductility. Large volume fraction of both classical and fiber reinforcements reduced the penetration depth in this investigation. Especially, the use of wire mesh steel layers enhanced the penetration resistance of HPFRCC panels by reducing the penetration depth and the front and rear face damages.

In summary, the cost of the steel fibers used in the production of SFRCs is also an important parameter from the application point of view. Therefore, the volume fraction of steel fiber must be minimized to get an economical mixture by maximizing equivalent flexural tensile strengths (or critical residual strengths). Thus, numerical optimization can optimize any combination of either factors or responses. Prices of steel fibers with the high aspect ratio and high tensile strength are higher than those of the lower ones, but their performances are in parallel with corresponding to their prices. Since the designer is interested in the equivalent flexural tensile strengths (or critical residual strengths), but not in the price, SFRC producer should find an optimum solution. Additionally, in the determination of the performance classes of SFRCs, the concrete strength, the ductility of SFRC, durability and workability in the fresh state should be of concern.

ACKNOWLEDGEMENTS

This research was completed in the Civil Engineering Faculty at Istanbul Technical University (ITU). Most of concrete productions used in the studies were produced at Akçansa – Betonsa Technological Center and ISTON laboratories. In the production and testing of HPSFRCC panels for protective structures, the support of ISTON is acknowledged. The author wishes to acknowledge Scientific and Technological Research Council of Turkey (Project: 106G122-Kamu). The support given by BEKAERT is also gratefully acknowledged. The author acknowledges the help of Dr. A. Şafak Açar Özbek for editing the paper.

REFERENCES

- Akçay, B., and Taşdemir, M. A., 2012. Mechanical behavior and fiber dispersion of hybrid steel fiber self-compacting concrete, *Construction and Building Materials*, Vol. 28, pp. 287-293.
- Akçay, B., C., Şengül, M. A. Taşdemir, S. Haberveren, A. N., Kocatürk, G. Arslan, and M. Yerlikaya, 2007. Mechanical behavior of hybrid steel fiber reinforced self compacting concrete, *Proceedings of 3rd International Symposium on Sustainability in Cement and Concrete*, TCMA, Vol. 2, 21-23 May, pp. 953-962.
- Alaee, F. J., 2002. Retrofitting of concrete structures using high performance fiber reinforced cementitious composites (HPFRCCs), *PhD Thesis*, University of Wales, Cardiff, 220 p.
- Aral, M., Ö. Şengül, C. Taşdemir, and M. A. Taşdemir, 2012. Fracture studies on concretes with hybrid steel fibers, *BEFIB 2012 - 8th International Symposium on Fiber Reinforced Concrete*, 19-21 September 2012, Guimaraes, Portugal.
- Balaguru, P., R. Narahai, and M. Patel, 1992. Flexural toughness of steel fiber reinforced concrete, *ACI Materials Journal*, 89, pp. 541-546.
- Betterman, L. R., C. Ouyang, and S. P. Shah, 1995. Fiber-Matrix Interaction in Microfiber-Reinforced Mortar, *Advanced Cement Based Materials*, 2, pp. 53-61.
- Bayramov, F., T. Aydoner, C. Taşdemir, and M.A. Taşdemir, 2004a. An optimum design of steel fiber reinforced concretes under cyclic loading, *Proceedings of Fracture Mechanics of Concrete and Concrete Structures (FraMCoS 5)*, Vail-Colorado, 12-16 April, Vol. 2, pp. 1121-1128.
- Bayramov, F., C. Taşdemir, and M.A. Taşdemir, 2004b. Optimisation of steel fiber reinforced concrete by means of statistical response surface method. *Cement and Concrete Composites*, Vol. 26, pp. 665-675.

- Bayramov, F., C. Taşdemir, and M.A. Taşdemir, 2002. Optimum design of cement-based composite materials using statistical response surface method, *ACE 2002: Fifth International Congress on Advances in Civil Engineering*, 25-27 September, Istanbul, Turkey, pp.725-734.
- Bonneau, O., M. Lachemi, E. Dallaire, J. Dugat, and P-C., Aitcin, 1997. Mechanical properties and durability of two industrial reactive powder concretes, *ACI Materials Journal*, 94(4), pp.286-290.
- Campione, G., N. Miraglia, and M. Papia, 2001. Mechanical properties of steel fiber reinforced lightweight concrete with pumice stone or expanded clay aggregates, *Materials and Structures* 34, pp.201-210.
- Dugat, J., N. Roux and G. Bernier, 1996. Mechanical properties of reactive powder concrete, *Materials and Structures*, 29, pp. 233-240.
- DBV Recommendation, 1996. Basis for the design of industrial floor slabs out of steel fiber reinforced concrete, *Eigenverlag*, Wiesbaden.
- Falkner, H., Z. Huang, and M. Teutsch, 1995. Comparative study of plain and steel fiber reinforced concrete ground slabs, *Concrete International*, January, pp. 45-51.
- Fritz, C., 1991. Tensile testing of SIFCON, In Eds. Reinhardt and Naaman, *Proceedings of 1st International Workshop on HPRCCs*, June 23-26, Mainz, RILEM, pp. 518-528.
- Gökalp, I., O. T. Turan, M. Aydoğan, and M. A. Taşdemir, 2012. Experimental and numerical analysis of SFRC ground slabs under point loading on elastic sub-base, *BEFIB 2012 - 8th International Symposium on Fiber Reinforced Concrete*, 19-21 September 2012, Guimaraes, Portugal.
- Grünwald, S., 2004. Performance-based design of self-compacting fiber reinforced concrete that, *PhD Thesis*, Delft University of Technology.
- Güvensoy, G., A. İlki, F. Bayramov, C. Şengül, M.A. Taşdemir, N. Kocatürk, N., and Yerlikaya, M., 2004. Mechanical Behaviour of Ultra High Performance Steel Fibre Reinforced Concretes under Cyclic Loading Condition, *International Symposium on Ultra-High Performance Concrete*, 13-15 September, Kassel, pp. 649-660.
- JCI-DFRCC Committee, 2003. DFRCC Terminology and Application Concepts. *Journal of Advanced Concrete Technology* 1, No.3, pp. 335-340.
- Kmita, A., 2000. A New Generation of Concrete in Civil Engineering. *Journal of Materials Processing Technology*, 106, pp.80-86.
- Köksal, F., A. İlki, F. Bayramov, and M.A. Tasdemir, 2006. Mechanical Behavior and Optimum Design of SFRC Plates“, *Proceedings of Measuring, Monitoring and Modeling Concrete Properties, S.P. Shah Symposium*, Ed. M.S. Konsta-Gdoutos, pp.199-205.
- Lee, Y., K. Willam, and H.D. Kang, 1995. Experimental Observations of Concrete Behavior under Uniaxial Compression“, *In Proc. FramCoS-2*, July 25-28, Zurich, Switzerland, Vol.1, pp.397-414.
- Myers, RH, and Montgomery, DC, 1995. Response Surface Methodology: Process And Product Optimization Using Designed Experiment, John Wiley & Sons, New York.
- Özalp, F., Y. Akkaya, C. Şengül, B. Akçay, M. A. Taşdemir, and N. Kocatürk, 2007. Curing Effects on Fracture of High-Performance Cement Based Composites with Hybrid Steel Fibers, *Framcos 6, Fracture Mechanics of Concrete and Concrete Structures*, Vol.3, pp. 1377-1384.
- Richard, P., and M. Cheyrezy, 1995. Composition of Reactive Powder Concrete, *Cement and Concrete Research*, 25, pp.1501-1511.
- Taşdemir, M. A., 2010. High Performance Fiber Reinforced Cement Based Composites and Their Applications”, *İMO-JSCE Joint Symposium on Concrete Engineering*, 9 June 2010, Istanbul, pp. 1-16.
- Taşdemir, M.A., and E.G. Arslan, 2011. Mechanical Behavior and Applications of HPRCCs with Hybrid Steel Fibers: The ITU Experience, *6th International Conference on Fiber Concrete 2011: Technology, Design and Application*, 8-9 September, Prague.
- Taşdemir, M. A., C. Taşdemir, S. Akyüz, A.D. Jefferson, F.D. Lydon, and B.I.G. Barr, 1998. Evaluation of Strains at Peak Stresses in Concrete: A Three Phase Composite Model Approach, *Cement and Concrete Composites* 20, pp.301-318.
- Taşdemir, C., M.A. Taşdemir, N. Mills, and B.I.G. Barr, 1999. Combined effects of silica fume, aggregate type, and size on post peak response of concrete in bending. *ACI Materials Journal*, 96, pp.74-83.
- Taşdemir, M.A., H.N. Atahan, I. Gökalp, M. Yerlikaya, 2008. A Comparison of Workability and Mechanical Properties of Normal and Lightweight SCC Mixtures with and without Steel Fibers, *SCC 2008: Challenges and Barriers to Application*, Chicago. Also Published in *Concrete Plant International (CPI)*, April 2009, pp.58-61.
- Yalçın, M., 2009. Optimization and Performance Based Design of Steel Fiber Reinforced Concretes, *PhD Thesis*, Istanbul Technical University, Institute of Science and Technology, 205p.
- Yalçın, M., C. Tasdemir, M.A. Tasdemir, I. Gokalp, and M. Yerlikaya, 2008. Performance Based Design of SFRC for Serviceability and Ultimate Limit States, In: Ed. R. Gettu, *Fiber Reinforced Concrete: Design and Applications (BEFIB 2008)*, RILEM Publications S.A.R.L., pp.419-428.

- Yalçın, M., C. Taşdemir, M.A. Taşdemir, I. Gökalp, and M. Yerlikaya, 2010. Optimum design of normal and high strength SFRCs: limit states and performance classes“, *Proceedings of Fracture Mechanics of Concrete and Concrete Structures, FraMCoS 7*, Jeju – Korea.
- Yalçın, M., C. Taşdemir, M.A. Taşdemir, I. Gökalp, and M. Yerlikaya, 2011. Optimum Design of Conventional SFRCs and Their Performance Classes”, *6th International Conference on Fibre Concrete 2011: Technology, Design and Application*, 8-9 September, Prague.
- Yalçın, M., C. Şengül, C. Taşdemir, I. Gökalp, Z. Yüceer, and H. Ekim, 2007. Performance Based Design of Steel Fiber Reinforced Concrete, *Proceedings of 3rd International Symposium on Sustainability in Cement and Concrete*, TCMA, Istanbul, 21-23 May, Vol 2, pp. 931 -940.
- Yardımcı, M.Y., Baradan, B., and Taşdemir, M.A., “Effect of Fine to Coarse Aggregate Ratio on the Rheology and Fracture Energy of Steel Fibre Reinforced Self-Compacting Concretes”, *Sadhana*, Vol. 39, No: 6, 2014, pp.1447-1469.
- Yılmaz, B., A. Dinç, C. Şengül, Y. Akkaya, and M.A. Taşdemir, 2007. Effects of Cement/Powder Ratio on Workability and Mechanical Behavior of SFRCs. *Advances in Cement Based Materials and Applications in Civil Infrastructure-(ACBM-ACI)*, 12-14 December, Lahore, pp.721-731.

Fiber reinforced cementitious composites for retrofit of reinforced concrete members-A Review

Idris Bedirhanoglu¹, Alper Ilki²

¹ Associate Prof. Dr., Diyarbakir, Turkey

² Prof. Dr., Istanbul, Turkey

ABSTRACT: A wide range of research has shown that fiber reinforced cementitious composites are very effective for retrofitting of concrete members. In addition to superior mechanical performance, wide range of applicability and high durability are among key advantages of fiber reinforced cementitious composites. In this paper, a literature review on the use of fibers in retrofitting of reinforced concrete members is presented. In addition to the literature review, a summary of research works on retrofitting of concrete/reinforced concrete members making use of fibers (made of steel or glass) executed by the authors during last two decades is also presented.

1 INTRODUCTION

High durability, high strength, low cost, easy usage and easy accessibility anywhere locally, make concrete the most used construction material in the World. Today, the increasing popularity of concrete causes changes and progress in concrete properties. In particular, pursuant to the advances in concrete technology in recent years, it has been possible to produce special concrete with very high strength. However, high strength concretes typically exhibit brittle behavior. Especially for that reason, the research focuses on increasing the tensile strength, toughness and ductility of the concrete as well as increasing the concrete compressive strength. Existing works showed that the drawbacks can be overcome by adding fibers into the concrete mixture.

When these properties are imparted to concrete, this material becomes an alternative for other application purposes such as structural retrofitting. Compared to other common retrofitting techniques, such as external confinement using fiber reinforced polymers (FRPs), higher compression strength, shear strength, and flexural stiffness of fiber reinforced cementitious composites bring important advantages. According to Li (Li 2000) most of the applications of steel fibers are nonstructural where fibers are generally used in limiting the shrinkage. Furthermore, he concluded that fibers has some advantages over conventional steel reinforcement where the advantages include uniform reinforcement distribution, resistance to corrosion and savings in labor costs.

In 2000s, interest in structural retrofitting has started to increase. Particularly, for buildings where it is not possible to demolish and rebuild the structure, retrofitting becomes inevitable. Although retrofitting of structures is not a new matter (Fukuta et al. 1998, Ilki et al. 1998, Tankut et al. 1998), the use of high technology cementitious composites in retrofitting is a new issue. In this paper, an extensive literature review, including the authors' own research projects are outlined and conclusions based on this literature survey are presented with suggestions for further research.

2 FIBER REINFORCED CEMENTITIOUS COMPOSITES

2.1 Fibers

The history of fibers goes back to ancient Egyptian times where organic fibers were used to reinforce clay (Torah 2018). Today, a lot of different types of fibers are available according to the material they are made from, their shapes and sizes (ie. steel, micro-synthetic, macro-synthetic, glass, cellulose, natural, and poly-vinyl alcohol (PVA) fibers). These types of fibers have varying properties and applications. Steel fibers are generally used to enhance the toughness and post-crack load carrying capacity. It has been five decades since fibers had been brought to the attention of academic society (Romualdi and Mandel, 1964). A variety of steel fibers in different shapes are available: straight, crimped, hooked single, hooked collated, and twisted (Tadepalli et al. 2009). The oldest and most basic steel fiber type is a straight fiber, cut from smooth cold drawn wire. Unfortunately, such fibers do not ensure the full utilization of the strength of steel because of a lack of appropriate bond (anchorage) to the matrix. It was realized that the anchorage of fibers can be drastically improved by modifying the fiber shape, resulting in a wide range of steel fiber types, some of which are illustrated in Figure 1 (ACI 544 1996, Naaman 2003). Each of the types was additionally varied by diameters and length (Maidl 1995, Katzer 2006). Steel fibers can be classified in four groups in terms of shape of the fibers; 1- completely flat, 2- wavy along its length, 3- wavy wires in the shape of half moon, 4- hook-ended (Figure 1). There are some research works on the effect of shape of fibers (Bayasi and Soroushian 1991, Balaguru and Shah, 1992, Wafa and Ashour 1992, Banthia and Trottier 1995, Dugat et al. 1996). As a result of these works the common point is that since it has a crucial effect on the bond between fibers and concrete, effect of the shape of fibers cannot be ignored.

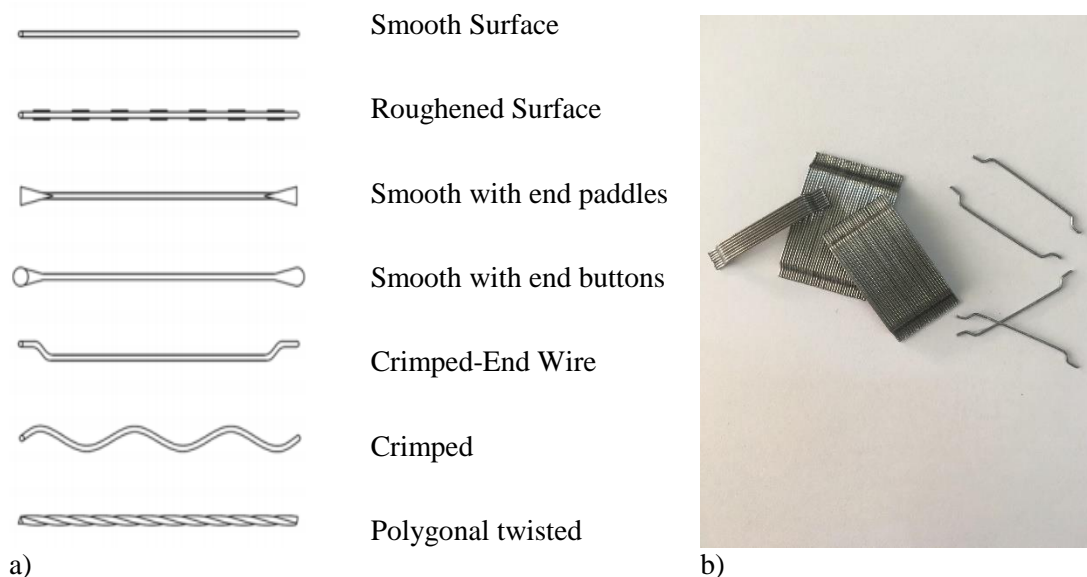


Figure 1. a) Different shape of steel fibers (adapted from ACI 544, 1996; Naaman 2003), b) steel fibers (Dramix ZP 305)

2.2 Fiber reinforced cementitious composites and applications

The recent research works provided remarkable information on improving concrete properties through use of different types of fibers. Various types of concretes with fibers were developed such as, Fiber Reinforced Cementitious Composites (FRCC), Fiber Reinforced Concrete (FRC), Fiber Reinforced Mortar (FRM), Ductile Fiber Reinforced Cementitious Composites (DFRCC), Slurry Infiltrated Fiber Concrete (SIFCON), Ductile Fiber Reinforced Cementitious Composites (DFRCCs), High Performance steel Fiber Reinforced Cementitious Composites (HPFRCCs), Ultra High Performance Fiber Reinforced Concrete (UHPFRC), Precast-HPFRCC, Engineered Cementitious Composites (ECC), Slurry Infiltrated Mat Concrete (SIMCON), Reactive Powder

Concrete (RPC), sprayed Glass Fiber Reinforced Concrete (GFRC) and Glass Fiber Reinforced Mortar (GFRM) (ie. Bayasi ve Soroushian 1991, Balaguru ve Shah, 1992, Wafa and Ashour 1992, Banthia and Trottier 1995, Naaman et al. 1996, Dugat et al. 1996, Gao et al. 1997, Li et al. 2000, Wang and Lee 2007, Farhat et al. 2007, Brühwiler and Denarié 2008, Comert et al. 2014, Ates et al. 2018).

Fiber reinforced concrete (FRC) has been used successfully in structures subjected to bending and/or shear such as slabs on grade, highway bridge slabs, piles, tunnel linings, architectural concrete, precast elements, offshore structures, structures in seismic regions, thin and thick repair, crash barriers, footings, blast resisting structures, nuclear reactors and various hydraulic structures (Figure 2). FRC exhibits better performance not only under static and quasi-statically applied loads but also under fatigue, impact, and impulse loadings and under environmentally imposed cracking (Higashiyama and Banthia, 2008).



a) Tunnel lining (Riva Railway) b) Precast panels (courtesy of Mehmet Yerlikaya)

2.3 Effect of steel fibers on concrete properties

Steel fibers change the behavior of concrete in all types of concrete. Particularly mechanical properties of steel fiber reinforced concrete derived by fiber types, volume, tensile strength, slenderness, orientation and dispersion of fibers. The matrix concrete strength and processing cementitious composites such as using extrusion technique are also can be count as another parameter that affects the strength of steel fiber reinforced concrete. A small amount of fibers could also increase toughness evidently where for every certain target volume of steel fibers to be used in concrete is changed generally between 0.5% to 6% in terms of volumetric ratio of concrete (Balaguru and Shah, 1992, Richard and Chezezy 1994, Gao et al., 1997, Akkaya 2000, Akkaya et al., 2000, Qian and Stroeven 2000, Akkaya and Shah 2001, Gutiérrez et al., 2005, Bayramov ve diğ., 2004a, Bayramov ve diğ., 2004b, Bedirhanoglu and Ilki, 2009).

3 RETROFITTING THROUGH USING STEEL FIBER REINFORCED CONCRETE

Past studies on the use of steel fibers particularly for retrofitting are summarized and evaluated in this section. Before this, some key works on the improvement of steel fiber reinforced concrete was touched upon briefly.

High-strength fiber-reinforced concrete has been studied by many researchers (Shah 1991, Li et al. 1993, Shannag et al. 2001, Shannag et al. 2005, Lu and Hsu 2006, Li et al. 2015). The Strain-Hardening Engineered Cementitious Composites have been developed with the aid of fracture mechanics and micromechanics by Li et al. (2000). Only a few sets of material tests were conducted and they conclude that because of the strain-hardening property of ECC this material behaves like steel. Effect of steel fibers addition on mechanical properties of concrete and RC beams was investigated by Altun et al. (2007) and they observed that increase both in load carrying capacity and toughness with addition of steel fibers to RC beams for mixture ratios of 30 to 60 kg/m³ is negligible. Several studies demonstrated that fiber can be used to replace transverse reinforcement (Meda et al., 2005, Minelli et al., 2006). Shear strength of SFRC beams

without web reinforcement were investigated by Kwak et al. (2002). Particularly remarkable (69 to 80%) increase in strength was observed with smallest shear span ratio ($a/d=2$, where a : shear span and d : effective depth of the beam). Behavior of Uni-Directional Cloth (UDC) Glass fiber reinforced concrete (GFRP) laminate-retrofitted steel fiber reinforced concrete (SFRC) beams was also investigated by Rajeshguna et al (2008). In their work, 3 and 5 mm UDCGFRP laminates bonded to tension side of the beam with epoxy resin. They observed that UDCGFRP strengthened SFRC beam resulted in more than 60% higher load carrying capacity. Behavior of frames with steel fiber addition was studied by Arslan and Dogan (2015). They concluded that steel fibers postponed the formation of cracks. A different approach was used by Boscato and Russo (2009) where they applied a thin layer of SFRC with different thicknesses to the surface of reinforced concrete (RC) slab and they observed a good bonding between RC slab and SFRC material and the first crack load was enhanced with different extend depending on the thickness of SFRC layer.

Blast resistance was studied by some researchers (Kalman, 2010; Cargile et al., Yusof et al. 2010, Bazgir, 2016; Li et al. 2015, Li et al. 2017 ie.). In work done by Kalman (2010) steel fibers was added to reinforced concrete to improve blast resistance. Kalman did a reasonable thing since for higher blast resistance greater mass and flexibility are required. It was concluded that steel fibers delay the failure mechanism in steel fiber reinforced concrete and this delay in failure mechanism results in reducing flying debris when compared to conventional RC.

Mahmud et al. (2013) investigated size effects on the structural strength of UHPFRC beam members. It was seen that up to 150 mm depth effect is very little. From experiments and finite element analysis (ABAQUSTM) it is clear that size effect is negligible up to 300 mm in depth. Singh et al. (2017) have modified the damage plasticity model to simulate the bending behavior of steel fiber concrete with finite elements. By conducting large-scale material tests, they developed a finite element model that yields quite reasonable results by calibrating material behavior via these tests.

It has been about two decades that steel fiber reinforced concrete has been used as a retrofitting material. Alaei (2002) and Alaei and Karihaloo (2003) retrofitted beams with prefabricated composite panels (CARDIFRC). They observed significant increases in the shear and flexural capacity of CARDIFRC-strengthened beams. They also developed an analytical model to predict moment resistance and load-deflection response of CARDIFRC-strengthened beams. First works on column retrofitting with SFRC were done by Ilki. Ilki et al. (2004) and Ilki et al. (2009) used prefabricated-HPFRCC to retrofit columns through external confinement. They reported that precast-HPFRCC panels used for external confinement increased the ductility and strength of retrofitted rectangular columns under axial loads as well as under the combined action of axial loads and reversed cyclic flexure. Shannag et al. (2002) used a 25-mm thick jacket of cast-in place HPFRCC to repair interior reinforced concrete (RC) beam-column joints. They observed a significant improvement in the behavior of HPFRCC-retrofitted weak connections. Ravichandran and Jeyasehar (2012) used ferrocement to retrofit exterior ductile and non-ductile beam-column joints. In addition to joints, beams were also retrofitted in their experimental study. They observed increases in energy dissipation achieved by retrofitting non-ductile joints with ferrocement. In addition to joints, ferrocement retrofit has also been used for beams and columns by Kumar et al. (2007). In tests on full-scaled beams carried out by Martinola (2007), it has been found that strengthening with HPFRCC was very effective, especially deformations under service loads decreased by 12 times. This decrease in deformations corresponds to pretension behavior. They found that the HPFRCC material adhered very well to the surface after a simple blasting of the existing concrete surface. Lastly, they found that the 40 mm HPFRCC thickness are well enough thickness for retrofitting. Rajeshguna et al. (2008) RC beams casted with %1 steel fibers were retrofitted with wrapping FRP. Enhancement both in load resistance and ductility were reached. Martinola et al. (2010) tested 3 large scaled beams retrofitted with 40 mm-HPFRCC bonding on 3 sides of the beams with and without longitudinal reinforcement. They conclude that due to easy and quick curing and casting a single thin layer of HPFRCC is a promising retrofitting technique.

Ruano et al. (2014) retrofitted beams with steel fiber reinforced concrete containing 30 and 60 kg/m³ of steel fibers. They found that the retrofitting is effective however the results were scattered. Beams were retrofitted with SFRC jacketing by Gonzalo et al. (2014). Repaired and retrofitted specimens showed excellent behavior in terms of strength and deformability. It was also seen that the addition of fibers to the concrete had an important effect on the prevention of the debonding of the jacketing from the beams.

Hussein and Amleh (2015) observed that the bending capacity of the beams increased by 54-90% when they made the pulling area of the beams from the concrete layer containing 1.5-2% steel fiber. They also observed a significant increase in their shear capacity and they have proposed a model for calculating the shear capacity. Paegle (2015) investigate characterization and modelling of FRC for structural applications. Lampropoulos et al. (2016), through the experimental and finite element analysis concluded that the wrapping of UHPFRC on three sides are an effective reinforcement method for beams. They also observed 30% reduction in shrinkage in case of 3% steel fiber addition to concrete. Anuradha and Britto (2016) tested 9 beam specimens retrofitted by bonding Steel Fiber Reinforced Ultra-High Strength Concrete (SFRUHSC) strip with 3-mm epoxy and found that load carrying capacity and serviceability of specimens were enhanced up to around 10%. Tanarslan (2017) increased the bending capacity of the beams retrofitted with UHPFRC by 30% to 200% and stated that UHPFRC was an effective method for increasing the bending capacity.

Mostosi et al. (2011) Retrofitted beams with HPFRC mortar with direct surface application (without epoxy). They concluded that strength of beams increases with increase in plate thickness.

Rosignoli et al. (2012) retrofitted actual scaled columns with pouring 40 mm thick layer of SFRC on four sides of the column. They concluded that retrofitted columns gain both strength and ductility with a thin layer of SFRC. Furthermore, the core concrete would have better durability performance with this thin layer of SFRC.

Hassanean et al. (2012) retrofitted beams with U-Shape SFRC jacketing with various thickness and steel fiber content. They used shear connector to improve the bond between SFRC jacket and concrete surface of the beam. They conclude that presence of shear connectors in the jacket play an important role in bond enhancement between the main beam and the jacket and prevent the debonding.

Lee et al. (2018) studied the effects of blast-induced local damages on the flexural strength of blast-damaged and repaired specimens. Specimens were repaired with steel fiber reinforced cementitious composite (SFRCC) as well as carbon fiber-reinforced polymer (CFRP) sheets and tested for flexural strength measurements. From test results, they concluded that replacing damaged concrete cover with SFRCC is adequate for repairing the blast-damaged RC members.

Lejano (2013) examined increase in axial load capacity of the columns by being wrapped with different materials. The study concludes that all retrofitting techniques were successful in increasing the strength of the column. However, it is the 2% steel FRM jacket that showed the best increase in strength among all cases. Lejano (2017) used FRM as a jacketing material for retrofitting RC columns. Both steel and polymer fibers were used. The results indicate that the FRM jackets are effective as a retrofitting material for RC column.

Wang and Lee (2007) retrofit joints with RC jacketing and Ultra-High Strength Steel Fiber-Reinforced Concrete (UFC) replacing in joint. They concluded that despite more tests were needed, good performance in terms of strength and durability for -18 and +4.4 °C were observed. RC joints with very low strength concrete were retrofitted with precast-HPFRCC plate bonding to joint surface through epoxy application by Bedirhanoglu (2009) and Bedirhanoglu et al. 2013. Precast-HPFRCC plate bonding resulted in increase in both strength and deformability. Tsonos (2009) also retrofitted beam-column joints cast with low strength concrete with UHSFC Jacketing to columns and the joints. Bedirhanoglu et al. (2012) compared performance of FRP and

prefabricated-HPFRCC retrofitted beam column joints and they conclude that prefabricated-HPFRCC plate bonding is also a convenient retrofitting method.

Table 1. Literature review

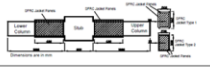

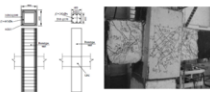


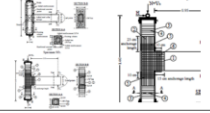
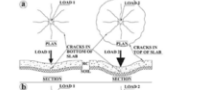
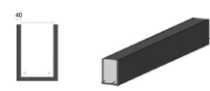
Researchers	Year	Fiber Types	Fiber Volume (%)	Mortar Types	Retrofitting Types	Reason, Deficiency (Excitation)	RC Members	Concrete Strength (MPa)	Mortar Strength (MPa)	Parameters	Number of Specimens	Conclusion	Details
Ilki et al.	2004	Steel Fibers		SFRC	SFRC bonding	Lap splice	Column	10	90	Plate thickness	6	Ductility enhanced but attention should be paid to the bonding of the SFRC	
Farhat et al.	2007	Steel Fibers		CARDIF RC	CARDIFRC strip bonding	Moment, shear	Beam	60	200	Cycles, side bonding	6	Thanks to fibers beam was not affect by thermal cycles between 0-90 °C. To prevent shear failure CARDIFRC must be bonded side of the beam, too.	
Wang and Lee	2007	Steel Fibers	40 kg/m ³	UFC	RC Jacket/UFC replacing in Joint	Shear/No Hoops at Joint	BC Joints	34	182	-	3	more tests needed, good performance in terms of strength and durability -18 and +4.4 °C	
Bedirhanoglu et al.	2008	Steel Fibers	4	Prefabricated-HPFRCC	HPFRCC bonding with epoxy	Shear	Concrete Panels	10	135	HPFRCC thicknesses, anchorage	8	remarkably higher shear strength and deformability were possible, particularly when the anchored to the concrete specimens properly prefabricated HPFRCC panels were	
Rajeshguna et al.	2008	Steel Fibers	1	SFC	FRP laminates	Flexure	Beam	66	-	-	4	with %1 steel fibers were retrofitted with wrapping FRP	
Tsonos	2009	Steel Fibers-ZP30/0.6	1,5	UHSFC	UHSFC Jacketing	shear and ductility	Column and joint	8,5	106		6	This new innovative method was found to be much more effective than the conventional reinforced concrete jackets and especially the FRP-jackets.	
Boscato and Russo	2009	Steel Fibers	5	SFRC	Pouring SFRC	Bending	Slab	25	-	SFRC thickness	5	Crack patterns has influenced by SFRC thicknesses	
Martinola et al.	2010	Steel Fibers		HPFRCC	40-mm HPFRCC application	Moment, shear	Beam	22	177	Longitudinal reinforcement and jacket	3	building codes require to verify the strengthened structure both at the ultimate limit state and at the serviceability limit state	

Table 1. Literature review (continued)

Researchers	Year	Fiber Types	Fiber Volume (%)	Mortar Types	Retrofitting Types	Reason, deficiency (Excitation)	RC Members	Concrete strength	Mortar strength	Parameters	Number of specimens	Conclusion	Details
Mostosi et al.	2011	Steel Fibers		HPFRC	HPFRC application without epoxy	shear	Beam	33		Jacket thicknesses, bonding, mortar application	4		
Rosignoli et al.	2012	Steel Fibers		HPFRC Jacket	Pouring SFRC	Axial load, flexure	Column	20	130			Increases in both strength and ductility	
Corvez and Masson	2013	Steel Fibers		UHPFRC	UHPC application to walls	impermeability	Wall		133			They find the retrofitting method very promising.	
Bedirhanoglu et al.	2013	Steel Fibers	4	Prefabricated-HPFRCC	HPFRCC bonding with epoxy	Shear	Joints	10	135	HPFRCC thickness, anchorage	8	Remarkably higher shear strength and deformability were possible, particularly when the anchored to the concrete specimens properly prefabricated HPFRCC panels were	
Mahmud et al.	2013	Steel Fibers	2	UHPFRC	NA	size effects	beam	NA	150	Beam depth	15	Size effect is negligible up to 150 mm in depth	
Gonzalo et al.	2014	Steel Fibers	30-60 kg/m ³	SFRC	SFRC plate bonding	Shear	Beam				18	The experimental program showed the possibility of performing the retrofitting at work place.	
Anuradha and Brito	2016	Steel Fibers	2	SFRUHS C	SFRUHS C strip with 3-mm epoxy	Flexure/serviceability	Beam	46	122	Plate thickness	9	Load carrying capacity and serviceability enhanced	
Koo and Hong	2016	Steel Fibers	1.5	UHPFRC	UHPFRC jacketing	Flexure/ductility	Column	29	145	Plate thickness	4	Load carrying capacity and serviceability enhanced	

Retrofitting of brick infill wall with using steel fibers was studied by Sevil et al. (2010). They applied steel fiber reinforced mortar (SFRM) onto the hollow brick infill of a reinforced concrete (RC) structure. Mortar with plasticizer, 2% volume of steel fiber and 20-mm-thick layer of SFRM came out to be the optimum mortar mixture to be used as a strengthening material.

Corvez and Masson (2013) used steel fibers in retrofitting of nuclear reactors. UHPFRC used for the reinforcement and air-tightness of the inner walls of nuclear reactor and they find the retrofitting method very promising in retrofitting of such structures.

UHPFRC was used as jacketing in order to retrofit columns by Koo and Hong (2016). Four nearly full-scaled specimens were cast and one of the specimens was used as reference specimen while the others retrofitted with 30 mm and 50 mm UHPFRC jacketing. The last specimen was retrofitted with 50 mm UHPFRCC jacket and D10@150 mm hooks. As a result of experimental work, it was seen that a small amount of UHPFRCC jacket brings much more shear strength.

RPC was used to retrofit beams by Kathik and Sundaravadivelu (2017). 10-mm and 20-mm thick layer of RPC resulted in 10% and 23% increase in load respectively.

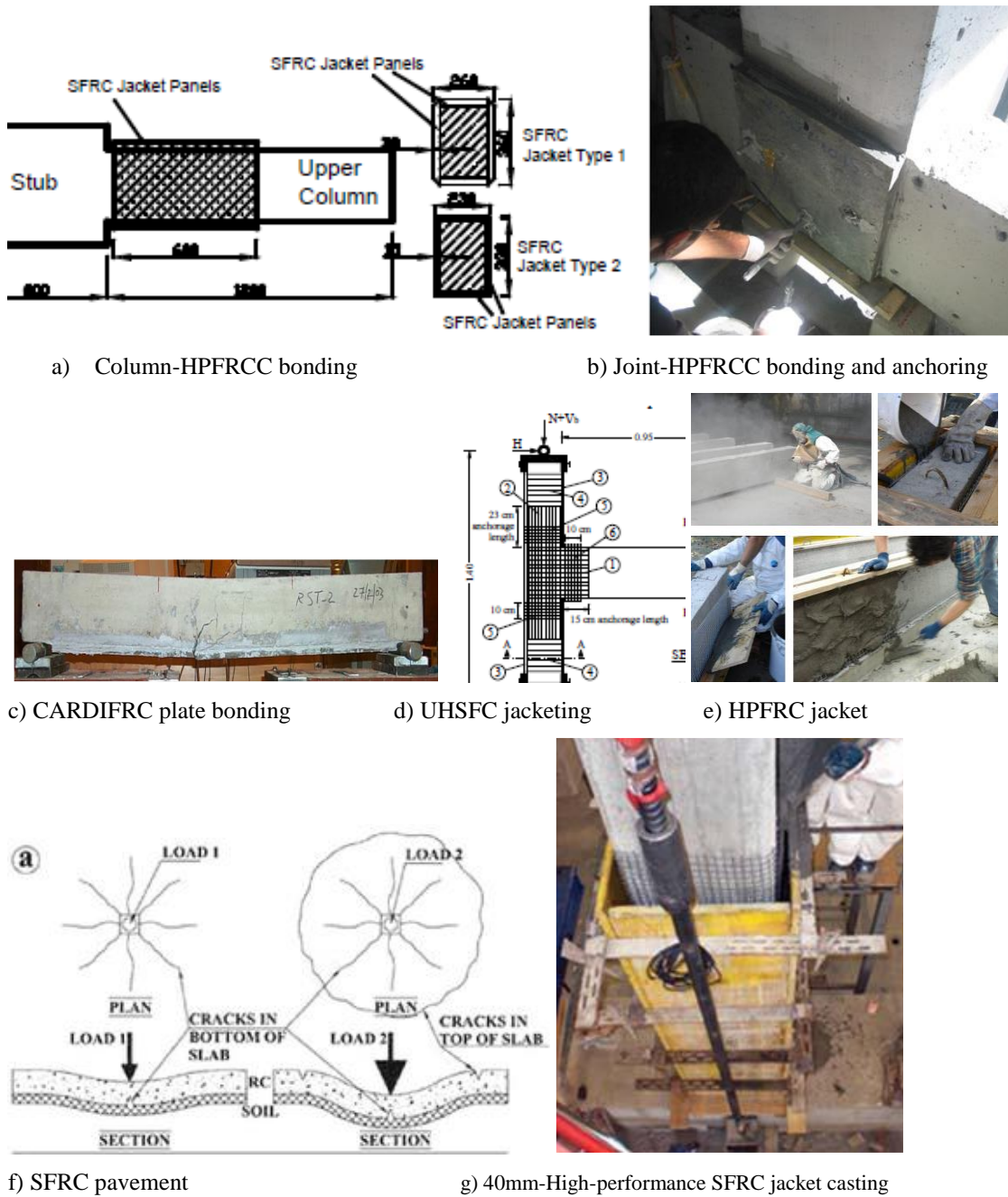


Figure 3. Retrofitting techniques developed with using steel fiber reinforced concrete material; a) Ilki et al. 2006, b) Bedirhanoglu et al. 2008, c) Farhat et al. 2007, d) Tsonos 2009, e) Mostosi et al. 2011, f) Boscato and Russo 2009, g) Rosignoli et al. 2012.

A summary of main details of research works on retrofitting RC members with using steel fibers are presented in Table 1. As seen steel fiber reinforced concrete has been used for concrete panels, beams, columns, joints for different purposes such as increasing axial load resistance, shear resistance, flexural strength, ductility, impermeability and limiting cracks in nuclear reactors, blast resistance etc.

The most efficient retrofitting is obtained in case of increasing shear strength, where the worst results were obtained in case of SFRC confining to increase axial load and ductility under axial

load. Precast applications, casting at site and spraying applications are groundbreaking developments in use of steel fibers in retrofitting of RC members.

The main retrofitting schemas developed with using steel fiber reinforced concrete are given in Figure 3, briefly. It can be concluded from Table 1 and Figure 3 that the main developed techniques with steel fibers can be listed as following:

- 1- Prefabricated composite panels (CARDIFRC)
- 2- Prefabricated-HPFRCC
- 3- 25-mm thick jacket of cast-in place HPFRCC
- 4- Ferrocement application
- 5- SFRC jacketing
- 6- UHPFRC wrapping
- 7- Bonding Steel Fiber Reinforced Ultra-High Strength Concrete (SFRUHSC) with epoxy
- 8- HPFRC mortar with directly surface application
- 9- Pouring 40 mm thick layer of SFRC
- 10- U-Shape SFRC jacketing with addition with shear connectors
- 11- Replacing damaged concrete cover with SFRCC+ wrapping with carbon fiber-reinforced polymer (CFRP)
- 12- Both steel and polymer fibers included FRM jacketing
- 13- RC jacketing and Ultra-High Strength Steel Fiber-Reinforced Concrete (UFC) replacing in joint
- 14- UHSFC Jacketing to columns and the joints
- 15- High performance SFRC jacket casting

4 EXPERIMENTAL AND ANALYTICAL WORKS CARRIED OUT BY AUTHORS

Experimental and analytical works carried out by authors are presented here briefly. It should be noted that the results of these works were presented in different publications elsewhere (Ilki et al 2004, Ilki et al 2006a, Ilki et al 2006b, Bedirhanoglu et al. 2007, Bedirhanoglu et al. 2008, Bedirhanoglu and Ilki 2009, Ilki et al 2009, Bedirhanoglu et al. 2012, Comert et al. 2014 and Ates et al. 2018).

4.1 *Cylinder specimens*

Work in this section was targeted to improve the mechanical properties of mortar to be used in the production of high performance steel fiber reinforced cementitious composite (HPFRCC) panels for retrofitting applications. First of all, silica sands and fly ash are mixed for 1 minute and then cement is added to the mixture. Water and admixture were poured slowly during mixing. At the end after getting a workable mortar, steel fibers are added. General casting procedure is summarized in Figure 3. In the experimental study, hot curing, separation of the fibers before appending the mixture, corrosion of the fibers and the amount of steel fibers were the main test variables. Standard cylinder and standard disk samples produced for this purpose were subjected to axial pressure and splitting tensile tests as shown in Figure 4.

As a result of these experiments, it has been seen that hot curing, pre-separation of the fibers and the ratio of the steel fiber have a positive effect on mechanical properties such as tensile strength, ductility and toughness. Three days hot cured (≈ 90 °C) specimens showed the performance of 28 days normal cured (≈ 21 °C) specimens in terms of mechanical properties. Gain in strength and ductility was given in Tables 2 and 3 briefly. Table 2 shows that there is no significant increase in compressive strength and elastic modulus with increasing volume of steel fibers. On the other hand, there are a major increase in tensile strength and the ductility through increasing amount of steel fibers (Table 3). A summary of schematic representation of stress-strain behavior in case of compression forces was presented in Figure 5. This schematic graph clearly shows positive effects of steel fibers up to a certain level (less than 6%) on the toughness of high performance concrete.

It can be concluded from this work that 4% volumetric amount of steel fibers can be a reasonable upper bound for developing strength and deformability properties of high performance concrete.



Figure 3. Mixing process of steel fibers concrete



Figure 4. Cylinder splitting and compression tests

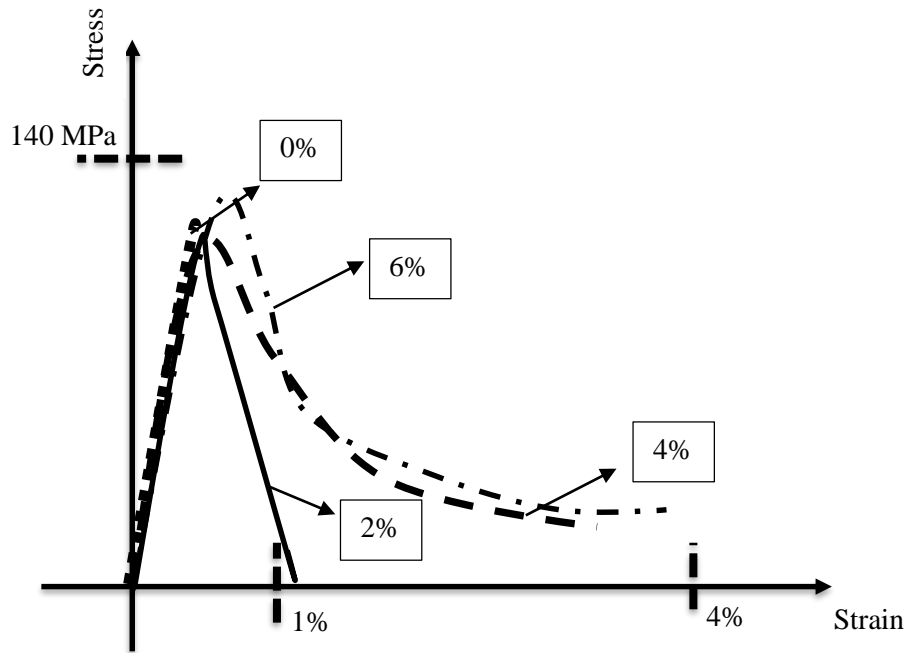


Figure 5. Comparison of compression behavior of specimens with different fiber content (modified from Bedirhanoglu et al. 2007)

Table 2 Outline of splitting tension and compression test results

Volumetric fiber content (%)	Mean values at 28. days		
	Average Compressive Strength $f_{c,ort}$ (MPa)	Average Elastic Modulus $E_{c,ort}$ (GPa)	Splitting Tension Strengths at 12 and 28 Days
0	115.2	40.6	6.7-7.2
1	110.8	38.4	8.5-8.3
2	118.1	40.4*	11.1-13.6
3	119.4	41.2	14.2-14.1
4	116.2	39.4	14.2-13.8
5	118.6	39.1	17.2-15.6
6	132.4	42.3	18.6-17.7

* Average of two data while the others are average of three data

Table 3 Strain values

Volumetric fiber content (%)	Mean values at 28. days		
	$\epsilon_{c,(fco)}$	$\epsilon_{c,(fco)}$	$\epsilon_{c,(fco)}$
1	0.0051	0.0058	1.13
2	0.0053	0.0055	1.09
3	0.0060	0.0069	1.14
4	0.0073	0.0083	1.15
5	0.0060	0.0085	1.42
6	0.0080	0.0106	1.34

4.2 Beam specimens

To test effect of steel fibers on high strength concrete fracture energy of steel fiber reinforced concrete (SFRC) evaluated through using test procedure proposed by RILEM (RILEM TC 50, 1985). Beam specimens were casted and tested with three point loading test setup. To assess the fracture energy of SFRC three point bending tests were carried out using displacement control. A 100 kN capacity Instron 5500R machine was used in the tests (Figure 6). In three point loading tests loading rates were 0.05 mm/minute and 0.1 mm/minute for the ascending and descending branches of load-displacement curves, respectively. On the other hand, in the tests of specimens without steel fibers the loading rate was 0.0175 mm/minute during the entire test. The displacements were measured at the middle point of the beams. Mechanical properties such as fracture energy, bending strength and toughness of the specimens were obtained from load-displacement curves. The maximum reached displacement was 10 mm for specimens with steel fibers (Figure 7). For the tests of specimens without steel fibers the behavior was very brittle and the specimen failed around 0.03% drift ratio. Figure 8 shows that fracture energy increases with increasing amount of steel fibers while the relation between fracture energy and amount of steel fibers is not linear. Beam tests also show a parallel correlation with cylinder tests in terms of necessity for limiting the fiber volume with respect to a reasonable upper bound. As a result, beam tests showed that the bending strength and toughness increased significantly with increasing amount of steel fibers up to a level.



Figure 6. RILEM beam tests (RILEM TC 50-FCM 1985, Bedirhanoglu 2009)

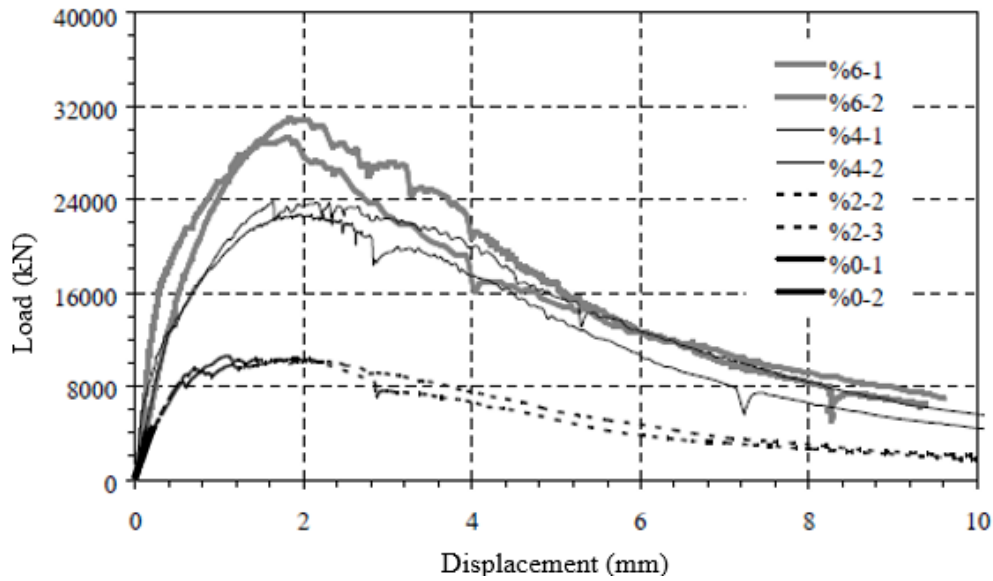


Figure 7. Load-deflection curves (Bedirhanoglu and Ilki 2009)

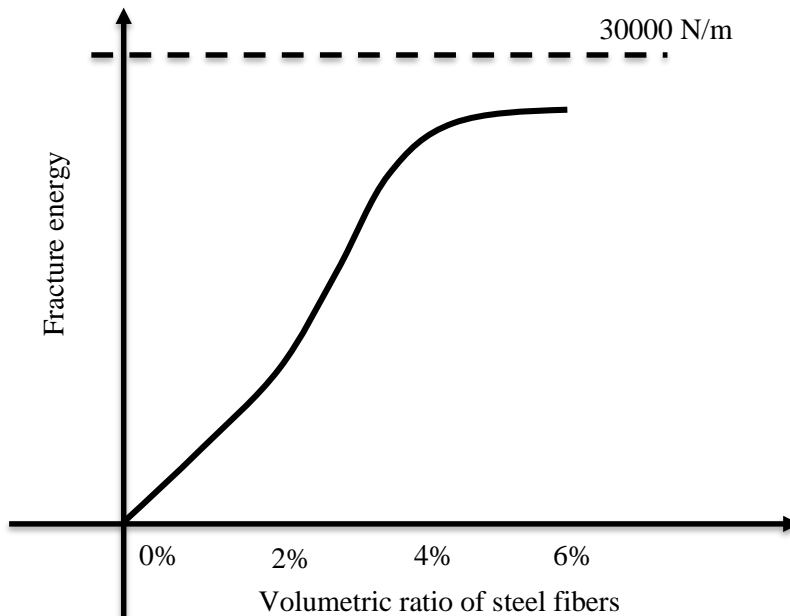


Figure 8. Schematic representation of change in fracture energy with increasing amount of steel fibers (Bedirhanoglu 2009)

4.3 Retrofitting of concrete panels

Material tests which were explained in former sections lead design of a SFRC mortar can be efficiently used in retrofitting application thanks to its superficial mechanical properties. In this part, through using developed SFRC mortar, high performance fiber reinforced cementitious composite (HPFRCC) plates were casted. The main target of this work is to test performance of precast-HPFRCC plates as a strengthening technique for retrofitting of reinforced concrete (RC) members against shear forces. Convenient application of precast-HPFRCC plates was also studied. Experimental work included tests of reference specimens and tests of specimens retrofitted with precast-HPFRCC panels (Figure 9). The precast-HPFRCC panels were either only bonded on the specimens using epoxy mortar or anchored to the specimen by steel bolts as well as epoxy bonding (Figure 10). The specimens were tested under diagonal tension (Bedirhanoglu et al. 2010). For doing tests of retrofitted specimens a simple testing method was utilized. The

behavior of the specimens under the same loading conditions was also investigated through a theoretical study by employing non-linear finite element analysis (FEM) (Figure 11). The retrofitted members were found to exhibit a much better performance in terms of strength and deformation capability. The anchorage application was found to positively affect this improved performance (Figure 12). In this figure DS-O-a and DS-O-b are reference specimens while the others are retrofitted specimens with different thickness of precast-HPFRCC panel with or without anchorage. Experimental results and theoretical results obtained from FEM analysis were also compared (Figure 13). It was seen that finite element analysis is successful to predict the load carrying capacity of the original and the retrofitted specimens as well as the vertical load–vertical strain relationship of the original specimen. For this relation, however, the FEM model needs development for the retrofitted specimens.



Figure 9. HPFRCC retrofitting application (Bedirhanoglu 2009)

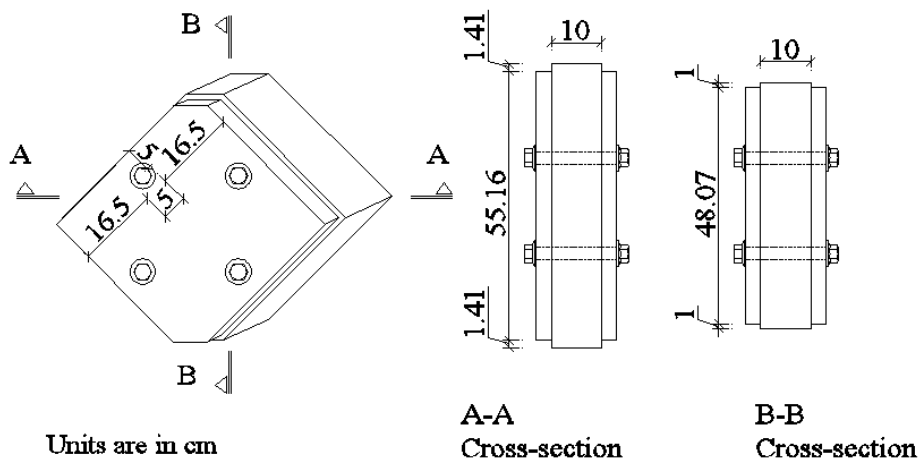


Figure 10 The geometry of specimens and anchorage applications.

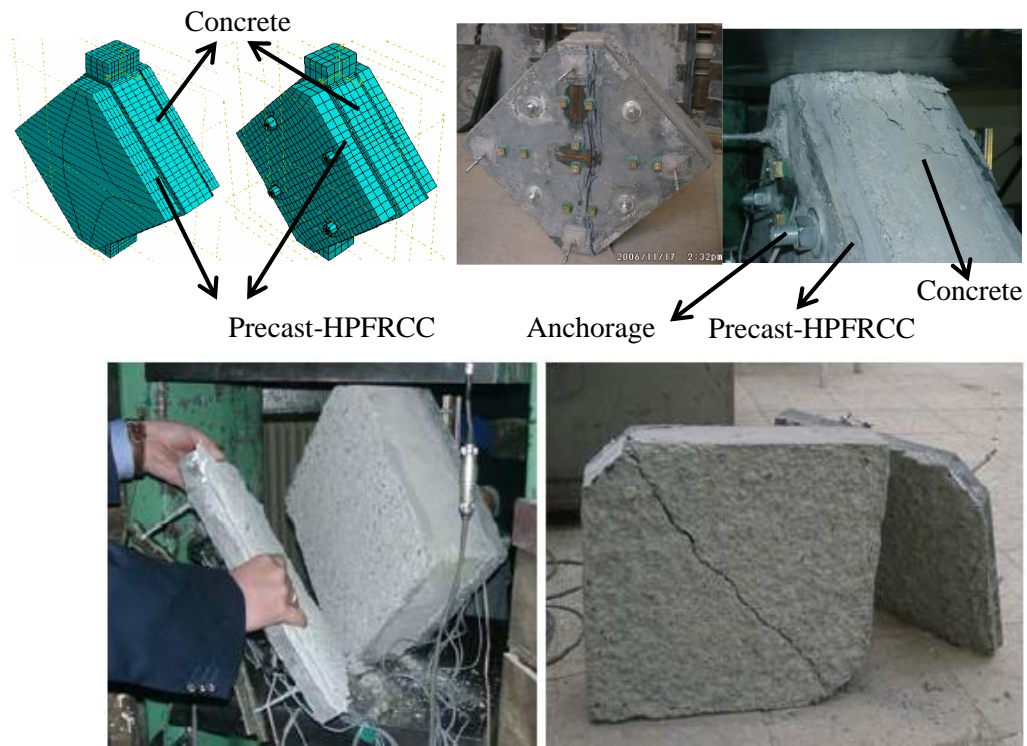


Figure 11 Finite element model and typical failure modes of retrofitted specimens

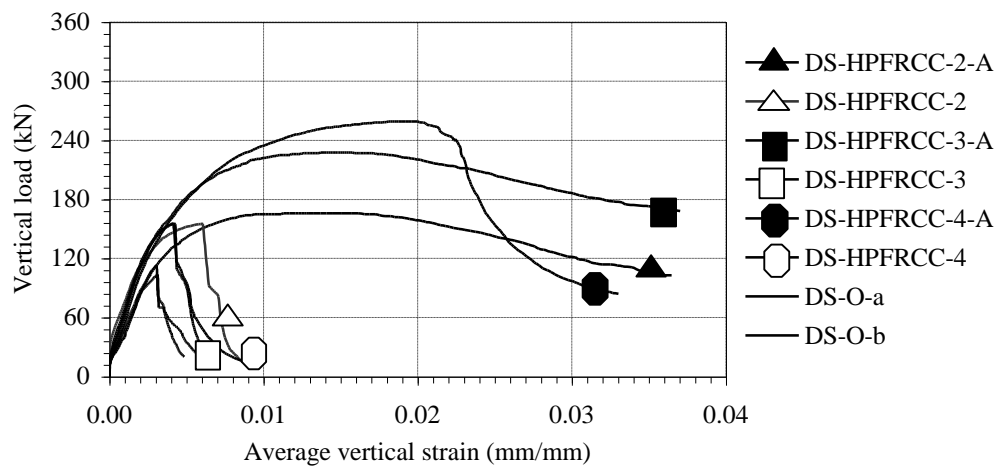
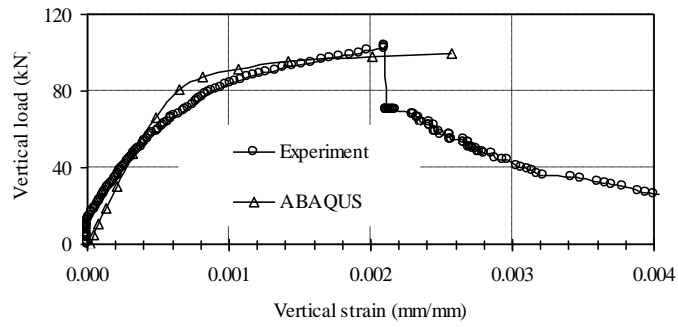
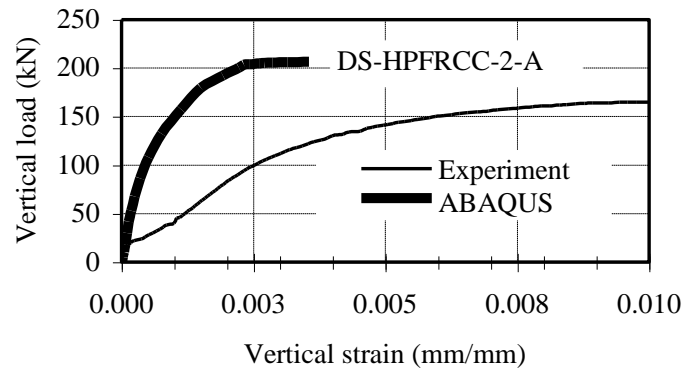


Figure 12 Comparison of experimental results of vertical load-average vertical strain relationships for all specimens (here A and numbers represent anchorage and plate thicknesses of HPFRCC, respectively).



a) Reference specimen



b) Sample retrofitted specimen

Figure 13 Vertical load-vertical strain relationships of reference specimen (experimental and numerical results).

4.4 Retrofitting RC columns

4.4.1. Axial compression tests

Efficiency of precast-HPFRCC plates in case of confining squat columns were investigated in this section (Ilki et al. 2006). For this purpose, a few series of squat RC columns with different cross sectional aspect ratios such as 1, 2 and 3 were used.

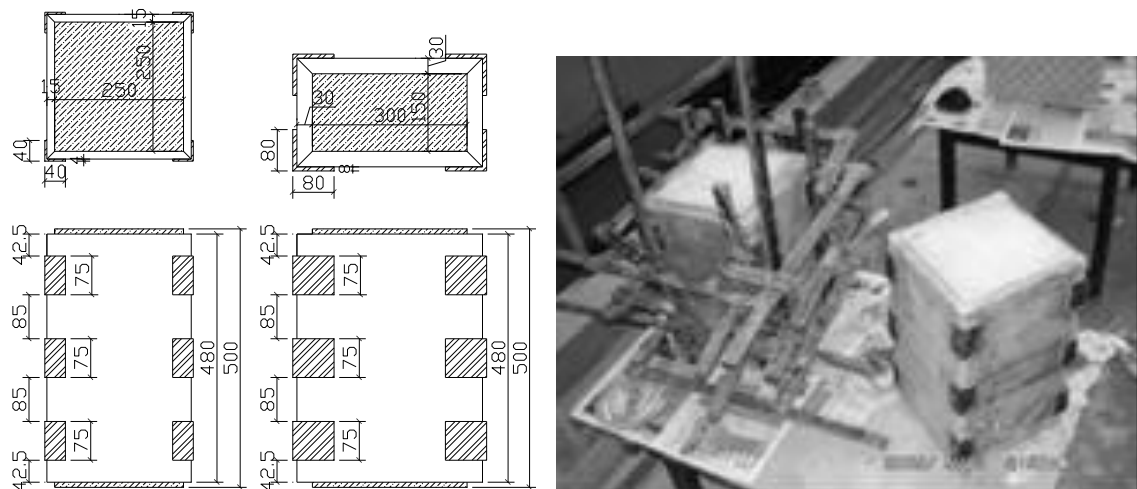


Figure 14. Retrofitted specimens with confining SFRCC panels (adapted from Ilki et al. 2006)

As seen from Figure 15 the SFRC bonding as jacketing is an effective method in case of uniaxial excitation, too. As shown in Figure 15 the areas under the curves increase due to SRFCC panels retrofitting, where this increase is more pronounced in case of smaller cross section aspect ratios.

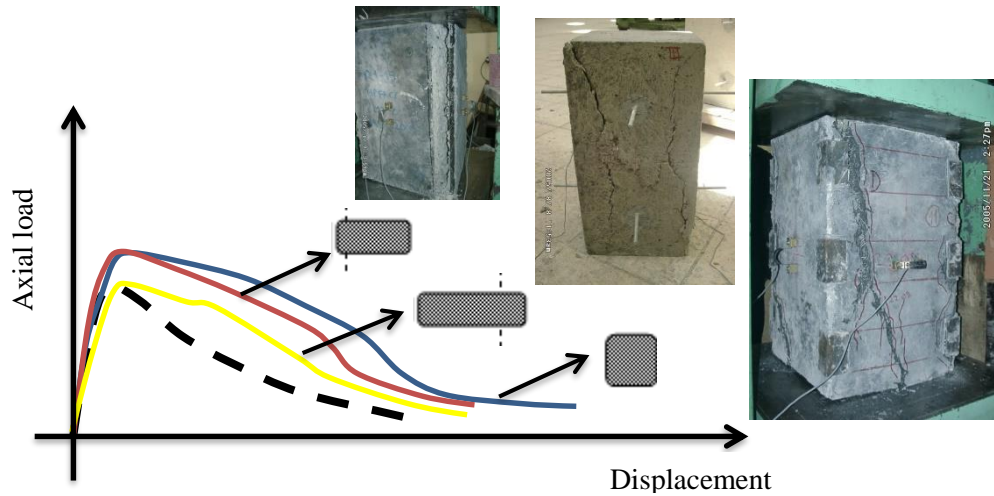


Figure 15. Schematic representation of experimental results in terms of axial load-displacement (adapted from Ilki et al. 2006)

4.4.2. Bending tests with constant axial load

Efficiency of precast-HPFRCC plates were tested through retrofitting columns with low strength concrete, continuous longitudinal bars and insufficient lap splice length (Ilki et al. 2004, Ilki et al. 2009). Precast-HPFRCC plates were bonded to column faces at potential plastic hinging zone through epoxy. For better bonding steel corners were also used in the intersection of plates bonded to adjacent faces. Figure 16.a shows precast-HPFRCC plates while Figure 16.b shows preparation of column face for bonding plates. HPFRCC plate bonding and steel corner application were given in Figures 16.c, d and e. Test setup is shown in Figure 16.f.

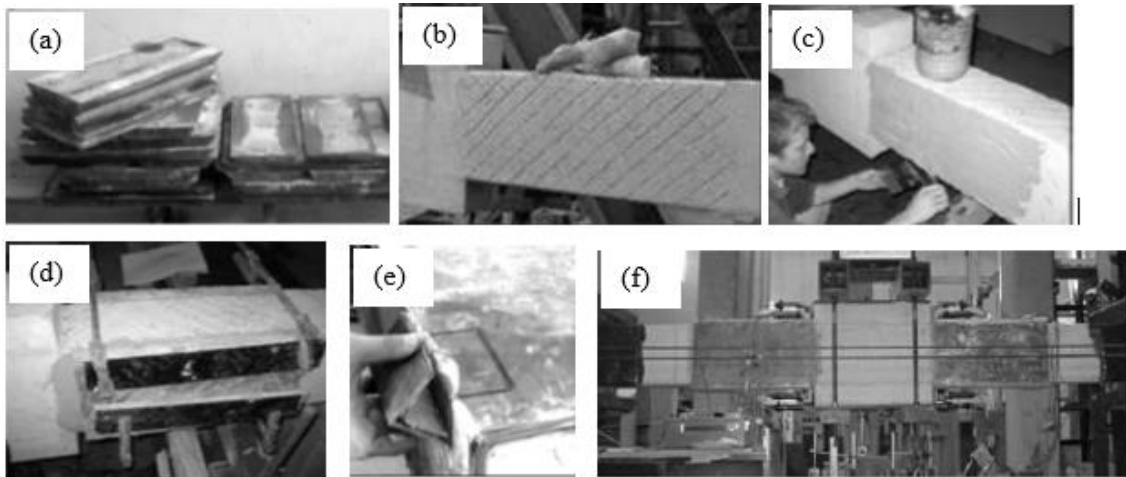


Figure 16. (a) Prefabricated HPFRCC panels, (b) preparation of surfaces of columns, (c) application of epoxy to surface of column (d) installation of HPFRCC panels on the columns and bonding of steel corners (e) application of steel corner (f) test of retrofitted specimen (modified from Ilki et al. 2004)

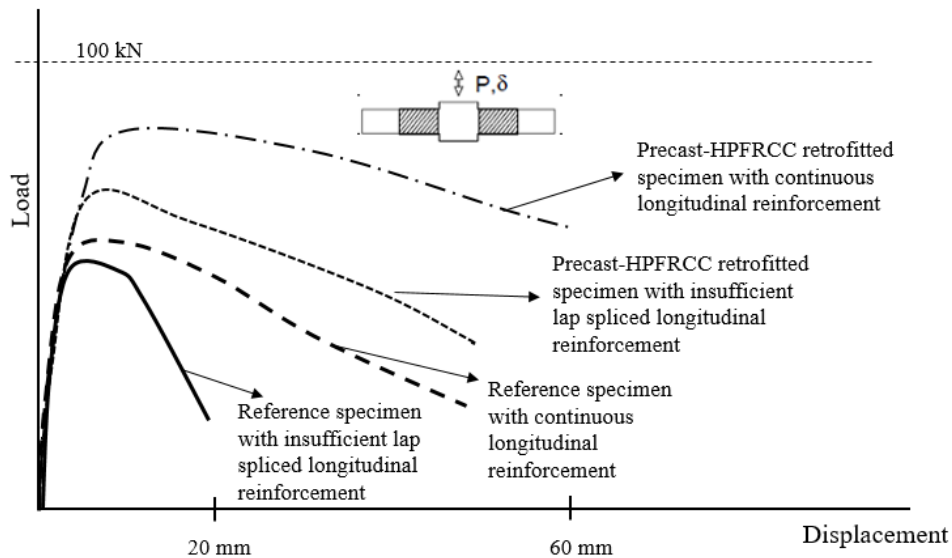


Figure 17. Schematic representation of load-displacement envelopes for reference and retrofitted specimens (modified from Ilki et al. 2004)

No matter the longitudinal reinforcement is continuous or lap spliced both reference specimens failed in a brittle manner before reaching their flexural capacity while retrofitted specimens shows a better performance. All the results of this experimental works are summarized with schematic graphs given in Figure 17. As seen in this figure reference specimens neither with lap spliced and nor with continuous longitudinal reinforcement show a ductile failure. With precast-HPFRCC applications it is intended to change brittle failure of reference specimens to a ductile behavior. Successful results were obtained only in case of continuous longitudinal bars. This clearly shows that precast-HPFRCC retrofitting is not fully effective in preventing lap splice failure and the increasing load carrying capacity. Both load carrying capacity and ductility was increased in case of precast-HPFRCC retrofitted specimen with continuous longitudinal reinforcement. 30-mm HPFRCC panel thickness is enough to prevent buckling of longitudinal bars.

4.5 Retrofitting of beam-column joints

In this section, work on the retrofitting of beam column joints will be presented. The target of joint tests was to investigate the seismic behavior of deficient exterior reinforced concrete beam-column joints constructed with low-strength concrete and plain reinforcing bars (as seen in Figure 18) retrofitted with prefabricated HPFRCC panels. For this purpose, four full-scale beam-column-slab-transverse beam sub-assemblies were tested under constant column axial load and reversed static cyclic lateral loads (Figure 13). To prevent slippage of beam longitudinal bars from the joint core, 90-degree hooks of beam longitudinal bars were welded as shown in Figure 19. For joint retrofitting, precast-HPFRCC plates were bonded and anchored to beam-column joint panel region (Figure 20).

Tests showed that retrofitting of joint cores with prefabricated HPFRCC panels provided considerable enhancement, both in strength and in displacement capacity, provided that the panels are properly anchored to the joint core and the slippage of the beam longitudinal bars in the joint core is prevented (Figure 21).

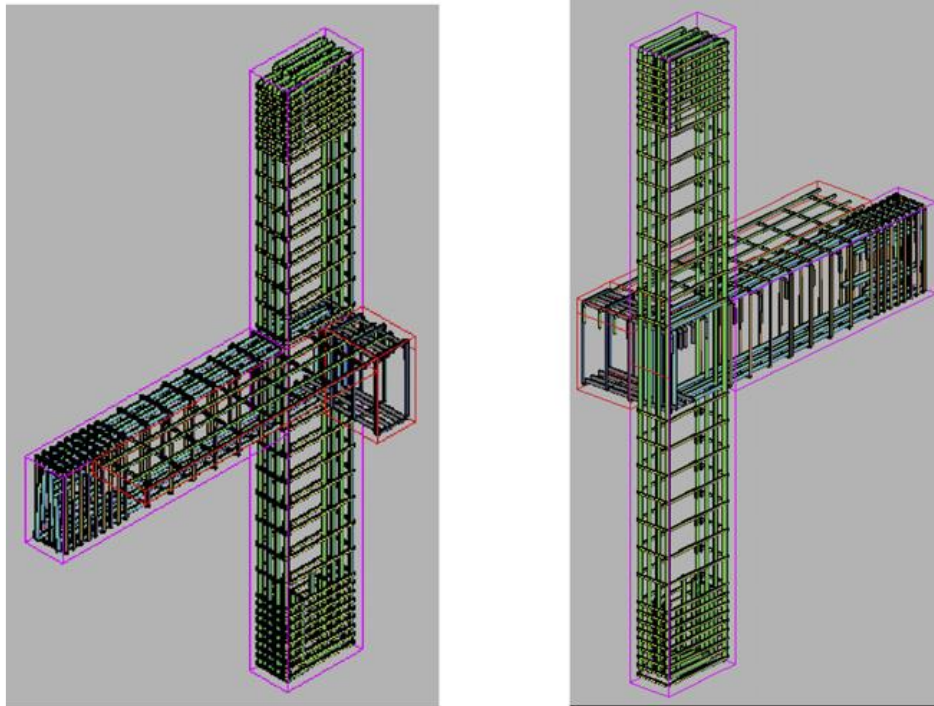


Figure 18. Detail of joint specimens



Figure 19. Welding application

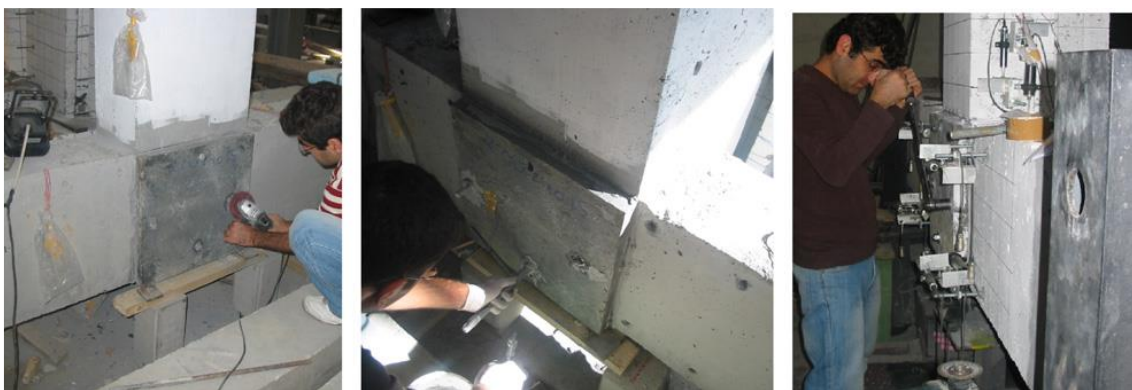


Figure 20. Retrofitting process (horizontal member is the column and the vertical member is the beam)

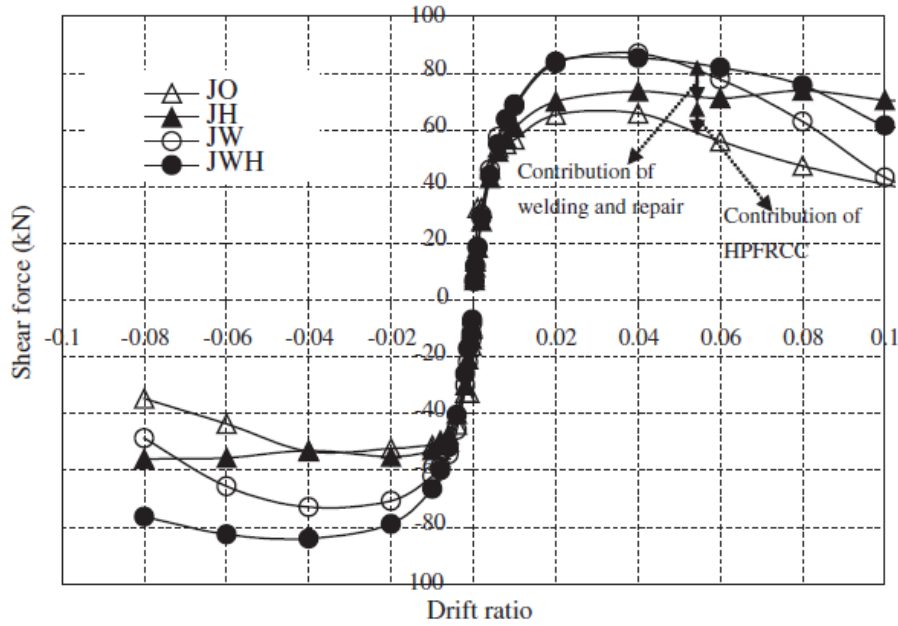


Figure. 21. Comparison of envelopes of shear force-drift ratio relationships (JO: Reference specimen, JW: reference specimens with welding of hook of beam longitudinal bars JH: retrofitted specimen without application of welding and JWH: retrofitted specimens with welding application).

An analytical model was also developed to predict the strengths of the reference and retrofitted specimens (Figure 22). The normalized shear capacity-drift ratio graph obtained for reference specimen with welding of hooks of beam longitudinal bars shown in Figure 22.a. This relationship was used as a model for representing the contribution of concrete to the joint shear resistance. A schematic representation of contribution of different parts to the load carrying capacity of retrofitted specimens is given. Analytical model is compared with the experimental results of specimen with weld and specimen with weld and HPFRCC retrofitting in Figure 23. Figure 23 shows compatibility between analytical and experimental results.

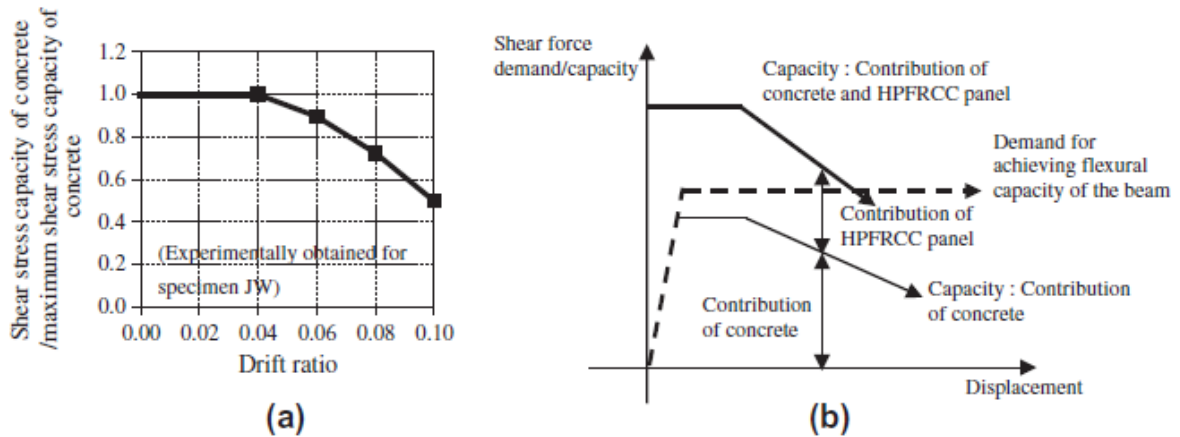


Figure. 22. (a) Variation of shear stress capacity of concrete in the joint with drift ratio and (b) contribution of concrete and HPFRCC panel as a function of drift ratio.

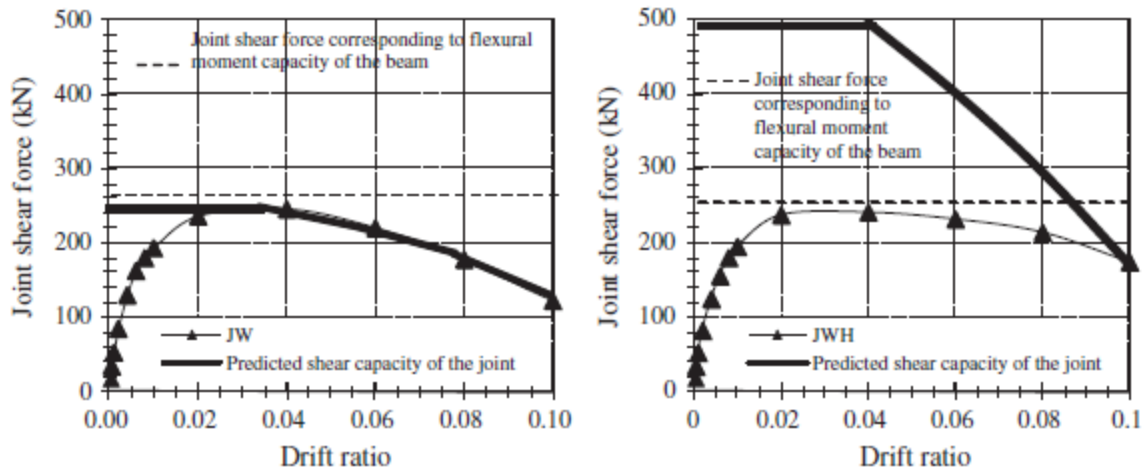
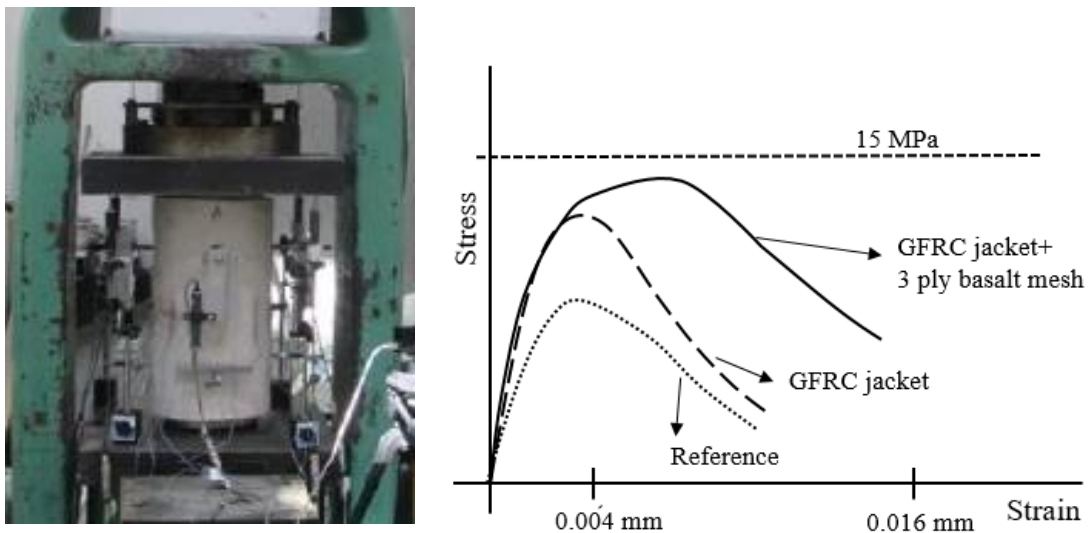


Figure. 23. Comparison of analytical and experimental results.

4.6 Retrofitting of columns with basalt mesh

Large number of concrete prisms retrofitted by using basalt textile reinforced sprayed glass fiber reinforced mortar (GFRM) were produced and tested under axial load (Ates et al. 2018). Both cylinder and rectangular specimens with cross-sectional aspect ratios of 1, 2 and 3 were tested under axial load (Figure 24.a). As a result, it was seen that significant contribution of external jacketing on the axial behavior was obtained especially for circular specimens while for the rectangular ones, the confinement effectiveness decreased as the cross-sectional aspect ratio increased. As clearly can be seen in Figure 24.b, addition of basalt textile reinforcement inside the sprayed GFRM matrix resulted in behaviors with increased consistency for the post peak behavior (Figure 24.b).



a)

b)

Figure. 24. Comparison of analytical and experimental results (adapted from Tore et al. 2015).

To investigate performance of same technique in retrofitting RC members under both flexure and axial load, flexure critical column specimens with low strength and low amount of transverse reinforcement are retrofitted with basalt mesh reinforced with sprayed glass fiber reinforced

concrete (GFRC) jacketing as seen in Figure 25. Specimens were tested under very high axial loads such as 50-70% of axial load capacity of the specimens. Effectiveness of the retrofitted specimen in terms of ductility can be clearly seen from damage condition of reference and retrofitted specimens at large drift ratios as seen in Figure 26.



Figure. 25. Retrofit application of basalt mesh (Comert et al. 2014).

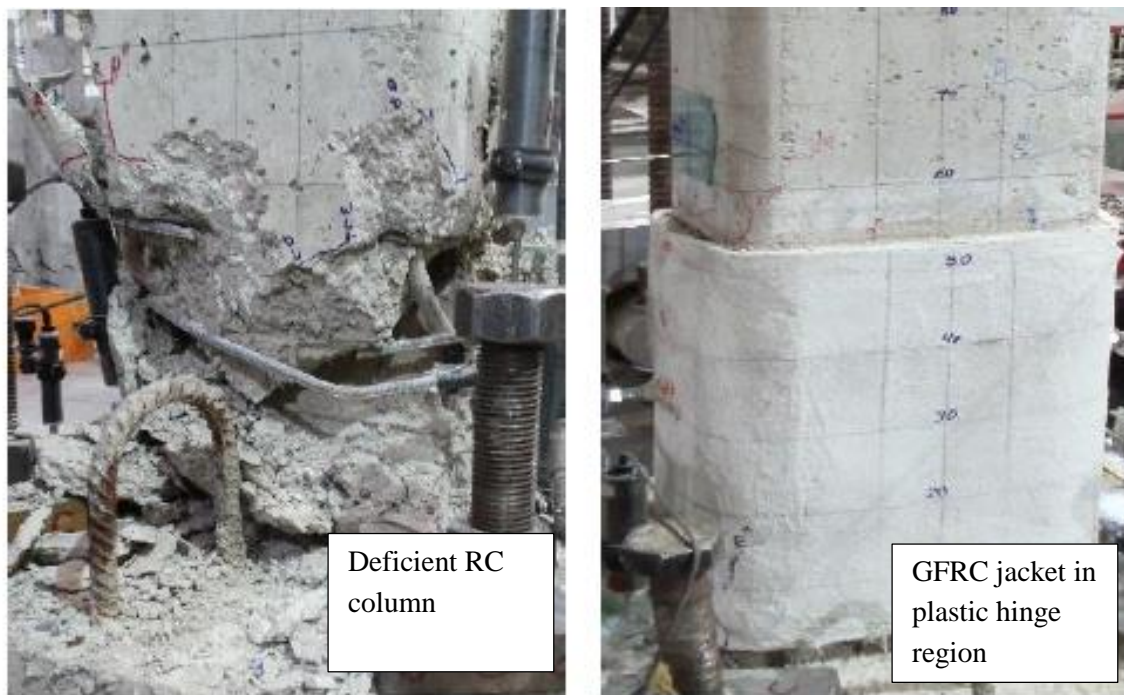


Figure 26. Conditions of reference and retrofitted specimens at 4% and 8%, respectively (Comert et al. 2014).

5 CONCLUSIONS AND RECOMMENDATIONS FOR FURTHER RESEARCH

5.1 Conclusions

In this study, a review on retrofitting of reinforced concrete members through fiber reinforced cementitious composites is presented. Additionally, a brief summary of past research executed by the authors during last two decades on retrofitting with fiber reinforced cementitious composites is presented. Other than conventional cast-in-situ production of fiber reinforced cementitious

composites, prefabrication and application through spraying are also possible. Examined studies show that fiber reinforced cementitious composites are very effective for retrofitting of concrete members. Beams, columns, joints and walls can be strengthened for enhancing shear resistance, flexural strength and ductility not only for better structural performance under vertical loads but also for improved performance under seismic actions. Other than possessing superior mechanical characteristics, wide range of applicability and high durability are important advantages of fiber reinforced cementitious composites. These make fiber reinforced cementitious composites a good option for limiting crack widths, improving impermeability and blast resistance as well. Since the integrity of concrete is kept even after remarkable damage due to contribution of fibers, improvement of the post-crack behavior results in reducing flying debris during a blast induced loading.

5.2 Further research

The behavior of fiber reinforced cementitious composites and the interaction of the fiber reinforced cementitious composites with existing reinforced concrete in retrofitting depend on many parameters including volume fraction, geometry of fibers and interface characteristics between fiber reinforced cementitious composites and existing reinforced concrete members. Further research on these issues may result in better performance and more feasible solutions. Such further research may also lead to more realistic modeling of fiber reinforced cementitious composites, which can bring improvements in design standards. With such improvements, design codes for strengthening with fiber reinforced cementitious composites can also be established.

REFERENCES

- ABAQUS 2008. Standard user's manual, version 6.7. Hibbitt, Karlsson and Sorensen, Inc.
- ACI 544. 1996. *Report on Fiber Reinforced Concrete*. ACI Committee 544, Farmington Hills, MI: American Concrete Institute.
- ACI 544. 2010. *Report on the Physical Properties and Durability of Fiber-Reinforced Concrete*. ACI Committee 544.5R-10, Farmington Hills, MI: American Concrete Institute.
- Akkaya, Y. 2000. Microstructural characterization of high performance fiber reinforced cement composites, PhD Thesis, Northwestern University, Illinois.
- Akkaya, Y., Peled, A., and Shah, SP. 2000. Parameters Related to Fiber Length and Processing in Cementitious Composites, RILEM, *Materials and Structures*, 33, 515-524.
- Akkaya, Y., and Shah, SP. 2001. Effect of fiber dispersion on multiple cracking of cement composites, *Journal of Engineering Mechanics*, ASCE, 127, 311-316.
- Alaee FJ, Karihaloo BL. 2003. Retrofitting of reinforced concrete beams with CARDIFRC. *ASCE Journal of Composites for Construction*, 7:174-186.
- Alaee, FJ. 2002. *Retrofitting of concrete structures using High Performance Fiber Reinforced Cementitious Composite (HPFRCC)*. PhD Thesis, University of Wales, Cardiff.
- Altun, F., Köse, M. Yilmaz, C., Ari, K. and Durmuş, A. 2007. Experimental investigation of reinforced concrete beams with and without steel fiber under explosive loading, *Indian Journal of Engineering and Materials Sciences*, 14, 419-426.
- Anuradha, R., and Britto, XJ. 2016. Structural rehabilitation of beams with steel fibre reinforced UHSC strips, *International Journal of Advanced Engineering Technology* E-ISSN 0976-3945
- Arslan MH., and Dogan G. 2015. Beton içinde kullanılan çelik tellerin betonarme çerçevenin davranışına olan etkisi, *International Burdur Earthquake & Environment Symposium (IBEES2015) Uluslararası Burdur Deprem ve Çevre Sempozyumu 7-9 May*, Mehmet Akif Ersoy University, Burdur-Türkiye.
- Ates, AO., Khoshkholghi, S., Tore, E., Marasli, M. and Ilki, A. 2018. Sprayed glass fiber reinforced mortar with or without basalt textile reinforcement for jacketing of low strength concrete prisms, *ASCE, Journal of Composites for Construction*, accepted August.
- Balaguru, P.N., and Shah, S.P. 1992. Fiber reinforced cement composites, *McGrawHill, New York*.
- Banthia, N. and Trottier, JF. 1995. Concrete reinforced with deformed steel fibers Part II: Toughness characterization, *ACI Materials Journal*, 92, 146-154.
- Bayasi, Z. and Soroushian P. 1991. Fiber type effects on the performance of steel fiber reinforced concrete, *ACI Materials Journal*, 88, 129-134.

- Bayramov F., İlki A., Taşdemir C., Yerlikaya M., Taşdemir M.A. and Yerlikaya M. 2004a. SFRCs for concrete roads in heavily trafficed situations, *The 9th International Symposium on Concrete Roads*, Istanbul, Turkey, April 4-7.
- Bayramov F., Tasdemir C., and Tasdemir MA. 2004b. Optimization of steel fibre reinforced concretes by means of statistical response surface method. *Cement and Concrete Composites*, 26(6), 665-675.
- Bazgir, A. 2016. The Behaviour of steel fibre reinforced concrete material and its effect on impact resistance of slabs, *Submitted for the Degree of Master of Philosophy in Structural Engineering, City University London, School of Mathematics, Computer Science&Engineering*.
- Bedirhanoglu, I. 2009. The behavior of reinforced concrete columns and joints with low strength concrete under earthquake loads: an investigation and improvement. *Istanbul Technical University, Turkey*, Ph.D. Thesis:700.
- Bedirhanoglu, İ., Candan, Y., İlki, A., and Taşdemir, M.A. 2007. Çelik lif içeriği sıcak kür ve lif korozyonunun çimento esaslı yüksek performanslı kompozitlerin mekanik davranışına etkisi (Effect of steel fibre content, hot curing and corrosion of fibre on the mechanical behavior of cement based high performance composites-in Turkish). *7. National Concrete Congress*, Istanbul, Turkey, 28-30 Kasım. 215-223.
- Bedirhanoglu, I., and İlki, A. 2009. HPFRCC for rehabilitation of reinforced concrete members with low strength concrete. *ITU Journal/d, Engineering*, 8(6),146-156 (in Turkish).
- Bedirhanoglu, I., İlki, A., Incecik, O. and Kumbasar, N. 2008. Retrofit of concrete panels with prefabricated HPFRCC Plates, *14th World Conference on Earthquake Engineering*, 14WCEE, Beijing, China, 12-17 October.
- Bedirhanoglu, I., İlki, A., and Kumbasar, N. 2012. Innovative techniques for seismic retrofit of reinforced concrete joints. *ACES Workshop: Innovative Materials and Techniques in Concrete Construction*, October 10-12, Corfu, Greece. [Invited Paper]
- Bedirhanoglu I., İlki, A., and Kumbasar, N. 2013. Precast fiber reinforced cementitious composites for seismicretrofit of deficientrcjoints – A pilot study. *Engineering Structures*, 52. 192-206. DOI: 10.1016/j.engstruct.02.020
- Boscato, G., and Russo, S. 2009. Experimental investigation on repair of RC pavements with SFRC. *Concr Repair Rehab Retrofitting II-Alexander*; ISBN:978-0-415-46850-3.449-458.
- Brühwiler, E., and Denarié, E. 2008. Rehabilitation of concrete structures using ultra-high performance fiber reinforced concrete. In: *The second International Symposium on Ultra High Performance Concrete, UHPC-2008*, March 05 - 07, Kassel, Germany, 1-8.
- Cargile, J.D. O’Neil, EF., and Neeley, BD. (NA). Very-high-strength concretes for use in blast-and-penetration-resistant structures. *The AMPTIAC Quarterly*, 6(4), 61-66.
- Comert, M., Hajihosseini, S., Nasrinpour, A., Ates, A. O., Demir, C., Marasli, M., and İlki, A. 2014. Seismic retrofit of sub-standard RC columns through basalt mesh reinforced sprayed GFRC jacketing. *FRC 2014 Joint ACI-fib International Workshop*, July, Montreal, Canada.
- Corvez D. and Masson B. 2013. UHPFRC Solutions for the retrofit of nuclear reactor containment walls, *RILEM-fib-AFGC Int. Symposium on Ultra-High Performance Fibre-Reinforced Concrete, UHPFRC 2013 – October 1-3, Marseille, France*.
- Dugat, J., Roux, N. and Bernier, G. 1996. Mechanical properties of reactive powder concretes, *Materials and Structures*, 29, 233-240.
- Farhat, F.A., Nicolaidis, D., Kanellopoulos, BL., and Karihaloo, BL. 2007. High performance fibre-reinforced cementitious composite (CARDIFRC) – performance and application to retrofitting, *Engineering Fracture Mechanics*, 74, 151-167.
- Fukuta, T., Hiraishi, H., Okada, T. 1998. Repair and retrofit of buildings after the 1995 Great Hanshin Awaji earthquake disaster. *The 2nd Japan-Turkey Workshop on Earthquake Engineering*, Istanbul, Turkey.
- Hassanean Y., Assaf K., Raheem S., and Arafa A. 2012. Behavior of repaired R.C. beams by using steel fiber concrete jacket and subjected to short time repeated loading, *Journal of Engineering Sciences*, Assiut University, 40(5), 1309-1324, September.
- Higashiyama, H., and Banthia, N. 2008. Correlating flexural and shear toughness of light weight fiber-reinforced concrete. *ACI Materials Journal*, 105(3):251-257.
- Hussein, L., and Amleh, L. 2015. Structural behavior of ultra-high performance fiber reinforced concrete-normal strength concrete or high strength concrete composite members. *Construction and Building Materials* 93, 1105–1116

- Gao, J., Sun, W., and Morino, K. 1997. Mechanical properties of steel fibre reinforced, high-strength, lightweight concrete, *Cement and Concrete Composites*, 19, 307-313.
- Gutiérrez, R.M., Diaz, LN., and Delvasto, S. 2005. Effect of pozzolons on the performance of fiber-reinforced mortars, *Cement and Concrete Composites*, 27, 593-598.
- Güvensoy, G., Bayramov, F., Ilki, A., Sengul, C., Tasdemir, MA., Kocaturk NA. and Yerlikaya, M. 2004. Mechanical behavior of high performance steel fiber reinforced cementitious composites under cyclic loading condition, *International Symposium on Ultra High Performance Concrete*, September 13-15, Kassel, Germany.
- Ilki, A., Akgun, D., Goray, O., Demir, C., and Kumbasar, N. 2006-a. Seismic strengthening of low strength concrete columns by external confinement using prefabricated SFRCC panels, *Proceedings of the 19th Australasian Conference on the Mechanics of Structures and Materials*, P.J. Moss and R.P. Dhakal, eds., University of Canterbury, Christchurch, New Zealand, December, 393–399.
- Ilki, A., Akgun, D., Goray, O., Demir, C., and Kumbasar, N. 2006-b. Retrofit of concrete members with externally bonded prefabricated SFRCC jackets, *Proceedings of the 16th European Conference on Fracture*, M.S. Konsta-Gdoutos, ed., Xanthi, Greece, July. 625-632.
- Ilki, A. Darilmaz, K. Bakan, I. Zorbozan, M. Yuksel, E. Saruhan, H., and Karadogan, F. 1998. Jacketing of prefabricated columns. The 2nd Japan-Turkey Workshop on Earthquake Engineering, Istanbul, Turkey.
- Ilki, A., Demir, C., Bedirhanoglu, I., and Kumbasar, N. 2009. seismic retrofit of brittle and low strength rc columns using fiber reinforced polymer and cementitious composites, *Journal of Advances in Structural Engineering*, 12(3), 325-347, [BEST PAPER AWARD-2009]. DOI: 10.1260/136943309788708356
- Ilki, A., Yilmaz, E., Demir, C., and Kumbasar, N. 2004. Prefabricated SFRC jackets for seismic Retrofit of non-ductile rectangular reinforced concrete columns. *13th World Conference on Earthquake Engineering*, Vancouver, B.C., Canada, August 1-6.
- Kalman, D. 2010. Use of steel fiber reinforced concrete for blast resistant design. *Msc Thesis submitted to Department of Architectural Engineering and Construction Science College of Engineering*, Kansas State University, Manhattan, Kansas.
- Kathik, S., and Sundaravadivelu, K. 2017. Retrofitting of reinforced concrete beams using reactive powder concrete (RPC), *IOP Conference Series: Earth and Environmental Science*, 80, 1-9.
- Katzer, J. 2006. Steel fibers and steel fiber reinforced concrete in civil engineering. *Pacific Journal of Science and Technology*. 7(1):53-58.
- Koo I. and Hong S. 2016. Strengthening RC columns with ultra-high performance concrete. *The Structures Congress Jeju Island, Korea*, August 28-September 1.
- Kumar, PR. Oshima, T. Mikami, S., and Yamazaki, T. 2007. Studies on RC and ferrocement jacketed columns subjected to simulated seismic loading. *Asian Journal of Civil Engineering (Building and Housing)*, 8(2). 221-225.
- Kwak, YK., Eberhar, MO., Kim, WS., and Kim, J. 2002. Shear strength of steel fiber-reinforced concrete without stirrups. *ACI Structural Journal*, 99(4), 530-538.
- Lampropoulos, AP., Paschalis, SA., Tsioulou, OT., and Dritsos, SE. 2016. Strengthening of reinforced concrete beams using ultra high performance fibre reinforced concrete (UHPFRC), *Engineering Structures* 106, 370-384.
- Lee J., Shin H., Min K., and Yoon Y. 2018. A preliminary study of reactive powder concrete as a new repair material, *Construction and Building Materials* 21, 182–189.
- Lejano, BA. 2013. Confinement effects of different retrofitting materials on the axial strength of reinforced concrete columns, *7th IEEE International Conference Humanoid, Nanotechnology, Information Technology Communication and Control, Environment and Management (HNICEM)*, The Institute of Electrical and Electronics Engineers Inc. (IEEE) – Philippine Section 12-16 November Hotel Centro, Puerto Princesa, Palawan, Philippines.
- Lejano, BA. 2017. Evaluation of different fiber reinforced mortar as retrofitting materials for RC columns, *International Journal of GEOMATE*, July, 13(35), 40 – 47.
- Li, VC. Stang, H., and Krenchel, H. 1993. Micromechanics of crack bridging in fiber reinforced concrete. *Mater Struct*, 26(162), 486–94.
- Li, VC. 2000. Large volume, High performance applications of fibers in civil engineering, *Journal of Applied Polymer*, 83, 660-686.
- Li, V.C., Horri, H., Kabele, P., Kanda, T., and Lim, YM. 2000. Repair and retrofit with engineered cementitious composites. *Engineering Fracture Mechanics*, 65, 317-334.
- Li, J. Wu, C. Hao, H. and Su, Y. 2015. Investigation of ultra-high performance concrete under static and blast loads. *International Journal of Protective Structures* 6(2), 217-235.

- Li, J. Wu, C. Hao, H., and Liu, Z. 2017. Post-blast capacity of ultra-high performance concrete columns. *Engineering Structures*, 134, 289–302.
- Lu X, Hsu CTT. 2006. Behavior of high strength concrete with and without steel fiber reinforcement in triaxial compression. *Cement and Concrete Research*, 36(9), 1679–85.
- Mahmud, G. Hassan, A., and Yang Z. 2013. Experimental and numerical studies of size effects of ultra high performance steel fibre reinforced concrete (UHPFRC) beams, *Construction and Building Materials* 48, 1027-1034.
- Maidl, BR. 1995. *Steel Fibre Reinforced Concrete*. Ernst&Sohn.
- Maringoni, . Meda, A. Mostosi, S., and Riva, P. 2012. Strengthening of RC members by means of high performance concrete. *American Concrete Institute, ACI Special, Publication*; 289:201–213.
- Meda, A. Minelli, F. Plizzari, GA., and Riva, P. 2005. Shear behaviour of steel fibre reinforced concrete beams, *Materials and Structures*. 38(3), 343-351.
- Martinola, G. Meda, A. Plizzari, GA., and Rinaldi, Z. 2007. An application of high performance fiber reinforced cementitious composites for R/C beams strengthening, *FRAMCOS 6*, Catania, Italy, June 18–21.
- Martinola, G. Meda, A. Plizzari, GA., and Rinaldi Z. 2010. Strengthening and repair OS RC beams with fiber reinforced concrete. *Cement and Concrete Composites*, 32(9), 731-739.
- Minelli, F., and Plizzari, GA. 2006. Steel fibers as shear reinforcement for beams. *Proceedings of The Second Fib Congress*, Naples, Italy, 5-8 June, abstract on page 282- 283, full length paper available on accompanied CD, pp.12.
- Mostosi, S. Meda, A. Riva, P., and Maringoni, S. 2011. Shear strengthening of RC beams with high performance jacket, *fib Symposium PRAGUE*.
- Naaman, AE. Paramasivam, P. Balazs, GL. Eibl, J. Erdelyi, L., and Hassoun NM. 1996. Reinforced and prestressed concrete using HPFRCC matrices. *High performance fiber reinforced cementitious composites*. RILEM Proc; 31, 291–348.
- Naaman, A. 2003. Engineered Steel Fibers with Optimal Properties for Reinforcement of Cement Composites, *Journal of Advanced Concrete Technology*, 1(3), 241-252.
- Naaman, A. 2008. High performance fiber reinforced cement composites. *High-Performance Construction Materials*, DOI: 10.1142/9789812797360_0003.
- Paegle, I., and Fischer, G. 2015. Modeling the load-deformation response of FRC structural members, *International Conference High Performance Fiber Reinforced Cement Composites 6*.
- Qian, CX., and Stroeven, P. 2000. Fracture properties of concrete reinforced with steel–polypropylene hybrid fibers. *Cement and Concrete Composites*. 22(5), 343–351.
- Rajeshguna, R., Suguna, K., and Raghunath, PN. 2008. Experimental study on steel fiber reinforced concrete beams strengthened with fibre reinforced polymer laminates. *International Journal of Engineering Science and Innovative Technology*, 3(4), 696-705.
- Ravichandran, K., and Jeyasehar, C. 2012. Seismic retrofitting of exterior beam column joint using ferrocement. *International Journal of Engineering and Applied Sciences (IJEAS)*, 4(2), September.35-58.
- Richard, P., and Cheyrezy, MH. 1994. Reactive powder concretes with high ductility and 200-800 mpa compressive strength, *American Concrete Institute, ACI SP-144*, 507-518.
- RILEM TC 50-FMC. 1985. Determination of fracture energy of mortar and concrete by means of three point bend tests on notched beams, *Materials and Structures*, 18(106), 285-290.
- Romualdi, JP., and Mandel, JA. 1964. Tensile strength of concrete affected by uniformly distributed closely spaced short lengths of wire reinforcement. *ACI Journal*, proc. 61(6).
- Rosignoli, D. Simonelli, F. Meda, A., and Rosignoli, R. 2012. High-performance fiber-reinforced concrete jacketing in a seismic retrofitting application. *Concrete Repair Bulletin*:26–31.
- Ruano, G. Isla, F. Pedraza, RI. Sfer, D., and Luccioni, B. 2014. Shear retrofitting of reinforced concrete beams with steel fiber reinforced concrete. *Construction and Building Materials* 54(1): 646–658.
- Sevil, T. Baran, M. Bilir, T., and Canbay E. 2010. Use of steel fiber reinforced mortar for seismic strengthening, *Construction and Building Materials* 25, 892–899.
- Shah SP., 1991. Do fibers increase the tensile strength of cement-based matrices. *ACI Materials Journal*, 88(6), 595-602.
- Shannag, MJ., Barakat, S., and Jaber, F. 2001. Structural repair of shear-deficient reinforced concrete beams using SIFCON. *Magaz Concr Res*, 53(6), 391–403.
- Shannag, MJ., Abu-Dyya, N., and Abu-Farsakh, G. 2005. Lateral load response of high performance fiber reinforced concrete beam–column joints. *Construction and Building Materials*, 19(7), 500–508.

- Shannag, MJ., Barakat, S., and Abdul-Kareem, M. 2002. Cyclic behavior of HPFRC-repaired reinforced concrete interior beam-column joints. *Materials and Structures*, 35, 348-356.
- Singh, M. Sheikh, AH, Mohamed Ali, MS. Visintin, P., and Griffith, MC. 2017. Experimental and numerical study of the flexural behaviour of ultra-high performance fibre reinforced concrete beams, *Construction and Building Materials* 138, 12–25.
- Tadepalli, P. Mo, Y. Hsu, T., and Vogel, J. 2009. Mechanical properties of steel fiber reinforced concrete beams.. Austin, TX: ASCE. *Structures Congress*, 1039-1048.
- Torah, 2018. Exodus *Part-5*, in a *dictionary of the Bible.*, edited by W.R.F. Browning. *Oxford Biblical Studies Online*, <http://www.oxfordbiblicalstudies.com/article/opr/t94/e1935> (accessed Nov 4, 2018).
- Tanarlan, HM. 2017. Flexural strengthening of RC beams with prefabricated ultra-high performance fibre reinforced concrete laminates, *Engineering Structures* 151, 337–348.
- Tankut, T., and Ersoy, U. 1998. Seismic repair/strengthening of RC structures-METU research. *The 2nd Japan-Turkey Workshop on Earthquake Engineering*, Istanbul, Turkey.
- Tore, E. Comert, M. Demir, C. Ilki, A., and Marasli, M. 2015. Seismic retrofit of columns using basalt mesh reinforced GRC jacket. *GRC 2015*, Dubai.
- Tsonos, AG. 2009. Steel fiber high-strength reinforced concrete: a new solution for earthquake strengthening of old R/C structures, *Earthquake Resistant Engineering Structures VII*, 153-164.
- Wafa, FF., and Ashour, SA. 1992. Mechanical properties of high-strength fibre reinforced concrete, *ACI Materials Journal*, 89, 449-455.
- Wang, YC., and Lee, MG. 2007. Ultra-high strength steel fiber reinforced concrete for strengthening of RC frames. *Journal of Marine Science and Technology*, 15(3), 210–218.
- Yusof, MA., Noraman, N. Arffin, A. Zain FM., and Risby, R., and Ng, CP. 2010. Normal strength steel fiber reinforced concrete subjected to explosive loading. *International Journal of Sustainable Construction Engineering and Technology*, 1(2), 127-136.

Regular Papers

Influence of adjacent channel bolts on the lip capacity of anchor channels – a connection to withstand typhoons and earthquakes

Christoph Mahrenholtz¹

¹ Jordahl GmbH, Berlin, Germany

ABSTRACT: Anchor channels are cast in concrete and allow, after curing and stripping of the formwork, the connection of components using channel bolts. Because of the mechanical interlock between concrete, anchor channel, and channel bolt, anchor channel-channel bolt-systems are very reliable and therefore a perfect fastening solution for connections which are safety relevant and extremely loaded, e.g. due to typhoons and earthquakes.

For this reason, anchor channels with channel bolts became worldwide popular and design rules were codified in Europe and in the USA. However, the whole framework of the design rules is not fully consolidated to date. Therefore some design rules in Europe and in the USA slightly differ. Following a brief introduction of the design rule framework in Europe and in the USA, the influence of adjacent channel bolts on the lip capacity of anchor channels is discussed.

Tests were carried out to study the influence of adjacent channel bolts on the shear lip capacity of anchor channels. The tests allowed the verification of a proposed model on the basis of a model for the calculation of the tension lip capacity. The corresponding equation is proposed for the completion of the design rules in the USA. Because of several advantages, it is suggested to mirror the equations to Europe.

1 INTRODUCTION

Anchor channels with channel bolts allow versatile possibilities to conveniently connect components to reinforced concrete structures. Advanced anchor channel-channel bolt-systems reliably take up static and cyclic loads even under extreme conditions to be anticipated in typhoon battered and earthquake prone regions, e.g. for the fixation of outdoor M&E equipment, steel platforms and ladders, or curtain wall elements (Figure 1).

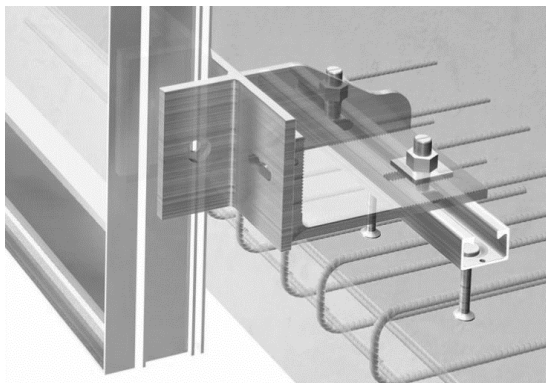


Figure 1. Connection of curtain wall elements using anchor channels and two adjacent channel bolts, e.g. for the façade of the Marina Bay Sands project, Singapore.

According to the recent building design codes, concrete anchors including anchor channels with channel bolts have to be qualified if used for safety relevant connections. Because of their high load capacity, anchor channels with channel bolts are typically used to fix heavy loads and therefore in general require qualification. Beside the careful selection of suitable and certified products by the specifier, a professional structural design by the engineer is required for a safe connection with anchor channels and channel bolts.

The design rules for anchor channel-channel bolt-systems are mostly based on the general design rules developed for steel fasteners anchored in concrete. The many and partly unique failure modes of anchor channel-channel bolt-systems, however, require additional and often quite complex design rules. The framework of these design rules is explained below following the presentation of further background information.

2 BACKGROUND

The development of anchor channels with channel bolts more than 100 years ago was driven by the need to connect components, e.g. transmission belts, to the then upcoming reinforced concrete structures (Figure 2a). T-bolts are locked into C-channels which are fitted with anchors and cast flush in reinforced concrete elements. Conventional smooth anchor channels with smooth channel bolts allow the transfer of tension loads (N) and shear loads (V) perpendicular to the channel. To enable the load transfer also along the axis of the channel, serrated anchor channels and matching serrated channel bolts were developed in the 1980s (Figure 2b), making the load transfer in all directions possible. These systems are very reliable since the installation of anchor channel as well as channel bolt is failsafe and the load is transferred in all directions by mechanical interlock. Moreover, the displacements to be anticipated are small – not only under static loads but even under cyclic loads. Advanced serrated anchor channel-channel bolt-systems are for these reasons a good choice for applications subjected to typhoons and earthquakes (Mahrenholtz et al (2017)).

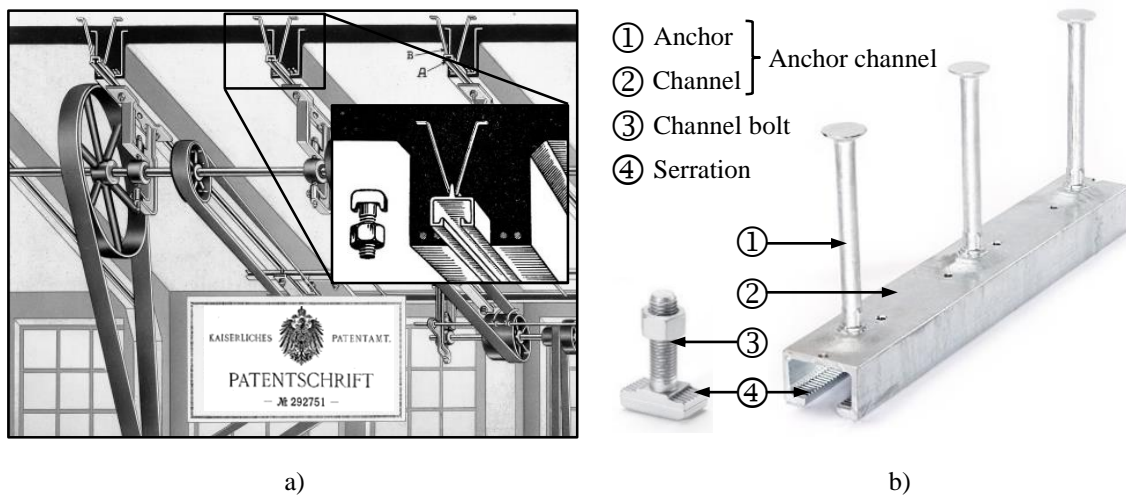


Figure 2. a) Anchor channels with channel bolts were invented by Jordahl in 1913; b) Serrated anchor channel components and matching serrated channel bolt.

For installation, the anchor channel is hot glued or nailed to the formwork (Figure 3a). Anchor channels are generally furnished with filler material to prevent concrete slurry leaking into the profile during concreting. After the concrete is set and the formwork is stripped off, the filler is removed (Figure 3b and c). Channel bolts are then inserted and twisted in the slot of the anchor channel to allow fastening of components at any point along its length (Figure 3d).

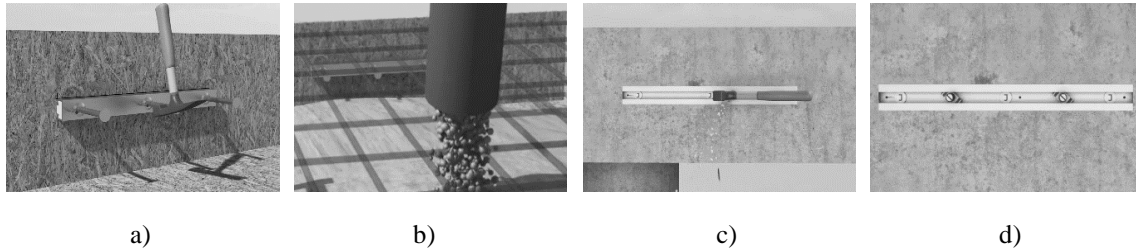


Figure 3. Installation sequence a) attaching of anchor channel to formwork, b) casting of concrete, c) removing of filler, d) twisting-in of channel bolt.

Anchor channels with channel bolts became very popular for the connection of components with steel base plates to the reinforced concrete structure mainly because of the following benefits:

- Quick and easy installation of the anchor channel during concreting
- Tolerances compensation by adjusting the position of channel bolt along the anchor channel
- Robust load transfer due to mechanical interlock (bolt-channel, anchor-concrete)
- Unlike anchor plates no on-site welding is required, thus no weld quality issues, or fire risks
- Unlike post-installed anchors no drilling required thus no cut reinforcing and silica dust
- Later positional adjustment, or replacement of attached components is made easy at any time

3 DESIGN

Some design equations are semi-empiric and require product dependent parameters to be determined during the qualification. The most important qualification guidelines for anchor channels with channel bolts are the European Assessment Document EAD 330008-03-0601 (2018) in Europe and the Acceptance Criteria AC232 (2018) in the USA. In Europe, qualification is documented by European Technical Assessment (ETA) certificates, e.g. ETA-09/0338 (2013), and does not yet address seismic qualification due to the lack of regulation. In the USA, Evaluation (Service) Reports (E(S)R), e.g. ER 0293 (2013) and ESR-2854 (2016), may include seismic qualification even for applications designed according to the more demanding Seismic Design Categories (SDC).

In Europe, the design provisions for concrete anchors including anchor channels with channel bolts are provided in the pre-norm CEN/TS 1992-4 (2009) whose revision FprEN 1992-4 (2016) has just been formally approved to become EN 1992-4 (2018), i.e. Part 4 of the Eurocode 2, the design code for concrete structures. The amendment FprCEN/TR 17080 (2016) was written to allow the design of anchor channels which channel bolts are loaded in the longitudinal direction. The latest revision of the design code for concrete structures in the USA, ACI 318 (2014), provides design rules for post-installed and cast-in anchors in Section 17. The design rules for anchor channel-channel bolt-systems are not yet included. For this reason, AC232 provides amendments to the relevant clauses of ACI 318 to allow the design of anchor channels and channel bolts. Also the fib Bulletin No. 58 (2011), published by the Fédération International du Béton (fib), includes design rules for anchor channels with channel bolts. A revision is on the way to reflect the latest developments in the field of the design of anchorages in concrete.

In contrast to the typically rotational symmetric post-installed and cast-in single point anchors with little more than the basic steel, concrete breakout and pullout failure modes, the geometric complex anchor channel-channel bolt-systems (Figure 4) may develop 18 different failure modes if loaded in tension and shear (Mahrenholtz (2016)). The design equations to calculate the load and resistance corresponding to the individual failure modes are organized according to the main

axis, i.e. in tension (z-direction), perpendicular shear (y-direction) and longitudinal shear (x-direction). The calculation of the loads as well as of the resistances are partly different in Europe and in the USA, calling for harmonization (Mahrenholtz et al (2017)).

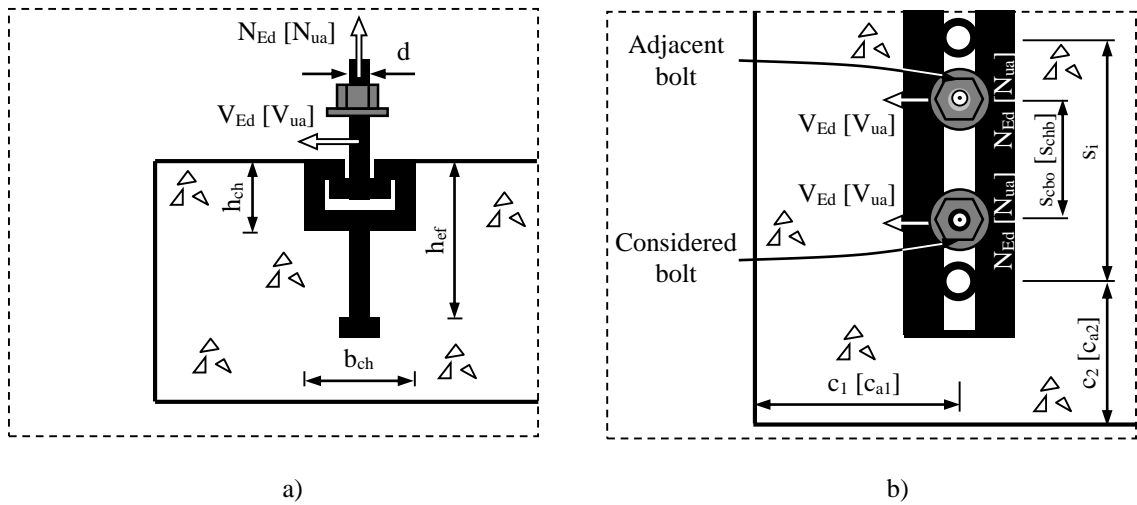


Figure 4. Schematic drawing of anchor channel with channel bolt loaded in tension and shear (steel base plate not shown): a) Cross section; b) Top view (denomination in square brackets according to ACI 318/AC232 if deviating from EN 1992-4).

The capacities are determined by analytically developed equations, by experimentally tested values (in the course of the qualification), or a mixture of both. A good example for the latter is the lip capacity corresponding to the lip failure (Figure 5a).

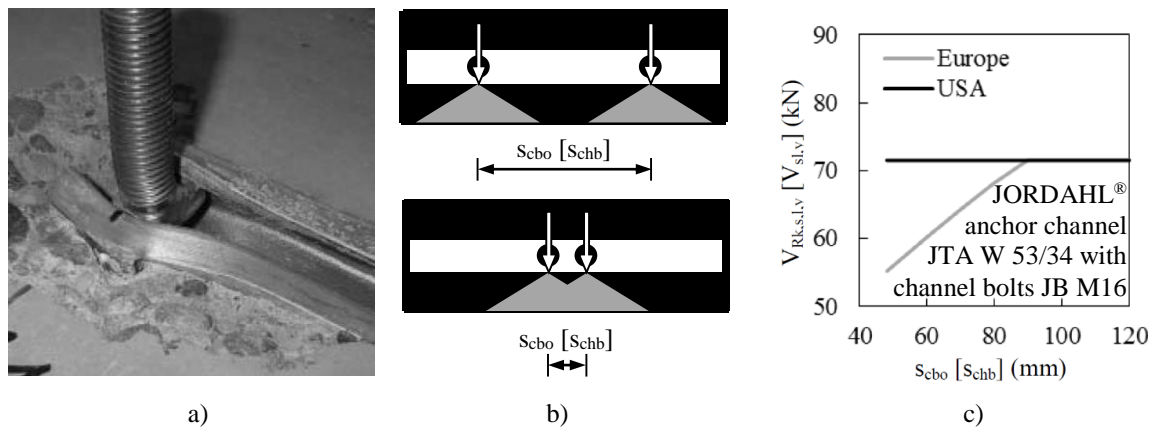


Figure 5. a) Photo of lip failure in shear after testing (Potthoff (2008)); b) Schematic of influencing adjacent channel bolts acting on the lip of the anchor channel; c) Comparison of calculated shear lip capacity in Europe and in the USA for a typical example (Mahrenholtz et al (2017)).

Lip failure is the excessive plastic deformation of the anchor channel where the loaded channel bolt is positioned. In Europe and in the USA, the value of the full basic lip capacity is determined experimentally during qualification due to the absence of reliable design models (Eligehausen et al (2007)). For tension loads, the influence of adjacent channel bolts on the lip capacity is taken into account analytically as a function of the channel bolt distance denominated s_{cbo} in Europe and s_{chb} in the USA (in the following, denomination according to ACI 318/AC232 is given in square brackets if deviating from EN 1992-4). In Europe, the equation used to account for the overlapping stress fields at the lip of the anchor channel resulting from shear loads (Figure 5b) is basically identical to the equation provided for tension loading. In contrast to the calculation of

the tension lip capacity, the reduction of the shear lip capacity due to the negative influence of adjacent channel bolts is not yet taken into account in the USA (Figure 5c).

Table 1 provides an overview how to calculate the lip capacity of anchor channel-channel bolt-systems. It is noteworthy that the quantitative difference between the equations stipulated in Europe and in the USA to account for the influence of adjacent channel bolts on the tension lip capacity of anchor channels is only minor. In the course of the harmonization of design rules, however, the influence of adjacent channel bolts on the shear lip capacity of anchor channels should be taken into account in the USA. This includes also the minimum spacing of adjacent channel bolts which is defined as $3d$ in the USA (AISC 360-10 (2010)), where d is the diameter of the channel bolt. Furthermore, the equations provided in Europe should be improved to provide a definition of the lip capacity also in case of two influencing adjacent channel bolts, one at each side of the considered channel bolt.

Table 1. Current definition of lip capacities in Europe and in the USA.

Europe: EN 1992-4, TR 17080, ETA	USA: ACI 318, AC232, E(S)R
Tension	
$N_{Rk,s,l} = N_{Rk,s,l}^0 \cdot \psi_{1,N}$ $N_{Rk,s,l}^0$ according to ETA $\psi_{1,N} = 0.5(1 + s_{cb0}/s_{1,N}) \leq 1$ $s_{1,N}$ according to ETA $(s_{1,N} = 2b_{ch}$ according to EAD 330008-03-0601 (2018))	N_{sl} if $s_{chb,i} \geq 2b_{ch}$, else $N_{sl} / (1 + \Sigma[(1 - s_{chb,i}/2b_{ch})^2 \cdot N_{ua,i}^b/N_{ua,1}^b])$ N_{sl} according to E(S)R $s_{chb} \geq 3d$ $N_{ua,1}^b$ load considered channel bolt $N_{ua,i}^b$ load adjacent channel bolt
Shear	
$V_{Rk,s,l,y} = V_{Rk,s,l}^0 \cdot \psi_{1,V}$ $V_{Rk,s,l}^0$ according to ETA $\psi_{1,V} = 0.5(1 + s_{cb0}/s_{1,V}) \leq 1$ $s_{1,V}$ according to ETA $(s_{1,V} = 2b_{ch}$ according to EAD 330008-03-0601 (2018))	$V_{sl,y}$ according to E(S)R (Currently, no reduction to account for the influence of adjacent channel bolts on the lip capacity of the anchor channel)

4 TESTS

Since the influence of adjacent channel bolts on the shear capacity of anchor channels is arguable, tests were required to shed light on this phenomenon (Mahrenholtz et al (2017)). Anchor channel and channel bolts are no uniform linear system because of the arbitrarily distribution of anchors and channel bolts at discrete locations along the channel. For qualification, the lip capacity of the anchor channel is therefore tested on channel bolts positioned at an anchor and between the anchors to determine the decisive value to be reported in the qualification certificate. For common anchor channel-channel bolt-systems, however, the lip capacity in shear may be assumed to be independent from the position of channel bolts: The ratio of the anchor channel lip capacity in shear is in general about 1.00 if tested on channel bolts positioned at the anchor and between two anchors (Figure 6).

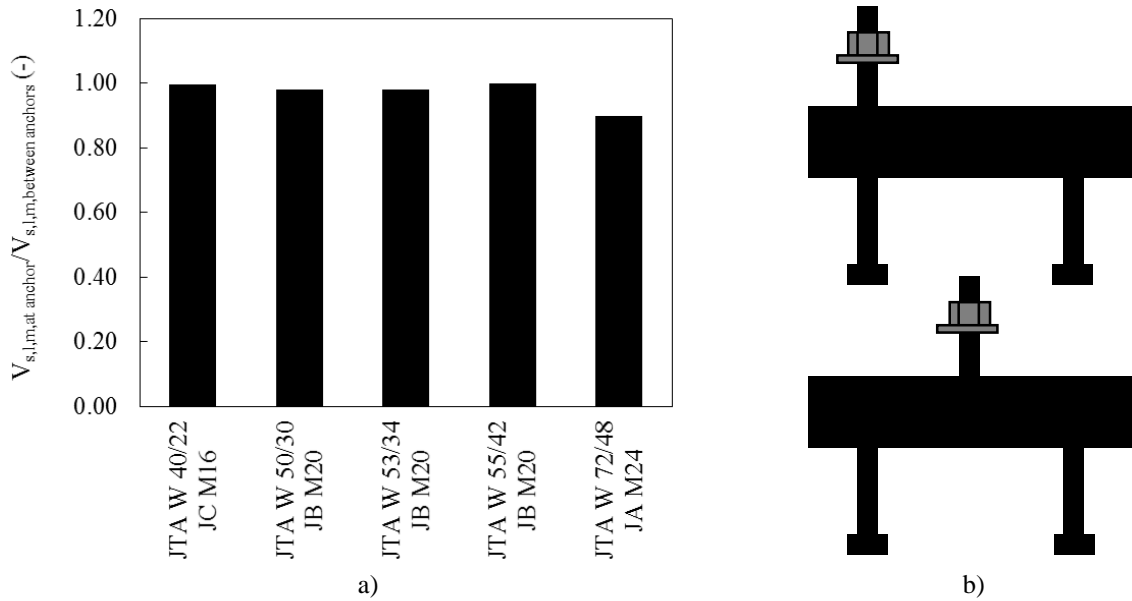


Figure 6. a) In general insignificant influence of channel bolt position on shear lip capacity of anchor channels (for most common JORDAHL® anchor channels JTA with matching channel bolts JA, JB, JC after Eligehausen et al (2015)); b) Position of channel bolt at the anchor and between the anchors of the channel.

Because the influence of adjacent channel bolts is therefore deemed not to be a function of the position with regard to the anchor channel, the test program (Table 2) included only tests on channel bolts symmetrically positioned between the two anchors of the tested channel. Thus, the effect of influencing adjacent channel bolts is not blurred by eccentricity effects. In total, 3 test series *i*, each with 3 repeats, were carried out with varying spacing of the channel bolts. Tests on single channel bolts were not carried out. Instead of, tests on two channel bolts with a large spacing of $s_{chb}/d [= s_{cbo}/d] = 7.5$ were carried out for which an influencing effect is precluded because the stress fields at the lip of the anchor channel do not overlap. For this reason, the tested mean lip capacity $V_{s,l,m}$ of this test equals to the basic mean lip capacity $V_{s,l,m}^0$.

Table 2. Test program, results and evaluation.

Series	Repeats	s_{cho}/d [s_{chb}/d]	$V_{s,l,m}$ (kN)	COV (%)	$V_{s,l,m}/V_{s,l,m}^0$ (-)	$V_{s,l}/V_{s,l}^0$, Eq. 1 (-)	$V_{s,l}/V_{s,l}^0$, Eq. 2 (-)
1	3	2.5	81.2	9.3	0.79	0.75	1.00
2	3	5.0	101.2	7.9	0.98	1.00	1.00
3	3	7.5	102.8	5.8	1.00	1.00	1.00

Apart from the loading fixture for *two* JORDAHL® channel bolts JC M16 (grade 8.8, hot-dip galvanized), the test setup (Figure 7) was identical to the arrangement used for qualification testing (EAD 330008-03-0601 (2018)). The JORDAHL® anchor channels JTA W 40/22 (hot-rolled, hot-dip galvanized) were cast in the concrete test members with sufficient edge distance to preclude concrete breakout failure. The test members were placed before a support which took over the reaction forces of the actuator loading the anchor channel-channel bolt-system in shear. Lifting forces were tied down to the strong floor.

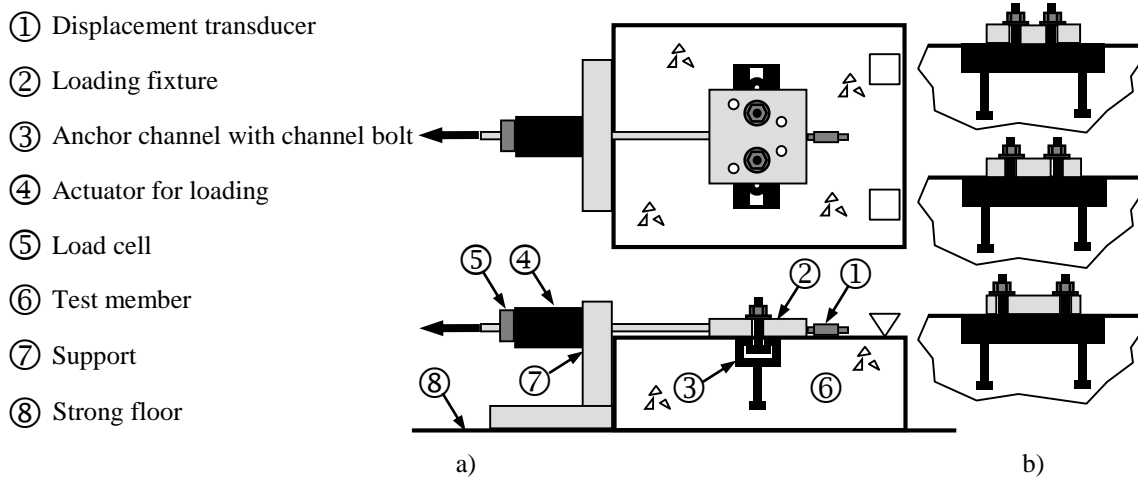


Figure 7. Schematic of test setup: a) Top and cross section; b) Details showing the tested anchor channel with 3 channel bolt positions.

To eliminate friction, PTFE sheets were placed between loading fixture and test member (Figure 8a). A load cell and a displacement transducer were installed to record load-displacement curves (Figure 8b).

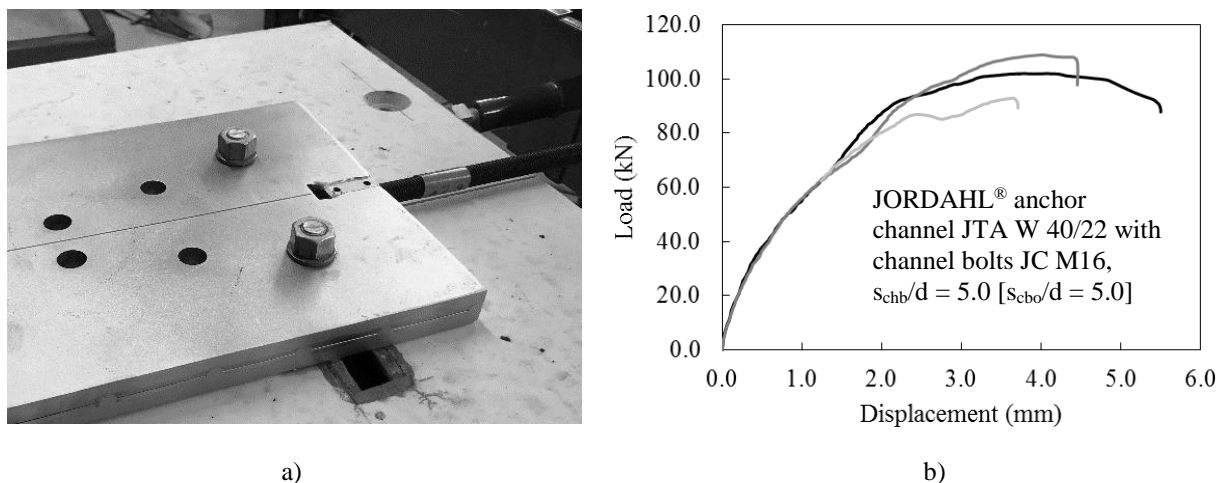


Figure 8. a) Close-up photo of completed test setup (PTFE not visible); b) Load-displacement curves (example test series).

All tests were terminated when a distinct load drop indicated the matured lip failure. The ultimate loads, indicating the lip capacities, showed acceptable coefficients of variation (COV) for all test series (Table 2). The ratio $V_{s,l,m}/V_{s,l,m}^0$ of the tested mean lip capacities represents the tested influence of adjacent channel bolts. The influence is deemed to be insignificant for a spacing of 5.0d but pronounced for a spacing of 2.5d where the determined ratio $V_{s,l,m}/V_{s,l,m}^0$ shows a reduction of about 25% (Table 2). The deformed lips visualize this finding (Figure 9): The zones of deformation are completely separated or just contact each other if tested with a channel bolt distance of 7.5d or 5.0d, respectively. In contrast, one joint zone of deformation exists, if the channel bolts loaded the anchor channel at a close distance of 2.5d.

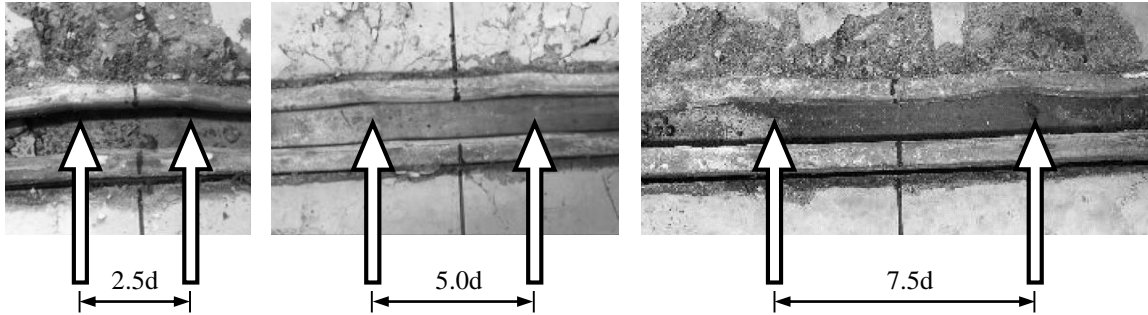


Figure 9. Photos of tested anchor channels after removing fixture and channel bolts.

5 MODEL

In the following, the test results are compared with two equations to calculate the influence of adjacent channel bolts on the shear lip capacity of the anchor channel if the spacing s_{cbo} [s_{chb}] is smaller than the characteristic spacing of $s_{l,v} = 2b_{ch}$. The influence is expressed by the ratio of the actual lip capacity $V_{s,l}$ and the basic lip capacity $V_{s,l}^0$ smaller 1.00.

Assuming the indicative value of $s_{l,v} = 2b_{ch}$ (FprEN 1992-4 (2016)) as the characteristic spacing for lip failure under shear, the equation codified in Europe (Table 1) for $s_{cbo} < 2b_{ch}$ [$s_{chb} < 2b_{ch}$] may be rewritten as follows:

$$\begin{aligned} V_{s,l}/V_{s,l}^0 &= 0.5(1 + s_{cbo}/2b_{ch}) \\ &[= 0.5(1 + s_{chb}/2b_{ch})] \end{aligned} \quad (1)$$

As an alternative, the equation stipulated in the USA to take into account the influence of adjacent channel bolts loading the anchor channel in tension (Table 1) for $s_{cbo} < 2b_{ch}$ [$s_{chb} < 2b_{ch}$] and $s_{cbo} \geq 3d$ [$s_{chb} \geq 3d$] may be adapted for shear. For two equally loaded channel bolts as in the tests, the ratio $V_{Ed,i}/V_{Ed,0}$ [$V_{ua,i}^b/V_{ua,0}^b$] yields 1.00 and only one spacing $s_{cbo,i} = s_{cbo}$ [$s_{chb,i} = s_{chb}$] exists:

$$\begin{aligned} V_{s,l}/V_{s,l}^0 &= 1 / (1 + \sum[(1 - s_{cbo,i}/2b_{ch})^2 \cdot V_{Ed,i}/V_{Ed,0}]) = 1 / (1 + (1 - s_{cbo}/2b_{ch})^2) \\ &[= 1 / (1 + \sum[(1 - s_{chb,i}/2b_{ch})^2 \cdot V_{ua,i}^b/V_{ua,0}^b]) = 1 / (1 + (1 - s_{chb}/2b_{ch})^2)] \end{aligned} \quad (2)$$

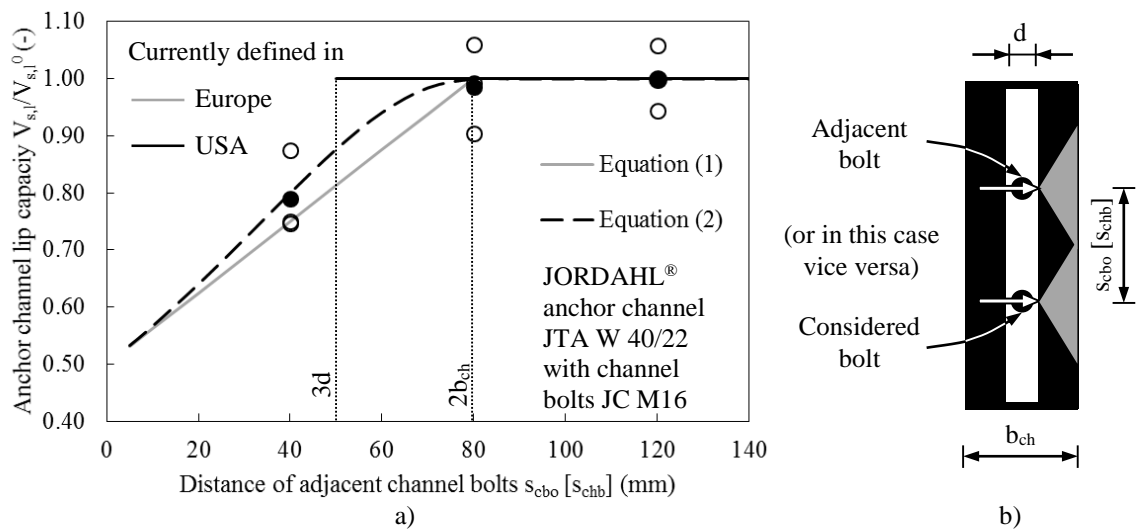


Figure 10. a) Representation of tested and modeled influence of adjacent channel bolts on the shear lip capacity of the anchor channel; b) Illustration of denominations.

The representation of tested and modelled influence of adjacent channel bolts on the lip capacity of the anchor channel (Figure 10) shows that Equation 1 estimates the influence conservatively. Equation 2 appears to be an even better match and has a smooth transition from the range where adjacent bolts do and do not have an influence. Moreover, the equation can be applied also if there are two adjacent bolts.

For these reasons it is suggested to use Equation 2 in Europe and in the USA to take the influence of adjacent channel bolts with a spacing smaller $2b_{ch}$ on the shear lip capacity of the anchor channel into account (Table 3). Furthermore, the more advanced provisions stipulated in the USA to account for the effect of adjacent channel bolts on the tension lip capacity of anchor channels should be mirrored to Europe where $2b_{ch}$ should be stipulated as a standard value for $s_{l,N}$ and $s_{l,V}$. The minimum bolt spacing of $3d$ appears to be a reasonable requirement to allow the proper manufacturing of the holes in the fixture and the correct installation of the bolts.

Table 3. Suggested definition of lip capacities in Europe and in the USA.

Europe: EN 1992-4, TR 17080, ETA	USA: ACI 318, AC232, E(S)R
Tension	
$N_{Rk,s,l} = N_{Rk,s,l}^0 \cdot \psi_{l,N}$	N_{sl} if $s_{chb,i} \geq 2b_{ch}$, else
$N_{Rk,s,l}^0$ according to ETA	$N_{sl} / (1 + \sum[(1 - s_{chb,i}/2b_{ch})^2 \cdot N_{ua,i}^b / N_{ua,1}^b])$
$\psi_{l,N} = 1 / (1 + \sum[(1 - s_{cbo}/b_{ch})^2 \cdot N_i^b / N_0^b]) \leq 1$	N_{sl} according to E(S)R
$s_{cbo} \geq 3d$	$s_{chb} \geq 3d$
N_0^b load considered channel bolt	$N_{ua,1}^b$ load considered channel bolt
N_i^b load adjacent channel bolt	$N_{ua,i}^b$ load adjacent channel bolt
Shear	
$V_{Rk,s,l,y} = V_{Rk,s,l}^0 \cdot \psi_{l,V}$	V_{sl} if $s_{chb,i} \geq 2b_{ch}$, else
$V_{Rk,s,l}^0$ according to ETA	$V_{sl} / (1 + \sum[(1 - s_{chb,i}/2b_{ch})^2 \cdot V_{ua,i}^b / V_{ua,1}^b])$
$\psi_{l,V} = 1 / (1 + \sum[(1 - s_{cbo}/b_{ch})^2 \cdot V_i^b / V_0^b]) \leq 1$	V_{sl} according to E(S)R
$s_{cbo} \geq 3d$	$s_{chb} \geq 3d$
V_0^b load considered channel bolt	$V_{ua,1}^b$ load considered channel bolt
V_i^b load adjacent channel bolt	$V_{ua,i}^b$ load adjacent channel bolt

It is noteworthy that the impact is low for common anchor channel-channel bolt-systems since the range between $s_{cbo} < 2b_{ch}$ [$s_{chb} < 2b_{ch}$] and $s_{cbo} \geq 3d$ [$s_{chb} \geq 3d$] is small and the potential influence of adjacent channel bolts on the lip capacity of the anchor channel may be secondary and seldom relevant for the overall capacity of the system.

6 SUMMARY

Following a brief introduction of anchor channels with channel bolts as a perfect solution for typhoon and earthquake loaded connections, the most relevant background is presented. It is discussed that the overlapping stress fields of adjacent channel bolts reduce the anchor channel lip capacity. The review of the current design rules show that the influence of adjacent bolts is differently handled in Europe and in the USA. In Europe, the influence is taken into account for shear loading in analogy to tension loading, however, the influence of two adjacent bolts is not defined. In the USA, the influence is taken into account for tension loading but not for shear loading, though a minimum spacing according to the recommended distance between centres of the holes is required.

Three tests series were carried out to quantify the influence of adjacent channel bolts on the shear lip capacity of the anchor channel and to study whether the current European model for shear loading or the adaption of the US American model for tension loading is more suitable to describe the influence. The evaluation of the test results showed that the US American equation for tension

loading modified for shear loading has a better match and, moreover, avoids the limitation of the European equation with regard to the number of adjacent bolts.

In conclusion, it is suggested to add an equation in the USA to account for the effect of adjacent channel bolts on the shear lip capacity of anchor channels on the basis of the equation for the calculation of the tension lip capacity. The equations should be mirrored to Europe. Further research is suggested to substantiate the correctness of the suggested equation for the complete range of common anchor channel-channel bolt-systems. The views expressed in this paper are the views of the author only and do not necessarily reflect the views of Jordahl GmbH.

REFERENCES

- AC232, 2018, Acceptance criteria for anchor channels in concrete elements. International Code Council Evaluation Service, Inc. (ICC-ES), Whittier, California
- ACI 318, 2014, Building code requirements for structural concrete (ACI 318-14) and commentary (ACI 318R-14), American Concrete Institute, Farmington Hills, Michigan
- AISC 360-10, 2010, Specification for structural steel buildings. American Institute of Steel Construction, (AISC), Chicago, Illinois
- CEN/TS 1992-4, 2009, Design of fastenings for use in concrete – Part 4-1 – 4-5. Technical Specification, European Committee for Standardization (CEN), Brussels
- EAD 330008-03-0601, 2018, Anchor channels. European Assessment Document, OJEU 2018/C /, EOTA
- Eligehausen, R. and K. Schmid, 2015, Assessment of Jordahl anchor channels K28/15, K38/17, W50/30, W53/34, W55/42 and W72/48 with round anchors for anchoring in concrete in accordance with AC232. Assessment report 10_61_1, IEA
- Eligehausen, R., J. Asmus, D. Lotze and M. Potthoff, 2007, Ankerschienen (Anchor channels). *Beton-Kalender 2007*, Part 2, 377-435, Ernst & Sohn, Berlin
- EN 1992-4, 2018, Eurocode 2: Design of concrete structures – Part 4: Design of fastenings for use in concrete. European Committee for Standardization (CEN); EN 1992-4
- ER 0293, 2013, Evaluation Report on Jordahl Anchor Channels JTA and Channel Bolts, IAPMO Uniform Evaluation Service
- ESR-2854, 2016, Evaluation Service Report on Jordahl anchor channel system in uncracked and cracked concrete. ICC-ES Evaluation Service
- ETA-09/0338, 2013, European Technical Approval for Jordahl-anchor channel JTA
- fib Bulletin No. 58, 2011, Design of anchorages in concrete. Guide to good practice. Bulletin No. 58, Fédération International du Béton (fib)
- FprCEN/TR 17080, 2016, Design of fastenings for use in concrete – Anchor channels – Supplementary rules. European Committee for Standardization (CEN); Technical Report, prenorm for formal vote
- FprEN 1992-4, 2016, Eurocode 2: Design of concrete structures – Part 4: Design of fastenings for use in concrete. European Committee for Standardization (CEN); EN 1992:2016, prenorm for formal vote
- Mahrenholtz, C., 2016, Non-seismic and seismic qualification and design of anchor channels with channel bolts. *Joint ASC and AEES Conference*, Melbourne
- Mahrenholtz, C., J. Lambton and F. Julier, 2017, Suitability of anchor channels with channel bolts for use in nuclear power plants. *Proceedings of the 24th International Conference on Structural Mechanics in Reactor Technology (SMiRT 24)*, Proceeding Div VI, Busan
- Mahrenholtz, C. and D. Neumann, 2017, Influence of adjacent channel bolts on channel shear lip capacity. Presentation at CAMA
- Mahrenholtz, C. and A. Sharma, 2017, Comparison of design rules for anchor channels with channel bolts. *Proceedings of the 3rd International Symposium ConSC2017 (Connections between Steel and Concrete)*, Stuttgart
- Potthoff, M., 2008, Tragverhalten und Bemessung von Ankerschienen unter Querbelastung (Load bearing behaviour and design of anchor channels under shear loads). Dissertation, University of Stuttgart (in German)

Study on the behavior of RC beams strengthened with CFRP laminates under pure torsion using finite element analysis and *fib* Bulletin 14 method

Muhanad Mohammad Majed¹, Mohammadreza Tavakkolizadeh²

¹ Ph.D. Student, Department of Civil Engineering, Ferdowsi University of Mashhad, Mashhad, Iran

² Assistant Professor, Department of Civil Engineering, Ferdowsi University of Mashhad, Mashhad, Iran

ABSTRACT

This paper discussed analytical and finite element (FE) studies on behavior of CFRP (Carbon Fiber Reinforced Polymer) strengthened reinforced concrete (RC) beams under pure torsion. Behavior of rectangular reinforced concrete beams strengthened with CFRP laminates under pure torsion was studied using finite element method by ABAQUS. Results were compared with the experimental data collected from previous studies. The finite element ultimate torsional capacity showed good agreement with the experimental results. In addition, the analytical methods suggested by *fib* Bulletin 14 was used to predict value of effective CFRP strain and the torsional moment capacity. The difference between FE capacity of control and strengthened beams was less than 11%. The comparison between the design approaches suggested by *fib* Bulletin 14 with previous experimental results discussed and compared.

1 INTRODUCTION

Very few studies focused on torsion beams strengthening using FRP. The torsion is considered a minor effect in some cases, while it becomes critical in cases such as horizontally curved beams, members of a space frame, eccentrically loaded beams, spandrel beams, and spiral staircases are typical examples of structural elements subjected to major torsional moments and hence torsion cannot be neglected in design of such members. Therefore, it is important to understand the behavior of RC members subjected to twisting about its longitudinal axis, known as torsion.

Testing of FRP-strengthened concrete elements in torsion has been very limited. Some tests have been conducted by Täljsten (1998) who proven that torsional strengthening of beams with rectangular cross sections is viable with CFRP wrapping *fib* (2001). Panchacharam & Belarbi (2002) presented an experimental work to study the behavior and performance of reinforced concrete members strengthened with externally bonded Glass FRP (GFRP) sheets subjected to pure torsion. Six RC spandrel beams were tested by Salom et al (2004). Assuming that the torsional moment capacity is a function of only the amount and spacing of the torsional reinforcement, the nominal torsional capacity of the control specimen can be estimated using the equation given in (ACI318M-02) (2002). Hii & Al-Mahaidi (2006) tested six medium scale RC beams of 500 mm x 350 mm cross section and 2500 mm long; where two specimens were solid sections while the rest were box sections with 50 mm thick walls and flanges. Hii & Al-Mahaidi (2006) performed an experimental and numerical investigation on torsional strengthening of solid and box-section reinforced concrete beams using CFRP laminates. CFRP and GFRP-strengthened RC beams with a rectangular cross-section have been tested by Ameli et al. (2007) and the results then were compared with those obtained from the nonlinear finite element program ANSYS.

Chalioris (2008) used an experimental program includes 14 rectangular and T-shaped beams were tested under pure torsion. Torsion failure is an undesirable brittle form of failure as showed by Deifalla & Ghobarah (2010).

Numerical studies using finite FE have been carried out by many researchers to understand the overall behavior of concrete members with and without FRP strengthening. Chellapandian et al. (2017) Analytical and finite element studies on the behavior of Reinforced Concrete (RC) column elements strengthened using a hybrid Carbon Fiber Reinforced Polymer (CFRP) laminates and externally bonded fabric is explored in this study a numerical model of column elements is developed using a commercial software ABAQUS. Dawood (2013) examined the behavior and performance of solid and box section RC Beams and found that the increase in torsional strength enhances torsional strength when using CFRP composites. For this purpose, that researcher used the ANSYS (FE) program to model the beam. The torsional behavior of RC members strengthened with CFRP laminates presented by Allawi (2006) using two different software DIANA version 9.0 and P3DNFEA. Alabdulhady et al. (2017) described the results of numerical simulation performed using LS-DYNA to investigate the torsional behavior of reinforced concrete beams strengthened with externally bonded fiber reinforced cementitious Matrix (FRCM) composite.

The current study is aimed to explore more information about RC beams strengthened with externally bonded CFRP and subjected to pure torsion numerically with different strengthening schemes. The simulation is performed with software program ABAQUS/CAE 2016. Torsional strength, torque and angle of twist per unit length response are evaluated and compared with experimental results to validate the model and determine its accuracy. *fib* Bulletin 14 (2001) described here and compared with experimental data. The model is capable of predicting failure for concrete materials. Both cracking and crushing failure modes but in this study, failure criteria for CFRP strengthened beams were not considered. They are needed to define a failure surface for the concrete. The results of FE were plotted until the beams reached failure in the experimental study.

2 VALIDATION OF FE AND *fib* BULLETIN 14 METHOD

For FEA validation the specimens tested is taken from other researchers previously published by Chalioris (2008). The beams selected for the purpose of the numerical simulation in this paper were Ra-Fs150 (2) and Ra-S5.5/75 for group Ra, Rb-F (1) and Rb-S5.5/160 for group Rb. The details of tested beams are summarized in Table 1.

Table 1. Details of the test beams used for validation.(Chalioris, 2008)

Beam	Flexural reinforcement	Shear reinforcement	Type of strengt hening	n_f mm ()	A_f/S_f (mm)	ρ_{sl} %	ρ_{st} %	ρ_{ft} %
Ra-Fs150(2)	4Ø8	-	Wrappi ng with 150 mm width strips spaced 300mm apart	2	0.11	1.01	-	0.33
Ra-s5.5/75	4Ø8	Ø 5.5/75	-	-	-	1.01	0.67	-
Rb-F(1)	4Ø8	-	Full wrappi ng	1	0.11	0.45	-	0.22
Rb-s 5.5/160	4Ø8	Ø 5.5/160	-	-	-	0.45	0.22	-

For fib Bulletin 14 method validation, five beams strengthened with CFRP (Ra and Rb) were considered. Details of these beams are listed in Table 2 and their experimental test setup is shown in Figure 1. Additional information of the experimental work and setups may be found in references (Chalioris, 2008).

3 FINITE ELEMENT ANALYSIS FOR EXPERIMENTAL RESULTS

To study more thoroughly the torsional behavior of reinforced concrete beams strengthened with CFRP, a nonlinear finite element analysis has been carried out to analyze experimentally tested beams. The analysis was performed by using the FE using software program ABAQUS. A nonlinear finite element model is proposed in this study to Simulate the torsional behavior of FRP strengthened RC beams for various parameters using ABAQUS. Modelling details are discussed in the following sections. The verification is done in order to check the validity and accuracy of the finite element procedure. The accuracy of the finite element models was determined by ensuring that the ultimate torque was reasonably predicted with the experimental results, and the torque - twist and torque are close to the experimental curves.

Table 2. Details of strengthening and testing beams.(Chalioris, 2008)

Beam	b , h mm	ϵ_{fu} $\times 10^{-2}$	f'_c MPa	t_f mm	E_{fu} GPa	θ Deg	β Deg	Experimental values Ultimate Torque kN.m	Ultimate Torque Refrence kN.m	Ultimate torque ($T_{f,CFRP}$) kN.m
Ra-F(1)	100,200	1.5	27.5	0.11	230	45	90	4.86	2.389	2.479
Ra-F(2)	100,200	1.5	27.5	0.22	230	45	90	6.65	2.389	4.261
Ra- Fs150(2)	100,200	1.5	27.5	0.11	230	45	90	3.018	2.389	0.629
Rb- Fs200(1)	150,300	1.5	28.5	0.05	230	45	90	9.315	6.951	2.364
Rb- Fs300(1)	150,300	1.5	28.5	0.05	230	45	90	7.52	6.951	0.569

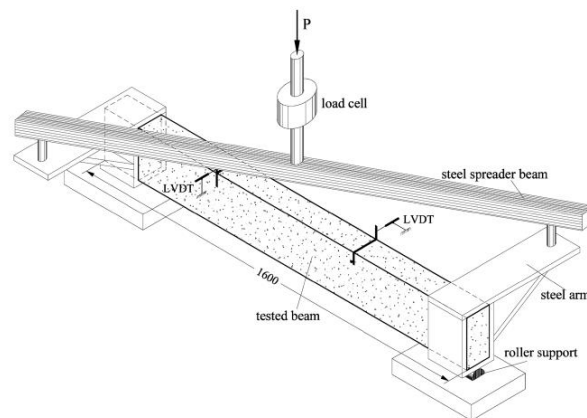


Figure 1. Experimental test setup for RC beam under torsion Chalioris (2008)

3.1 Model geometry

3.1.1 Concrete idealization

The modelled beam in ABAQUS is shown in Figure 2. Concrete damaged plasticity available in ABAQUS/STANDARD. Concrete is modelled using three dimensional eight node solid brick elements with three Translational degrees of freedom at each node (C3D8R). Behavior of concrete in compression and tension are different, and the damage plasticity approach is adopted to model the concrete. Isotropic and linear elastic behavior of concrete both in compression and tension are defined Using Young's modulus and Poisson's ratio, nonlinear behavior is defined in terms of inelastic Strain and corresponding yield stress, parabolic model is used to define the compressive stress strain curve, Failure ratios for concrete used in the model are reported in Table 3.

Table 3. Parameters for FE Modelling

Dilation angle	Eccentricity	Bi-axial to uni-axial compressive strength ratio	K	Viscosity parameter
36	0.1	1.16	0.67	0

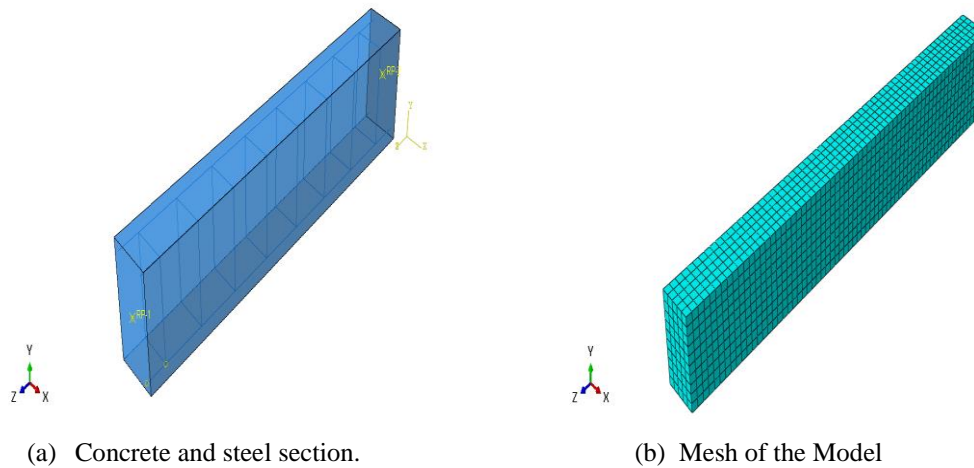


Figure 2. Finite element discretization of different components

3.1.2 Reinforcing bar idealization

The modeled of the longitudinal and stirrups rebars in ABAQUS is shown in Figure 3. The embedded element technique is used to specify that steel reinforcement element are embedded in host concrete elements. Steel reinforcing bars were modeled using material model type plastic. The parameters needed are the modulus of elasticity E, Poisson's ratio and yield stress. The modulus of elasticity and yield strength are listed in

Table 4. Longitudinal and transverse reinforcements are modeled with three dimensional; two noded truss elements (T2D3), elastic perfectly plastic stress strain relationship is assumed for steel under both compression and tension, Steel being an isotropic material; linear elastic behavior

is defined by elastic modulus and Poisson's ratio. Perfectly plastic behavior is defined using any two points on the yield line in terms of inelastic strain and yield stress.

Table 4. Reinforcement material properties

Rebar diameter (mm)	Yield Stress (MPa)	Modulus of Elasticity (GPa)
8	560	200
5.5	350	200

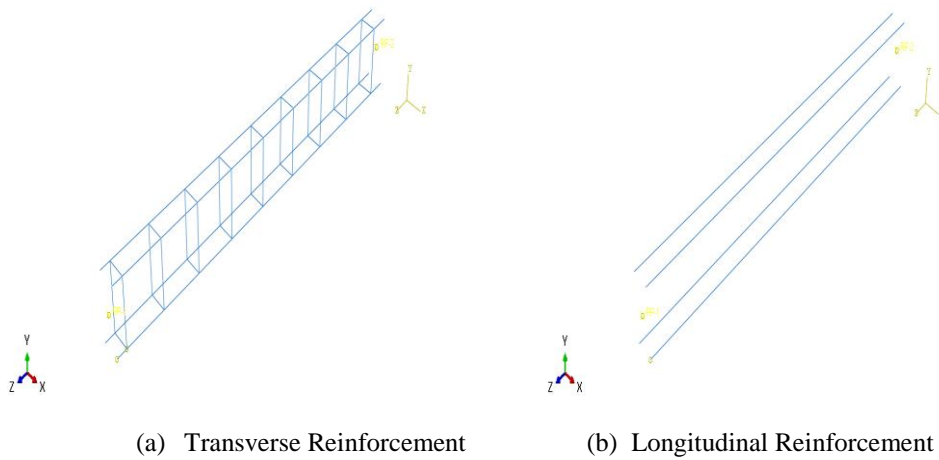


Figure 3. Finite element discretization of different components

3.1.3 CFRP idealization

The modeled of full wrapping and wrapping with strips in ABAQUS is shown in Figure 4. FRP (S4R) is modelled using three dimensional shell element. The main parameters needed in this model are E and shear modulus G in three orthogonal directions, and fiber direction is defined by a vector. The properties of fibers are listed in Table 5.

Table 5. Properties of the CFRP used in the present study

Properties	CFRP (SikaWrap-200c)
Thickness (mm)	0.11
Tensile strength (MPa)	3900
Modulus of Elasticity (GPa)	230

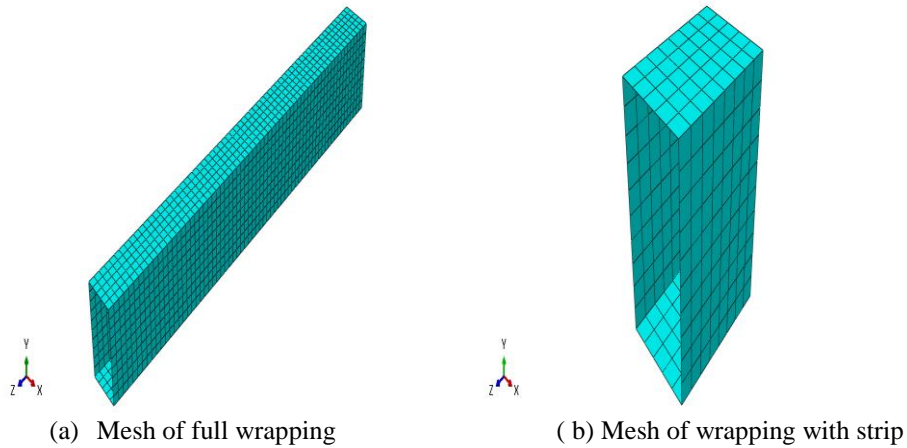


Figure 4. Finite element discretization of different components

3.1.4 Interaction: Concrete

Concrete - steel interaction is modelled using embedded region constraint which is a built-in interaction in ABAQUS. Steel interaction is modelled using embedded region constraint which is a built-in interaction in ABAQUS. Perfect bond is also assumed to define the interaction between Concrete and FRP for simplification using a tie constraint. Table 6. summarizes the type of element and material behavior used for all specimens.

Table 6. Element type and Idealized stress strain curve of materials

Material	Element type	Idealized curve
Concrete	Solid-C3D8R	Parabolic
Steel	Truss-T3D3	Elastic –perfectly plastic
FRP	Shell-S4R	Elastic

4 RESULTS

4.1 Ultimate torque

Finite element and experimental results for overall torsional moment behavior are compared for the tested beams. Analytical predictions are validated with the experimental results taken from previous study and a good agreement was found. The values of ultimate torsion (kN.m) and ultimate angle of twist per length (rad/m) of tested beams obtained from the theoretical study (ABAQUS/CAE.2016) and experimental tests are reported in

Table 7. Results obtained from FE show that the model was able to predict the ultimate torque with difference in the range of 1-11%. Considering the bond properties of FRP and concrete my yield improved results. The influence of FRP is less significant before cracking of the concrete and this led to accurate prediction of the cracking torque and corresponding twist. However, the ultimate torque and corresponding twist were reasonably captured. The boundary condition plays very important role in the calculations of FE analysis.

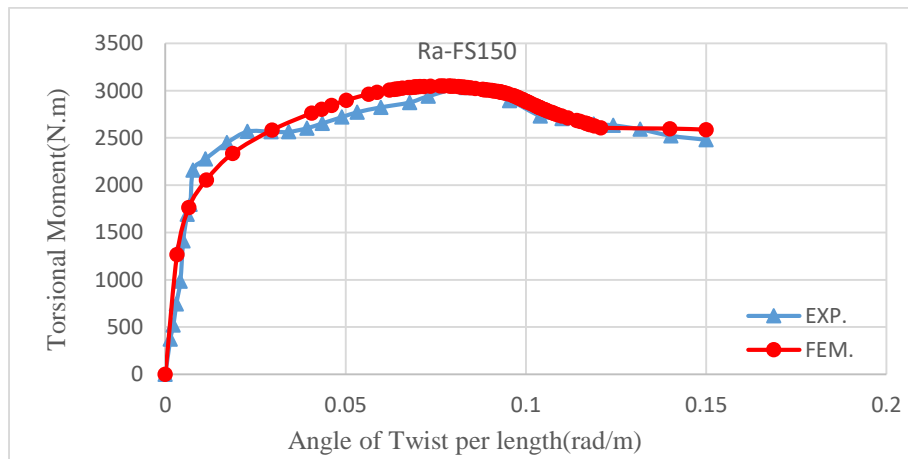
Table 7. Experimental and theoretical ABAQUS ultimate torque results for the control and strengthened beams

Specimen	Cracking torque (k N-m)		Cracking twist (rad/m)		Peak torque T_u (k N-m)		Peak twist θ_u (rad/m)		$\frac{T_{u,EXP.}}{T_{u,FEM.}}$	$\frac{\theta_{u,EXP.}}{\theta_{u,FEM.}}$
	EXP.	FEM.	EXP.	FEM.	EXP.	FEM.	EXP.	FEM.		

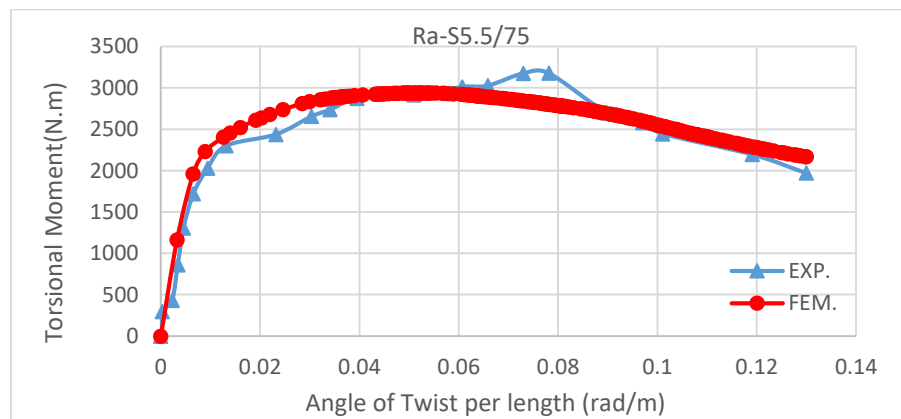
Ra-Fs150(2)	2.219	1.762	0.009	0.0065	3.018	3.049	0.088	0.076	1.01	1.15
Ra-S5.5/75	2.250	2.230	0.013	0.0089	3.156	2.940	0.078	0.052	1.07	1.5
Rb-F(1)	8.794	8.779	0.009	0.0077	10.050	10.27	0.071	0.027	1.021	0.37
Rb-S5.5/160	6.924	7.660	0.009	0.0088	6.924	7.7	0.009	0.0075	1.11	1.2

4.2 Torque – Twist behavior

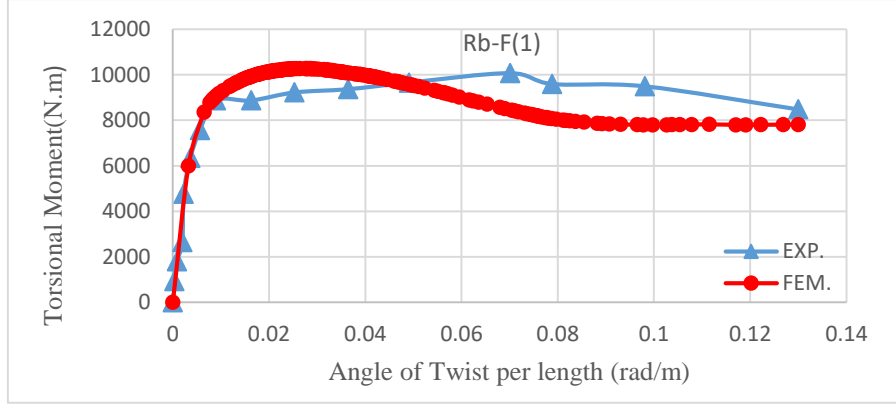
Torque-twist behavior of the all specimens predicted by model is offered in Figure 5 shows the comparison between experimental and FE results of overall torque - twist behavior of all tested beams. In general, it can be noted from the torque - twist curve that the finite element analysis are agree well with the experimental results during the full range of behavior. The FE models accurately predicted the cracking torque and cracking twist peak values of torque and peak twist were also captured reasonably well.



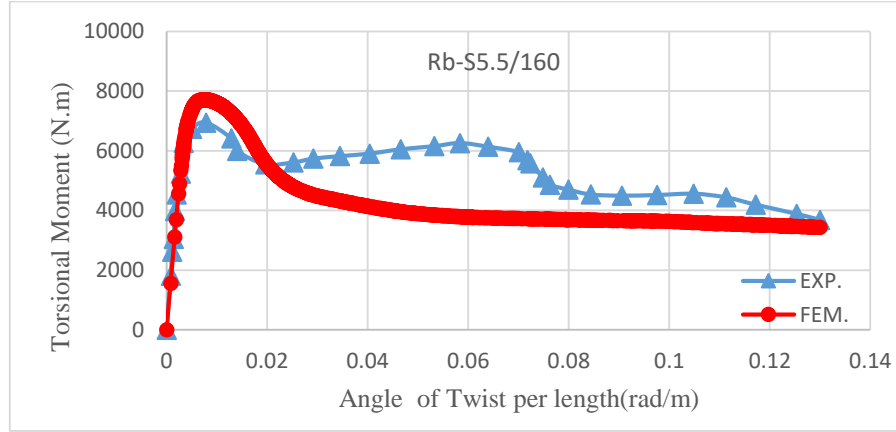
(a) Ra-Fs150 (2)



(b) Ra-S5.5/75



(c) Rb F (1)



(d) Rb-S5.5/160

Figure 5. Comparison of FEM results and experimental data for beams

5 ANALYTICAL METHODS (*FIB*-14 GUIDELINE METHOD (*FIB*,2001)

Ghobarah et al. (2002) and (Salom et al., 2004) have proposed a simple limiting FRP strain value.

$$\varepsilon_{fe} = \frac{T_f S}{2A_0 A_f E_f (\cos \alpha + \sin \alpha)} \quad (5.1)$$

Ameli et al. (2003), Panchacharam & Belarbi (2002) and Hii & Al-Mahaidi (2007) adopted *fib*-14 guideline method of predicting the effective CFRP strain. These analytical methods can be discussed below and compared to a data base compiled from the previous study data.

$$T_{n,FRP} = 2\varepsilon_{fde} E_{fu} A_f S_f^{-1} A_c (\cot \theta + \cot \alpha) \sin \alpha \quad (5.2)$$

$$\varepsilon_{f,calc} = \frac{T_{f,exp}}{2 E_{fu} A_f S_f^{-1} A_c (\cot \theta + \cot \alpha) \sin \alpha} \quad (5.3)$$

$$\varepsilon_{fk,e} = K \varepsilon_{f,e} \leq \varepsilon_{max} \quad (5.4)$$

$$\varepsilon_{fd,e} = \frac{\varepsilon_{fk,e}}{\gamma_f} \quad (5.5)$$

where ($A_f = b_f t_f$) is the area of fiber strip/wrap; (b_f) is the width of FRP strips; ($K = 0.8$) is used to define the characteristic effective FRP strain ($\varepsilon_{fk,e}$); (S_f) is center to center spacing of FRP strips; (t_f) is the thickness of fiber laminate; (α) is the angle between principal fiber

orientation and longitudinal axis of member; ($\epsilon_{fd,e}$) is the design value of effective fiber strain; $\epsilon_{max} = 5000$ micro-strain for shear case as stated by (*fib*, 2001) while the (ACI Committee 400, 2002) suggest limited value of 0.004 ; (γ_t) is the material safety factor for the FRP (range 1.2 - 1.5 in *fib* bulletin 14); and (θ) is the angle of crack to longitudinal axis.

The effective fiber strain (ϵ_{fe}) is:

For completely wrapped sample

$$\epsilon_{fe} = 0.17 \left(\frac{f_{cm}^{2/3}}{E_f \rho_f} \right)^{0.3} \epsilon_{fu} \quad (5.6)$$

And for samples strengthened with strips:

$$\epsilon_{fe} = \min 0.8 \left[0.65 \left(\frac{f_{cm}^{2/3}}{E_f \rho_f} \right)^{0.56} \times 10^{-3}, 0.17 \left(\frac{f_{cm}^{2/3}}{E_f \rho_f} \right)^{0.3} \epsilon_{fu} \right] \quad (5.7)$$

Where f_{cm} is the compressive strength of concrete in MPa, E_f is in GPa and. ρ_f is the CFRP reinforcement ratio.

Table 8. Comparison between experimental and calculated CFRP torsional contribution predicted by *fib*-14 Method

Beam	$T_{f,CFRP}$ KN.m (Test)	$T_{f,CFRP}$ KN.m (<i>fib</i> -14)	$T_{f,CFRP}$ KN.m ($\epsilon_{f,CFRP}=0.004$)	$\frac{T_{f,CFRP,EXP}}{T_{f,CFRP}(FIB-14)}$	$\frac{T_{f,CFRP,EXP}}{T_{f,CFRP}(\epsilon_{f,CFRP}=0.004)}$	CFRP Strain Level	
						Analytical CFRP Strain	
						ϵ_{fe} Calculate $\times 10^{-3}$ Ghobarah & Salom et al.	ϵ_{fe} <i>fib</i> -14 Calculate $\times 10^{-3}$
Ra-F(1)	2.479	3.477	2.522	1.40	1.017	2.449	5.376
Ra-F(2)	4.261	5.648	5.044	1.32	1.18	2.105	4.366
Ra-Fs150 (2)	0.629	0.676	0.646	1.07	1.027	0.621	2.092
Rb-Fs200 (1)	2.364	2.3194	2.181	0.98	0.922	2.076	3.923
Rb-Fs300 (1)	0.569	1.427	0.727	2.5	1.277	0.499	3.923

The determination of effective CFRP strain (ϵ_{fe}) is based on partial safety factor (γ_f) equals to 1.3 and $k = 0.8$ CFRP torsional contribution based *fib*-14 expression for effective strain is compared with experimental results in Table 8. It can be seen the results are in good agreement with the test result and in encouraging when used maximum allowable value for effective CFRP strain of 0.004 according to the recommended ACI Committee 440 (2000) while the torsional contribution of CFRP predicted by *fib*-14 (2001) is generally un conservative in defining the effective CFRP strain (ϵ_{fe}) when associated to the experimental results. That is because of limited available data on the behavior of reinforced concrete members strengthened with CFRP subjected to torsion at that time and the suggested torsion model by *fib*-14 (2001) is based on similar cracking mechanism of shear.

6 CONCLUSIONS

Numerical and analytical studies were carried out on strengthened beams elements under pure torsion. A non-linear finite element model was developed using ABAQUS and was calibrated with the test results. From the results and observation the following major conclusions can be drawn presented in this study:

1. The finite element simulation shows good agreement with the experimental results. Maximum difference in ultimate strength was (1-11%) for the strengthened and control beams.
2. The slight difference between the results from finite element models and experimental results indicate that the assumption of full interaction between CFRP composite and concrete is reasonable.
3. The nonlinear finite element model was able to capture the behavior of RC beams with and without FRP strengthening techniques under pure torsion.
4. The only torsional design method for reinforced concrete members strengthened with CFRP recommended by *fib-14* was found to be generally un conservative. Therefore, future improvement is needed for *fib-14* guideline to make it suitable as a design method for torsional strengthening.
5. A value of 0.004 for the characteristic effective CFRP strain (ϵ_{fke}) suggested by ACI Committee 440 is shown to be an optimum value for design purposes.

REFERENCES

- Alabdulhady, M. Y. et al. (2017). Finite element study on the behavior of RC beams strengthened with PBO-FRCM composite under torsion. *Composite Structures* (Vol. 179). Elsevier Ltd.
- Allawi, A. A. (2006). Nonlinear analysis of reinforced concrete beams strengthened by CFRP in torsion, (December).
- Ameli, M., Ronagh, H. R., & Dux, P. F. (2003). Experimental investigations on FRP strengthening of beams in torsion, (Fib 2001).
- Ameli et al. (2007). Behavior of FRP strengthened reinforced concrete beams under torsion. *Journal of Composites for Construction*, 11(2), 192–200.
- Chalioris, C. E. (2006). Experimental study of the torsion of reinforced concrete members, 23(6), 713–737.
- Chalioris, C. E. (2008). Torsional strengthening of rectangular and flanged beams using carbon fibre-reinforced-polymers – Experimental study, 22, 21–29.
- Chellapandian, M., Prakash, S. S., & Rajagopal, A. (2017). Analytical and Finite Element Studies on Hybrid FRP Strengthened RC Column Elements under Axial and Eccentric Compression. *Composite Structures*.
- Committee, ACI (2002). Guide for the design and construction of externally bonded frp systems for strengthening concrete structures reported by ACI Committee, *ACI*, 440, 45.
- Dawood, M. B. (2013). Nonlinear analysis of solid and box-section rc beams strengthened in torsion with CFRP reinforcement. *Journal of Babylon University/ Engineering Sciences*, 21(1), 11–26.
- Deifalla, A., & Ghobarah, A. (2010). Full torsional behavior of RC beams wrapped with FRP: analytical model. *Journal of Composites for Construction*, 14(3), 289–300.
- FIB. (2001). Externally bonded FRP reinforcement for RC structures, *International Federation for*

Structural Concrete (fib) (Vol. 14).

- Ghobarah, A., Ghorbel, M. N., & Chidiac, S. E. (2002). Upgrading torsional resistance of reinforced concrete beams using fiber-reinforced polymer, (November), 257–263.
- Hii, A. K. Y., & Al-Mahaidi, R. (2006). An experimental and numerical investigation on torsional strengthening of solid and box-section RC beams using CFRP laminates, *Composite Structures*, 75(1–4), 213–221.
- Hii, A. K. Y., & Al-Mahaidi, R. (2007). Torsional capacity of CFRP strengthened reinforced concrete beams, *Journal of Composites for Construction*, 11(February), 71–80.
- Panchacharam, S., & Belarbi, A. (2002). Torsional behavior of reinforced concrete beams strengthened with FRP composites, First FIB Congress, 1–11.
- Salom et al., 2004. (2004). Torsional strengthening of spandrel beams with fiber-reinforced polymer laminates, *Journal of Composites for Construction*, 8(2), 157–162.
- Täljsten, B. (1998). Strengthening of concrete structures for shear with CFRP-fabrics: test and theory. In International Conference on Concrete Under Severe Conditions: 21/06/1998-24/06/1998 (Vol. 2, pp. 1298–1310).

Experimental and numerical investigation of cyclic response of precast hybrid beam-column connections

Sadık Can Girgin¹, İbrahim Serkan Mısıır², and Serap Kahraman³

¹ Assistant Professor, Department of Civil Engineering, Dokuz Eylül University, Izmir, Turkey

² Associate Professor, Department of Civil Engineering, Dokuz Eylül University, Izmir, Turkey

³ Professor, Department of Civil Engineering, Dokuz Eylül University, Izmir, Turkey

ABSTRACT: Moment-resisting beam-column connections including emulative and mechanical components are widely used solutions in precast construction practice. Hybrid (emulative-welded) beam-column connections are constructed by welding of corbel plates to beam end plates where beam bottom longitudinal rebars are welded, and casting of concrete through the designated gaps in beam tops and column elements at site. Experimental studies reveal that strain demands in welded rebars increase near the connection due to the discontinuity in the reinforcement and leads to premature rupture under tensile forces. This study presents experimental and numerical cyclic behavior of precast hybrid connection specimens, one of which has unbonded lengths at the ends of beam bottom flexural reinforcements to improve the overall cyclic behavior. Numerical simulation models with lumped and hybrid numerical modeling approaches are studied for precast connections. The hybrid numerical model includes truss-based elements for beam-column connections and fiber-based elements for beams and columns. Numerical models represent the strength, stiffness and energy dissipation characteristics of precast beam-column connection tests satisfactorily.

1 INTRODUCTION

Precast concrete frame structures are designed to resist seismic forces without significant strength and stiffness degradation for structural elements under reversed cyclic loading. During past earthquakes, it was revealed that seismic detailing of beam-column connections affected the seismic behavior and performance of precast concrete structures (Saatcioglu et al., 2001; Senel et al., 2013). Hybrid (emulative-welded) connections are commonly used in precast construction practice. Hybrid connections are constructed by welding longitudinal rebars to plates embedded to precast beams and casting concrete through the formed gaps in beam and column elements at site. Ertas et al. (2006) tested one exterior ½ scaled beam-column connection subjected to displacement based cyclic loading. Yuksel et al. (2015) tested five half scale exterior beam-column connections with slabs under monotonic and cyclic loading conditions and proposed improvements for seismic behavior. During the above-mentioned tests, significant strength degradations were reported before 3.5% drift ratio due to rebar rupture in the vicinity of connection.

Unbonding of reinforcing bars over a length in precast beam and column elements has been studied in order to reduce strain demands and prevent rupture of reinforcing bars (Priestley et al., 1999). Pampanin et al. (2001) proposed an analytical approach to obtain unbonded length based on Monolithic Beam Analogy for precast frames with ductile connections. Unbonding of reinforcing bars in RC beams has been applied in a specified length for simulation of corrosion (Sharaf et al., 2002; Kotsovos et al., 2015). Unbonded length approach has been adapted for hybrid beam-column connections to reduce the strain demands of welded beam longitudinal rebars (Girgin et al., 2017). However, modeling the effect of unbonding in reinforcing steel bars is still challenging, because compatibility conditions are not valid for RC cross sections with

unbonded rebars. It is required in some seismic codes that (ACI 318, 2005; Turkish Earthquake Code, 2007), proper analytical models or experimental studies must be performed to verify the equivalence in cyclic behavior between new proposed precast moment-resisting connections and monolithic connection. Nonlinear cyclic behavior of reinforced concrete elements, analytical modeling approaches are classified as lumped plasticity and distributed plasticity models.

Lumped plasticity models are used to simulate nonlinear behavior of structural elements with concentrated nonlinearities in a finite element length. Zero-length rotational springs or moment-curvature relations within a specified length which follow nonlinear hysteretic models can be assigned to the ends of beam-column elements. Ibarra et al. (2005) presented peak-oriented hysteretic model including stiffness and strength properties for numerical simulation of reinforced concrete structural elements. Lignos et al., (2013) modified the model by adding cyclic deterioration parameters.

Distributed plasticity models with fiber-based beam-column elements provide sufficient estimation for local response parameters such as curvature and strains. Element cross section is discretized into fibers at integration points along the element length. Force-based formulation for nonlinear beam-column elements has advantages over the displacement-based formulation, because equilibrium is satisfied at each section and end node for force interpolation function (Kostic et al., 2012). Jeong et al. (2008) suggested a fiber-based analytical model for post-tensioned bridge columns to achieve constant strains in unbonded rebars in the plastic hinge length. Trono et al. (2013) proposed an analytical model for the end region of rocking bridge columns including concrete fiber sections and separate truss elements for unbonded rebars. Jnaid et al., (2014) developed a finite element analysis model and validated experimental tests on beams with unbonded reinforcement. Vertical spring elements were used in the model to represent loss of bond between concrete and reinforcing steel.

Truss-based modeling approaches have been studied for design and analysis of RC members subjected to shear, flexure and axial forces. Panagiotou et al. (2012) improved existing truss modeling approaches by including mesh size effects and biaxial effects for diagonal elements in compression. Moharrami et al. (2015) enhanced the truss model for analysis of shear-critical RC columns including the contribution of aggregate interlock effects. Xing et al. (2018) studied a hybrid numerical model for beam-column joints of non-ductile frames including nonlinear cyclic truss model for connection region and distributed plasticity model for beams and columns.

This study presents the summary of experimental results of two half-scale precast concrete hybrid interior connections tested under cyclic loading (Girgin et al., 2017). Additionally, numerical simulations of precast connections were performed by applying lumped plasticity and distributed plasticity modeling approaches by computer program OpenSees (McKenna et al., 2014). A hybrid numerical model was proposed for the proposed connection with unbonded rebars including fiber-based elements for beams, columns and truss elements for connection region.

2 EXTENDED SUMMARY OF EXPERIMENTAL STUDY

An experimental research program was conducted in Dokuz Eylul University, Structural Engineering Laboratory with the collaboration of Turkish Precast Concrete Association to verify the results of some improved details and possible enhancements in the cyclic behavior of precast hybrid interior beam-column connections. In this scope, one monolithic (reference) and five interior hybrid connections were tested, and some improvements were proposed for the design (Girgin et al., 2017). During the first stage of the study, SP1, SP2, and SP3 specimens with various welding coefficients (α) were tested. It should be note that, in the scope of Turkish Earthquake Code (2007), seismic connection forces are multiplied by a welding coefficient (a) to obtain the design forces for welded connections of precast concrete structures. At the second stage, SP1 and SP3 specimens were improved considering the failure modes observed in the previous tests. SP1-R and SP3-R represents the revised specimens by adapting the unbonded length concept,

generally applied in post-tensioned connections. As part of this comprehensive research program, test results of SP3 and SP3-R precast connections are presented in this study.

2.1 Description of test specimens

Geometry, reinforcing and welding details of the precast connections (SP3 and SP3-R) are shown in Figure 1. Figure 1(d) shows the fillet welding detail of beam bottom longitudinal rebars to beam support plate (PL-1). Tests on precast connections by Yuksel et al. (2015) showed that butt welding of transverse rebars to beam support plate at the connection may cause rupture and significant strength degradation. They proposed to weld the stirrups to additional steel plates welded to corbel plate to prevent rupture. For this purpose, vertical steel plates (PL-2) were welded to beam support plate (PL-1) for both sides as shown in Figure 1(d).

Previous experimental studies on post-tensioned beam-column connections showed that rupture of mild rebars at earlier drift ratios could be prevented by using unbonded length approach (Cheek et al., 1994). For this purpose, SP3-R specimen as the revised version of SP3 considering the observed failure modes during the tests was constructed with an unbonded lengths (L_u) with 10 times the rebar diameter (d_b). Unbonded length (L_u) is selected between the proposed values of 100 and 200 mm defined in ACI 550.2R-13 (2013). Since significant buckling was observed prior to rupture of longitudinal rebars during the tests, additional ties were used as shown in Figure 2(a) in the beam sections to prevent buckling for SP3-R specimen. Beam, column cross-sections and application of unbonded length for longitudinal rebars with a steel sleeve are shown in Figure 2.

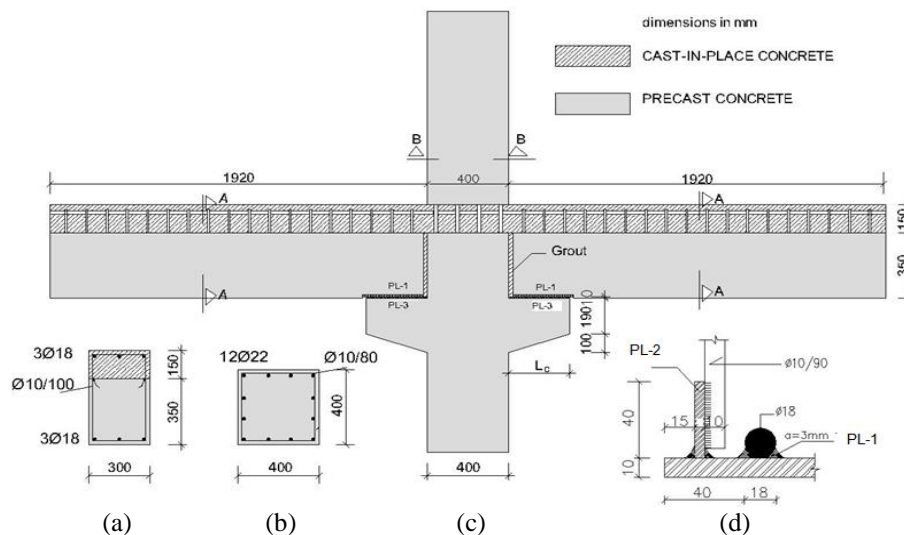


Figure 1. (a) Beam cross-section, (b) Column cross-section, (c) Precast beam-column connection, (d) corbel rebar (Girgin et al., 2017a).

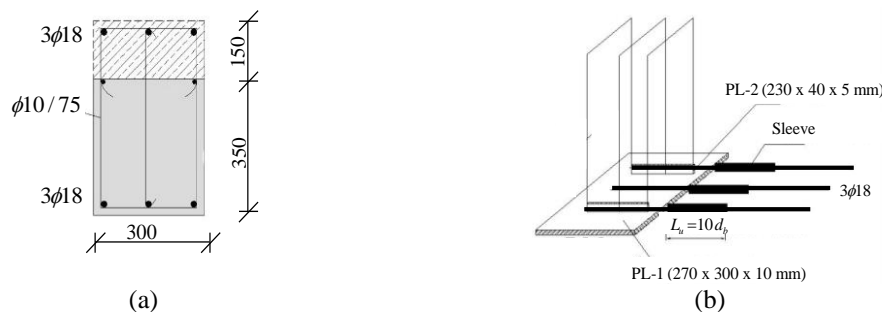


Figure 2. Geometry and welding details for SP3-R specimen: (a) Beam cross section, (b) Unbonding of beam longitudinal rebars (Girgin et al., 2017a)

Average concrete strength was 42 MPa for beam and column elements, while 35 MPa for the topping concrete at the test day. Beam and column elements were constructed separately in the precast facility as shown in Figs. 3(a)-(c). Beam longitudinal rebars were welded to beam support plate and stirrups were welded to vertical steel plates as shown in Figs. 3(a)-(b), respectively. Figure 3(c) shows columns with corbels constructed with a 15 cm gap in the joint for topping concrete. Column and beam elements were transported to the DEU Structural Engineering Lab. At first, precast columns were kept in a vertical position, and the precast beams were placed on the corbels; subsequently beam support plates (PL-1) were welded to corbel plates (PL-3) as shown in Figure 3(d). Finally, topping concrete was poured and construction processes of the specimens were completed.

2.2 Experimental set-up

Experimental set-up was designed according to ACI 374.1.05 (2005) and components of experimental set-up is shown in Figure 4a. Figure 4b shows the location of a precast specimen in the test set-up and points of contraflexure of the beam-column connection subassembly. Beam ends were fixed in vertical direction from 1800 mm from the column axis while column was supported with hinge at the top and bottom. Axial load was applied corresponding to 8% of axial load capacity of the column and kept constant during cyclic reversals.

Lateral cyclic displacements were applied at the top of the column with increasing amplitude from 0.15% to 4.0% drift ratios. Drift ratios are defined considering the uncertainties in strong ground motions and structural properties for beam-column connection sub-systems. Tests are continued up to 3.5% drift ratio to observe the whole post-peak behavior of the connections which is required by ACI 374.1.05 (2005). Drift ratio is defined as Δ/H_c , where Δ is the lateral displacement and H_c is the height of the column (2310 mm) between hinges (Girgin et al., 2017a).

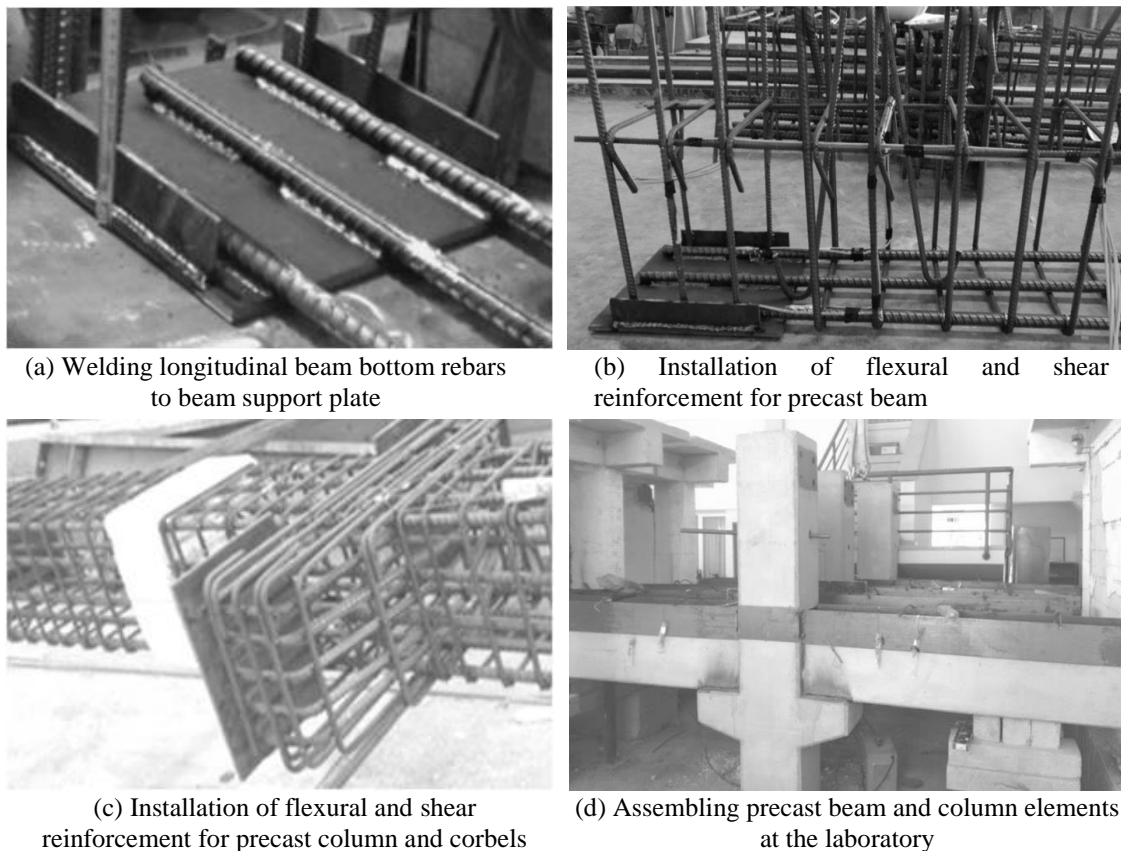


Figure 3. Construction process of interior precast beam-column connection specimens (Girgin et al., 2017a)

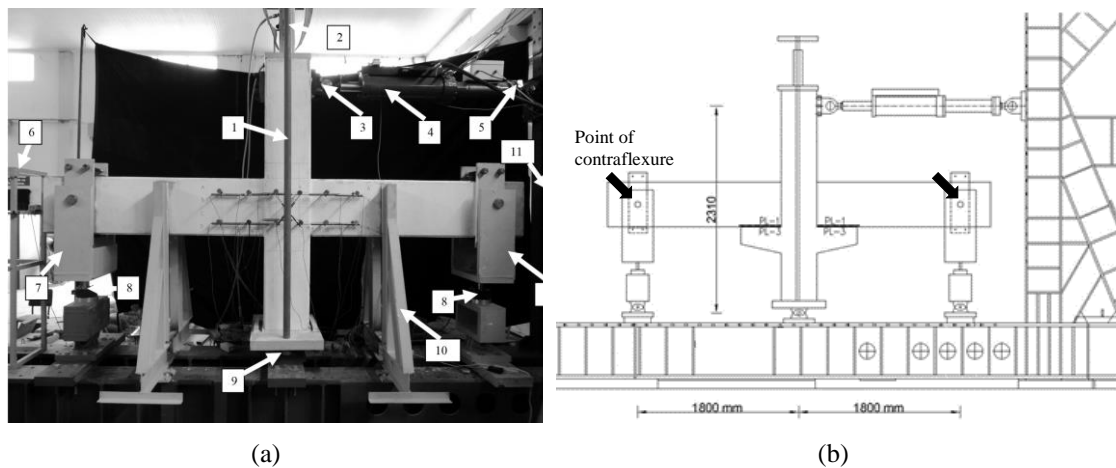


Figure 4. (a) Components in experimental set-up: (1) axial load frame, (2) hydraulic jack, (3) hinge, (4) actuator, (5) load cell, (6) reference frame, (7) pendulum support, (8) load cell, (9) fixed support, (10) out-of-plane support frame, (11) steel reaction frame (b) Location of test specimens in the loading system and points of contraflexure of the beam-column connection subassembly (Girgin et al., 2017a)

2.3 Experimental results

Tests were continued up to the drift ratio at which the specimens showed significant strength degradation. Flexural, shear cracks and concrete spalling were observed damages for the beam ends while diagonal hairline cracks occurred at the joints. Beam bottom longitudinal rebars showed significant buckling after spalling of concrete near the connection. Subsequently, welded longitudinal rebars ruptured at the connection for SP3 specimen. Longitudinal rebar buckling of beams was prevented with added ties for revised specimen SP3-R. Lateral load- drift ratio relationships for precast beam-column connections are shown in Figure 4. As seen in the figures, in-cycle strength degradation was occurred after the buckling and continued with the rupture of longitudinal reinforcements for SP3 specimen. 20% with some pinching behavior was observed for pull and push directions for SP3 specimen at 3.5% drift ratio (Figure 5a). SP3-R specimen showed no pinching behavior and buckling of rebars so significant increase in energy dissipation was observed (Figure 5b). Damage states of the connection specimens at 2.75% drift ratio are shown in Figure 5c and 5d.

3 NUMERICAL SIMULATION MODELS

OpenSees computer program (McKenna et al., 2014) was used to simulate the experimental results of precast connections. OpenSees nonlinear force-based beam-column elements with linear geometric transformation were implemented for beam and column elements, Gauss-Lobatto integration with two integration points was used for each element. Cyclic response of numerical model was computed using displacement-based algorithm. Six Newton-Raphson iterations followed by 500 Newton with initial tangent iterations were used. The same time step increment selected for experimental study was used for analysis. Energy increment was used to maintain the residual error in the range of 10^{-5} tolerance value.

3.1 Lumped plasticity model

Lumped plasticity model is only employed for SP3 specimen which doesn't have unbonded length. Linear frame elements were used for beam, column, and corbel sections with rigid end zones, and nonlinear rotational springs with hysteresis model parameters were defined in the vicinity of the corbel sections where nonlinear behavior is mainly concentrated (Figure 6). Modified Ibarra-Medina-Krawinkler (IMK) deterioration model with peak-oriented hysteretic

response was used to determine rotational spring parameters for the simulation of experimental behavior. Monotonic backbone curve of the IMK model is given in Figure 7 (Lignos et al., 2013).

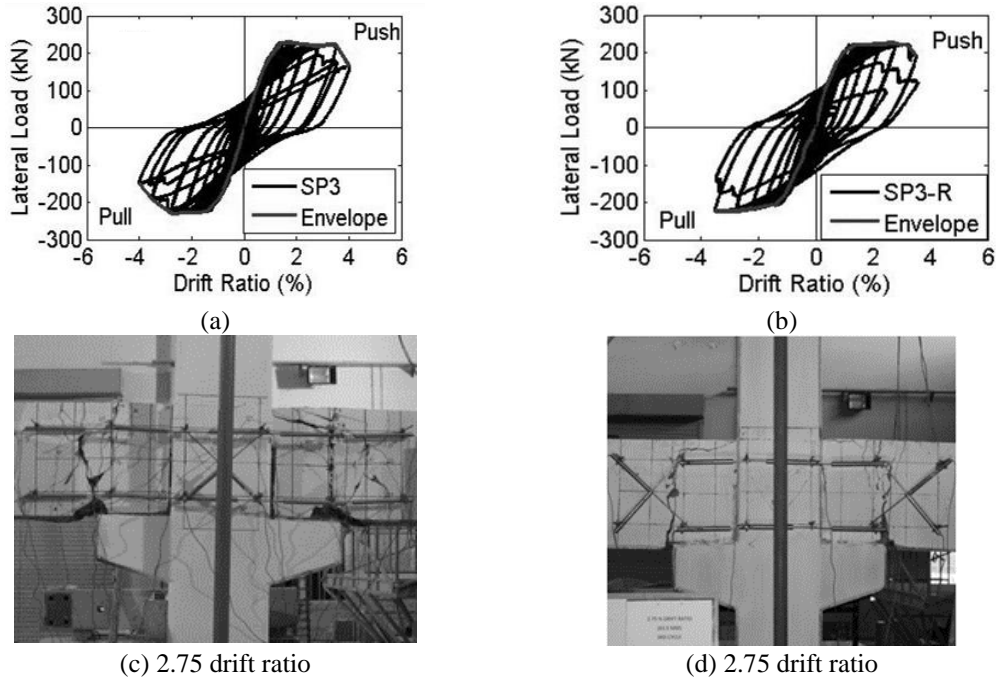


Figure 5. Lateral load-drift ratio relationships and damage states at 2.75% drift ratio for SP3 (a and c) and SP3-R (b and d) specimens. (Girgin et al., 2017a).

Hysteretic model parameters include elastic stiffness (K_0), yield moment (M_y), capping moment (M_c), residual moment (M_r), pre-capping rotation (θ_p), post-capping rotation (θ_{pc}) and ultimate rotation (θ_u). Also, cyclic deterioration parameter (λ_s), unloading stiffness deterioration parameter (c_k) and residual strength ratio (γ) were defined in the model (Ibarra et al. 2005).

Biskinis et al. (2004) proposed an equation for the chord rotation at yield (θ_y) for beam-column elements with rectangular cross sections including flexure ($\theta_{flexure}$), shear (θ_{shear}) and bar slip (θ_{slip}) deformations as

$$\theta_y = \underbrace{\phi_y \frac{L_s + a_v z}{3}}_{\theta_{flexure}} + \underbrace{0.0013 \left(1 + 1.5 \frac{h}{L_s} \right)}_{\theta_{shear}} + \underbrace{a_{sl} \frac{0.13 \phi_y d_b f_y}{\sqrt{f_c'}}}_{\theta_{slip}} \quad (1)$$

where ϕ_y is the yield curvature; L_s is the shear span; h is section depth; [$a_v z$] is the tension shift due to diagonal cracking; z ($=d-d'$) is the internal lever arm; $a_v = 1$ when there is diagonal cracking at flexural yielding; d_b is the diameter of tension reinforcement; a_{sl} is a coefficient for pull-out of rebars ($a_{sl} = 1$ if pull-out of longitudinal bars is occurred) and f_y and f_c' are the material yield and compressive strengths for steel and concrete, respectively.

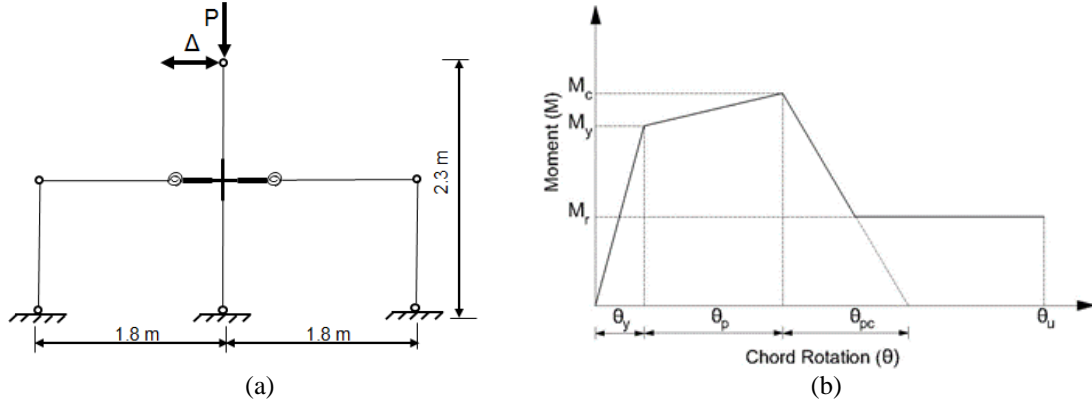


Figure 6. (a) Lumped plasticity model for the connection specimen, (b) Monotonic backbone curve of the mod-IMK model

For precast specimen, $\phi_y = 0.012$ (1/m), $h = 500$ mm, $d_b = 18$ mm, $L_s = 1450$ mm, $a_v = 1$, $a_{sl} = 1$, $f_y = 487$ MPa and $f_c' = 42$ MPa and so the Eq. 1 yields $\theta_y = 0.0116$ rad. Mod-IMK with peak-oriented hysteretic model which is defined for the rotational springs were calibrated using the experimental data and the parameters are summarized in Table 1.

Table 1. Peak-oriented hysteretic model parameters

Specimen	K_0 (kN.m/rad)	M_y (kN.m)	λ_s	Θ_p (rad)	Θ_{pc} (rad)	Θ_u (rad)	χ
SP3	15,720	180.8	1.0	0.046	0.1	0.25	0.5

3.2 Hybrid numerical simulation model

Bowers (2014) proposed a numerical model for shear deficient beam to column connections. This model has been extended to represent the precast hybrid connections tested by the authors. Joint panel, end regions of beams and columns and the gussets are modeled by nonlinear cyclic truss elements, and the rest is represented by distributed plasticity model. For frame elements, nonlinear force-based beam-column model with two integration points is used. Reinforcement layout and positions of the longitudinal rebars in the test specimens are reflected to nonlinear truss model. Horizontal, vertical and diagonal truss elements are used in the model considering the reinforcement and concrete regions. Inclination angle of diagonal elements is considered as 41° . Nonlinear concrete trusses in the vertical and horizontal directions account for tension stiffening effects. Nonlinear truss model is connected to distributed plasticity model with rigid elements as shown in Figure 7.

Concrete truss elements followed a stress-strain law provided by Lu and Panagiotou (2014) as shown in Figure 8, where f_c' is the compressive strength at $\epsilon_0 = 0.2\%$ strain for unconfined concrete. Ultimate strain (ϵ_u) of concrete is adjusted considering the mesh-size effects. For concrete truss elements in horizontal and vertical direction, tensile strength is taken as $f_t = 0.33\sqrt{f_c'}$ (MPa), and a softening portion is taken into account considering the tension stiffening. Compressive stresses in diagonal truss elements are scaled down with a coefficient (β) based on the transverse strains to account for biaxial stress state. The stress-strain relationship in reinforcing steel is determined by Giuffr -Menegotto-Pinto (GMP) steel material model. The initial modulus of concrete is calculated by $E_c = 5000\sqrt{f_c'}$ (MPa).

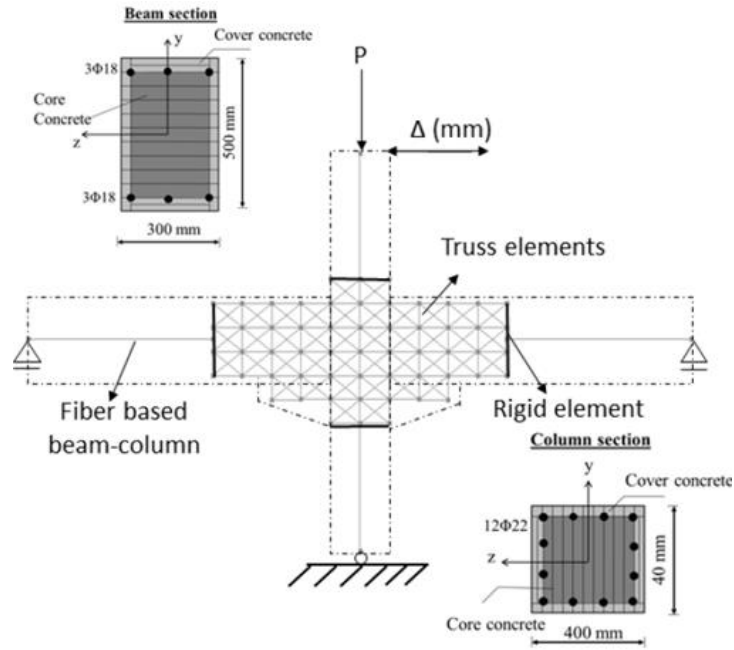


Figure 7. Hybrid numerical simulation model and truss elements for connection region (Girgin et al, 2017b)

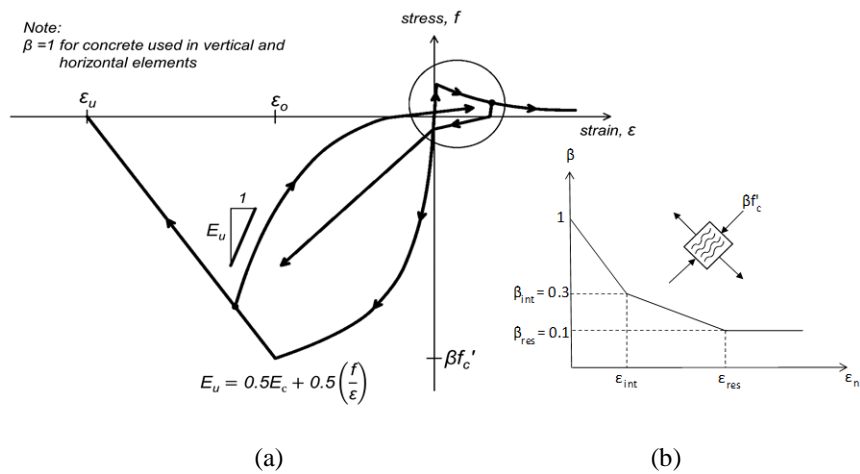


Figure 8. (a) Stress-strain relationship of concrete material model, (b) Relation between reduction factor and normal strain (Lu and Panagiotou, 2014).

3.3 Analysis results

The lateral load-drift ratio responses were computed under cyclic and monotonic loads using lumped plasticity model and hybrid numerical models; comparisons with the experimental data are shown in Figure 9. LP model computed strength degradation in a good agreement with the SP3 connection experimental results, but the model couldn't capture pinching due to shear failures after 2.75% drift ratio. Hybrid model with fiber-based and truss-based elements for beam and columns computed strength and stiffness quite well up to the second cycle of 3.5% drift ratio. The peak strength in the numerical model was computed 1.15 times the experimentally measured.

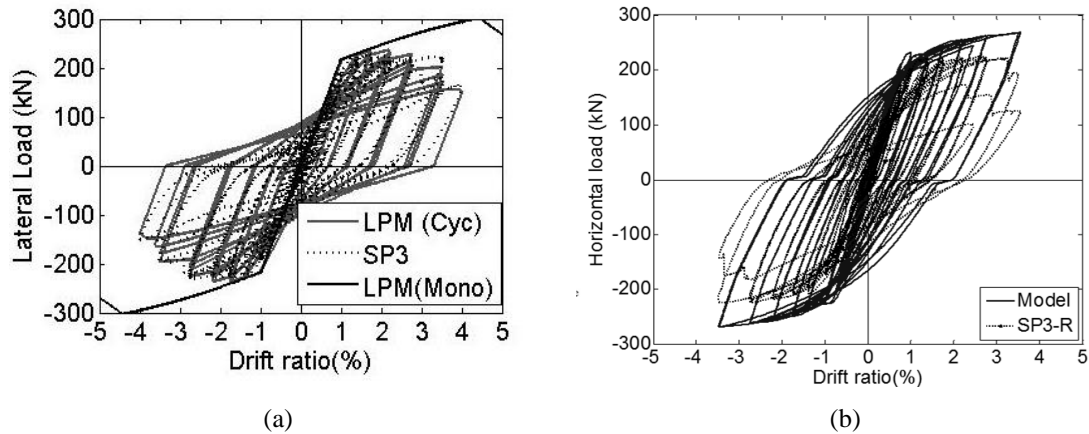


Figure 9. Comparison of measured and computed responses for (a) SP3 connection with lumped plasticity model and (b) SP3-R connection specimen with hybrid model

4 CONCLUSIONS

This study investigates the seismic performance and the efficiency of numerical modeling approaches for precast hybrid (emulative-welded) beam-column connections. Hybrid beam-column connections are constructed by welding longitudinal rebars to plates embedded to precast beams and casting concrete through the formed gaps in beam and column elements at site. A recently proposed beam-column connection includes design details with unbonding of beam welded rebars and implementing additional ties for beams in the vicinity of the welded connection. Experimental work of precast interior hybrid connections and numerical simulations using lumped plasticity and distributed plasticity approaches in OpenSees were performed and the results are presented. A numerical model is proposed for precast connections with unbonded rebars including fiber-based elements for beams, columns and truss elements for unbonded rebars. Based on the test results and numerical simulations following conclusions can be made:

Under cyclic loading, it is shown that the ultimate strains of welded rebars can be decreased utilising unbonded length approach to succeed higher top drift ratios. But in this case, additional ties should be used to prevent buckling of welded longitudinal rebars prior to rupture can be improved with these modifications. Therefore, it has been concluded that the implementation of both design details is required to improve the strength, stiffness and energy dissipation characteristics of precast specimens. Numerical simulation models satisfactorily captured the lateral load-drift ratio responses and initial stiffnesses in comparison with the experimental results. Numerical studies provide sufficient input for design practice of precast concrete structures.

REFERENCES

- ACI Committee 318 (2005). Building code requirements for structural concrete and commentary, ACI 318.05, American Concrete Institute, Michigan, U.S.A.
- ACI Committee 374 (2005). Acceptance criteria for moment frames based on structural testing and commentary, ACI 374.1.05, American Concrete Institute, Michigan, U.S.A.
- ACI Committee 550 (2013). Design guide for connections in precast jointed systems, ACI 550.2R-13, American Concrete Institute, Michigan, U.S.A.
- Biskinis, D.E., Roupakias, G.K., and Fardis, M.N. (2004). Degradation of shear strength of reinforced concrete members with inelastic cyclic displacements. *ACI Structural Journal*, 101(6), 773-783.
- Bowers, J.T. (2014). Nonlinear cyclic truss model for beam-column joints of non-ductile RC frames. M.Sc. thesis, Virginia Polytechnic and State University.

- Cheok, G. S., and Stone, W. C. (1994). Performance of 1/3 scale model precast concrete beam column connection subjected to cyclic inelastic loads. Report No. 4. Report No, NISTIR 5436, Building and Fire Research Laboratory, NIST, Gaithersburg, MD, 59.
- Ertas, O., Ozden, S., and Ozturan, S. (2006). Ductile connections in precast concrete moment resisting frames. *PCI Journal*, 51(3), 66-76.
- FEMA P-795 (2011). Quantification of Building Seismic Performance Factors: Component Equivalency Methodology, Federal Emergency Management Agency.
- Girgin, S.C., Misir, I.S. & Kahraman, S. *Int J Concr Struct Mater* (2017a). Experimental cyclic behavior precast hybrid beam-column connections with welded components, 11: 229-245. <https://doi.org/10.1007/s40069-017-0190-y>
- Girgin, S.C., Misir, I.S. & Kahraman, S. (2017b). Seismic performance factors for precast buildings with hybrid beam-column connections, *Procedia engineering* 199: 3540-3545.
- Ibarra, L. F., Medina, R. A., and Krawinkler, H. (2005). Hysteretic models that incorporate strength and stiffness deterioration. *Earthquake Engineering and Structural Dynamics*, 34 (12), 1489-1511.
- Jeong, H. I., J. Sakai, and Mahin, S. A. (2008). Shaking table tests and numerical investigation of self-centering reinforced concrete bridge columns. PEER Report 2008/06 Pacific Earthquake Engineering Research Center, College of Engineering. University of California, Berkeley.
- Jnaid, F. and Aboutaha, R.S. (2014). Residual flexural strength of reinforced concrete beams with unbonded reinforcement. *ACI Structural Journal*, 111(6), 1419-1430.
- Kostic, S., and Filippou, F. (2012). Section discretization of fiber beam-column elements for cyclic inelastic response. *Journal of Structural Engineering*, 138, 592-601.
- Kotsovos, G. M., Vougioukas, E. and Kotsovos, M. D. (2015). Behaviour of reinforced concrete beams with non-bonded flexural reinforcement. *Magazine of Concrete Research* 67.10: 503-512.
- Lignos, D.G., and Krawinkler, H. (2013). Development and utilization of structural component databases for performance-based earthquake engineering. *Journal of Structural Engineering*, 139, 1382-1394.
- Lu, Y. and Panagiotou, M. (2014). Three-dimensional cyclic beam-truss model for non-planar reinforced concrete walls, *Journal of Structural Engineering*, 140(3).
- McKenna, F., Fenves, G. L., Scott, M. H., and Jeremic, B. (2014). Open system for earthquake engineering simulation. Berkeley, CA., University of California. <<http://opensees.berkeley.edu>>.
- Moharrami M., Koutromanos I., Panagiotou M., Girgin S.C. (2015) Analysis of shear-dominated RC columns using the nonlinear truss analogy, *Earth. Eng. and Str. Dyn.*, 44(5), 677-694.
- Pampanin, S., Priestley, M. J. ve Sritharan, S. (2001). Analytical modeling of the seismic behaviour of precast concrete frames designed with ductile connections. *Journal of Earthquake Engineering*, 5 (3), 239-367, 2001.
- Panagiotou, M., Restrepo, J. I., Schoettler, M., and Kim, G. (2012). Nonlinear cyclic truss model for reinforced concrete walls, *ACI Structural Journal*, 109(2), 205-214.
- Priestley, M.J.N., Calvi, G.M. and Kowalsky, M.J. (2007). *Displacement-Based Seismic Design of Structures* (1st ed.). Italy: IUSS Press.
- Saatcioglu, M., Mitchell, D., Tinawi, R., Gardner, N.J., Gillies, A.G., Ghobarah, A. and Lau, D. (2001). The August 17, 1999 Kocaeli (Turkey) earthquake-damage to structures. *Can. J. Civ. Eng.*, 28(4), 715-737.
- Senel, S., and Palanci, M. (2013). Structural aspects and seismic performance of 1-story precast buildings in Turkey. *Journal of Performance of Constructed Facilities*, 27 (4), 437-449.
- Sharaf, H., and Soudki, K. (2002). Strength assessment of reinforced concrete beams with unbonded reinforcement and confinement with CFRP wraps. 4th Structural Specialty Conference of the Canadian Society for Civil Engineering.
- Trono, W., Jen, G., Ostertag, C. and Panagiotou, M. (2013). Tested and modeled seismic response of a rocking, post-tensioned HyFRC bridge column. *Proc., 7th National Seismic Conf. on Bridges and Highways*. Buffalo, NY: MCEER, State Univ. of New York at Buffalo.

- Turkish Earthquake Code (2007). Specifications for Buildings Constructed in Disaster Areas. TEC 2007, Ministry of Public Works and Settlement, Ankara, Turkey.
- Xing C., Koutromanos I., Leon R., and Moharrami M. (2018). Computational simulation of RC Beam-to-Column Connections Under Earthquake Loading, Eleventh US National Conference on Earthquake Engineering, Los Angeles, CA, USA.
- Yuksel, E., Karadogan, H. F., Bal, I. E., Ilki, A., Bal, A., and Inci, P. (2015). Seismic behavior of two exterior beam-column connections made of normal-strength concrete developed for precast construction. *Engineering Structures*, 99 (157-172).

A simplified performance based rapid seismic assessment method for mid-rise reinforced concrete structures

Halil Görgün¹, Derman Kaya², Mehmet Emin Öncü¹, and Senem Yılmaz Çetin¹

¹ Department of Civil Engineering, Dicle University, Diyarbakır, Turkey

² Social Security Institution, Diyarbakır, Turkey

ABSTRACT: During the last five decades, severe earthquakes occurred in Turkey have showed that most of the existing buildings are weak against earthquake movements. Seismic design codes generally necessitate structural analyses in detail. In this study, Performance Based Rapid Seismic Assessment Method (PERA) has been modified. The horizontal deflected profile of critical story has also been considered during the evaluation of whole building performance. The comparison of the results with the seismic safety evaluation method analyses carried out for 2880 different situation representing structures in Turkey is given. A very reliable agreement has been obtained among the results.

1 INTRODUCTION

Earthquakes occurring in the last 50 years, such as Lice/Diyarbakır-Turkey (1975), Spitak-Armenia (1988), Marmara-Turkey (1999), Gujarat-India (2001), Sumatra-Indonesia (2004), Kashmir-Pakistan (2005), Sichuan-China (2008), Haiti (2010), Tohoku-Japan (2011), Erciş/Van-Turkey (2011), Pakistan (2013) and Iran-Iraq (2017) clearly showed that a large number of existing buildings in seismic regions all around the world particularly in less or underdeveloped countries is vulnerable against earthquakes. For this reason, the safety of these buildings should be evaluated for determining the vulnerable ones against seismic action thinking that Turkey is on very active fault lines, such as the North Anatolian Fault, the East Anatolian Fault, and the densely populated regions are on these fault lines. The final official Turkish government assessment, 66% of the territory of Turkey is located in the first and second earthquake zone, and about 71% of the population lives in these regions. Turkey's Active Fault Line Map was updated 21 years later (Figure 1), while there are 326 active faults in Turkey, 485 segments can produce magnitude determined to be 5.5 and higher earthquakes. It is not possible if the earthquake resistance of our existing buildings is examined with the principles of Turkish Seismic Code (TSC, 2007) and Regulation on the Determination of Risky Structures (RDRS, 2013) and if it is required to determine earthquake resistance quickly. For this reason, with the introduction of the urban regeneration process in Turkey, it has become necessary to use simpler methods, but with reliable results, in a shorter time. The process and procedures of a building at risk by RDRS method (2013) is given in Figure 2. There are many methods related to seismic safety assessment procedure in literature (FEMA P-154; 1988a, 2002a and FEMA P-155; 1988b, 2002b, 2015 and Sucuoğlu, 2007).

EARTHQUAKE HAZARD MAP OF TURKEY

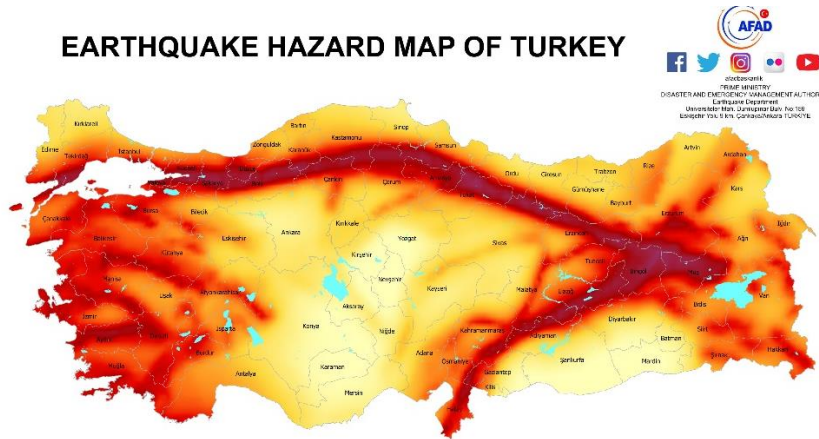


Figure 1. Earthquake hazard map of Turkey (2018)

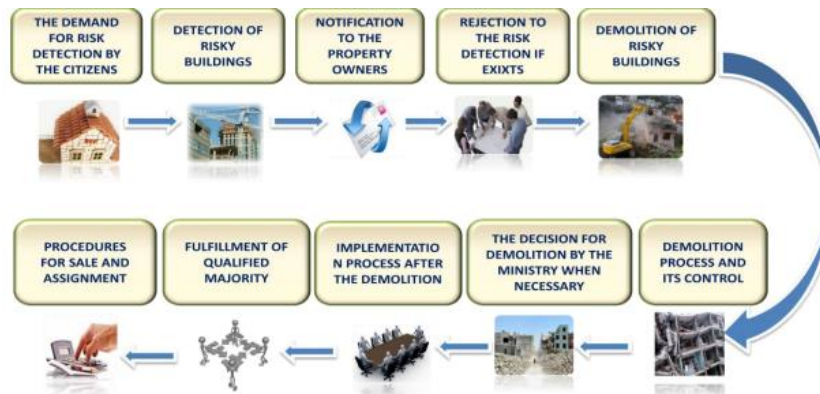


Figure 2. The process and procedures of a building at risk (Ministry of Environment and Urbanisation of Turkey) (2017)

In the risk assessment method they have developed, using the building parameters that can be observed from the street, the number of building free floors, soft floors, heavy projections, visible building quality) a risk sequence can be made. Also, methods of seismic performance analysis of existing buildings are given in codes and guidelines (e.g., TSC, 2007; NZSEE, 2012; Eurocode 8 Part 3, 2005; ASCE 41, 2006). The details of these approaches are given in Ilki et al. (2014). In addition to detailed structural analyses that can take considerable time and computing resources, while these methods are applied when large stocks of vulnerable buildings in developing countries are taken into account on-site inspection studies are required. Ilki et al. (2014), proposed a simpler method than the methods of codes which minimizes the level of field investigations. This method involves a simpler approach and is more reliable than the other methods in the literature. The first vibration mode of earthquake effect is proposed for dominant reinforced concrete frame structures. It is proposed that Performance Based Rapid Seismic Assessment Method (PERA) by Ilki et al. (2014). This method based on member tributary area concept and the various simplifications and assumptions related to the structural analysis and performance-based evaluation with using Muto principles (1956) and also performance criteria of the TSC (2007) are considered.

2 PERA (2014) PROCEDURE

It is clearly showed from results of recent earthquakes that most of existing structures in earthquake zones are weak to against seismic loads (2014). In order to avoid similar catastrophic consequences of earthquakes, it is necessary to sort the buildings with weak earthquakes and take

the necessary precautions. And a performance-based quick evaluation procedure should be presented for comparison with conventional code-based seismic in less time and at lower cost. Most of these assumptions are mentioned in this method for many RC frame structures in Turkey. In addition to modification may be required for other countries. However, the methodology of Ilki et al. (2014) is useful in all seismic regions, where reinforced concrete buildings are widespread.

The seismic performance of RC frame buildings was evaluated according to TSC 2007's performance-based assessment principles in the method of Ilki et al. (2014). TSC 2007 consider irregularities of the building and detailed structural characteristics, together with local soil class and the earthquake zone where the building is located. The ratios of demand / capacity of structural elements should be obtained to determine the building performance. First, elastic internal force demands, and capacities are determined, then the demand / capacity ratios for each building element are calculated. Then, member damage levels are determined depending on the demand / capacity ratios and inter-story drifts. The expected failure modes of the structural elements, confinement properties and levels of axial and shear forces are taken into account when determining the damage levels. And finally, level of seismic performance of the building is determined. The PERA method (2014) follows a similar approach to the TSC 2007. This method significantly reduces the duration of on-site inspections and simplifies the stages of analysis and evaluation. This method estimates damage levels of the columns of the ground story and its inter-story. The flexural strength and moment capacity of the beams are estimated based on reinforcement rates and beam measurements observations on typical building structures. In addition, the method assumes the reinforcement configuration of the columns. The structural irregularities shown in Table 1 as defined by TSC (2007) are considered through penalty coefficients in the PERA method (2014). The amount of data required is less than the rapid and pre-evaluation methods mentioned above and determination of concrete quality with limited number of tests, stirrup spacing and type of reinforcing bars and use of different modes of comparisons, make the algorithm more realistic than classical methods.

Table 1. Penalty coefficients for structural irregularities

Irregularity	Penalty coefficient	Irregularity	Penalty coefficient
A-Irregularities in plan		B-Irregularities in elevation	
A1-Torsional irregularity	0.85	B1- Inter-story strength irregularity (weak story)	0.95
A2- Floor discontinuities	0.95	B2- Inter-story stiffness irregularity (soft story)	0.85
A3- Projections in plan	0.95	B3- Discontinuity of vertical Sstructural elements	0.95

The PERA method (2014) assumes that the ground story of the building is the critical story as defined in the RDRS (2013) under seismic loads. The base shear force (V_b) is given Eq. (1), where A_0 is the effective ground acceleration, W is building weight ($G + 0.3Q$), G and Q are the dead and live loads, respectively. The spectrum coefficient $S(T)$ and the corner periods T_A and T_B are as defined in TSC (2007).

The natural vibration period of the building is estimated by Eq. (2). Taking into account the effects of the high vibration modes used in the TSC (2007) approach, Eq. (1) uses a coefficient of 0.85. The 'n' used in Eq. (2) is the number of stories contributing to the first vibration mode on the investigation side. Detailed calculations should be done to calculate the natural period of construction in a more complex way.

$$V_B = 0.85WS(T)A_0 \quad (1)$$

$$T = 0.2 n \quad (2)$$

The base shear force (V_b) is distributed among the ground story columns in two principle directions of the building according to Eq. (3), where I_i and h_i are the moment of inertia and heights of the columns, respectively, in the direction investigated.

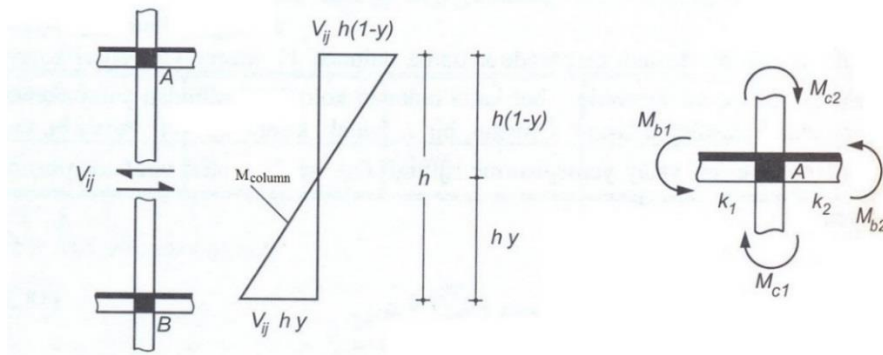


Figure 3. Variation of earthquake moments in the beam and columns.

In Equation 4. V_{ij} is the column shear force, h is the height of the ground story and y is a coefficient for determination of the inflection point of the column, such that the product of y and h gives the location of the point of zero moment from the base of the column (Figure 3).

$$V_{ij} = V_b \left(\frac{\frac{I_i}{h_i^3}}{\sum \frac{I_i}{h_i^3}} \right) \quad (3)$$

$$M_{et} = V_{ij}h(1 - y) , M_{eb} = V_{ij}hy \quad (4)$$

The y coefficient is calculated by Eq. 5.

$$y = y_0 + y_1 + y_2 + y_3 \quad (5)$$

In the PERA method (2014), assuming $y = y_0$, ignoring $y_1 + y_2 + y_3$ coefficients. y_0 values are given in Muto (1956) for sway loading for wind and seismic loading separately.

In the PERA method (2014), the first and last (exterior) axes are called x_1, x_2 and y_1, y_2 in the x -direction and in the y -direction of the structure, respectively. The corner columns are showed x_1y_1, x_2y_1 , etc (Figure 4).

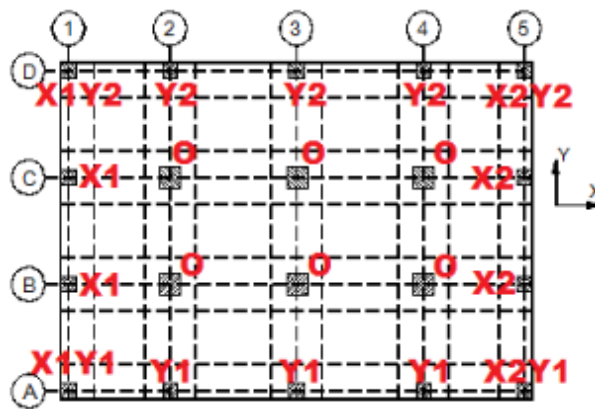


Figure 4. Coding of the columns (corner, edge, interior)

3 THE PROPOSED METHOD

In this study, Performance Based Rapid Seismic Assessment Method (PERA, 2014) has been modified. The present study is an alternative to the PERA method (2014) for reinforced concrete frame buildings. The proposed methodology makes use of approaches of very well-known Smith method (1969). Point of contra-flexure occurs at the middle of all members of the frame in Smith method (1969), as shown schematically in Figure 5.

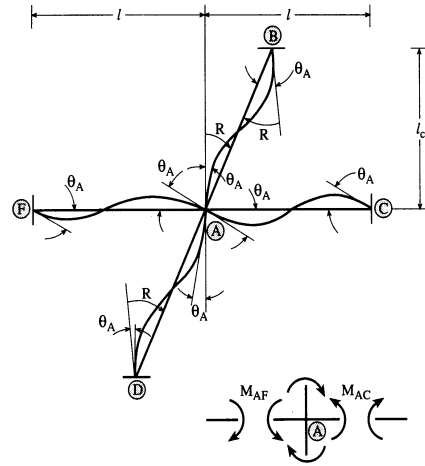


Figure 5. Sub-assembly model for unbraced (sway) frame for Smith method (1969)

Smith method (1969) presented an approach for estimating the inflection point of the beam and columns. The basic assumptions made in development of the Smith method (1969) are listed as follows, referring to Figure 5: a) Joints (A) and (C) are on a straight line (axial deformation of columns is negligible), b) Joints (A) and (D) are on a straight line (floors are infinitely rigid in their own planes), c) The rotations at joints (F) and (C) are equal in magnitude, d) The rotations at the ends of the columns are equal in magnitude e) Point of contra-flexure occurs at the middle of all members of the frame. In the Smith method (1969), the inflection point coefficient is taken as $y = y_0 + y_1 + y_2 + y_3 = 0.50$ giving the location of the point of zero moment at the mid height of the column from the base of the column as shown in Figure 5. This assumption is very important to prevent the possibility of using wrong y_0 value by practicing engineers and saving time on calculating individual $y_0 + y_1 + y_2 + y_3$ values.

4 APPLICATION AND COMPARISON OF THE PROPOSED METHOD RESULTS WITH THE OTHER PREDICTIONS

The results of the analysis of proposed methods are compared with the TSC (2007) method, RDRS (2013) method, and PERA method (2014). The results are obtained from 720 analysis cases for 15 existing buildings (numbered B1 to B15) that are located in Başiskele/Kocaeli-Turkey. B1-B6 buildings were investigated by Ozcelik (2014) and B7-B15 buildings were investigated by Vulas (2014). Typical floor plans of B1-B6 are showed in Figure 6 and main characteristics of the B1-B15 buildings are presented in Table 2. As seen in Table 2, all buildings are located in Earthquake zone 1. Number of stories of the buildings varies between three or four. Most of the building were built between the years 1975 and 2000 according to TSC (1975). Characteristic of reinforcing bars of older buildings, constructed before 2000, are S220 and characteristic of reinforcing bars of other buildings are S420. The buildings were analyzed under horizontal loads along two principle axes in plain. The compressive strengths of concrete were assumed 10, 14 and 20 MPa and local soil classes are given Z2 and Z3.

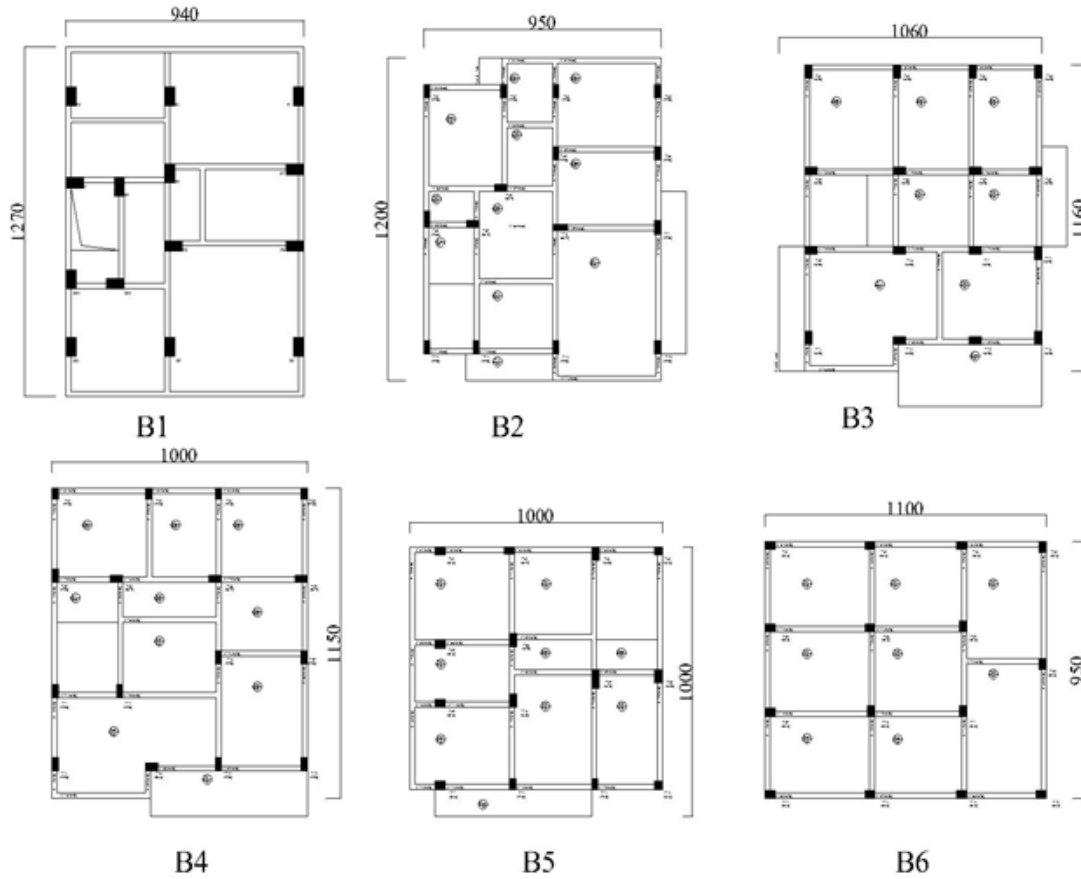


Figure 6. Existing buildings typical floor plans (adopted from Ozcelik, 2014) (dimensions are in cm)

The results were obtained from 720 different analysis cases [15 (number of buildings) x 3(C10, C14, C20) x 2(Z2, Z3) x 2(confinement, No confinement) x 4(+X, -X, +Y, -Y directions)] for 15 buildings. The total 720 analysis cases were performed according to TSC 2007 and the RDRS (2013) procedures by using Sta4CAD (2007), structural analysis software, by Ozcelik (2014) for B1-B6 buildings and by Vulas (2014) for B7-B15 buildings. Also, the total 720 analysis cases were performed by Ilki et al. (2014) by using PERA. The analysis steps of the PERA (2014) procedure were used in this present study by replacing Muto method (1956) with Smith method (1969). Comparison of the results for the 720 different cases obtained using the TSC (2007), the RDRS (2013) approach, the PERA method (2014), and the proposed method, in this study, are given in Tables 3-7. 720x4=2880 cases have been compared in detail for the four methods.

Table 2. General characteristics of buildings

Building	Number of stories	Average dimensions in plan (m)	Constructed year	Reinforcement type	Stirrup/spacing diameter (mm)	Confinement zone
B1	4	9.4x12,7	1990	S220	8/200	Yes
B2	4	9.5x12.0	1990	S220	8/200	No
B3	4	10.6x11.6	1990	S220	8/200	No
B4	3	10.0x11.5	1990	S220	8/200	No
B5	3	10.0x10.0	1990	S220	8/200	Yes
B6	3	11.0x9.5	1990	S220	8/200	No
B7	3	8.6x10.2	1974	S220	8/150	No
B8	3	9.5x9.0	1974	S220	8/150	Yes
B9	3	9.0x10.5	1974	S220	8/150	No
B10	3	9.1x9.75	1979	S220	8/150	No
B11	3	9.9x8.8	1979	S220	8/150	No
B12	3	9.8x10.25	1979	S220	8/150	No
B13	3	13.25x10.15	2001	S420	8/300	No
B14	3	14.5x9.5	2003	S420	8/120	Yes
B15	3	9.4x14.7	2005	S420	8/120	Yes

Table 3. Summation of predictions of the TSC (2007) and the RDRS (2013) methods

		TSC 2007		
		Safe	Unsafe	Total
RDRS (2013)	Safe	210	66	276
	Unsafe	33	411	444
	Total	243	477	720

Table 4. Summation of predictions of the TSC (2007) and the PERA (2014) methods

		TSC 2007		
		Safe	Unsafe	Total
PERA (2014)	Safe	151	96	247
	Unsafe	92	381	473
	Total	243	477	720

Table 5. Summation of predictions of the TSC (2007) and the proposed methods

		TSC 2007		
		Safe	Unsafe	Total
Proposed	Safe	192	145	337
	Unsafe	51	332	383
	Total	243	477	720

Table 6. Summation of predictions of the proposed method and other methods

Method	Number of buildings		
	Safe	Unsafe	Total
TSC 2007	243 (34%)	477 (66%)	720 (100%)
RDRS	276 (38%)	444 (62%)	720 (100%)
PERA	247 (34%)	473 (66%)	720 (100%)
Proposed	337 (47%)	383 (53%)	720 (100%)

Table 7. Summation of predictions of the proposed method and other methods (low and high risk cases are considered separately)

Method	Number of buildings		
	Safe	Unsafe	Total
TSC 2007	243 (100%)	477 (100%)	720 (100%)
RDRS	210 (86%)	411 (86%)	621 (86%)
PERA	151 (62%)	381 (80%)	532 (74%)
Proposed	192 (79%)	332 (70%)	524 (73%)

The results of the analyses using the RDRS (2013) are given in Table 3 and are compared with the rigorous analysis by TSC (2007). 243 out of 720 analysis cases (34%) unbend to pre-collapse performance level, whereas 477 cases (66%) correspond to collapse performance level. In another word, TSC 2007 marks 66% of the examined cases as highly vulnerable to earthquakes. Estimations of the RDRS (2013) Method indicate 276 safe and 444 unsafe cases, which correspond to 38% and 62% of the 720 analysis cases, respectively (Table 3 and Table 6). These results show a good agreement between the RDRS (2013) and the TSC 2007 (34% and 66%, respectively). Also, if low and high risk cases are considered separately, estimations of the RDRS (2013) method are again in reasonably good agreement with the predictions of the TSC 2007 method. The safe cases estimated by the TSC 2007 and by the RDRS (2013) were 243 and 210, respectively (86% achievement according to TSC 2007). Similarly, the unsafe cases estimated by the TSC 2007 and by the RDRS (2013) were 477 and 411, respectively (again 86% achievement according to TSC 2007). The ratio of 86% can be deemed an acceptable ratio of agreement. Also, out of 720 total safe and unsafe (life safety or collapse prevention and collapse) analysis cases found by TSC 2007, the RDRS method (2013) simultaneously found 621 low and high risk cases (86% success with respect to TSC 2007), shown in Table 7. The results of the analyses using the PERA (2014) are given in Table 4 and are compared with the rigorous analysis by TSC (2007). If estimations of the TSC (2007) are accepted as reference values, as given in Table 3, the results of the PERA method (2014) show 247 safe and 473 unsafe cases corresponding to 34% and 66% of the 720 analysis cases, respectively. These values give good, if conservative, agreement with TSC 2007 (34% and 66%, respectively). In addition to, if safe and unsafe cases are considered separately as before, the results of the PERA method (2014) once again give good agreement with the TSC 2007 method. Out of 243 safe cases (life safety or collapse prevention) predicted by the TSC 2007, 151 were also obtained as safe by the PERA method (2014) (62% success with respect to TSC 2007). Similarly, out of 477 unsafe (collapse) analysis cases predicted by TSC 2007, the PERA method (2014) simultaneously predicted 381 cases as unsafe (80% success with respect to TSC 2007). The 62% and 80% match found for safe and unsafe cases, respectively. Similarly, out of 720 total safe and unsafe (life safety or collapse prevention and collapse) analysis cases predicted by TSC 2007, the PERA method (2014) simultaneously predicted 532 low risk and high risk cases (74% success with respect to TSC 2007), shown in Table 7.

A comparison of the building performances for the 720 cases found using the rigorous TSC 2007 approach, the proposed method is compared in Table 5. The predictions of the proposed method plumb to 337 safe and 383 unsafe cases, which match 47% and 53% of the 720 analysis cases, respectively. These values point to an acceptable level of accuracy between the values of the proposed method and the TSC 2007 (34% and 66%, respectively). Again, if safe and unsafe cases are considered separately, predictions of the proposed method are in reasonably good agreement with the predictions of the TSC 2007 method. Out of 243 safe cases (life safety or collapse prevention) predicted by the TSC 2007, 192 were also identified as low risk by the proposed method (79% success with respect to TSC 2007). Similarly, out of 477 unsafe (collapse) analysis cases predicted by TSC 2007, the proposed method simultaneously predicted 332 cases as high-risk (70% success with respect to TSC 2007). The 79% and 70% match found for both safe and unsafe cases, respectively. The effect of concrete cube compressive strength, presence of adequate confinement, and soil conditions, on the estimations of the TSC 2007 approach are also observed. The percentage of unsafe cases generally tends to decrease with increasing concrete compressive

cube strength values, as expected, for all parameter groups. Both existence of adequate confinement and soil condition parameters, for a given concrete strength, seem to be quite influential on the classification of performance according to the TSC 2007. Similarly, out of 720 total safe and unsafe (life safety or collapse prevention and collapse) analysis cases predicted by TSC 2007, the proposed method simultaneously predicted 524 low risk and high risk cases (73% success with respect to TSC 2007), shown in Table 7.

Finally, summation of the predictions of the TSC (2007), the RDRS (2013) approach, the PERA method (2014) and the proposed method are given in Tables 6-7. Accordingly, the predictions of the RDRS (2013), the PERA method (2014) and the proposed method are again in reasonably good agreement with the predictions of the TSC 2007 method. The 86% match obtained by using the RDRS (2013), the 62% and 80% match obtained by using the PERA method (2014) and the 79% and 70% match obtained by using the proposed method for safe and unsafe cases, respectively, can be considered an acceptable ratio of agreement, which can be encountered also while carrying out rigorous structural analysis utilizing slightly different assumptions in TSC (2007). Besides overall comparison of the predictions of the TSC 2007 and the proposed methods, the effect of significant variables, including concrete quality, confinement, and soil conditions, on the performance prediction of the proposed method were evaluated by Ilki et al. (2014). It has been reported that highly successful prediction rates were obtained relative to the TSC 2007 results. The 86%, 74% and 73% match obtained by using the RDRS (2013), the PERA method (2014) and the proposed method, respectively for safe and unsafe cases, can be considered an acceptable ratio of agreement. The proposed method (79%) gives better results than the PERA method (2014) (62%) in finding low cases as shown in Table 7.

5 CONCLUSIONS

A simplified version of the PERA method for predicting rapid seismic safety evaluation of existing medium-rise reinforced concrete frame structures has been proposed. In this study, the performance based rapid seismic assessment method (PERA) has been modified. The analysis steps of the PERA procedure was used by replacing Muto method by Smith method. The integrity of the presented method is validated for common medium-rise reinforced concrete frame structures for which the first mode of vibration is dominant. The proposed method, for safe and unsafe cases, can be considered an acceptable level of agreement. A good agreement is obtained between the proposed method, the PERA method and conventional detailed seismic safety assessment analyses carried out for 720 different cases representing typical medium –rise reinforced concrete frame buildings in Turkey. A comparison of the building performances for the 720 cases found using the rigorous TSC 2007 approach, the proposed method is given. The predictions of the proposed method plumb to 337 safe and 383 unsafe cases, which match 47% and 53% of the 720 analysis cases, respectively. These values point to an acceptable level of accuracy between the values of the proposed method and the TSC 2007 (34% and 66%, respectively). It should be noted that the pace of the application of the proposed method is remarkably higher than conventional structural performance assessment methods. Not only the accuracy of the presented method is acceptable for structures with limited structural irregularities, but also the pace of the implementation is considerably higher than current conventional structural performance assessment methods in practice. Further study is required for evaluating and improving the reliability of the proposed rapid seismic assessment method for structures with significant irregularity defined in conventional structural performance assessment methods and structures having shear walls in two principle directions.

REFERENCES

- ASCE 41: Seismic Rehabilitation Standard, American Society of Civil Engineers, 2006, Washington DC, USA.
- Bal, I.E., Gulay, F.G. and Tezcan, S.S., 2008. A new approach for the preliminary seismic assessment of RC buildings: P25 scoring method, *Proceedings of the 14th World Conference on Earthquake Engineering*, Beijing, China.

- Eurocode, 2005, Seismic Design of Buildings. Part 3: Assessment and Retrofitting of Buildings, European Committee for Standardization; Brussels, Belgium.
- Earthquake hazard map of Turkey, 2018, AFAD.
- FEMA P-154: Rapid Visual Screening of Buildings for Potential Seismic Hazards: A Handbook, Federal Emergency Management Agency, 1988a, Washington D.C., USA.
- FEMA P-154: Rapid Visual Screening of Buildings for Potential Seismic Hazards: A Handbook, Second Edition, Federal Emergency Management Agency, 2002a, Washington D.C., USA.
- FEMA P-155: Rapid Visual Screening of Buildings for Potential Seismic Hazards: Supporting Documentation, Federal Emergency Management Agency, 1988b, Washington D.C., USA.
- FEMA P-155: Rapid Visual Screening of Buildings for Potential Seismic Hazards: Supporting Documentation, Second Edition, Federal Emergency Management Agency, 2002b, Washington D.C., USA.
- FEMA P-155: Rapid Visual Screening of Buildings for Potential Seismic Hazards: Supporting Documentation, Third Edition, Federal Emergency Management Agency, 2015, Washington D.C., USA.
- Hassan, A.F. and Sozen, M.A., 1997, Seismic Vulnerability Assessment of Low-Rise Buildings in Regions with Infrequent Earthquakes, *ACI Structural Journal*, 94(1): 31-39.
- Ilki, A., Comert, M., Demir, C., Orakcal, K., Ulugtekin, D., Tapan, M. and Kumbasar, N., 2014, Performance based rapid seismic assessment method (PERA) for reinforced concrete frame buildings, *Advances in structural engineering*, 17(3):pp. 439-459.
- Ministry of Environment and Urbanisation of Turkey, www.csb.gov.tr, 17.10.2017.
- Ministry of Public Works and Settlement of Turkey, 1975, Turkish Seismic Design Code; Ankara, Turkey.
- Muto, K., 1956, Seismic analysis of reinforced concrete buildings, *Proceedings of the First World Conference on Earthquake Engineering*, Berkeley, California, USA.
- Ozcelik, M.U., 2014, Seismic assessment of existing buildings using PERA, RDRS and TSC 2007, M.Sc. Dissertation, Istanbul Technical University, Istanbul.
- Performance based rapid seismic assessment method (PERA) for reinforced concrete frame buildings, *Advances in structural engineering*, 17(3): 439-459.
- Recommendations for Assessment and Improvement of the Structural Performance of Buildings in Earthquakes, 2012, New Zealand Society for Earthquake Engineering, New Zealand.
- Regulation on the Determination of Risky Structures, 2013, (RDRS): Ankara, Turkey.
- Standard for Seismic Capacity Assessment of Existing Reinforced Concrete Buildings: Japanese Building Disaster Prevention Association, 1990, Ministry of Construction of Japan.
- Sta4CAD, 2007, Structural Analysis for Computer Aided Design, Sta Engineering Consultancy Ltd., Istanbul, Turkey.
- Stafford Smith, B. and Carter, C., 1969, A method of Analysis for Infilled Frames, *Proceedings of the Institution of Civil Engineers*, 44(1): 31-48.
- Sucuoglu, H., Yazgan, U. and Yakut, A., 2007, A screening procedure for seismic risk assessment in urban building stocks, *Earthquake Spectra*, 23(2): 441-458.
- Turkish Seismic Design Code (TSC), 2007, Ankara, Turkey.
- Vulas, Y., 2014, Rapid performance seismic assessment method (PERA) for existing reinforced concrete frame buildings, M.Sc. Dissertation, Istanbul Technical University, Istanbul.
- Yakut, A., 2004, Preliminary seismic performance assessment procedure for existing RC buildings, *Engineering Structures*, 26(10):1447-1462.

Flexural behaviour of fabric reinforced cement-based composites in strengthening of masonry walls

Mustafa Esat GÜNEŞ¹, Zehra Canan GİRGIN² and Bekir Yılmaz PEKMEZCİ³

¹ Yıldız Technical University, Istanbul, Turkey

² Yıldız Technical University, Istanbul, Turkey

³ Istanbul Technical University, Istanbul, Turkey

ABSTRACT: The fabric reinforced mortar composites are widely utilized for the seismic retrofit of masonry walls subjected to in-plane and out-of-plane actions. Therefore, to define the structural behavior of these composites are getting importance. In masonry walls with small lateral stiffness, out-of-plane failure via snap-through mechanism represents a serious life-safety problem. Out-of-plane behavior is dominated by the flexural performance of composite retrofitted wall. For this reason, to test the flexural performance of composite on plates may be a practical approach to predict out-of-plane behavior of composite under seismic excitation. In this study, the flexural behavior of fabric reinforced cementitious mortar (FRCM) was investigated for three type one-layer glass fabrics. Three-point bending tests were conducted on the plates which the fabric was positioned in tension region at sub half of the cross-section. Flexural strengths and deflections were compared at 7 and 28 curing days. The effect of fabric geometry and stiffness as well as the interaction between fiber mesh and cement based matrix were observed, possible failure modes and crack types were discussed.

1 INTRODUCTION

In recent years, fabric reinforced FRM (Fabric Reinforced Matrix), or TRM (Textile Reinforced Mortar), systems are widely used in applications of strengthening or repairing of existing masonry/reinforced concrete structures. These systems are composed of the high strength textile immersed in a matrix. If the binding material is cement in mortar, this material is commonly named FRCM (Fabric Reinforced Cementitious Matrix). The main aim of matrix reinforced with high strength textiles in 2D grid-like alignment or multiaxial configuration is to get the maximum tensile performance from fibers.

In the current literature, in-plane masonry behavior induced by seismic loads is represented by mostly direct tensile tests on FRCM coupons, e.g. Leone et al. (2017), De Santis et al. (2017), Lignola et al. (2017) despite several difficulties on clamping conditions of the samples (De Santis et al. 2015). A recommendation document, RILEM TC 232-TDT (2016), was also published about the test method to determine the load bearing behavior of tensile specimens made of textile reinforced concrete. On the other hand, masonry walls, e.g. slender load bearing walls or infill walls, are subjected to out-of-plane behavior accompanying instability problem which may lead a serious life-safety problem during seismic excitations as well. The snap-through mechanism under consideration can be represented by flexural tensile loading. Thus, to conduct bending tests on composite plates may be suggested by simulating out-of-plane bending of masonry wall more realistically, only a few studies are available in the current literature (Portal et al. 2017, Kamani et al., 2017).

In some experiments, multi-layer FRCM composite samples are tested under direct tension (Donnini et al. 2017, Raoof et al. 2016, Larrinaga et al. 2014). In the applications of masonry strengthening, 1-layer FRCM is commonly used, multi-layer FRCM on masonry wall may not be efficient (Kamani et al. 2017) as well. Thus, in this study, three-point bending tests are conducted on 1-layer FRCM plate specimens to practically predict the flexural tensile performance in retrofitted masonry walls subjected to out-of-plane action.

2 MATERIALS AND EXPERIMENTAL PROGRAM

Commercially available three types of alkali resistant (AR) glass fiber mesh were used in this experimental study. Specimens are composed of one layer of textile reinforcement embedded into cement based mortar. The characteristics of matrix and three textiles are described below.

2.1 Mix proportion and material properties


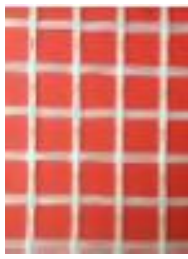
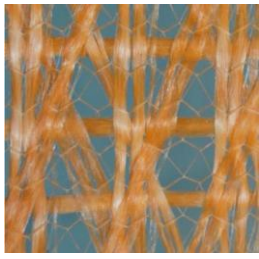
The matrix consists of Portland cement (CEM I 42.5 N), sand (max. size 1.0 mm) and water (Table 1). Low-strength matrix was designed for the consistent performance to those of masonry wall. Mechanical properties of mortar was determined according to BS EN 1015-11. Three-point bending tests on 40mm×40mm×160 mm prisms and then compressive tests on two remaining broken parts were carried out.

Table 1. Proportion of mix and mechanical properties of mortar

Mix		Mortar matrix	
Water/Cement	Cement/Sand	Compressive Strength (MPa)	Flexural Strength (MPa)
0.8:1	1:3	6.7	1.26

As three different types of glass fiber fabrics, GF1 and GF2 are two types of unbalanced bidirectional glass-fiber mesh, GF3 is a multiaxial hybrid glass-synthetic fabric that glass fiber is aligned in four directions. Mechanical characteristics specified by the manufacturer are given in Table 2.

Table 2. Mechanical properties of fabrics

Fabric Name	GF1		GF2		GF3
					
Fiber Type	AR-Glass		AR-Glass		Multiaxial Hybrid
Nominal Weight (g/m ²)	670		340		330
Covering Weight (g/m ²)	120		57		-
Grid Spacing (mmxmm)	Warp	Weft	Warp	Weft	-
	35.0	39.0	34.5	27.6	
Thickness (mm)	2.3		1.9		1.2
Fiber Alignments	0°	90°	0°	90°	0°, 60°, 90°, 120°
Strength (kN/5 cm)	13.9	12.45	2.9	3.25	-
Ultimate Elongation (%)	<5	<5	3.0	2.95	5.65

2.2 Specimen preparation and test setup

The experimental work addresses the characterization of the flexural performance on the 250 mm × 50 mm × 13 mm FRCM plate specimens in accordance with ASTM C947-03 (2009) (Figure 1). Total 30 plates for three textile types (Figure 2a) were tested in three-point bending tests in 7 and 28 days. Five specimens were prepared for each fabric type (3 fabrics × 2 curing ages × 5 = 30 specimen). Fabric reinforced specimens will be defined with the same names of GF1, GF2, GF3, as well.

In the preparation stage of specimens, at first, cement based mortar was poured into the molds up to 3 mm thickness, then, fabrics at appropriate sizes were fixed manually. The warp yarns of the fabrics were orientated longitudinally such that they carry the tensile stresses occurred at the sub half of the cross section caused by bending moment. Then, the remaining mortar was placed on the reinforcement in the mould (Figure 2b). The mixture was vibrated for a thirty seconds. After 24 hours later, the demolded samples were stored in a sealed and moist environment of $25\pm 3^{\circ}\text{C}$ until testing days.

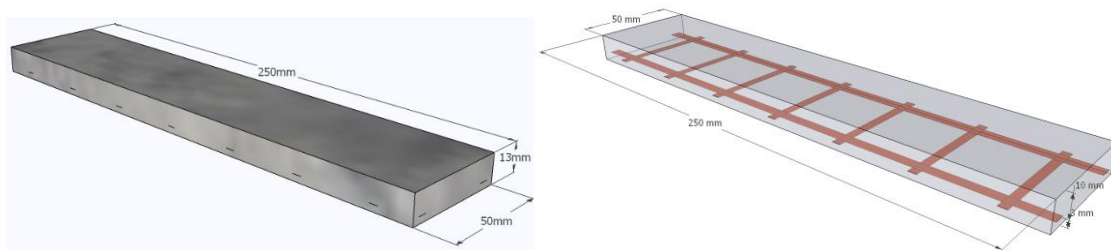


Figure 1. Schematic representations of plate specimens for GF1 and GF2 type of fabrics

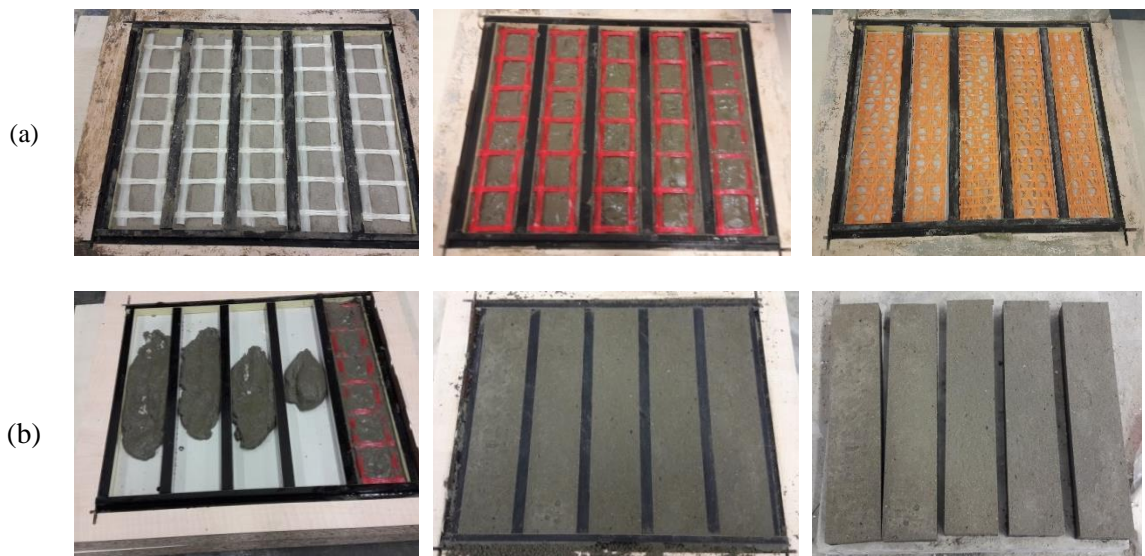


Figure 2. (a) Three types of fabrics (b) Production stages of plate specimens

The tests were performed in a deformation controlled testing machine (MTS Criterion Model 43) at a strain rate of 1.8mm/min and ended at 30% lower level than ultimate (peak) load (P_u). Three-point bending test setup is illustrated in Figure 3 with a real photo.

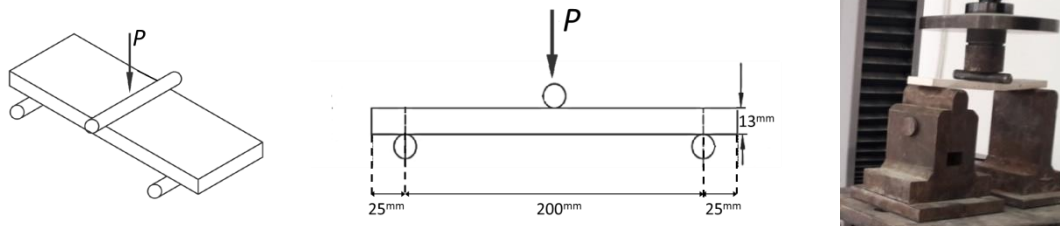


Figure 3. Three-point bending test set up

3 TEST RESULTS AND DISCUSSION

This research focuses the effect of three type glass fiber fabrics on the flexural properties of reinforced cement composite by comparisons. Load-deflection curves and failure modes are investigated on plate specimens.

Three phases are observed in load-deflection graphs (Figure 4). First phase is linear elastic and corresponds to the un-cracked phase. After first cracking (P_{cr} , D_{cr}), in the second phase, a significant increase up to the ultimate load (P_u , D_u) is under consideration. Third phase, namely softening, begins after peak load and continues until 30% loss ($0.7P_u$, D_{max}), then the loading protocol is terminated. In the second and third phase, local breakdown in adherence may be detected in fiber mesh-matrix interface. For all plate samples, first crack occurred at $D_{cr}=0.3-0.6$ mm mid-span deflection and $P_{cr}= 50$ to 65 N load level.

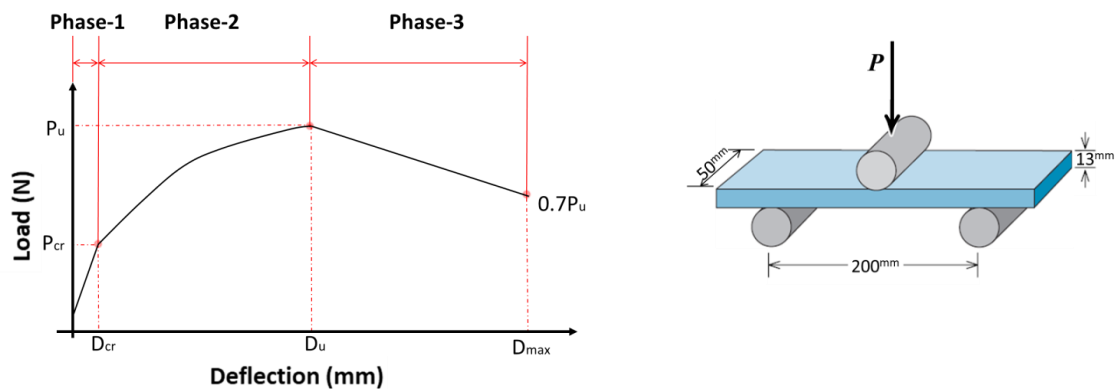


Figure 4. Schematic graph of three zones

3.1 Test results

In GF1 plate samples, the ultimate loads in 7 and 28 days are very close to each other (Figure 5). In addition, the load-deflection graph displays 28-day deflection capacity to be significantly better than 7-day one. Sharp drops through debonding in 7-day specimens, before/after the peak load to failure, considerably disappears in 28 days, thus softening phase proceeds more gradually with less brittle behavior.

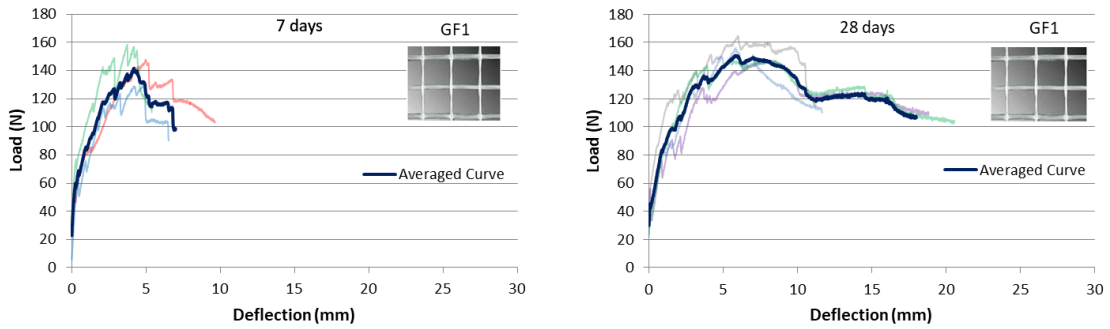


Figure 5. 7 and 28-day load-deflection diagrams of GF1 specimens and averaged curves

There is no significant variation in flexural properties for GF2 specimens (Figure 6). In 7 and 28 days, ultimate loads and deflection capacities are very close, this means that there is a ductile behavior as a result of the compatibility between the rigidities of fiber mesh and matrix during the curing period.

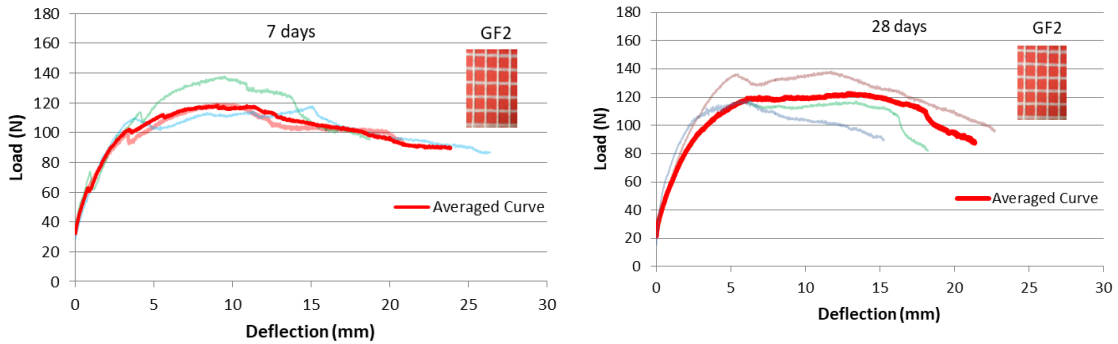


Figure 6. 7 and 28-day load-deflection diagrams of GF2 specimens and averaged curves

In multiaxial hybrid glass-synthetic fiber-fabric GF3 specimens, ultimate load and deflection increased from 7 days to 28 days (Figure 7). Brittle behavior in 7-day samples is observed, the deflection capacity improves about two times up to 28 day.

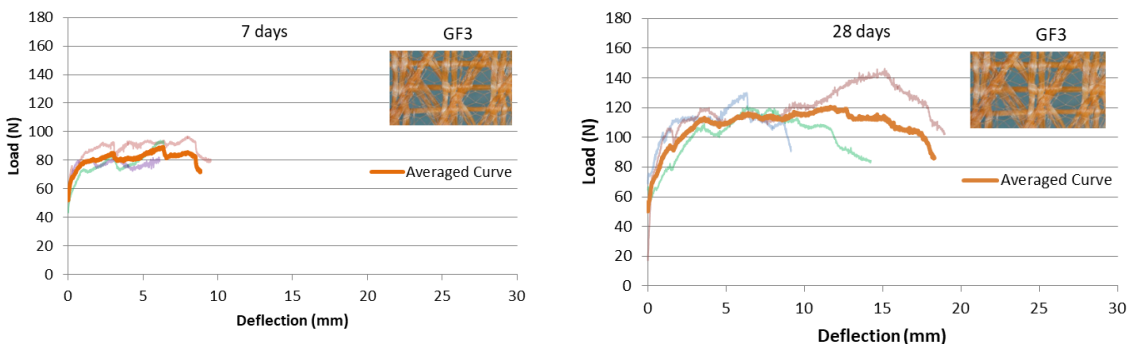


Figure 7. 7 and 28-day load-deflection diagrams of GF3 specimens and averaged curves

3.2 Discussion of findings

Averaged characteristics and curves for three fabric type are given in Table 3 and Figure 8. Slightly improvement (6-13%) in flexural strengths is detected from 7 days to 28 days for all fabric types.

Table 3. Load-deflection mean values in ultimate states

		GF1	GF2	GF3
7 days	P_u (N)	141.64	118.23	90.91
	D_u (mm)	4.15	11.35	6.72
	D_{max} (mm)	6.99	23.98	8.83
28 days	P_u (N)	150.68	122.75	118.11
	D_u (mm)	5.93	12.93	12.01
	D_{max} (mm)	18.26	21.39	18.13

GF1 reaches the highest peak strength (141.64 N) but with limited deflection (4.15 mm) in 7 days. Then, the deformation capability increases, however it is more limited compared with GF2 in 28 days. In GF1, the decrement rate in softening phase following peak load is faster than GF2. Relatively brittle behavior may be attributed to the incompatibility between stiff mesh and matrix due to probably surface treatment of fabric as well as rising in fiber content. Flexible fabric type GF2 maintains its deflection capacity from 7 days to 28 days, the adherence between fiber and matrix indicates the ductile failure mode.

Although the ultimate deflection of GF3 is small in early curing period, very significant improvement is detected later. In 28 days, a load-deflection curve quite similar to GF2 is attained along the bending direction. Surface treatment of this fabric is not so stiff as GF1, nominal weight is very close to GF2.

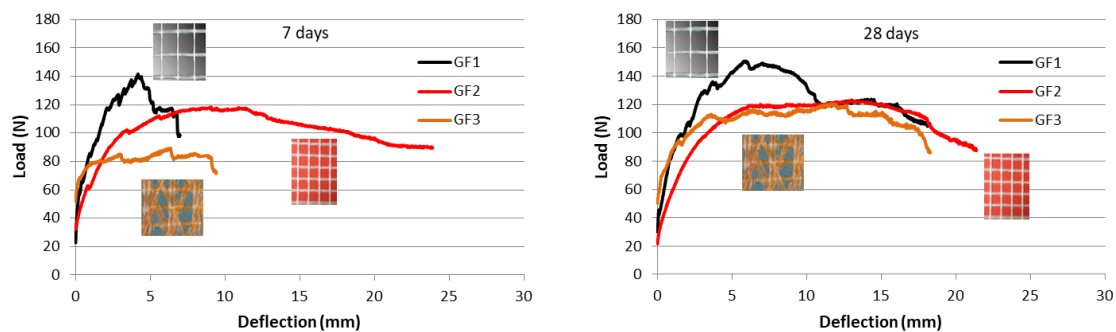


Figure 8. 7 and 28-day averaged load-deflection curves for GF1, GF2, GF3

When the crack formation in 28-day samples is investigated, the different cases are assessed. The photographs from the tensile region and side faces as well as the close views to fabrics in the samples are given in Table 4. Photographs during the flexure test are also given to explain crack propagation in Figure 9.

Only one sharp and deep transverse crack is noticed in GF1 to be different from GF2 with fine and multiple cracks. For GF1, an inner and partial longitudinal crack from middle region to support region, that indicates to the inter-laminar shear deformations, may be possible as well. In GF2, any longitudinal crack was not observed, flexural failure mode is dominant.

Multiaxial hybrid fabrics are useful to enhance mechanical characteristics of FRCM composite (Peled et al. 2009). Inter-laminar shear slippage (delamination) possibility in FRCM composites

was referred in the current literature (Promis et al. 2010; Urban and Stempniewski, 2012). Herein, the cracks progress from middle region to supports along 3 mm thickness at the tensile region of the cross-section toward the failure. The delamination inside cementitious matrix, contrary to fiber reinforced polymers (FRP), are of little importance (Bellini and Mazotti 2016), the good adhesion of mortar to the masonry should be assured. Nevertheless, it may be suggested that improvement in shear behaviour may be recommended to attain max. flexural capacity (Promis et al. 2010). Possible debonding between glass and synthetic fibers of GF3 samples was not detected in the hybrid fiber system, full integrity between fibers was observed.



Figure 9. Views of cracked samples from test setup

Table 4. Cracking modes of plate samples

<p>GF-1</p> 	 	
<p>GF-2</p> 	 	
<p>GF-3</p> 	 	

4 CONCLUSION

In this study, out-of-plane bending performance of FRCM-retrofitted masonry walls in earthquake prone regions were practically investigated through three-point bending test on plate specimens. The following results can be drawn from the findings of this study:

- Stiff glass fiber mesh (GF1) leads higher peak load but declines rather fast beyond it, its deformation capacity is limited due to the incompatibility between stiff mesh and low-strength mortar matrix. This type of fabric may be more effective in high-strength matrix. Partial slippage, or delamination, in tension region and one thick transverse crack is detected toward failure.

- Flexible glass fiber meshes (GF2) conform well to low-strength matrix. In 7 and 28 days, the ductile behavior in load-deflection curve is followed with higher deflection capacity, ductile transverse multi-crack formations and better adherence without delamination compared with GF1.
- Multiaxial hybrid GF3 samples show a similar behavior to GF2 in 28 days, bending performance may be enhanced by eliminating shear slippage in the tension region. Debonding between glass and synthetic fibers is not observed. Multiaxial orientation of fibers may provide strengthening concerning two-way bending moments in masonry wall during out-of-plane bending.
- Three- or four-point bending tests on plates may be useful to predict out-of-plane performance after strengthening in masonry walls with small lateral stiffness. Thus, the required precautions for FRCM strengthening may be practically determined prior to large scale masonry wall tests.
- Further researches via aging tests are needed to predict the flexural performance after long-term environmental conditions in FRCM composites.

REFERENCES

- ASTM International, ASTM C947-03. (2009). Standard test method for flexural properties of thin-section glass-fiber-reinforced concrete (using simple beam with third-point loading).
- Bellini, A., Mazzotti, C. Bond behavior and tensile properties of FRCM composites applied on masonry panels. In *Structural Analysis of Historical Constructions: Anamnesis, Diagnosis, Therapy, Controls: Proceedings of the 10th International Conference on Structural Analysis of Historical Constructions (SAHC, Leuven, Belgium, 13-15 September 2016)*,(p. 322).
- De Santis, S., de Felice, G. (2015). Tensile behaviour of mortar-based composites for externally bonded reinforcement systems. *Composites Part B: Engineering*, 68, 401-413.
- De Santis, S., Carozzi, FG., de Felice, G., Poggi, C. (2017). Test methods for textile reinforced mortar systems. *Composites Part B: Engineering*, 127, 121-132.
- Donnini, J., Corinaldesi, V. (2017). Mechanical characterization of different FRCM systems for structural reinforcement. *Construction and Building Materials*, 145, 565-575.
- EN, B. (1999). 1015-11, Methods of test for mortar for masonry–Part 11: Determination of flexural and compressive strength of hardened mortar. *European Committee for Standardization, Brussels*.
- Kamani, R., Dolatabadi, M.K., Jeddi, A.A.A. (2018). Flexural design of textile-reinforced concrete (TRC) using warp-knitted fabric with improving fiber performance index (FPI). *The Journal of The Textile Institute*, 109(4), 492-500.
- Larrinaga, P., Chastre, C., Biscaia, H. C., San-José, J. T. (2014). Experimental and numerical modeling of basalt textile reinforced mortar behavior under uniaxial tensile stress. *Materials & Design*, 55, 66-74.
- Leone, M., Aiello, M. A., Balsamo, A., Carozzi, F. G., Ceroni, F., Corradi, M., Mazzotti, C. (2017). Glass fabric reinforced cementitious matrix: Tensile properties and bond performance on masonry substrate. *Composites Part B: Engineering*, 127, 196-214.
- Lignola, G. P., Caggegi, C., Ceroni, F., De Santis, S., Krajewski, P., Lourenço, P. B., Zuccarino, L. (2017). Performance assessment of basalt FRCM for retrofit applications on masonry. *Composites Part B: Engineering*, 128, 1-18.
- Peled, A., Mobasher, B., Cohen, Z. (2009). Mechanical properties of hybrid fabrics in pultruded cement composites. *Cement and Concrete Composites*, 31(9), 647-657.
- Portal, N. W., Thrane, L. N., Lundgren, K. (2017). Flexural behaviour of textile reinforced concrete composites: experimental and numerical evaluation. *Materials and Structures*, 50(1), 4.
- Promis, G., Gabor, A., Maddaluno, G., Hamelin, P. (2010). Behaviour of beams made in textile reinforced mineral matrix composites, an experimental study. *Composite Structures*, 92(10), 2565-2572.

- Raof, S. M., Koutas, L. N., Bournas, D. A. (2016). Bond between textile-reinforced mortar (TRM) and concrete substrates: experimental investigation. *Composites Part B: Engineering*, 98, 350-361.
- RILEM Technical Committee 232-TDT (2016). Recommendation of RILEM TC 232-TDT: test methods and design of textile reinforced concrete: Uniaxial tensile test: Test method to determine the load bearing behavior of tensile specimens made of textile reinforced concrete. *Materials and Structures*, 49, 4923-4927.
- Urban, C. M., Stempniewski, L. (2012). Comparison of different earthquake strengthening methods for masonry buildings. In *15th World Conference on Earthquake Engineering*, (p. 697).

A Study on effect of steel fiber content on minimum reinforcement ratio of high strength reinforced concrete beams

Muhammed Gümüş¹, and Abdussamet Arslan²

¹ Civil Engineering Department at Gazi University, Ankara, Turkey

² Civil Engineering Department at Gazi University, Ankara, Turkey

ABSTRACT: Effect of volume fraction of steel fiber on the minimum reinforcement ratio of high strength reinforced concrete (HSRC) beams was investigated experimentally. The main parameters in the proposed study were volume fraction of steel fibers and longitudinal reinforcement ratios. Therefore, nine fiber reinforced concrete beams and three plain beams were manufactured and tested under four point loading. Test results were criticized regarding minimum reinforcement ratio by fracture mechanics approximation. Therefore, critical brittleness number was obtained from the comparison between characteristic length and brittleness number. Using critical brittleness number, a proper model giving the minimum reinforcement ratio was proposed. Finally, validation of the proposed model has been performed as the comparison of the equation with several reported models.

1 INTRODUCTION

Flexural members should ensure the ductile behavior as well as the target strength under bending loads. The ratio of the longitudinal reinforcement area located at tensile zone to the beam cross section area is described as reinforcement ratio. It is the main parameter governing flexural response of RC beams. When the reinforcement ratio is equal to the limit ratio namely minimum reinforcement ratio, required minimum flexural ductility is obtained. However, when the reinforcement ratio is smaller than the minimum reinforcement ratio, beam is considered as unreinforced flexural member and represents a sudden failure. Ožbolt and Bruckner (1999) defines the minimum reinforcement ratio that it must assure (i) stable flexural behavior when the beam reaches the moment at first crack and (ii) when the ultimate moment is approximately equal to moment at first crack. To prevent the unstable crack propagation and accordingly brittle response of reinforced concrete (RC) beams, Eurocode 2 (2004) and ACI committee 318 (2008) define the lower limit for reinforcement area.

In the ACI committee 318 (2008) on structural concrete, required longitudinal reinforcement ratio is derived by the equalizing ultimate moment of RC beam to the moment at first crack of plain concrete beam at a certain rate. Hence, the lower limit of reinforcement ratio for high strength concrete (HSC), whose compressive strength is greater than 100 MPa, beam with rectangular cross section is expressed as;

$$\rho_{min} = 0.25 \frac{\sqrt{f_{ck}}}{f_{yk}} \geq \frac{1.4}{f_{yk}} \quad (1)$$

Where, f_{ck} and f_{yk} represent the characteristic compressive strength and yield strength of the reinforcement, respectively.

In Eurocode 2 (2004) at the section for general rules for buildings, minimum reinforcement ratio is expressed for both rectangular and T-beams. However, average tensile strength derived from characteristic compressive strength is used instead of flexural tensile strength given as following relationship:

$$\rho_{min} = 0.26 \frac{f_{ctm}}{f_{yk}} \geq 0.0013 \quad (2)$$

Where, f_{ctm} represents average uniaxial tensile strength of concrete and it could be obtained by using the compressive cylinder strength of concrete.

The codes are entirely depend on the compressive strength of the concrete and the yield strength of reinforcement. They ignore some important parameters such as fracture energy which particularly important for fiber reinforced concrete members. This means, tensile properties of HSC with dispersed steel fiber are not considered in the evaluation of critical reinforcement ratio. However, Henager and Doherty (1976), Wafa and Ashour (1992) and Koksai et al. (2008) stated that randomly distributed steel fibers increase the flexural and direct tensile strength as well as the fracture energy rather than compressive strength of concrete. Moreover, Karihaloo (2015) reported that compressive failure of the concrete is also nothing other than concentration of local micro fractures due to over stretching of the bonds.

On the other hand, Carpinteri (1984) stated that fracture mechanic approach is one of the method to evaluate the mechanical and failure behavior of beams with low reinforcement ratios. The method is based on the linear elastic fracture mechanic principles and takes into account the bridged crack model. In accordance with the analytical procedures of bridged crack model, it was found that the flexural response of beam is related to the brittleness number (N_p) as follows:

$$N_p = \frac{\rho f_{yk} h^{0.5}}{K_{Ic}} \quad (3)$$

Where ρ , h and K_{Ic} are the longitudinal reinforcement ratio, beam depth and critical stress intensity factor, respectively. In fact, N_p is a measure of ductility of the RC flexural member, though it is called brittleness number. The larger value of the N_p , the more ductile response is achieved under bending loads and vice versa. A critical value of brittleness number (N_{pc}) is defined depends on the average compressive strength (f_{cm}) in order to distinguish the brittle and ductile behaviours by Bosco and Carpinteri (1992) as follows:

$$N_{pc} = 0.1 + 0.0023 f_{cm} \quad (4)$$

Therefore minimum reinforcement ratio is achieved by substituting Eq.4 into Eq.3 as following:

$$\rho_{min} = (0.1 + 0.0023 f_{cm}) \frac{K_{Ic}}{f_{yk} h^{0.5}} \quad (5)$$

Carpinteri et al. (2014) investigates the minimum reinforcement ratio by numerical study through the non-linear fracture mechanics. To confirm the validity of numerical model, simulation results were calibrated by experimental results. A parametric study was conducted by means of numerical model to reveal the minimum reinforcement ratio by using compressive strength of concrete and beam depths as variables. Therefore, main two parameters governing the response of RC beams were determined using dimensional analysis and then the relationship between them was defined as hyperbolic curve. The minimum reinforcement ratio for rectangular cross section beam was derived by substituting the general equation of hyperbolic curve into Eq.3 as follows:

$$\rho_{min} = 0.27 \frac{K_{Ic}^{0.3} f_{ctm}^{0.7}}{f_{yk} h^{0.15}} \quad (6)$$

Besides Bosco and Carpinteri (1992) and Carpinteri et al. (2014), many studies have been conducted to evaluate minimum longitudinal reinforcement ratio for flexural members without dispersed steel fiber by Bosco et al. (1990), Bosco et al. (1990), Bosco and Carpinteri (1992), Ozbolt and Bruckner (1999), Ozcebe et al. (1999), Shehata et al. (2003), Fantilli et al. (2005), Rao et al. (2008), Carpinteri and Corrado (2011) and Carpinteri et al. (2014). However limited

experimental attempts by Dancygier and Savir (2006), Dancygier and Berkover (2016) and Yoo et al. (2017) evaluating the steel fiber effect on the flexural behavior of RC beam with low reinforcement ratios are exist. Dancygier and Savir (2006) and Dancygier and Berkover (2016) stated an interesting result that use of dispersed steel fibers in concrete mix considerably decreases the flexural ductility of lightly reinforced RC beams. Therefore, the reinforcement ratio for the beam with dispersed steel fibers should be higher than that of the beam without steel fibers.

2 RESEARCH SIGNIFICANCE

Majority of the conducted studies on the topics of minimum reinforcement ratio in flexural members focused on the RC beams manufactured by plain concrete. However, it is a well-known fact that incorporation of the steel fiber remarkably increases the fracture energy of the concrete. With this in mind, effect of the steel fiber on the minimum reinforcement ratio of HSRC beam remains unclear. Therefore, the objective of the present study is to investigate by fracture mechanics how the steel fiber in various ratios effects the mechanical response of lightly reinforced concrete beams and to determine the relationship between the required minimum reinforcement ratio of HSRC beams and steel fiber content. For this purpose, brittleness number (N_p) of the RC beams and characteristic length (L_{ch}) of the concrete are used. It should be noted that L_{ch} was introduced by Hillerborg et al. (1976) to study ductility of concrete, and for the plane stress condition, L_{ch} is as follows:

$$L_{ch} = \frac{K_{Ic}^2}{f_t^2} \quad (7)$$

Where f_t is the tensile strength of the concrete. L_{ch} is related to the intrinsic ductility of the concrete mixture and it increases as the ductility of the concrete mixture increases.

In the present study, three RC beams without steel fiber and nine RC beams with steel fiber were tested under four-point flexural loading. The test results were analyzed regarding to the minimum reinforcement ratio required for minimum ductility. Then a comparison between the suggested equation and some models by Bosco and Carpinteri (1992), Eurocode 2 (2004), ACI committee 318 (2008) and Carpinteri et al. (2014) was developed to confirm the validity of proposed equation on minimum reinforcement ratio.

3 MATERIALS AND METHODS

Twelve RC beam specimen was manufactured by HSC and tested under four point loading to investigate the effect of dispersed steel fiber on the minimum reinforcement ratio. Silica sand whose maximum size of aggregate was smaller than 1mm, silica fume and CEM I-52.5N Portland cement were used to cast HSC. Super plasticizer was employed to compensate the decreased workability due to low water/binder ratio.

Hook-end steel fibers were used into the mixes at different volume fraction to evaluate the effect of steel fiber on the required minimum reinforcement ratio. Mechanical and geometrical properties of steel fibers given by manufacturer are indicated in Table 1. Ingredients content for all types of mixture are given in Table 2 as kg/m^3 . The letter of S and the following number in the name of mixture type represent the steel fiber concrete and percentage volume fraction of the steel fiber respectively.

Average compressive and tensile strengths of the concrete types were determined by 6 cubes with a dimension of 100 mm and 4 cylinders with a dimension of 75x150 mm for each types. In order to determine the fracture energies of the concrete mixes, 3 rectangular specimens having dimensions of 100x100x500 mm were casted. The notch having 5 mm width and 30 mm depth was opened at the center of the beams. Then, specimens were tested by three point bending tests with the span length of 400 mm. Mechanical properties of concrete mixes are given in Table 3. It should be noted that quantities given in the table are average values.

All of the RC beams had the same rectangular cross section with the dimensions of 150x200 mm and same span length which is 1200 mm. Four point loading was applied onto the beams. Details of the instrumentations and test setup is given as in Fig.1. Mid span deflection was directly obtained regardless of support deflection thanks to rigid steel rod mounted on the RC beam as to be the one end of rod is fixed and the other is roller. Title of the RC specimens was assigned as concrete type and following letter of R representing the reinforcement and the following number representing the percentage of reinforcement ratio (i.e., 0.17%, 0.33% and 0.50%). Longitudinal reinforcements were selected such as Smaller, Equal and Bigger than the minimum reinforcement ratio given by Eurocode 2 (2004), and the corresponding cover thickness was selected as 12 mm for all specimens. Moreover, sufficient stirrups were used within the high shear zone to prevent the RC beams from shear failure. Longitudinal reinforcements and stirrups used in the present study had a nominal diameter of 8 and 5 mm, respectively. The steel bars used as longitudinal reinforcements showed a clear yield point with 500 MPa yield strength.

Rigid load transfer beam was located at the top of RC beam to bifurcate the single point applied load such that 200 mm constant bending moment region was obtained. The bending force was applied through the experiment was around 45 minutes. One support of the RC beams was arranged as fixed, whereas the other was roller to provide statically determined system. Applied force and vertical mid-span deflection were recorded by 200 kN capacity load cell and 100 mm capacity LVDT, respectively. Normal strains located on the face of RC beams were determined through the strain gauges.

Table 1. Properties of steel fibers

Fiber type	Length (mm)	Diameter (mm)	Aspect ratio	Young's modulus (MPa)	Tensile strength (MPa)	Density (kg/m ³)
Steel	30	0.55	60	210	1500	7850

Table 2. Quantity of ingredients as kg/m³

Concrete type	Water	Cement	Silica sand	Superplasticizer	Silica fume	Steel fiber
S0	198	990	1210	29.7	148.5	-
S33	198	990	1210	29.7	148.5	25.9
S67	198	990	1210	29.7	148.5	51.8
S100	198	990	1210	29.7	148.5	77.7

Table 3. Mechanical properties of hardened concrete

Concrete type	Compressive strength (MPa)	Splitting tensile strength (MPa)	Fracture Energy (N/m)	Young's Modulus (MPa)	Stress intensity factor, K_{Ic} (N/mm ^{1.5})
S0	105.8	5.7	107	39825	65.28
S33	126.7	8.3	445	39985	133.39
S67	120.3	11.9	1149	41062	217.21
S100	109.2	15.4	2115	43369	302.86

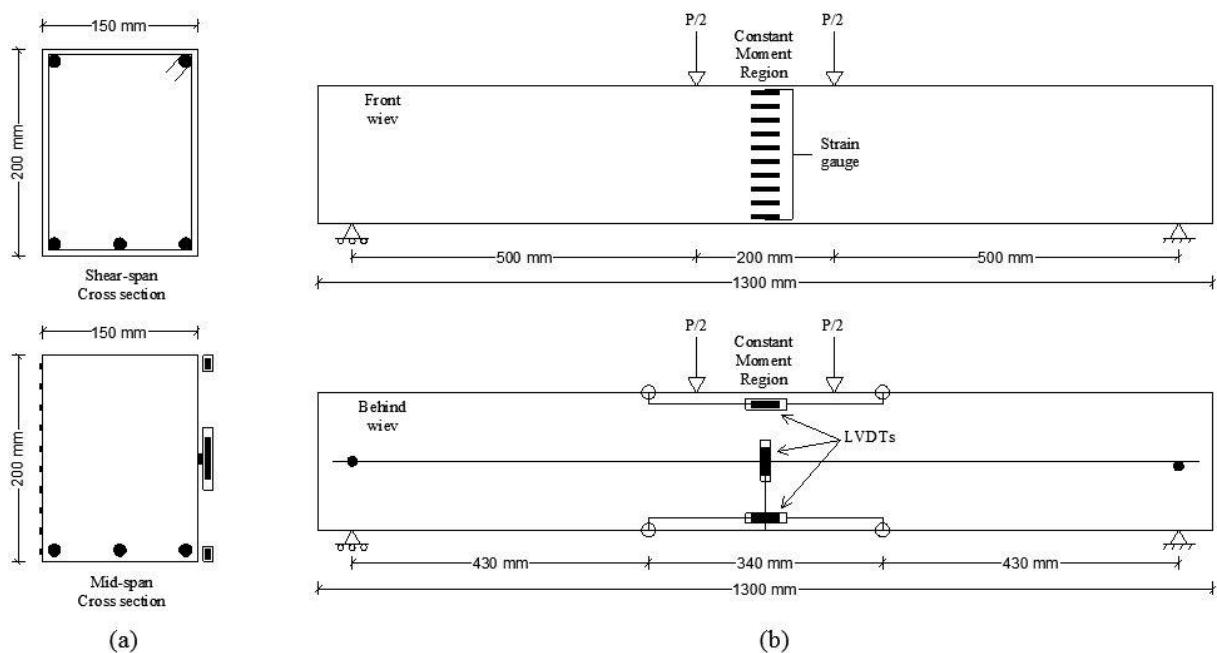


Figure 1. Specimen detail: (a) cross section and (b) scheme and measurements

4 RESULTS AND DISCUSSIONS

The experimental load-displacement curves of the RC beams are given in Fig.2. It can be seen from the plots that steel fiber increases the yield load of the RC beams independent from the reinforcement ratio. Rapid decrease in load capacity was observed for the specimen SOR17 and S100R17 after the maximum load and gradual decrease was observed for the beams S33R17, S67R17, S67R33, S100R33 and S100R50 after the yielding loads. Such a behavior may be attributed to the pull out mechanism of steel fibers. It should be noted that shear behavior had never been observed for the RC beams due to combined effect of used steel fiber and stirrups, in accordance with experimental results by Sahoo and Sharma (2014).

It can be clearly seen that the flexural responses of the RC beams after yield load were governed by steel fiber content rather than main longitudinal reinforcement ratios in Fig 2. When the most bottom region of the RC beam reaches its expansion limit, a formation of flexural crack with the cohesive zone takes place. Tensile strength of the fibers in cohesive zone and that of main reinforcement increases by the increment of applied load. RC beams reached the yield strength as

soon as the main reinforcement yields, and width of the flexural crack begun to develop further. Steel fiber started debonding from concrete matrices, so cohesive zone raised towards middle of the cross section by replacing real crack. From the experimental observations, it could be said that lesser the reinforcement ratio, more the effect of steel fiber on the flexural response of lightly reinforced RC beams.

Minimum reinforcement ratio must be used in RC members to prevent the beam as plain concrete beam. The experimental results are evaluated with respect to fracture mechanics principles as described previously. Therefore, L_{ch} of the HSC mixture suggested by Hillerborg et al. (1976) and brittleness number of the RC beam by Carpinteri (1984) were comparatively plotted and shown in Fig.3. It has been observed that an increment in the steel fiber content reduces the brittleness number (i.e., structural ductility) of the RC beams. The main reason to that is the increasing stress intensity factor, while reinforcement ratio, yield strength of the beam and dimension of the cross section is constant. However, increasing steel fiber ratio improved the mixture ductility of HSC because of the fact that steel fiber increased the tensile strength of the concrete, though it increased the fracture energy and stress intensity factor more than that of tensile strength as in Table 3.

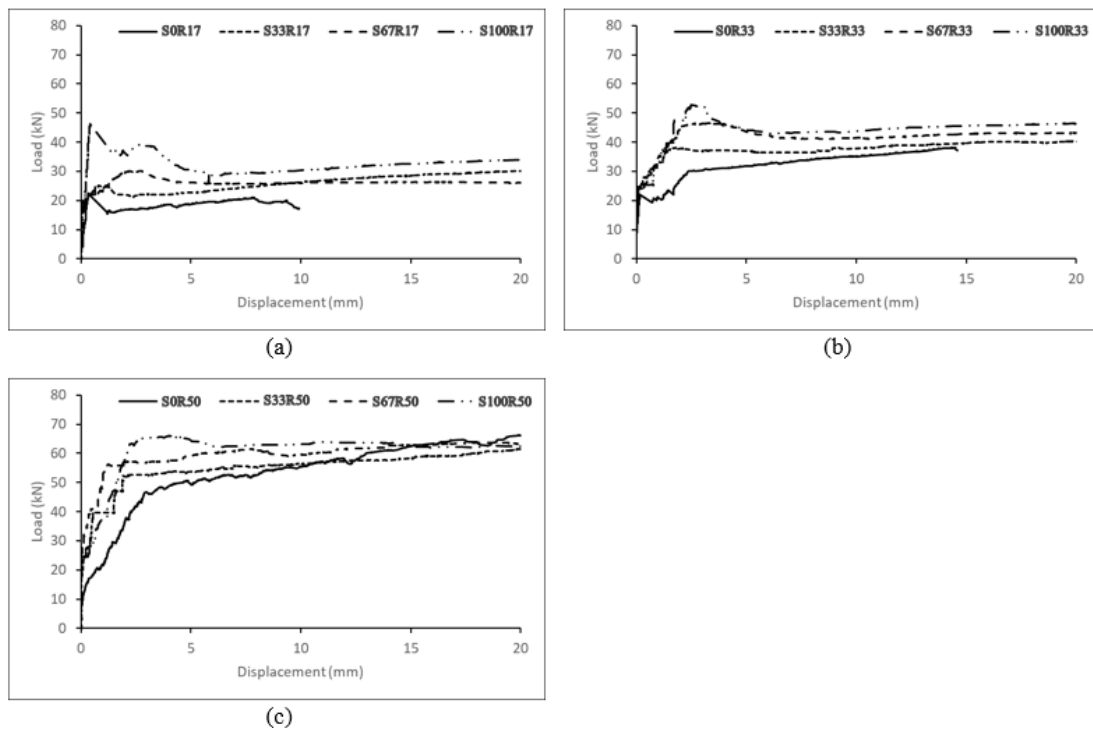


Figure 2. Load-displacement curves according to: (a) $g=0.17\%$, (b) $g=0.33\%$ and (c) $g=0.50\%$

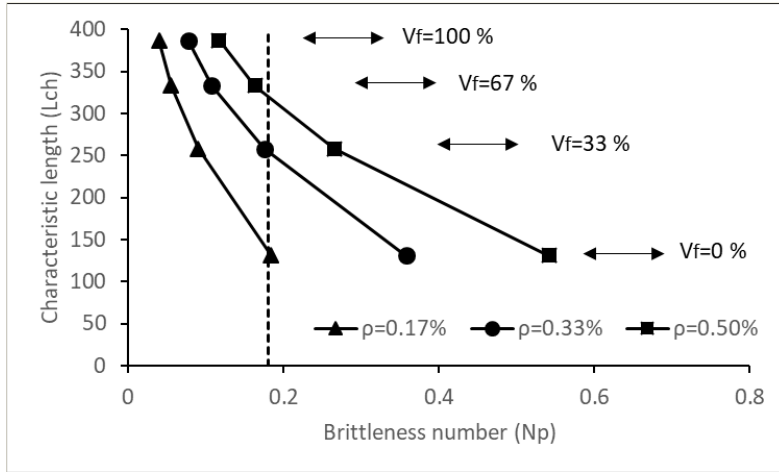


Figure 3. Concrete mixture ductility versus RC beams ductility

A typical non-linear relationship between the structural ductility and mixture ductility resulted from quadratic form of the tensile strength in the L_{ch} seen in Fig.3. Flexural ductility of the RC beams for the same concrete mixture ductility decreased as the fiber content was increased. Increment in the fiber content compelled the RC beams with low reinforcement ratio towards the more brittle behavior. Because, the use of the steel fibers decrease the number of flexural cracks and limit the width of fracture process zone on front of the main flexural crack. In order to clarify the expression, crack patterns observed at the end of the experiments within the constant moment zone of RC beams are given in Fig.4. Number of the flexural cracks spread on the RC beams with lowest steel fiber content and plain concrete increases as the reinforcement ratio increases. However, it decreased with the increasing fiber content for the beams with 0.33% and 0.50% reinforcement ratio.

Similar to the test results from this study, Koksal et al. (2008) reported that incorporating the steel fiber into concrete increases the material ductility of the mixture, though Dancygier and Savir (2006) and Dancygier and Berkover (2016) stated that it reduces the structural ductility of the lightly reinforced RC beams. Therefore, it can be said that there should be a constant brittleness number giving minimum structural ductility. Crack patterns, load-displacement curves and the concrete's ductility-RC beam ductility variations given in the three figures are considered together in order to control whether a constant critical brittleness number is exist or not. It was seen that the beams having a decrement in their load bearing capacity after yielding and having only a single crack in the constant moment region were located to the left side of dashed line on the Fig.3. Therefore intersection point between dashed line and the x axis was obtained as 0.18, which is reasonably close to the minimum brittleness number defined by Rao et al. (2008). The constant brittleness number obtained as 0.18 which will be used to determine the minimum reinforcement ratio for fiber reinforced RC beams. Therefore, a new equation is obtain giving minimum reinforcement ratio as follows:

$$\rho_{min} = 0.18 \frac{K_{IC}}{f_y h^{0.5}} \tag{8}$$

In order to test the reliability of the proposed equation, it was compared with several model suggested by ACI committee 318 (2008), Eurocode 2 (2004), Carpinteri et al. (2014) and Bosco and Carpinteri (1992). Minimum reinforcement ratios for HSRC without and with steel fiber are comparatively represented in Table 4. It should be noted that some suggested equations by Eurocode 2 (2004) and Carpinteri et al. (2014) includes the average uniaxial tensile stress, f_{ctm} , derived from cylinder compressive strength of concrete. However, use of the steel fiber increases tensile strength rather than compressive strength of the HSC. Therefore the table is subdivided into two sections in which the average uniaxial tensile strength f_{ctm} and splitting tensile strength

f_t of the concrete used in the models by Eurocode 2 (2004) and ACI committee 318 (2008) for Table 4-a and Table 4-b, respectively.

The results given in a tabulated form for all models and proposed equation is also shown graphically for both situation in Fig.5. From the Fig.5a it is observed that the model by Bosco and Carpinteri (1992) gives overestimated results especially for higher fiber volume fractions. On the other hand results from the model by ACI committee 318 (2008) was not affected by increasing steel fiber content due to dependence of the model on the compressive strength of HSC. Dancygier and Savir (2006) and Dancygier and Berkover (2016) stated that the reinforcement ratio should be increased as the fiber content increases for beams with low reinforcement ratio. Therefore, recommended equation by ACI committee 318 (2008) on minimum reinforcement ratio may be revised depending on the tensile characteristics of HSC with fiber.

Another important comparison may be achieved by comparing Fig.5a and Fig.5b with regard to the model results by Eurocode 2 (2004) and Carpinteri et al. (2014). Such a comparison illustrated that if the experimentally obtained splitting tensile strength is used in the models, the proposed equation and models give similar results particularly in higher fiber dosages. Consequently, it can be concluded that from all these observations, material properties obtained by experiments yield more accurate results for the models in determination of minimum reinforcement ratio.

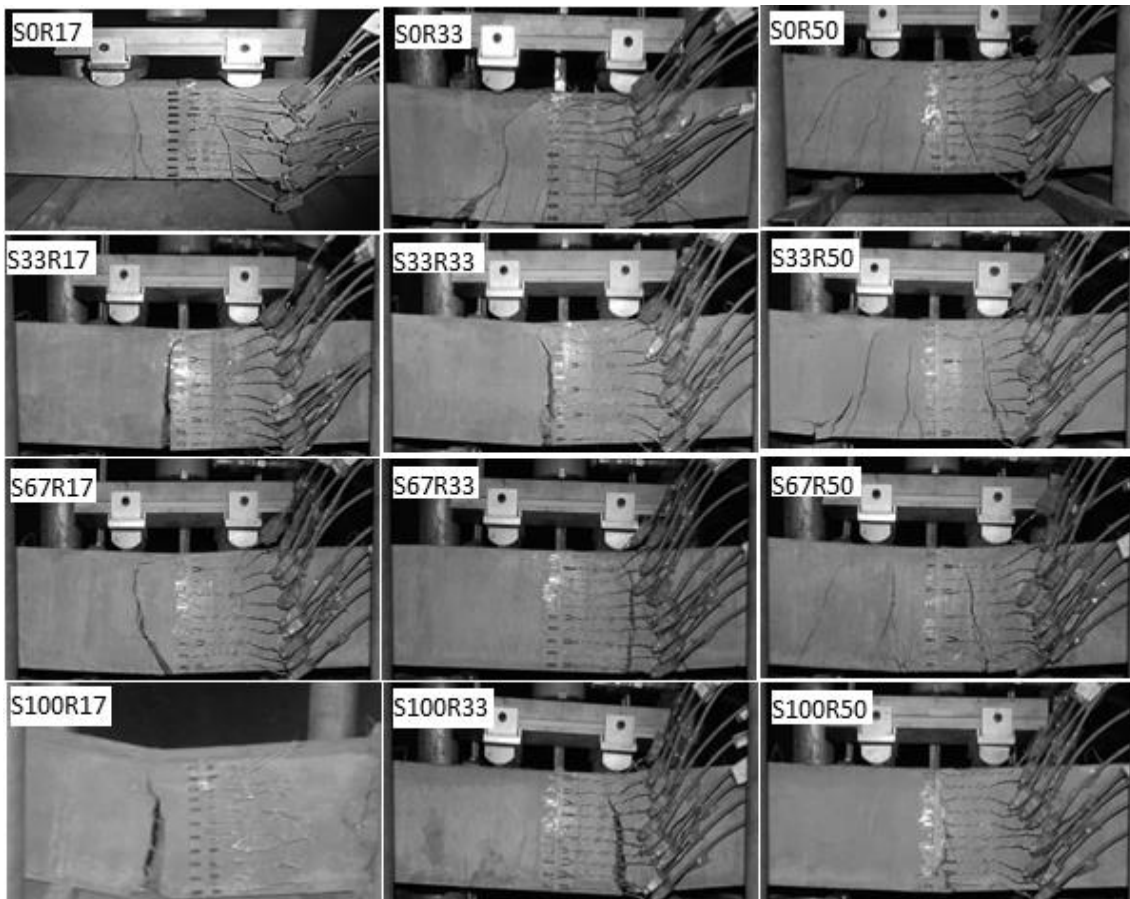


Figure 4. Crack patterns of the beams at the end of the tests

5 CONCLUSION

In the present study, the effect of steel fiber content on the minimum reinforcement ratios were investigated. Twelve RC beam specimens were tested experimentally under four point bending loading conditions. Test results from the experimental study may be concluded as follows:

Table 4. Mechanical properties and minimum reinforcement ratios

Concrete type	f_{ctm} (MPa)	ρ_{min} (%)						
		(a)					(b)	
		Model (1)	Model (2)	Model (3)	Model (4)	Proposed Equation	Model (2)	Model (3)
S0	4.88	0.45	0.25	0.26	0.28	0.17	0.27	0.27
S33	5.23	0.49	0.27	0.34	0.66	0.34	0.39	0.43
S67	5.13	0.48	0.27	0.38	1.03	0.55	0.56	0.64
S100	4.94	0.46	0.26	0.41	1.34	0.77	0.72	0.85

Model (1) - ACI 318-08 (2008); Model (2) – Eurocode 2 (2004); Model (3) - Carpinteri et al. (2014); Model (4) - Bosco and Carpinteri (1992)

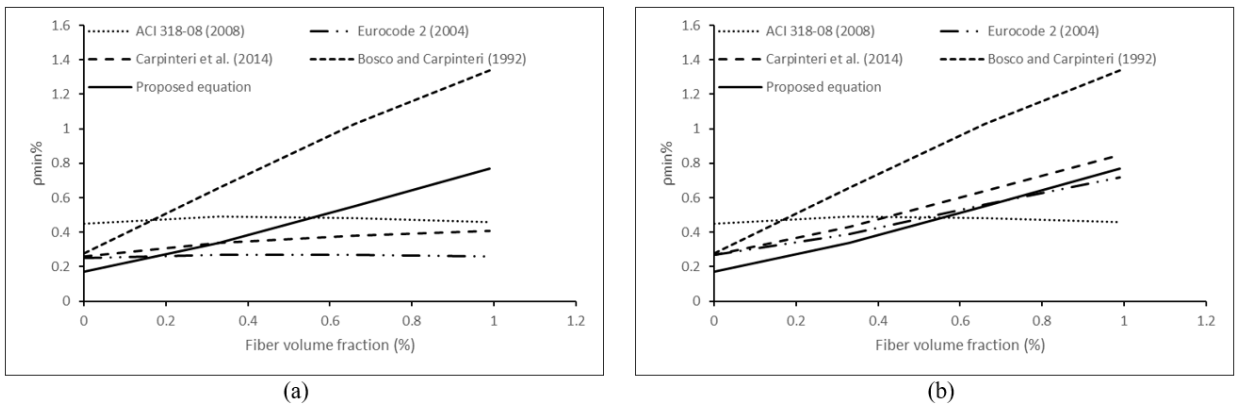


Figure 5. Minimum reinforcement ratio versus steel fiber content for: (a) average uniaxial tensile strength and (b) splitting tensile strength

- The beams with the reinforcement ratio of 0.17% represent a brittle behavior independent from the fiber volume fraction.
- Increasing steel fiber content clearly improves the yield load capacity of the RC beams due to the superior mechanical clamping between fiber and concrete after first crack.
- Final crack patterns of RC beams in particular for 0.50% reinforcement ratio demonstrated that increasing fiber content decreases the flexural ductility of the beams reducing the number of flexural crack and the length of the plastic hinge.
- Critical brittleness number was determined as 0.18 from the comparison between concrete's ductility-RC beam ductility plot and crack patterns. Then the equation giving minimum reinforcement ratio was proposed based on solely fracture properties of concrete.
- Some further experimental and theoretical studies based on concrete fracture characteristics could be performed and suggestions could be made on the existing rules for the minimum reinforcement ratio to the existing codes.

REFERENCES

- ACI Committee 318. 2008. *Building Code Requirements for Structural Concrete (ACI 318-08) and Commentary (ACI 318R-08)*. Farmington Hills, MI: American Concrete Institute.
- Bosco, C., A. Carpinteri, and PG. Debernardi, 1990, Fracture of reinforced-concrete - scale effects and snap-back instability. *Engineering Fracture Mechanics*, 35(4-5): 665-677.
- Bosco, C., A. Carpinteri, and PG. Debernardi, 1990, Minimum reinforcement in high-strength concrete. *Journal of Structural Engineering-Asce*, 116(2): 427-437.
- Bosco, C, and Carpinteri A. 1992. *Fracture mechanics evaluation of minimum reinforcement in concrete structures. Applications of Fracture Mechanics to Reinforced Concrete*. Ed: A. Carpinteri. London: Elsevier Applied Science, 347-377.
- Carpinteri, A. 1984, Stability of fracturing process in rc beams. *Journal of Structural Engineering-Asce*, 110(3): 544-558.
- Carpinteri, A., and M. Corrado, 2011, Upper and lower bounds for structural design of rc members with ductile response. *Engineering Structures*, 33(12): 3432-3441.
- Carpinteri, A., E. Cadamuro, and M. Corrado, 2014, Minimum flexural reinforcement in rectangular and t-section concrete beams. *Structural Concrete*, 15(3): 361-372.
- Dancygier, AN., and Z. Savir, 2006, Flexural behavior of hsfrc with low reinforcement ratios. *Engineering Structures*, 28(11): 1503-1512.
- Dancygier, AN., and E. Berkover, 2016, Cracking localization and reduced ductility in fiber-reinforced concrete beams with low reinforcement ratios. *Engineering Structures*, 111: 411-424.
- Eurocode 2. 2004. *Eurocode 2: Design of Concrete Structures, Part 1-1: General Rules and Rules for Buildings*. Brussels: European Committee for Standardization.
- Fantilli, AP., D. Ferretti, and G. Rosati, 2005, Effect of bar diameter on the behavior of lightly reinforced concrete beams. *Journal of Materials in Civil Engineering*, 17(1): 10-18.
- Henager, CH., and TJ. Doherty, 1976, Analysis of reinforced fibrous concrete beams. *Journal of the Structural Division*, 102(1): 177-188.
- Hillerborg, A., M. Modéer, and PE. Petersson, 1976, Analysis of crack formation and crack growth in concrete by means of fracture mechanics and finite elements. *Cement and Concrete Research*, 6(6): 773-781.
- Karihaloo, BL. 2015, A new approach to the design of RC structures based on concrete mix characteristic length. *International Journal of Fracture*, 191(1-2): 147-165.
- Koksal, F., F. Altun, I. Yigit, and Y. Sahin, 2008, Combined effect of silica fume and steel fiber on the mechanical properties of high strength concretes. *Construction and Building Materials*, 22(8): 1874-1880.
- Ožbolt, J., and M. Bruckner, 1999, Minimum reinforcement requirement for rc beams. *European Structural Integrity Society*, 24(1): 181-201.
- Ozcebe, G., U. Ersoy, and T. Tankut, 1999, Minimum flexural reinforcement for T-beams made of higher strength concrete. *Canadian Journal of Civil Engineering*, 26(5): 525-534.
- Rao, GA., I. Vijayanand, and R. Eligehausen, 2008, Studies on ductility and evaluation of minimum flexural reinforcement in RC beams. *Materials and Structures*, 41(4): 759-771.
- Shao, DR., and A. Sharma, 2014, Effect of steel fiber content on concrete beams with and without stirrups. *ACI Structural Journal*, 111(5): 1157-1166.
- Shehata, IAEM., LCD. Shehata, and SLG. Garcia, 2003, Minimum steel ratios in reinforced concrete beams made of concrete with different strengths - theoretical approach. *Materials and Structures*, 36(255): 3-11.
- Wafa, FF., and SA. Ashour, 1992, Mechanical-properties of high-strength fiber reinforced-concrete. *Aci Materials Journal*, 89(5): 449-455.
- Yoo, DY., N. Banthia, and YS. Yoon, 2017, Experimental and numerical study on flexural behavior of ultra-high-performance fiber-reinforced concrete beams with low reinforcement ratios. *Canadian Journal of Civil Engineering*, 44(1): 18-28.

Author Index

A		K	
Al-Mahaidi, R.	22	Kahraman, S.	170
Al-Ogaidi, Y.	22	Kasuga, A.	41
Arslan, A.	200	Kaya, D.	181
B		M	
Bedirhanoglu, I.	122	Mahrenholtz, C.	149
Bourgund, U.	79	Majed, M. M.	159
C		Mısır, I. S.	170
Cetin, S. Y.	181	O	
D		Oncu, M. E.	181
Delgado, J. S.	1	P	
F		Palieraki, V.	89
Fernandez, F. A.	1	Pampanin, S.	58
G		Peiretti, H. C.	1
Genesio, G.	89	Pekmezci, B. Y.	191
Girgin, S. C.	170	Piccinin, R.	79, 89
Girgin, Z. C.	191	S	
Gorgun, H.	181	Sucuoglu, H.	13
Günes, M. E.	191	T	
Gümüş, M.	200	Tasdemir, M. A.	100
H		V	
Hashemi, M. J.	22	Vintzileou, E.	89
I		Y	
Ilki, A.	122	Yazdi, H. A.	22
Ishikawa, Y.	31	Z	
		Zadeh, M. T.	159

